2012

EXPERIMENTAL INVESTIGATION OF AUTOMATIC TRANSMISSION FLUID (ATF) IN AN AIR COOLED MINICHANNEL HEAT EXCHANGER

MD ABDUL QUAIYUM
University of Windsor

EXPERIMENTAL INVESTIGATION OF AUTOMATIC TRANSMISSION FLUID (ATF) IN AN AIR COOLED MINICHANNEL HEAT EXCHANGER

by

Md Abdul Quaiyum

A Thesis
Submitted to the Faculty of Graduate Studies
through Mechanical, Automotive, and Materials Engineering
in Partial Fulfillment of the Requirements for
the Degree of Master of Science at the
University of Windsor

Windsor, Ontario, Canada

2012

EXPERIMENTAL INVESTIGATION OF AUTOMATIC TRANSMISSION FLUID (ATF) IN AN AIR COOLED MINICHANNEL HEAT EXCHANGER

by

Md Abdul Quaiyum

APPROVED BY:

_____

Dr. Paul Henshaw
Department of Civil and Environmental Engineering

_____

Dr. Daniela Pusca
Department of Mechanical, Automotive, and Materials Engineering

_____

Dr. Amir Fartaj, Advisor
Department of Mechanical, Automotive, and Materials Engineering

_____

Dr. Bill Zhou, Chair of Defense
Department of Mechanical, Automotive, and Materials Engineering

January 30, 2012

DECLARATION OF ORIGINALITY

I hereby certify that I am the sole author of this thesis and that no part of this thesis has been published or submitted for publication.

I certify that, to the best of my knowledge, my thesis does not infringe upon anyone's copyright nor violate any proprietary rights and that any ideas, techniques, quotations, or any other material from the work of other people included in my thesis, published or otherwise, are fully acknowledged in accordance with the standard referencing practices. Furthermore, to the extent that I have included copyrighted material that surpasses the bounds of fair dealing within the meaning of the Canada Copyright Act, I certify that I have obtained a written permission from the copyright owner(s) to include such material(s) in my thesis and have included copies of such copyright clearances to my appendix.

I declare that this is a true copy of my thesis, including any final revisions, as approved by my thesis committee and the Graduate Studies office, and that this thesis has not been submitted for a higher degree to any other University or Institution.

ABSTRACT

Narrow-channels have been subjected to diversified research and application interests due to miniaturized geometry and lightweight, superior heat transfer characteristics, and better energy efficiency. Automatic Transmission Fluid (ATF) cooling is one of the most important challenges in the automotive industry due to its changing thermo-physical properties as a result of temperature and frictional environment which exist, inside the transmission. In this study, efforts have been accumulated to justify the suitability of Minichannel Heat Exchanger (MICHX) application in characterizing ATF cooling and its flow behaviours.

An experimental investigation has been conducted with the aid of a well-equipped closed loop thermal wind tunnel, which uses a wavy finned MICHX as the test specimen. During the experiment, ATF mass flow rates were varied to achieve Reynolds Number of $3 \leq Re_L \leq 30$. The effects of serpentines on ATF heat transfer and flow behaviours were investigated in a laminar flow regime. Heat transfer enhancement was observed due to the serpentine structure. The effects of dimensionless parameters; such as Reynolds number, Nusselt number, Prandtl number, Brinkman number, and Ekert number on heat and mass transfer characteristics were examined. Heat and mass transfer correlations were established while considering variable property ratio.

The investigation showed promising heat transfer characteristics and good agreement in flow-field with the established phenomena of MICHX.

DEDICATION

Dedicated to-

My beloved Mother who prays day and night,

Who loves me the most,

Who wishes all the best from the far.

ACKNOWLEDGEMENTS

First the author is greatly thankful to the Almighty, the Creator and the Sustainer.

The author likes to express his sincere gratitude and appreciation to his advisor Dr. Amir Fartaj for offering him the opportunity in conducting such a needful research. His diligent and distinctive guidance, supports, and judicious opinion throughout the research are gratefully honored. His expert supervision, thoughtful instruction, intellectual academic input, and incessant inspiration led the author to a successful completion of the research.

The author likes to thankfully recognize the advices from the committee members; Dr. Paul Henshaw and Dr. Daniela Pusca for their most valuable suggestions and comments which made the write-up more readable and informative.

The author offers his deep appreciation and gratefulness to Mr. Andy Jenner for his cordial technical supports and sincere efforts in remodeling the experimental setup.

Special thanks and acknowledgements are extended to Ms. Rose Gignac for providing the author with friendly secretarial supports throughout the program. Warm acknowledgement goes to Ms. Barb Denomey for her cordial assistance in all respect during the program in the Department of Mechanical, Automotive, and Materials Engineering.

The author gratefully recognizes the advice from Dr. Mesbah-ul Ghani Khan. Special thanks and gratitude are presented to Serena Askar for her sincere efforts in compiling the write-up and assistance during equipment operation. Continuous efforts, expense of valuable moments, and hard labor during the experimentation extended by Shahram

Fotowat, Mohammed Ismail, Mohammed Saadi, and Mr. Sarbadaman Dasgupta are inevitably acknowledged.

Lastly, the author likes to express his deep obligation to the Almighty for His blessings and kindness in successful accomplishment of the program.

TABLE OF CONTENTS

LIST OF TABLES

LIST OF FIGURES

NOMENCLATURE/ABBREVIATIONS

A	Cross-Sectional Area of Fluid Flow, *(m^2)*
A_{hx}	Total Channel Heat-Transfer Surface Area, *(m^2)*
A_{min}	Minimum Air-Flow Frontal Area, *(m^2)*
A_{Hxa}	Combined Available Air Heat-Transfer Surface Area, *(m^2)*
C_p	Specific Heat Capacity, *(J/Kg-K)*
C_{pL}	Liquid Specific Heat Capacity, *(J/Kg-K)*
C_{pa}	Air Specific Heat Capacity, *(J/Kg-K)*
C_h	Hot Fluid Heat Capacity Rate, *(J/s-K)*
C_c	Cold Fluid Heat Capacity Rate, *(J/s-K)*
C_L	Liquid Heat Capacity Rate, *(J/s-K)*
C_a	Air Heat Capacity Rate, *(J/s-K)*
C^*	Capacity Rate Ratio
cP	Centi-Poise, Unit of Dynamic Viscosity
cSt	Centi-Stroke, Unit of Kinematic Viscosity
C_{min}	Minimum Heat Capacity Rate, *(J/s-K)*
D	Channel Diameter, *(m)*
D_c	Serpentine Curvature Diameter, *(m)*
D_T	Thermal Diffusivity, *(m^2/s)*
D_h	Channel Hydraulic Diameter, *(m)*
D_{h_L}	Liquid-Side Channel Hydraulic Diameter, *(m)*
D_{h_a}	Air-Side Channel Hydraulic Diameter, *(m)*
D_e	Dean Number

D_o	Channel Outside Diameter, *(m)*
D_i	Channel Inside Diameter, *(m)*
E_c	Eckert Number
f	Friction Factor
f_d	Darcy's Friction Factor
f_f	Fanning's Friction Factor
f_{cort}	Friction Factor Corrected for Temperature with Variable Property Ratio
f_c	Friction Factor at Curvature Part of Channel (Serpentine Part)
f_s	Friction Factor at the Straight Part of the Channel
F	LMTD Correction Factor for Multi-pass and Cross-flow Heat Exchanger
g_c	Acceleration Due to Gravity, *(m/s^2)*
G	Mass Flux, *(kg/m^2-s)*
G_L	Liquid Mass Flux (Mass Flow Rate per Unit Area), *(kg/m^2-s)*
h	Heat Transfer Coefficient, *($W/m^{2-}K$)*
h_L	Liquid Heat Transfer Coefficient, *($W/m^{2-}K$)*
h_a	Air Heat Transfer Coefficient, *($W/m^{2-}K$)*
k	Thermal Conductivity, *(W/m-K)*
k_{al}	Thermal Conductivity of Aluminum, *(W/m-K)*
k_L	Thermal Conductivity of Liquid, *(W/m-K)*
L	Channel Length, *(m)*
L_a	Air Flow Length, *(m)*
L_{hy}	Hydrodynamic Entrance Length of Liquid, *(m)*
L_{Th}	Thermal Entrance Length of Liquid, *(m)*

$\dot{m}$	Mass-Flow Rate, *(kg/s)*
$\dot{m}_L$	Liquid Mass-Flow Rate, *(kg/s)*
$\dot{m}_a$	Air Mass-Flow Rate, *(kg/s)*
N_{Br}	Brinkman Number
Nu	Nusselt Number
Nu_L	Liquid Nusselt Number
Nu_a	Air Nusselt Number
Nu_c	Nusselt Number Corrected for Temperature with Variable Property Ratio
Nu_{Lc}	Liquid Nusselt Number Corrected for Temperature with Variable Property Ratio
Nu_m	Nusselt Number at Mean/Bulk Temperature
Nu_w	Nusselt Number at Wall Temperature
NTU	Number of Transfer Unit
P	Wetted Perimeter, *(m)*
P_{dyn}	Dynamic Pressure of Air, *(kPa)*
P_e	Péclet Number
Po	Poiseuille Number
Pr	Prandtl Number
Pr_L	Liquid Prandtl Number
Pr_g	Glycol Prandtl Number
ΔP	Pressure Drop, *(kPa)*
$\dot{Q}$	Heat Transfer Rate, *W*
$\dot{Q}_L$	Liquid Heat Transfer Rate, *W*

$\dot{Q}_a$	Air-Side Heat Transfer Rate, *W*
$\dot{Q}_{avg}$	Average Heat Transfer Rate, *W*
$\dot{Q}_{max}$	Maximum Heat Transfer, *W*
q_L	Heat Transfer Rate, *W*
R	Radius of Serpentine Curvature, *(m)*
R_e	Reynolds Number
Re_L	Liquid Reynolds Number
Re_g	Glycol Reynolds Number
Re_a	Air Reynolds Number
Re_{cr}	Critical Reynolds Number
R_L	Liquid-Side Thermal Resistance, *($^oK/W$)*
R_a	Air-Side Thermal Resistance, *($^oK/W$)*
R_{total}	Total Thermal Resistance, *($^oK/W$)*
R_w	Solid Wall Thermal Resistance, *($^oK/W$)*
T_{L_i}	Liquid Inlet Temperature, *(^oC)*
T_{L_o}	Liquid Outlet Temperature, *(^oC)*
T_{b_L}	Liquid Bulk Temperature, *(^oC)*
T_{a_i}	Air Inlet Temperature, *(^oC)*
T_{a_o}	Air Outlet Temperature, *(^oC)*
T_{b_a}	Air Bulk Temperature, *(^oC)*
T_{hi}	Hot-Fluid Inlet Temperature, *(^oC)*
T_{ho}	Hot-Fluid Outlet Temperature, *(^oC)*

T_{ci}	Cold-Fluid Inlet Temperature, *(^oC)*
T_{co}	Cold-Fluid Outlet Temperature, *(^oC)*
T_{s_i}	Channel inside Wall Temperature, *(^oC)*
T_{s_o}	Channel outside Wall Temperature, *(^oC)*
T_f	Film Temperature, *(^oC)*
T_{in}	Inlet Temperature, *(^oC)*
T_{out}	Outlet Temperature, *(^oC)*
T_b	Bulk Temperature, *(^oC)*
T_w	Wall Temperature, *(^oC)*
ΔT	Temperature Difference, *(^oC)*
ΔT_L	Liquid Temperature Difference, *(^oC)*
ΔT_a	Air Temperature Difference, *(^oC)*
ΔT_{lm}	Log-Mean-Temperature Difference, *(^oC)*
UA	Overall Heat Transfer Conductance, *($W/^oK$)*
V	Velocity, *(m/s)*
V_L	Liquid Velocity, *(m/s)*
V_a	Air Velocity, *(m/s)*
$\dot{\tilde{V}}$	Volume Flow Rate through the Channels, *(m^3/s)*
$\tilde{V}$	Pump Volume Flow Rate, *(m^3/s)*
V_{eff}	Volumetric Efficiency of Pump

τ_w	Wall Shear Stress, *(kPa)*
α	Thermal Diffusivity, *(m^2/s)*
ρ	Density, *(kg/m^3)*
ρ_L	Liquid Density, *(kg/m^3)*
ρ_a	Air Density, *(kg/m^3)*
ν	Kinematic Viscosity, *(centi-Stroke)*
μ	Dynamic Viscosity, *(kg/m-s, centi-Poise, (SSU) Saybolt Universal Seconds)*
μ_f	Film Dynamic Viscosity, *(centi-Poise)*
μ_L	Liquid Dynamic Viscosity, *(centi-Poise)*
μ_a	Air Dynamic Viscosity, *(centi-Poise)*
μ_m	Dynamic Viscosity of Liquid at Bulk/Mean Temperature, *(centi-Poise)*
μ_w	Dynamic Viscosity of Liquid at inside Wall Temperature, *(centi-Poise)*
η_a	Air Side Surface Efficiency
η_f	Fin Efficiency
m	Exponent for Friction Factor Correction with Variable Property Ratio Due to Temperature
n	Exponent for Nusselt Number Correction with Variable Property Ratio Due to Temperature
ε	Heat Exchanger Effectiveness

ASME	American Society of Mechanical Engineers
ASTM	American Society of Testing Materials
ATF	Automatic Transmission Fluid
CARB	California Air Resources Board
CVT	Continuously Variable Transmission
DAQ	Data Acquisition System
DFM	Digital Flow Meter
DPTD	Differential Pressure Transducer
EPA	Environmental Protection Agency
EU	European Union
HB	Heat Balance
HB_L	Liquid Heat Balance
HB_{avg}	Average Heat Balance
HVAC	Heating Ventilating and Air Conditioning
IFM	Impeller Flow Meter
ITMRL	Integrated Thermal Management Research Laboratory
LMP	Liter per Minute
MC	Micro-Channel
MICHX	Minichannel Heat Exchanger
NHTSA	National Highway Traffic Safety Administration
OTA	Oil To Air
PTD	Pressure Transducer
PTO	Power Take-Off

PCM	Power-Train Control Module
RTD	Resistance Temperature Detector
SAE	Society of Automotive Engineers
TC	Thermocouple
TCC	Torque Converter Clutch
TCM	Torque Converter Module
UPS	Undisruptive Power Supply
VLSI	Very Large Scale Integrated Circuit
VII	Viscosity Index Improver

CHAPTER I

INTRODUCTION

Although naturally occurring renewable-energy sources in the form of solar energy, wind energy, geothermal energy, etc., are abundantly available, the reserves of some forms of energy, such as fossil fuel and other mining-energy resources, are being diminished day by day. All types of energy resources are limited and need to be conserved. Heat is one of the most important energies, which has versatile applications in daily life. Industries cannot be imagined without the application of heat energy. Power generation, nuclear industries, mobile and aerospace application, space research, HVAC industries, marine and mining applications, chemical processing, petroleum, and forestry; all of these industries and sectors consume heat energy.

The Global Auto Report (2011) stated that between the 2000 to 2010 statistical years, 208.82 million cars were sold [1]. The International Organization of Motor Vehicle Manufacturers' statistics showed that in the 2010 manufacturing year, the total number for car and commercial vehicle production was 77,857,705 [2]. Such a huge number of vehicles in the market consume a significant amount of fossil fuel. Those vehicles need suitable thermal management systems to keep them appropriately functioning.

One of the largest industries utilizing heat from solar energy is the living plants that enact photosynthesis when they receive millions of tons of CO_2 and release O_2. The heat transfer between the plant and the environment usually occurs in all three modes: conduction, convection, and radiation. The heat is transferred through the process of conduction and convection in the form of sensible heat, and through the evaporation of water, which includes the processes of condensation, freezing, thawing, and sublimation

in the form of latent heat [3]. In this case the plant stomata are the heat exchangers which are the natural heat exchangers. When heat energy is in use, heat transfer occurs and two phenomena usually exist: the system persists either in heating or in cooling mode. During either of the modes, heat transfer occurs due to the temperature differences in the physical systems.

Appropriate devices allow easy heat transfer. Heat exchangers are the devices that participate in exchanging heat between two fluids in order to serve specific purposes given the conditions of temperature gradients. The purpose is to remove or to add heat as quickly as possible. Inside an engine cylinder heat is transferred from the burnt gases to the engine coolant through the engine block, but this system is not considered a heat exchanger. However, a device which is called the heat exchanger, allows quick heat removal from the hot engine coolant by the flowing air. So, there are specific differences among the terms heat transfer and heat exchangers. To evaluate the term 'heat exchanger,' there must be two fluids participating in exchange of heat between them. Among the participating fluids, one may be liquid and the other a gas, or both may be liquids. If a heat transfer system consists of only one liquid, it is known as heat sink [77].

Heat exchangers can be distinguished from one another based on working principles, geometry, construction, fluid-flow arrangements, types of fluids, and the fluid mixing conditions. Heat transfer in a heat pipe occurs based on the principle of latent heat with no change in temperature in the working fluid, while other heat exchangers work on the principle of differential temperature in the form of sensible heat. Space (NASA) is one of the largest sectors to use heat pipes. A contact heat exchanger works on the principle of making direct contact with the fluids, then mixing with each other, and finally

exchanging heat between them. The de-aerator, spray condenser, and wet cooling tower are the example of such a heat exchanger. The regenerative heat exchanger works based on the principle of heat storage. The common types of heat exchangers used in the industries are: shell and tube heat exchanger, plate heat exchangers, regenerative heat exchangers, adiabatic wheel heat exchangers, heat sinks, and channel heat exchangers. Based on the direction of the liquid flow, the common heat exchangers are: parallel-flow, countercurrent, and cross-flow heat exchangers. In parallel-flow heat exchangers, both fluids move in the same direction parallel to each other. In countercurrent heat exchangers, the fluids flow in opposite directions. Lastly in cross-flow heat exchangers, the fluid flow direction is perpendicular to each other. Heat exchangers may work with both of the fluids liquid, one liquid and the other gas, or both gases. Based on channel dimensions, especially the hydraulic diameter, or in another word the characteristic length scale, heat exchangers may be classified with different names. Mainly, two classification schemes are available in open the literature. The scheme proposed by Mehendale et al (2000) covered heat exchanger cores within the range of 1μm to 100μm as microchannels, 100 μm to 1mm as meso-channels, 1mm to 6mm as compact passages, and greater than 6mm as conventional passages [4]. This division was based simply upon the hydraulic diameter of the channels. The classifications on channels were further refined by Kandlikar et al (2003), who classified channels as: 'Conventional Channels': Dh >3mm, 'Minichannels': 3mm > Dh >200 μm, 'Microchannels': 200μm > Dh >10μm, 'Transitional Channels': 10μm > Dh >0.1μm, 'Transitional Microchannels': 10μm > Dh >1μm, 'Transitional Nanochannels': 1μm > Dh >0.1μm, and 'Molecular Nanochannels': 0.1μm ≤ Dh. A heat exchanger with a channel size less than 3mm is

called narrow-channel [5]. The American Society of Mechanical Engineers (ASME) usually adopts the latter classification refined by Kandlikar et al in distinguishing channel classification. The organization uses the name; Minichannel, Microchannel, and Nanochannel when publishing technical papers or journals which deal with work related to channel hydraulic diameters [6, 7]. The heat exchanger under the current investigation has a hydraulic diameter of 1mm. Hence, it sits in the classification category of Minichannel according to the ASME adoption. Based upon the historical development of channel classification, which is established and recognized by ASME, the heat exchanger used for the current study has been termed as the Minichannel Heat Exchanger (MICHX).

Channel size is very important in terms of heat transfer and fluid flow characterization. In the case of a single phase or two-phase liquid-gas heat exchangers, no fundamental change occurs in fluid-flow due to channel sizes up to 200μm. Below 200μm, manufacturing techniques and the cleanliness process are very important in light of their performance [5, 8].

Heat-transfer intensification and energy efficiency of the heat exchanging devices are the prime concern of several industries now-a-days. The optimal design of heat exchangers for minimum system losses and efficient heat transfer is a great challenge in terms of energy savings. The challenges exist because of the persisting phenomenon of entropy generation by the heat transfer process across a finite temperature difference, and of irreversible friction flows [9]. One way of enhancing heat transfer is the minimization of entropy generation and the maximization of the heat transfer coefficient. This can be achieved in numerous ways such as minimizing pressure drops and friction factors, by improved fabrication technologies, minimizing channel size, and adopting advanced

geometry such as the slab and serpentine structure which gives better performance over conventional heat exchangers [6, 10-11, 19, 25, 63-70].

Researchers are in search of devices that efficiently transform energy and be friendly to the environment & ecology. MICHXs are the subject of diversified research and application interest due to the: miniaturized geometry and lightweight, augmented heat transfer characteristics, and the versatility in their use [12, 17-18, 25]. The devices can play an important role in the real-world applications, even in cooling of viscous fluids like engine oil, engine coolant, and transmission fluid. The applications of such devices are extended in the field of HVAC systems in automotive industries or residential use.

Narrow channel heat-exchangers with a diameter of 1mm or less have high-heat transfer surface densities up to 10,000m^2/m^3 [13-18]. In the current study, the surface density of the heat exchanger is 4,000m^2/m^3, which is about six times higher than traditional compact heat exchangers. For flow in channels, the local heat transfer coefficient h is directly proportional to the fluid conductivity and inversely proportional to the channel hydraulic diameter. The relation is $h = Nuk/D_h$ where h is the coefficient of heat transfer, k is the fluid conductivity, and D_h is the channel hydraulic diameter or characteristic length. Therefore, two basic parameters lead to the heat-transfer enhancement: fluid conductivity (k) and channel geometry (D_h). To ensure heat transfer enhancement, designers need to consider either increasing the fluid conductivity or decreasing the channel hydraulic diameter. This historical concept was first developed and proved in 1981 by David B. Tuckerman, a PhD candidate under the supervision of Professor R. F. W. Pease (Stanford University USA), to the advent of systems employing high-density, very-large-scale integrated (VLSI) circuits that required effective, compact, and quick

heat removal [17-18]. Their pioneering work aimed at the cooling of high-speed digital circuits employing submicron channel lengths dissipating high heat. They were successful in constructing a very compact water-cooled heat sink, which was an integral part of the silicon substrate, and capable of maintaining 790 W/cm^2 power densities. Since then, many researchers intensified their interests to dig into the mystery of high thermal and hydrodynamic performances in minichannel and microchannels. Some researchers worked on developing mathematical models [12, 19], while others conducted experimental investigations. Kang, et al (2002) used de-ionized water as the working fluid, and found a volumetric heat transfer of 188.5 MW/m^3-K with an overall heat transfer coefficient of 24.7 kW/m^2-K. Their investigation was carried out with a prototype cross-flow microchannel heat exchanger in the laminar regime [10].

Although theoretically heat transfer enhancement occurs based on fluid property k, and channel geometry D_h, it is still an open question as to whether or not this concept fits for all kinds of channel geometries and fluid conductivities. Therefore, many investigators emphasized the necessity of further research in this area to develop a consensus for eliminating such arguments. Although the open literature shows that higher heat transfer intensification can be ensured by the MICHXs [6, 10-11, 19, 25, 63-70], most of the investigations were carried out using fluids such as water and ethylene glycol, while literature pertaining to the investigation of ATF is scarce. There is a need for in-depth investigation on MICHX for cooling ATF.

1.1 Motivation

Heat-transfer augmentation and miniaturized geometry of heat exchangers have intensified the propensity of researchers towards finding a match for real-world application, such as cooling of a nano-scale device (microchips) or a huge piece of equipment, like a spacecraft. Narrow-channel technology in heat transfer and fluid-flow applications are heading towards the replacement of the traditional heat exchangers [6, 10-11, 19, 25, 63-70]. MICHXs are able to mitigate industry energy needs through energy conservation and reduced exergy destruction. In recent years, appreciable developments in micro and mini-heat exchanger design & fabrication technologies have been achieved. Such achievements have enriched the research appeal to find better-performing heating or cooling devices. The heat exchanger under this study is a slab-structured single piece unit, which has a serpentine shape and wavy fins at the straight part after the serpentine (Figure 4.20 and 4.21). As this is a slab structured unit with parallel minichannels, no gap exists in between channels. Such a structure can prevent any wake region formation behind the channels, and allow a longer dwelling time that enables uniform temperature distribution over the slab. Heat duty, which is defined as the amount of heat transferred from 1kg of hot fluid to the 1 kg of cold fluid in one hour, is also an important factor in this case. The advantages of these MICHXs have been summarized below:

- They ensure elevated heat duty, even 315 MW/m^3-K or more because of the advanced design, [10-11].
- Surface density is very high, about 4,000 m^2/m^3; it is approximately six times higher than traditional compact heat exchangers [20-22].

- For HVAC applications, they have environmentally sound operation, structural robustness, better thermal performance, and corrosion resistance [20].
- For serpentine-structure MICHX: the serpentine develops new thermal boundary layers at each turn that enhance the heat transfer rate [23-24].
- MICHXs offer reduced thermal resistance of the liquid boundary layer due to high-performing material properties that allow quicker heat transfer.
- Reduced air-side pressure drop enhances fuel-cost cutting and indirectly saves the environment.

The MICHX under this study has been selected to characterize fluid-flow and heat transfer behaviours of ATF. Under the research plan, a complete set of experimental data on heat transfer, fluid flow, and design parameters have been anticipated. Although open literature showing the advantages of narrow-channel heat exchangers is abundant, studies dealing with heat transfer and fluid-flow characterization of ATF using the MICHX are still unavailable. Therefore, the need of an investigation on heat transfer behaviours and fluid flow characteristics of ATF in MICHX has been realized. In the current study, the motivation of selecting a flat geometry serpentine-slab test specimen is to quantitatively and qualitatively justify the ATF cooling strategies.

1.2 Objectives

Numerous investigations have been conducted on heat transfer and fluid flow behaviours of different fluids like water, ethylene glycol, water-diluted glycol, brine, and other low viscous fluids. However, studies on examining heat transfer and flow behaviours of ATF are not available in the open literature either for conventional or advanced narrow-

channel heat exchangers. Thus, the findings of the literature survey on ATF cooling characteristics unveiled the great necessity of further exploration on this material to fill in the gaps in research. Investigations on slab-structure serpentine MICHXs that are involved in examining heat and mass flow characteristics of non-viscous or very low viscous fluids are available. However, the scarcity of information pertinent to ATF cooling brought the study into light as a field of research interest. Cooling of ATF is one of the major challenges for the automatic transmission designer due to the variable property characteristics as a result of temperature variation. The response of the ATF thermo-physical properties to temperature and the flow behaviours prompted this study to use serpentine MICHXs in order to make a judgment on their industrial applicability based on experimental data. The main objectives of this study are summarized below:

- Perform a comprehensive study of previous works identifying heat transfer and fluid flow behaviours of different viscous fluids.
- Experimentally investigate heat-transfer characteristics of ATF in MICHX in the laminar regime and compare findings to other fluid behaviours using a similar test specimen.
- Experimentally investigate and identify temperature dependency of ATF fluid-flow and heat-transfer parameters with air-side temperature change while keeping ATF temperature constant.
- Investigation of heat transfer rates, *NTU*, effectiveness, friction factor & pressure drop behaviours, and overall thermal resistance with Re_L and/or mass flux.

- Investigate effects of dimensionless form of parameters: Reynolds number (Re_L), Nusselt number (Nu_L), Prandtl number (Pr), Brinkman number (N_{Br}), Ekert number (Ec), and Dean Number (De) on heat and mass transfer behaviours.
- Establish heat and mass transfer correlations among the parameters: specifically h_L and Nu_L with Re_L, Nu_L with Ec, Nu_L with N_{Br}, and ε-NTU with Re_L.
- Summarize information to the fulfillment of the potentiality of MICHX in the real-world applications, especially in automotive industries.
- Generate an experimental database for the ATF cooling strategy for further research on similar types of viscous fluids using similar heat exchangers.

A careful completion of such research objectives will ensure greatest achievement in the development of an initial guide for the transmission designers and provide a source of information for future projects.

CHAPTER II

REVIEW OF LITERATURE

Heat exchangers are the devices that allow quicker heat transfer from one media to another usually between liquid and gases in serving special purposes. Industries cannot be established without considering heat exchangers. Heat exchangers have versatile use in the real-world applications. Some of the important applications of such a heat exchanger can be summarized as: Food & Beverage industry which includes processing of dairy product, brewing, soft drink, fruit processing, etc.; Chemical Industry that includes petroleum processing, hydrocarbon processing, polymer processing, pharmaceutical product processing, etc.; Industrial application such as mining, automotive, pulp and paper, textile application, vegetable oil processing, sugar industry, etc.; Power sector such as power generation and distribution, HVAC application, and so on. Some of the important research areas related to the current investigation available in open literature are summarized in this chapter.

2.1 Heat-Transfer Characteristics at Laminar Flow in Minichannel

The heat-transfer characteristics of circular minichannels, either straight or serpentine configurations for developing or developed laminar flow, are not readily available in the open literature. For narrow-channel heat exchangers, the *Nu* can be found within the range of 0.21 to 16 times higher than that of the conventional heat exchangers. During the heat transfer and fluid flow in channels, for a partially developed flow, the local *Nu* may be higher than in the case of a fully developed flow. *Nu* for a particular fluid flowing through the heat exchangers can be estimated experimentally or from the available

correlations. Although few correlations for a developing laminar flow through traditional pipes are available in open literatures, the correlations for developing laminar flow in circular minichannel, especially serpentine multi-slab MICHX, is still rare. Khan et al (2010) developed correlation for 50% ethylene glycol flowing through a single straight slab MICHX [25]. The authors termed the current minichannel as microchannel in their literature. During the investigation, they found a heat-transfer correlation for a developing flow in the form of $Nu = 0.152Re_g^{0.4912}\ Pr_g^{0.33}$ within the Reynolds number range of $400 \leq Re_g \leq 1800$ while using 50% ethylene glycol as the working fluid. In their investigation, the authors claimed that the *Nu* value is higher than the values obtained from the conventional fully developed heat exchangers. They also claimed that it is even higher than the conventional thermally developing laminar flow correlation proposed by Gnielski. Dasgupta et al (2011) worked on the air side *Nu* investigation while using de-ionized water as a liquid and found correlation as $Nu_a = 0.3972Re_a^{0.3766}$. In this case, the authors claimed that *Nu* is higher than that of Tang and Tailor [6]. Therefore, how ATF behaves at cooling while flowing through the serpentine circular minichannel in the laminar flow regime may be considered as a field of interest.

2.2 Automatic Transmission Fluid

Motor vehicle performances are usually evaluated in terms of torque generation for wheel traction, tailpipe emissions, and fuel consumption over on-road mileage. The stringent emission legislation set by the Environmental Protection Agency (EPA), California Air Resources Board (CARB), and National Highway Traffic Safety Administration (NHTSA) for North America, or European Emission Standards for EU countries are

highly regulated. A shifting of the new emission standards applicable to new passenger cars, light-duty trucks, and medium-duty passenger vehicles, covering model years 2012 through 2016 set by EPA and NHTSA, enforced to cover 35.5 miles per gallon [26]. This new standard compelled the automotive industry to manufacture vehicle components that can ensure fuel economy improvements in order for meeting the set legislation. Vehicle Power-Train is mainly responsible for such emissions. In a motor vehicle the typical Power-Train includes a set of components that generate power, deliver power to the transmission, and finally to the wheel for generating traction force. The major components of this system include engine, transmission, Power Take-Off (PTO) shaft, differentials, and the wheels. The engine and transmission are the main components of the vehicle that control its performance. Although the engine is the prime source of emissions, the transmission also plays an indirect role in increased emissions. Thus, the pressure on the manufacturing companies can be elevated due to inefficiency of such components. Researchers and manufacturers are walking jointly on the same way to overcome such problems. Efforts are being accumulated on improving the efficiency of the Power-Train components, especially the transmission. However, the investigations dealing with the efficiency improvement of the transmission system, particularly cooling of ATF using the MICHX, are still unavailable in open literatures.

Automatic transmission fluid has a life of about 100,000 miles at 175^0F (80^0C). At a high temperature it produces a varnish on internal parts interfering with the operation of the transmission. Above 250^0F (120^oC), rubber seals harden, causing pressure loss and leaks. For every 20^0F (6.67^oC) increase in operating temperature above 175^0F, the life of the

fluid is cut in half, and above 240 ^{0}F, the life becomes nil [27-28, 31]. The lifetime of the transmission with the ATF temperature is shown in Figure 2.1 in summary format.

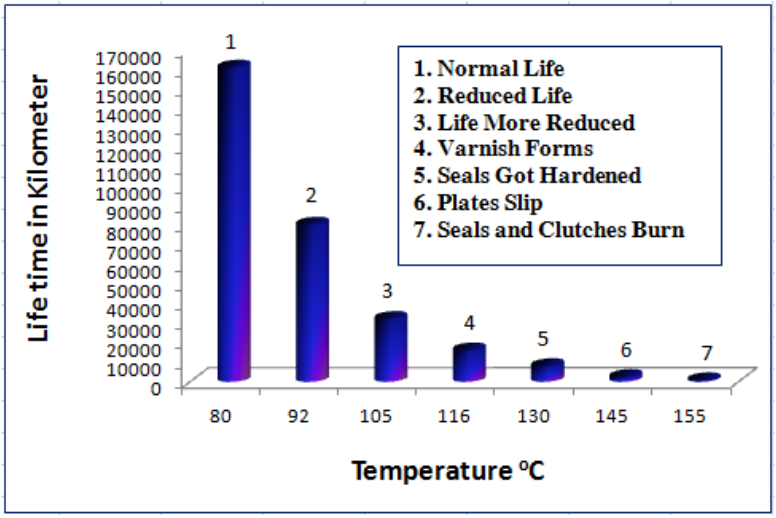

Figure-2. 1: Working Temperature of ATF and Transmission Life [27, 28]

In the petroleum industry, ATFs are known to be the most complex lubricants because of as many as 15 components in them to meet the requirements of automatic transmissions. The ATF usually performs five basic functions [29]:

(a) Transmit hydrodynamic energy in the torque converter.

(b) Transmit hydrostatic energy in hydraulic logic control circuits and servomechanisms.

(c) Lubricate shaft bearings, thrust bearings, and gears.

(d) Transmit sliding friction energy in bands and clutches.

(e) Act as a heat-transfer medium controlling automatic transmission operating temperatures.

What kind of automatic transmission fluid should be used in the transmission; this question is always answered by the manufacturers themselves. Various manufacturers of the transmission use different fluids and usually they do not match each other. Wrong use of ATF can affect the transmission performance. Shifting and engagement of the torque converter clutch (TCC) is usually controlled by the transmission control module (TCM). During the transmission in operation, the TCM electronic system considers many inputs in the transmission: including throttle position, engine speed, input-output speed, etc. The ECM and the TCM (together called PCM) work together based on some look-up values from control maps. A faulty control map from a wrong ATF may mislead the TCM causing a lot of trouble resulting in an inappropriate temperature rise. Therefore, an appropriate method of efficiently cool ATF is very important for the industries.

2.2.1 Transmission Efficiency

The improved transmission performance allows an enhanced engine efficiency and emission performance leading to overall vehicle performance and fuel economy. Salah, (2007) conducted an investigation on the Multiple Cooling Loops in Advanced Vehicle Thermal Management Systems. In the investigation, the author used an auxiliary heat exchanger located inside the radiator for transmission oil cooling. The research findings demonstrated that, appropriate Power-Train cooling can ensure vehicle fuel economy [30]. An appropriate cooling method can maintain the essential fluid properties. Semel, (2001) investigated stand-alone Oil to Air (OTA) transmission cooling strategy with thermostatic cold flow bypass valve. The study was conducted for improving the efficiency of the transmission by upgrading the warm-up system to minimize energy losses due to extremely viscous fluid at low temperatures [37].

2.2.2 Temperature Dependency of ATF

ATF performance is highly dependent on temperature, especially due to its quick response in changing the viscosity. The ATF properties significantly affect the transmission performance. Kemp, et al (1990) conducted an investigation on ATF and established correlations among various thermo-physical properties and temperature. In their study the author found that viscosity varies exponentially, while the other properties vary linearly with the variation in temperature. They established a correlation of Brookfield viscosity and temperature, as $Y = 51.565E^{(-0.1651T)}$. Here Y indicates Brookfield viscosity and T as temperature in ^{o}C. This relation is valid for low temperatures [31]. They found another correlation for the Kinematic viscosity at a higher temperature as $log\ (v + 0.7) = mlog(T) + C$ where T is the absolute temperature, and m & C empirical constants. The double log of viscosity and log of temperature allows interpolation and extrapolation as linear relations, but at temperatures below the cloud point the viscosity changes rapidly and does not follow linear relations for the mineral based lubricants [31-33].

The ATF viscosity is usually specified as kinematic viscosity, ν (centistokes) at $100^{o}C$ (ASTM D445) on the high-temperature range and Brookfield viscosity, μ (centipoises) which is reported as absolute viscosity at $-40^{o}C$ (ASTM D2983) on the low-temperature range [31-32, 34]. The viscosity of ATF varies within 5.50 - 8.00 cSt at $100^{o}C$ and generally under 20,000 cP at - $40^{o}C$ [31-32]. Most essential element properties of the ATF are: friction and friction durability, oxidation resistance, good sealing performance, operating at temperature extremes, non-corrosive to transmission components, and special antifoam properties. Rudnick, (1999) explained the physical and chemical

properties of ATF and its historical review, and also the performance level comparisons [35]. Henderson et al (1998) conducted an investigation on ATF fluidity at low and high temperatures. In Brookfield viscosity region, significant gelletion can occur due to wax crystal growth effects where the ATF behaves as a non-Newtonian fluid. However, at a kinematic viscosity region, it behaves as Newtonian fluid. The transition point is known as the cloud point (ASTM D2500) [32]. Basically, the cloud point is the temperature at which the gelletion or wax crystals start forming; it may plug the filter. For a typical ATF, the cloud point is -14^{o}C and for viscosity improved ATF it is -17^{o}C [31]. Sarker, et al (2002) conducted investigations to characterize rheological properties of ATF at low and high temperatures and outlined a cloud point at -7^{o}C. Furthermore, the findings of their investigation showed that the fluids with same kinematic and the Brookfield viscosities undergo a difference in viscosity values up to 40%, while the transmission works under the typical conditions [32/30]. Viscosity Index Improver (VII) helps in stabilizing the properties of the fluid at these temperatures. A low-viscosity ATF can reduce torque loss and improve the transmission efficiency. However, too low viscosity at a high temperature may decrease the fatigue life of metals. Kazuo et al (2003) studied low viscosity of ATF and reported on vehicle fuel economy. Their investigation showed that an improved ATF can reduce fuel consumption by 1.1-1.4% [36].

2.2.3 Newtonian and Non-Newtonian Behaviour of ATF

A fluid is said to be Newtonian fluid when it follows the expression, $\tau = \mu \partial v/\partial r$ where τ = shear stress, μ = dynamic viscosity, and $\partial v/\partial r$ is the velocity gradient perpendicular to the direction of shear [81]. ATF behaves as Newtonian and Non-Newtonian both depending

on temperature. So, the behaviours of non-Newtonian fluid also need to be studied. Rennie, et al (2007) numerically investigated Newtonian as well as non-Newtonian fluids flowing through double-pipe helical heat exchanger to examine thermo-physical properties. For Newtonian fluids, they found thermal dependency of viscosities, which have very little effect on the Nusselt number correlations, but significant effect on the pressure drops in the inner tube due to the change in average viscosity of the fluid with the change in average temperature. They studied the ratio between the pressure drops of the non-Newtonian fluid in a Newtonian fluid with change of the mass flow rate in the inner tube. Their investigation showed that the ratio of the pressure drops either decrease or increase with increasing flow rate in the inner tube, depending on conditions [39]. Other Newtonian and Non-Newtonian behaviour of fluids like ATF has been discussed in section 2.2.2.

2.2.4 Automatic Transmission Fluid Properties

Among the viscous fluids, ATF behaves very differently, especially with variation in temperature. So it is very important to know the properties and the fluid components. The following table gives an idea of the fluid components and their functions.

Table-2. 1: Automatic Transmission Fluid Properties

Components	Function of the components
Mineral oil	Base oil
Viscosity Index Improver (VII)	Helps in keeping the viscosity as much as unchanged during temperature change
Friction Modifier	Helps in improving friction characteristics

Pour Point dispersant	Helps in lowering pour point
Corrosion inhibitor	It prevents corrosion of bushings, thrust washers, bearings and other parts
Anti-wear	Helps preventing wear of gears, bushings, washers and other parts
Antioxidant	Control the oxidation during use
Dispersant	It controls the sludge and varnish
Foam Inhibitor	controls foam formation
Red Dye	Differentiate as ATF

The important thermo-physical properties are the viscosity, density, thermal conductivity, and the specific heat capacity which are usually applied for the heat-transfer characterization. These properties of ATF get changed with the change in temperature. They will be discussed in details in chapter 6. Among other properties of ATF, shear resistance is important. Viscosity Index Improver (VII) plays the role to keep the viscosity stable at higher and lower temperatures as much as possible. The VII are the long-chain polymers that get extended at higher temperature and shortened at the lower temperatures. The VIIs are usually composed of high molecular polymers, which have coiled chain. This coil size is related to the molecular weight. The high molecular weight polymers get sheared quickly [36]. So, there should be a balance in the molecular weight for choosing appropriate VII. In the transmission, especially due to frequent gear and clutch engagement and during pumping by the gear pump, the VII can be sheared into pieces resulting in permanent loss of viscosity. The temporary loss of viscosity may occur

due to shearing force that causes the VII molecule to be stretched and straitened. The base oil has smaller molecular weight than the VII, so it does not shear easily. It makes a thin film between the mating parts. An appropriate cooling can keep the ATF properties more stable during operation.

2.3 Viscous Effect of Liquid on Temperature Variation

Few researchers worked on examining the viscous effect of the liquid on temperature variations [38-53], while few others worked on pressure differential through MICHX [55-57]. Wang, et al (2004) investigated frictional characteristics of the highly viscous fluid in minichannels (D_h = *0.198–2.01 mm*) while using water and lubricating oil as the working fluids. The study was conducted with Reynolds number of 0.1 to 1500 [41]. In their investigation, it was found that the viscosity or the Prandtl number has negligible influence on the friction factor if the hydraulic diameter is greater than 1.0 mm. Obot et al (1997) observed similar results while working on water, ethylene glycol- water, and ethylene glycol within the Prandtl number range of $0.7 \leq Pr \leq 125.3$. Their result showed that the friction factor is independent of *Pr* in smooth pipes [58]. Nonino, et al (2006) carried out a parametric investigation on the effects of temperature-dependent viscosity in simultaneously developing laminar flow of a liquid for straight ducts while considering boundary condition at a uniform wall temperature [45]. Their numerical investigations showed that the viscosity varies exponentially with temperature variation in the entrance region for the laminar forced convection. Akehurst, (2001) conducted a study on V-Belt Continuously Variable Transmission (CVT) for his PhD work and checked the viscosity variation with temperature [59]. In his investigation, he found that the viscosity variation

with temperature change occurs in a power law manner where he obtained a polynomial best curve fit. Yang, et al (1995) developed a mathematical model to predict the heat transfer and fluid hydrodynamics during wet clutch engagement while considering viscous dissipation, ATF heat balance, and the effect of other thermo-physical properties [54]. So, consideration of viscous effect with temperature variation for designing transmission, cooling transmission oil, and designing the heat exchangers are very important.

2.4 Effect of Viscous Energy Dissipation

Hetsroni, et al (2005) made an analysis to verify the conventional theory to predict the hydrodynamic characteristics of Newtonian fluid flowing through micro-channels in the laminar regime with a hydraulic diameter range of $15\mu m \leq D_h \leq 4010\mu m$ and Reynolds number of $10^{-3} \leq Re \leq Re_{cr}$. Their investigation showed that to a fully developed laminar flow in circular micro-channels, an adiabatic increase in the fluid temperature may occur due to viscous dissipation as in the form of the following equation [60]:

$$\frac{\Delta T}{T_{in}} = 2\frac{v^2}{r^2}\left(\frac{L}{r}\right)\frac{Re}{C_p T_{in}} \tag{2.1}$$

where, r is the radius of microchannel channel, $\Delta T = T_{out} - T_{in}$, and ν is the kinematic viscosity. They also studied the effect of the viscous energy dissipation [60]. The study showed that under some conditions, the heat released due to viscous dissipation may cause changes in flow and temperature field. It may cause instability in the flow field.

C.P. Tso, and S.P. Mahulikar conducted an experimental investigation on water to study the viscous dissipation. They found an empirical relation of Nusselt number and the *Re*-

Pr numbers, $Nu/Re^{0.62}\ Pr^{0.33}$ on Brinkman Number (N_{Br}) in the range of $0.4559x10^{-5} \leq N_{Br} \leq 2.8333x10^{-8}$ while the Reynolds number, and the Prandtl number change in the ranges of $80 \leq Re \leq 107$, and $4.80 \leq Pr \leq 6.71$ [89]. They also noticed that at every small value of the Brinkman numbers ($N_{Br} \approx 10^{-8}–10^{-5}$), the effect of viscous dissipation on heat transfer may be considered non-realistic for flow in micro-channels.

The real effect of viscous dissipation on heat transfer can only be estimated if the dependence of the Nusselt number on the Brinkman number is determined at fixed values of the Reynolds and the Prandtl numbers. When N_{Br} is large as of the order of unity or larger, it can influence film temperature (T_f). If that is the case, even for a constant value of N_{Br} along the flow direction, the primary effect of N_{Br} occurs [89].

Koo, (2004) made an investigation on the effects of viscous dissipation on the temperature field and the friction factor while using dimensional analysis. He experimentally validated computer simulation results using water, methanol and iso-propanol as working fluids [42]. The investigation turned out that, for micro-conduits, viscous dissipation are a function of the channel aspect ratio, Reynolds number, Eckert number (*Ec*), Prandtl number, and conduit hydraulic diameter. In such a case of micro-conduits, even for a low Reynolds number, significant temperature increase may occur due to viscous dissipation in a fluid with high viscosity and low heat capacity. Morini, (2005) investigated that for forced convection through micro-channels, the conventional theory of Navier–Stokes equations cannot be considered as valid for predicting pressure drop and convective heat transfer coefficients when the hydraulic diameter is less than 1 mm. He developed a mathematical model to relate the heat generated due to viscous effects [49]. He obtained the model by considering a constant value of the viscosity so

that it gives the maximum value of the temperature rise related to the viscous heating. His model is (Temperature in Kelvin) [49]:

$$\frac{dT_b}{d_{xy}} = \left(4\frac{Ec}{Re}[fRe]\right)\frac{\Delta T_{ref}}{D_h} \tag{2.2}$$

Where, Ec is the Eckert number (*Eckert number* = $W^2/(2cp\Delta T_{ref}$, for the reference fluid)) The above equation holds if the micro-tube can be considered adiabatic.

Warnakulasuriya, et al (2008) investigated plate heat exchanger with an absorbent salt solution as highly viscous fluid, which has a high-temperature dependency. They established a correlation between the *Nu, Re*, and *Pr* and found the dependency of the heat-transfer coefficient on flow rate and that it is more pronounced at low flow rates. The Correlation relates the *Nu* with *Re* and *Pr* as $Nu = 0.292Re^{0.705}Pr^{0.35}$. They also realized the necessity of *Nu* correction due to the temperature dependency of viscous fluid and found a power law relation which they expressed in the form of $Nu = 0.292Re^{0.705}Pr^{0.35}\left(\frac{\mu_f}{\mu_m}\right)^{0.14}$; here, μ_f is the dynamic viscosity at film temperature and μ_m in mean temperature. They summarized that some factors may affect the heat exchanger performance and can cause (1) increased flow resistance at the end of the channels closer to outlet due to cooling down the fluid, (2) sedimentary buildups and solidifications at narrow part of flow passages, and (3) cold pockets at the end zone away from the main flow paths [38]. Viscous dissipation effects are very important for fluids with low specific heats and high viscosities, even in relatively low Reynolds number flows.

2.5 Scope of Current Research

Various investigations have been conducted on several working fluids either for heating or cooling purposes, while using different types of heat exchangers. However, the heat transfer and fluid-flow characteristics of an ATF still have a need of investigation due to the unavailability of information in open literatures. Although a few investigators conducted their study to apprehend the thermo-physical properties of ATF and its heat-transfer fluid-flow performances, the studies are limited to only inside the transmission [62]. The study on cooling strategies and heat-transfer characterization, using traditional or high performance heat exchanger, are still very sparse in open literatures. Even though an intensive literature survey has been accomplished, no literatures were available dealing with the ATF cooling, particularly with the aid of a MICHX. Therefore, the current study may be considered as a novel one that entails a detailed investigation on the applicability of a MICHX for transmission fluid cooling strategies.

A significant number of research articles, technical papers, journal publications, books, and open literatures have been carefully consulted. All those investigations deal with different channel geometry, channel size, fin type, tube arrangements, heat exchanger types, and types of fluids. Very few researchers have worked on slab structure minichannel of the serpentine shape. Their investigations mainly focused on the superiority of the cross-flow minichannel heat exchangers over the traditional ones while using water and 50% ethylene glycol. The chronological development of microfabrication techniques such as LIGA (a German acronym for Lithographic, Galvanoformung, Abformung which means Lithography, Electroplating, and Molding),

stereolithography, Laser beam machining, and Electroformation made the design and fabrications of mini and micro level heat exchangers easier. The heat exchanger under the current investigation is made of high-strength aluminum alloy that can withstand a pressure up to 15 Mpa due to the material and the fabrication method. Detailed plans have been made to examine the heat exchanger by placing it in a test chamber of a closed-loop thermal wind tunnel. A typical ATF has been selected to flow through the heat exchanger during the experiments. It has been anticipated that the current study is a novel work and after a successful completion of the study, the findings will be an extra addition to the industry-based information in the field dealing with the flow of mass and heat transfer.

CHAPTER III

DESIGN AND METHODOLOGY

In the current study, a Minichannel Heat Exchanger (MICHX) has been used as a test specimen. A typical automatic Transmission Fluid (ATF) has been taken as the liquid-side working fluid while conditioned air was blown in a cross-flow direction through the fins of the MICHX. For better distinguishing the fluids a subscript '*L'* for liquid and '*a'* for air have been adopted for the derivation and data analysis in the subsequent sections. It is assumed that the ATF is an incompressible fluid. Although ATF shows both Non-Newtonian and Newtonian behaviours depending on temperatures, the lowest temperature of the air has been maintained at 15^{o}C, so the ATF temperature can never be in the range of Non-Newtonian fluid. Therefore, all the calculations have been performed considering Newtonian fluid. Other considerations include; no effect of pressure drop on thermo-physical properties but the temperature-dependent properties like viscosity, density, specific heat capacity, thermal conductivity, Prandtl Number, etc. varies with the change in temperature. The wetted perimeter of the inlet and the outlet manifolds are 10 times bigger than the individual channel diameter, so the flow distributions are considered uniform. Based on the measured data all other required data and parameters have been deduced.

3.1 Key Assumptions

For a better data reduction and appropriate evaluation, the following assumptions were made:

1. The exchange of heat between the heat exchanger and the surroundings due to radiation or conduction is negligible because of appropriate thermal sealing.

2. No heat loss or gain by the air to or from the outside surroundings near the test chamber.

2. The condensation on the heat exchanger surface by the air is insignificant.

6. No heat generated by the air due to viscous dissipation.

7. During the ATF flow through the channels, the axial heat transfer due to conduction is negligible.

8. The kinetic and potential energy changes due to fluid movement from slab to slab through the serpentine are negligible.

3.2 Bulk Temperature and Thermo-physical Properties of ATF

For a temperature-dependent fluid, a selection of representative temperature for calculation is very important. The choice of selecting correct temperature should be based on the application such as a heat exchanger or heat sink. Muzychka, (2011) suggested that for a single fluid such as a heat sink, the better and easier approach is to use the inlet temperature and for two fluids like heat exchangers, better to consider the bulk mean temperature for the calculation [77]. The author further suggested that the most frequently used reference temperatures for defining the local heat transfer coefficient in an internal flow has traditionally been in terms of the bulk temperature [73, 77]. Many authors used bulk temperature for evaluating the thermo-physical properties of viscous

fluids [44, 46, 49, 52, 71, 78]. Shah, et al (2003) in their book, "Fundamentals of Heat Exchanger Design" (chapter 7, page-562), explained the reason of evaluating all properties at bulk temperature [71]. Based on the consideration of the authors, the bulk temperature as a representative temperature has been considered for the subsequent calculations.

The thermo-physical properties of the ATF include mainly the density, viscosity, thermal conductivity, specific heat, Prandtl number, etc., which will be evaluated in this text. As the bulk temperature has been considered the representative temperature, these properties have been evaluated based on the bulk temperatures for the ATF and the air. The bulk temperature for the ATF has been evaluated as the mean of the inlet and outlet temperatures given as:

$$T_{b_L} = \frac{T_{L_i} + T_{L_0}}{2} \tag{3.1}$$

The mean average temperature of air can be evaluated in the similar way as the mean of the air inlet and outlet temperatures:

$$T_{b_a} = \frac{T_{a_i} + T_{a_0}}{2} \tag{3.2}$$

The thermo-physical properties of ATF have been received from different sources. The viscosity and the density have been determined by Can-Am Instrument Limited, Canada for different temperatures. The ATF thermal conductivity and the specific heat capacity data have been checked from the SAE published paper with similar grade [31]. Appropriate curves have been best fitted, and any data required for the calculation have been taken from the fitted curves.

3.3 Dimensionless Fluid Flow and Heat Transfer Parameters

Dimensionless quantities are obtained from the product or ratio of the quantities which have dimensions or measuring units. After the product or making ratios, the units cancel out and the output is a result of dimensionless form. In engineering application especially in fluid mechanics analysis, a number of dimensionless parameters are employed to describe convective heat transfer. Numerous dimensionless parameters are commonly used in the field of heat transfer and fluid flow to characterize fluid behaviour. The most common dimensionless numbers are summarized here.

3.3.1 Reynolds Number (Re)

In fluid flow mechanics, Reynolds number (Re) is a very important parameter. It is named after the founder the British engineer and physicist, Osbourne Reynolds [76]. It is a dimensionless number which is the ratio of inertial forces to viscous forces. It quantifies the relative importance of these two types of forces for given flow conditions. It is the function of fluid velocity, density, flow cross-sectional area, characteristic length, and the viscosity. In a flow, usually the viscous effect within fluid acts for stabilizing the flow to organize it, whereas excessive fluid inertia tends to unorganized the flow. The resulting effect is that; either the flow is in laminar, transitional, or turbulent regime. Therefore, *Re* indicates the flow characteristics.

By definition, it can be shown as [76]:

$$Re_L = \frac{Inertia\ force}{Viscous\ force} = \frac{\rho V D_h}{\mu} = \frac{G D_h}{\mu} \tag{3.3}$$

Here G is the mass flux which is mass flow rate per unit cross-sectional area.

Re is a strong function of the fluid viscosity. In this expression, D_h is the characteristic length or in other words the hydraulic diameter. The characteristic length is generally expressed as:

$$D_h = \frac{4A}{P} \tag{3.4}$$

In the expression, *P* is the wetted perimeter. For a circular geometry, the following deduction can be made as:

$$D_h = \frac{4A}{P} = \frac{4\pi D^2}{4\pi D} = D \tag{3.5}$$

Therefore, for a circular geometry, the characteristic length is the channel diameter. Some authors have made their investigation and defined the characteristic length for any geometry. Muzychka, et al 2009, worked on non-circular geometry while investigating Pressure Drop in Laminar Developing Flow. The authors introduced a new characteristic length scale; the square root of the cross-sectional area through which the effect of duct shapes can be minimized. The hydraulic diameter of any geometry can be expressed as the square root of the channel cross-sectional area that can yield convenient results in fluid flow analysis [73-74, 79]. The authors claimed that $D_h = \sqrt{A}$, this characteristic length scale is superior to the conventional hydraulic diameter $D_h = 4A/P$. An expression for the Reynolds number of air flow can be obtained. The general expression is; $Re = \rho V D_h/\mu$.

$$Re_a = \frac{\rho V D_h}{\mu_a} \tag{3.6}$$

In this expression, D_h is the air flow hydraulic diameter.

3.3.2 Prandtl Number (Pr)

Prandtl number (*Pr*) is a fluid property. It is named after the German scientist, Ludwig Prandtl, who developed the concept of thermal boundary layer and got the idea of the number [76]. It is defined as the ratio of the momentum diffusivity to the thermal diffusivity. It is the function of the fluid properties such as viscosity, thermal conductivity, and the specific heat capacity. It can be expressed as [76]:

$$Pr = \frac{Momemtum\ Diffusivity}{Thermal\ Diffusivity} = \frac{\nu}{\alpha} = \frac{\mu C_p}{k_L} \tag{3.7}$$

Prandtl number contains no length scale and is dependent only on the fluid and the fluid states. In forced convection, heat transfer rate depends on the velocity boundary layer and the thermal boundary layer. The Prandtl number indicates the relative effectiveness of momentum as well as an energy transport by diffusion in the velocity and thermal boundary layers.

For a particular fluid, especially in the laminar regime the heat diffusion occurs quickly when $Pr << 1$, and slower when $Pr >> 1$ [75-76]. The fact implies that, compared to the velocity boundary layer, the thermal boundary layer is thicker when $Pr << 1$ and thinner when $Pr >> 1$. Liquid metal has $Pr << 1$ which indicates that liquid metal can offer higher thermal diffusion in heat transfer phenomenon. Oil has $Pr >> 1$which indicates slower thermal diffusion. In the current study, the working fluid is ATF, which has high viscosity yielding $Pr >> 1$.

3.3.3 Brinkman Number (N_{Br})

The Brinkman number is important for a viscous fluid. It is the measure of the viscous heating relative to the conductive heat transfer. It is the ratio of the heat production due to viscous forces, to the heat transferred from the wall to the fluid for heating or to the wall from the fluid for cooling. The Brinkman number is a dimensionless number related to heat conduction from a wall to a flowing viscous fluid. It is defined as the ratio of heat generated by viscous dissipation to the heat transferred by conduction. It is expressed as [94]:

$$N_{Br} = \frac{Viscous\ dissipation}{Thermal\ conduction} = \frac{\mu V^2}{k_L(T_b - T_w)} \tag{3.8}$$

It indicates the significance of the temperature rise in the fluid due to viscous dissipation. It can be an important factor for long flow pipes. ATF is a viscous fluid, so it may dissipate energy due to such viscosity even at low Reynolds number flow [42, 49].

3.3.4 Eckert Number (Ec)

Eckert number is named after Ernst R. G. Eckert. It is a dimensionless number which is usually defined based on a temperature difference, (not the bulk temperature). It expresses as the relationship between a kinetic energy and enthalpy of flow. It characterizes the viscous dissipation. It is defined as [95]:

$$E_c = \frac{kinetic\ Energy\ of\ flow}{Boundary\ layer\ enthalpy\ difference} = \frac{V^2}{C_p(T_b - T_w)} \tag{3.9}$$

It gives the idea of change in kinetic energy inside the channel due to inertia or velocity. The product of the Eckert number and the Prandtl number gives the Brinkman number. The numbers are explained more detailed in chapter-5.

3.3.5 Dean Number (De)

The Dean number is a dimensionless group in fluid mechanics. It is named after the British scientist W. R. Dean. He introduced this number 1920s (Dean, 1927, 1928) when he was studying fluid mechanics for fully developed laminar flow in a curved tube of circular cross section. This dimensionless number usually occurs in the study of flow in curved pipes and channels. It gives the ratio of the viscous force acting on a fluid flowing in a curved pipe to the centrifugal force. This is basically the Product of the Reynolds number and the square root of the ratio of the radius of the pipe to its radius of curvature. It can be expressed as [53, 92, 93]:

$$De = \frac{viscous\ force\ acting\ on\ a\ fluid\ flowing\ in\ a\ curved\ pipe}{centrifugal\ force}$$

$$De = \frac{\rho VD}{\mu}\left(\frac{D}{2R}\right)^{\frac{1}{2}} = Re\left(\frac{D}{2R}\right)^{\frac{1}{2}} \tag{3.10}$$

For a Newtonian flow, the curvature of the pipe axis induces centrifugal forces on the fluid which forms a secondary flow. The velocity profile began to change to be skewed towards the outer periphery due to the centrifugal force of the magnitude, $F_c = mV^2/r$. The force pushes the fluid outward along the symmetry axis resulting in secondary flow separation near the inner bend of the curved tube. It then returns along the upper and lower curved surfaces creating vortices.

The Dean number shows the flow characteristics due to curvature. The low Dean Numbers indicate that the axial-velocity profile remains parabolic, which are similar to the fully developed straight tube flow. The higher Dean number indicates that the velocity profile is distorted. The curvature ratio is another factor that governs the magnitude of the Dean number. For low curvature of the bend, the secondary flow intensity becomes higher. With the increase in Dean Number, the developing length also increases [53].

Due to the formation of Dean Vortices, the heat-transfer enhancement can occur. Dehghandokht et al (2011) carried out a numerical investigation on similar heat exchanger having only one serpentine within the Reynolds number range of 850 to 2200 for water and 400 to 1700 for the glycol-water mixture. In their investigation, they found that the velocity and thermal boundary layer get broken at the serpentine, and the new boundary layers start redeveloping [23-24].

3.3.6 Poiseuille Number (Po)

Poiseuille number is a dimensionless number. It is the product of channel friction factor and the Reynolds number. It is named after Jean Louis Poiseulle [76]. It is usually a constant and depends on the flow channel geometry. It is expressed as; $Po = fRe = Constant$ [76, 91]. For Darcy's friction factor, the product is 64 and for Fanning's friction factor the value is 16. The Hagen–Poiseuille equation is a physical law. It gives the pressure drop in a fluid flowing through a long tube in a straight path. To evaluate *Po*, some conditions to be met. The assumptions are that the flow is laminar, viscous; the fluid is incompressible, and the tube circular cross-section is constant where *L/D* is

substantially high. In the current study, the working fluid is viscous; the Reynolds numbers are very low, which gives a laminar flow. The channel diameter is constant, and the *L/D* is very high. So, evaluation of Po is very important. Even though this number is constant for an ideal case; there are discrepancies about the number, whether it is really constant for all kinds of channel geometry and hydraulic diameter sizes. *Po* is not applicable to the curved pipes due to flow vortices. Many authors found it higher than 64 for minichannel, while others got lower [79]. In the current study, it will be examined to verify the conventional values.

3.3.7 Nusselt Number (Nu)

The Nusselt Number (*Nu*) is a non-Dimensional number which was named after a German Engineer Ernst Kraft Wilhelm Nusselt [76]. It is a function of heat transfer coefficient, Channel geometry, and fluid conductivity. It is the ratio of the convective heat coefficient or convective conductance to pure molecular thermal conductance. This is expressed as [76]:

$$Nu = \frac{Convective\ Heat\ Transfer\ Coefficient}{Conductive\ Heat\ \boldsymbol{Transfer}\ Coefficient} = Nu_L = \frac{h_L D_h}{k_L} \tag{3.11}$$

Here, the hydraulic diameter D_h is explained earlier.

In the current study, the working fluid is ATF, which is highly viscous. As a viscous fluid the thermo-physical properties of the ATF dramatically vary with temperature changes. Although other thermo-physical properties such as density, thermal conductivity, and the specific heat capacity are changed with the temperature variation and affect the velocity and thermal distributions in the flow field, their contributions are less compared to the

viscosity [40, 75]. Temperature has a high effect on viscosity that affects other non-dimensional parameters, especially Nu when there is an internal flow. So the *Nu* of ATF should be compensated with viscosity for temperature. Two common schemes are usually used for compensating viscosity variation effect due to temperature. These are (a) reference temperature (the film average temperature scheme) and (b) the method of lumping the effects into the ratio of mean to wall fluid viscosity (μ_m/μ_w) [71-72, 75]. Method (a) requires the film average temperature which is difficult to maintain. Method (b) is more convenient to handle due to simplicity [71-72, 75]. For the temperature effect on viscosity, *Nu* of ATF can be corrected as follows:

$$\frac{Nu_c}{Nu_m} = \left(\frac{\mu_m}{\mu_w}\right)^n, \qquad Nu_c = Nu_m \left(\frac{\mu_m}{\mu_w}\right)^n \tag{3.12}$$

To calculate μ_w the inner wall surface temperature is required that can be calculated as:

$$T_w = T_{s_i} = T_{s_o} + \left(\dot{Q} * R_w\right) \tag{3.13}$$

The term R_w is the channel material thermal resistance. The thermal resistance of the wall (R_w), although it has been considered negligible for calculating overall thermal resistance in subsequent equations, can be calculated as:

$$R_w = \frac{ln\left(\frac{D_o}{D_i}\right)}{2\pi k_{al} L} \tag{3.14}$$

In the above equation D_o and D_i indicate the outer and inner diameter of the channel. The channels are spaced 1.00 mm from each other in the heat exchanger slab, and the thickness of the slab wall is 0.5 mm. So each channel has a metal thickness 0.50 mm all around. Therefore, to make the calculations easier, the surroundings of a single channel

has been considered circular and the above expression can be used to evaluate the channel wall thermal resistance for calculating wall temperature.

The Nusselt number is higher when the convective heat transfer is greater compared to conductive heat transfer of the liquid. In case of using nano-fluids, the fluid conductivity increases with the decrease in *Nu* values since, $Nu = hD/k$. Even so, in the case of conventional fluids, this phenomenon is not true. In such a condition, the heat-transfer coefficient is expected to be higher to characterize the fluid heat transfer.

3.3.8 Péclet Number (Pe)

The Péclet number is a dimensionless number which is important in the study of transport phenomena in fluid flow cases. It is the ratio of the rates of advection to the diffusion for a physical quantity of the flow. Another word it is the ratio of the bulk heat transfer to conduction heat transfer. It is also defined as the product of the Reynolds number and the Prandtl Number as [96]:

$$Pe = \frac{Rate\ of\ advection}{Rate\ of\ diffusion} = \frac{D_h V}{\alpha} = RePr \tag{3.15}$$

In engineering applications the Péclet number is often very large. In such situations, the dependency of the flow upon downstream locations is diminished, and variables in the flow tend to become 'one-way' properties. Thus, when modeling certain situations with high Péclet numbers, simpler computational models can be adopted.

A flow will often have different Péclet numbers of heat and mass flow. This can lead to the phenomena of double diffusive convection.

3.4 Heat Transfer Calculation

The fundamental equations mainly related to liquid-side heat-transfer calculations are summarized here.

3.4.1 Heat Transfer Rate and Heat Balance

Without considering any interference for a steady tube flow of a fluid, the conservation of energy equation can be expressed as:

$$\dot{Q} = \dot{m} C_p (T_{in} - T_{out}) \tag{3.16}$$

Where T_i and T_o are the inlet and outlet temperatures of the fluid respectively. The above equation is the general equation for estimating a heat transfer rate. For the ATF, the heat transfer rate can be formulated as:

$$\dot{Q}_L = \dot{m}_L C_{pL} (T_{Li} - T_{Lo}) = \dot{m}_L C_{pL} \Delta T_L \tag{3.17}$$

For the air side, heat-transfer rate can be expressed as:

$$\dot{Q}_a = \dot{m}_a C_{pa} (T_{ai} - T_{ao}) = \dot{m}_a C_{pa} \Delta T_a \tag{3.18}$$

The test chamber is perfectly insulated, so it is anticipated that there is no heat loss or gain from the surrounding. In that case, the rate of heat energy released from the hot ATF, and the rate of heat energy gained by the cold air should ideally be almost equal. This assumption may be valid for an ideal case but in practical situation, it usually does not happen. Therefore, it is necessary to verify the heat balance within what percentages they exist. Heat balance is basically the percentage deviation from the ideal case. To

evaluate the anticipation following Heat Balance (HB) equation can be expressed in the liquid heat transfer case as:

$$HB_L = \left(\frac{\dot{Q}_L - \dot{Q}_a}{\dot{Q}_L}\right) 100 \tag{3.19}$$

Due to measurement or instrumental uncertainties, the HB may not be zero. In such a case, for better data analysis, the average heat transfer rate needs to be considered. The average heat transfer rate is expressed as:

$$\dot{Q}_{avg} = \frac{\dot{Q}_L + \dot{Q}_a}{2} \tag{3.20}$$

Based on the average heat transfer rate, the HB can be evaluated as:

$$HB_{avg} = \left(\frac{\dot{Q}_L - \dot{Q}_a}{\dot{Q}_{avg}}\right) 100 \tag{3.21}$$

According to the ASME PTC 30-1991, the recommended Heat Balance (HB) limit is 15% [90]. For the current investigation, the HB has been evaluated based on both heat balance equations.

3.4.2 Heat Transfer Coefficient

The heat transfer coefficient (h) is very important in thermodynamics, and in mechanical and chemical engineering. It is defined as the amount of heat transferred through a unit area of a medium over a unit time per degree temperature gradient. It is used in calculating the heat transfer that typically occurs through convection or phase change. If the *Nu* and the length scale are known, h can be easily calculated as:

$$h_L = \frac{Nu_L k_L}{D_h} \tag{3.22}$$

Another way of calculating h_L is independent of the Nu_L values. In this case, the heat-transfer surface area, average heat transfer rate, and the temperatures of the channel inner surface and the surrounding fluid are needed. The expression is given below:

$$h_L = \frac{\dot{Q}_L}{A_{hx}(T_b - T_w)} \tag{3.23}$$

Here T_b indicates the bulk temperature of the surrounding fluid, here ATF, and T_w is channel wall temperature. T_b is sometimes referred to as fluid mean temperature. The above expression implies that the heat-transfer coefficient is the proportional coefficient between the heat flux and the temperature gradient which is basically the thermodynamic driving force to cause heat flow. The expression for calculating T_b and T_w have been shown earlier. As h_L can be independently calculated, Nu_L can be calculated based on the values of h_L.

3.4.3 Thermal Diffusivity

Thermal diffusivity is the measure of how faster a body can change its temperature. In transient heat-transfer problem, the distribution of temperature changes with time. It is the quantity that enters into the unsteady or transient heat-transfer situations and can be formulated as [76]:

$$D_T = \frac{Heat\ Conducted}{Heat\ stored} = \frac{k}{\rho C_p} \tag{3.24}$$

Where, D_T is the thermal diffusivity, k is thermal conductivity, ρ is the density and the C_p is the specific heat capacity. The higher the diffusivity, the more the capacity to adjust the temperature of the substances near the surroundings is.

3.5 Pressure Drop

In a heat exchanger device, pressure drop is one of the major factors governing the heat exchanger performances. The core pressure drop usually refers to the pressure drop in the straight flow path. The total pressure in a heat exchanger is the sum of the pressure at the straight path and the serpentine. The overall pressure drop depends on the geometric parameters of the device and the type of fluids which are summarized in the following sections.

3.5.1 Friction Factor (*f*)

Due to finite temperature difference, entropy is generated by the heat transfer in the heat exchanger. Another source of entropy generation is the irreversible dissipation of kinetic energy due to fluid friction. Therefore, friction factor is a function of kinetic energy, which is the result of the flow velocity. Fanning friction factor 'f_f' may be defined as the ratio of wall shear stress $\boldsymbol{\tau_w}$ to the flow kinetic energy per unit volume shown as [76]:

$$f_f = \frac{\tau_w 2 g_c}{\rho V^2} \tag{3.25}$$

Where, g_c is the proportionality constant in Newton's second law of motion.

The friction factor is a non-dimensional quantity and often related to the pressure head losses. In traditional pipe flow the *f* is usually known as the *Darcy's* friction factor (f_d) and it can be expressed as:

$$f_d = \Delta P \frac{D}{L} \frac{2}{\rho V^2} \tag{3.26}$$

$$\Delta P = f_d \frac{L}{D} \frac{\rho V^2}{2} \tag{3.27}$$

The concept of the friction factor helps in determining pressure drop for fully developed or developing laminar flow from the above equation. Using the friction factor a system pressure drop can be estimated in another way as:

$$\Delta P = \frac{f_d L \rho P V^2}{2A} \tag{3.28}$$

Where, P = channel perimeter.

Fluid thermo-physical properties and geometrical dimensions also play an important role in determining fluid pressure or the friction factor. The current study deals with a highly viscous fluid like ATF whose thermo-physical properties, especially the viscosity changes remarkably with the change in temperature. The friction factor is a function of fluid viscosity so; the change in viscosity affects the friction factor also. Therefore, the friction factor should be corrected for the viscosity based on temperature as shown below [71, 72, 75]:

$$\frac{f_{cort}}{f} = \left(\frac{\mu_m}{\mu_w}\right)^m \tag{3.29}$$

Many authors used the value of the exponent $m = 0.50$ [75].

In heat transfer and fluid flow analysis both of friction factors, Darcy's and Fanning's, are important. Ideally, there is no basic difference between the two friction factors. They are related to each other as follows [76]:

$$f_d = 4f_f \tag{3.30}$$

The above relationship between the friction factors is dependent on some factors related to the flow conditions such as; laminar or turbulent regimes, fully developed or developing, and also the channel geometry.

For a fully developed laminar flow, the friction factor is a function of Reynolds number. In such conditions, the relation is independent of roughness. For a circular cross-section and laminar flow, the relation is given as:

$$f_d = \frac{64}{Re}\ , or\ f_d Re = 64 \tag{3.31}$$

The above number is known as Poiseuille Number, which is a constant. In a fully developed laminar pipe flow; the flow is known as Hagan-Poiseuille flow.

3.5.2 Pressure Drop Due to Entrance Effect

As fluid enters into a tube or channel, the velocity profile starts developing along its length, and finally reaches to a fully developed flow which is termed as Hagen–Poiseuille flow. Usually, the flow condition of the entrance is considered as a uniform velocity condition. The pressure gradients in narrow channels are quite high. In case of a minichannel, the length of channel in the developing region forms a major part of the flow length. Therefore, pressure drops due to the entrance effect should be taken into

account. If the entrance length is so small compared to the total length of the channel or *L/D*, the entrance effect can be neglected.

3.6 Pipe Flow

The Heat Exchanger under the study contains 68 circular channels. Therefore, the channel flow can be considered as pipe flow with some exceptions. Fluid flows are usually characterized as laminar, transient and turbulent based on the Reynolds number (*Re*) which is mainly dependent on flow velocity and the fluid viscosity. Typically, *Re* values up to 2300 are termed as laminar flow but depending on channel geometry and length scale this value can be significantly lower to cause transient or turbulent flow regimes for *Re* values lower than 2300. ATF is a highly viscous fluid, and the channel diameter is only 1mm, so flow achieved during the experiment is always in a laminar regime. For a pipe flow two important phenomena always need to be considered; (a) Hydrodynamic entrance length and (b) Thermal entrance length. The entrance lengths imply the flow characters, whether developing or developed. Figure-3.1 shows the hydrodynamically developing and developed length, and regions. When a fluid starts flowing through a pipe, viscous effects due to the pipe wall develop. The region where viscous effects are important is referred to as the boundary layer. At a certain distance of the flow, the boundary layers reach the center line where the velocity gets the highest intensity.

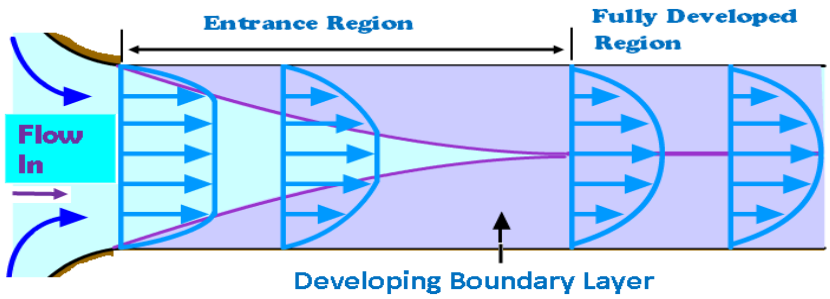

Figure-3. 1: Hydrodynamically Developing and Developed Boundary Layer

For laminar flow, the hydrodynamically developing entrance length can be calculated as [76]:

$$L_{hy} = 0.05ReD_h \tag{3.32}$$

The above expression clearly indicates that the hydrodynamic entrance length is the direct function of *Re* and length scale D_h. The geometry under the investigation has a length scale of 1 mm and the ATF is highly viscous, so the entrance length will obviously be very short, which implies the higher chances of hydrodynamically fully developed flow.

The thermal entrance length can be calculated as [76]:

$$L_{Th} = 0.05RePrD_h \tag{3.33}$$

$$L_{Th} = 0.05\frac{\rho V D_h}{\mu}\frac{\mu C_p D_h}{k}$$

$$L_{Th} = 0.05\frac{\rho V C_p D_h^2}{k} \tag{3.34}$$

The above expression specifies the relation of the thermal entrance length with a fluid property, the Prandtl number.

In a flow, pressure drop and friction factor are very important to characterize the flow. These factors are even more important for pipes or tubes with bend or curvatures. For the heat exchanger in the current investigation, each of the loops has four serpentine in sinusoidal orientation. Therefore, the pressure drop and the friction factor perceive higher importance in-depth investigations. ATF is a highly viscous fluid, so the conventional Bernoulli's theorem is not applicable to this study.

3.6.1 Pressure Drop in a Straight Tube

In a fully developed flow the pressure gradient, $\partial p/\partial x$ is constant. So, $\partial p/\partial x = (P_1 - P_2)/L = \Delta P/L$ [81, chapter 8]. Taking into account the wall shear stress ***(τ)*** that occurs due to the fluid viscosity *(μ),* the flow velocity in a tube at a distance *r* from the tube center can be expressed as:

$$V = \left(\frac{\Delta P}{4\mu L}\right)[R^2 - r^2] \tag{3.35}$$

Here, *R* is the tube radius. The volume flow rate in a conduit can be expressed as:

$$\dot{V} = AV = \int_0^R V 2\pi r dr = \int_0^R \left(\frac{\Delta P}{4\mu L}\right)[R^2 - r^2] 2\pi r dr$$

$$\dot{V} = \frac{\Delta P \pi R^4}{8\mu L} = \frac{\Delta P \pi D^4}{128\mu L} \tag{3.36}$$

From the above expression, the pressure drop as a function of channel diameter *D*, flow length *L*, flow velocity *V*, and the dynamic viscosity μ can be deduced as follows:

$$\Delta P = \frac{128\mu L\dot{V}}{\pi D^4}$$

$$\Delta P = \frac{128\mu LAV}{\pi D^4}$$

$$\Delta P = \frac{128\mu LV}{\pi D^4}\left(\frac{\pi D^2}{4}\right)$$

$$\Delta P = \frac{L}{D}\left(\frac{32\mu V}{D}\right) \tag{3.37}$$

Pressure drop may be computed analytically for a fully developed flow in a horizontal pipe once the flow average velocity is known [81]. In that case, Equation 3.37 can be applied.

3.6.2 Pressure Drop in a Curved Tube

For a curvature in pipe flow, the pressure drop cannot be calculated using the conversional pipe-flow equations. In the curved path, two pressure drops exist; the radial pressure drop and the axial pressure drop. The pressure drop in curved section is different from the straight section due to the fact of additional loss resulting from secondary flow. During the flow in a curved path, the centrifugal force causes the positive-pressure gradient which rises in the radial direction [53]. This positive-pressure gradient or the pressure drop can be calculated as [53]:

$$\Delta P_{radial} = 2\rho V^2\left(\frac{D}{D_c}\right) \tag{3.38}$$

Here D_c is the diameter of the curvature. If the Fanning friction factor is known, the pressure drop in the axial direction at the curved section (Equation 3.38) can be obtained by obtaining first the friction factor f_c at the curvature. The same pressure drop equation

used for the fluid flow through a straight tube can be used to calculate the pressure drop at the curved section [53]. In this case, the Fanning friction factor (f_f) should be replaced by (f_c) as [53]:

$$\Delta P_{axial} = \frac{4 f_c \left(\frac{L}{D}\right) \rho V^2}{2} \tag{3.39}$$

The equations (3.37) and (33.39) are fundamentally the same except their expression containing different parameters. Both equations should give the same result if the variables are handy. The friction factor at the curvature can be obtained using some expressions that will match the current study. Vashisth, et al (2008) made a review on the Potential Applications of Curved Geometries in Process Industry and summarized the correlations of f_s (friction factor at the straight part of the channel) and f_c (friction factor at the curved part of the channel) with other curvature parameters [53]. Most of the correlations are valid only for laminar flow in curved tubes. The correlations express the ratio of the Fanning friction factor at the curved tube to the straight tube under similar process parameters (f_c/f_s). If f_c/f_s can be computed as a comparison of the pressure drops in a curved tube to that in a straight tube, f_c can be used to estimate the pressure drops in equation (3.39).

White, (1929) formulated an empirical correlation for a circular geometry between the friction factors at the curvature and the straight part of the tube, and also the Dean number for that tube [86]. The correlation is shown as follows:

$$\frac{f_c}{f_s} = 1 - \left[1 - \left(\frac{11.6}{De}\right)^{0.45}\right]^{\frac{1}{0.45}} \tag{3.40}$$

Where, f_s is the friction factor at the straight part of the channel, and this is same as Darcy's friction factor in magnitude. *De* is the Dean number. For the case of $De < 11.6$, the ratio f_c/f_s comes to unity, which indicates that the friction factor at the curvature is equal in magnitude to the friction factor at the straight part of the tube for considering equation (3.39). Topakoglu, (1967) used the following analytical expression to find the correlation between f_c and f_s while considering circular tube for small *De* in a curved tube in laminar flow. The author formulated the relation as:

$$f_c = f_s\left(1 - 0.03058\left(\frac{De^2}{288}\right)^4 - 0.1833\left(\frac{De^2}{288}\right)\frac{1}{\lambda} + \frac{1}{48\lambda^2}\right)^{-1} \tag{3.41a}$$

$$\frac{f_c}{f_s} = \left(1 - 0.03058\left(\frac{De^2}{288}\right)^4 - 0.1833\left(\frac{De^2}{288}\right)\frac{D}{D_c} + \frac{1}{48}\left(\frac{D}{D_c}\right)^2\right)^{-1} \tag{3.41b}$$

Where, $\lambda = D_c/D$. To calculate the axial pressure drop the friction factor f_c should be replaced by the above equation. The axial and radial pressure drops are not vector quantities, so the total pressure drop will be the summation of the two pressure drops as [53]:

$$\Delta P = \Delta P_{radial} + \Delta P_{axial} \tag{3.42}$$

In the current study, the minichannel has four serpentine in each loop. So, it is very important to predict the effect of these serpentine in flow and the heat-transfer characteristics.

3.6.3 ATF Flow Rate in Laminar Regime

From the pressure drop equation for fluid flowing through a straight pipe, the velocity of the flow can be deduced as:

$$V = \frac{D}{L}\left(\frac{\Delta P D}{32\mu}\right) \tag{3.43}$$

In a fully developed laminar pipe flow, the traditional volume flow rate can be calculated as:

$$\dot{V} = AV = \frac{\pi D^2 V}{4}$$

$$V = \frac{4\dot{V}}{\pi D^2} \tag{3.44}$$

From the above equation with pressure drop, the following relation is valid for the volume flow rate:

$$\dot{V} = \frac{\Delta P \pi D^4}{128\mu L} \tag{3.45}$$

From the above relation, the mass flow rate can be obtained. Mass flow rate is the volume flow rate times the mass density. So, the mass flow rate is given by the following expression if the pressure drop for the flow is known.

$$\dot{m} = \rho\dot{\tilde{V}}, or\ \dot{m} = \frac{\rho \Delta P \pi D^4}{128\mu L} \tag{3.46}$$

For calculating mass flow rates, any of the above relations can be used as data are available. In the current study, the heat exchanger has 68 channels in each of the three

loops. So, in equation (3.47) for a known mass flow rate, the velocity of the flow can be related as:

$$V_L = \frac{4\dot{m}_L}{3*68\pi\rho D^2} = \frac{\dot{m}_L}{51\pi\rho D^2} \tag{3.47}$$

For the heat exchanger, the above equation will be used to calculate the velocity of ATF flow through minichannel heat exchanger.

3.7 Air Flow

In the current study, air flows through the fins in a perpendicular direction to the liquid mass flow direction. Hence, the MICHX in this case, is a cross flow heat exchanger. Detail information of the air flow is summarized in the subsequent sections.

3.7.1 Air Mass Flow Rate

The air side mass flow rate through the heat exchanger fins can be calculated based on the minimum free flow area through the fin and slab arrays. The air mass flow rate is given by:

$$\dot{m}_a = \rho_a V_a A_{min} \tag{3.48}$$

The integrated wind tunnel is provided with the pitot static tube near the upstream of the flow through the heat exchanger. This pitot static tube allows recording the dynamic pressure of the air flow. The pitot static tube is connected to a flow kinetic device which records the dynamic pressure. Using the dynamic pressure, the velocity of air can be obtained from the following expression:

$$V_a = C\sqrt{\frac{2P_{dyn}}{\rho}} \tag{3.49}$$

Where, V_a is the air velocity, ρ is the air density, P_{dyn} is the dynamic pressure measured through the flow kinetics, and C is the correction factor for the Pitot static tube. The manufacturers usually set the value of the factor C. For the current study, the pitot static tube which has been used to measure the dynamic pressure of air flow has a correction factor of 1. So the above equation reduces to:

$$V_a = \sqrt{\frac{2P_{dyn}}{\rho}} \tag{3.50}$$

3.7.2 Air-Side Reynolds Number (Re_a)

The air side Reynolds number (Re_a) can be calculated based on the air side velocity and mass flow rate. The classical formula for the air side Re_a is given below:

$$Re_a = \frac{\rho V_a D_{ha}}{\mu_a} = \frac{\dot{m}_a 4 L_a A_{min}}{A_{min}\mu_a A_{Hxa}}$$

$$Re_a = \frac{\dot{m}_a 4 L_a}{\mu_a A_{Hxa}} \tag{3.51}$$

Where, L is the air flow length, and the A_{Hxa} is the combined available heat transfer surface area including all fins and slabs of the heat exchanger. In the current study, the air flow length L = *100 mm or 0.10 m*, and the A_{Hxa} = *8.604* m^2 (physically measured and calculated). Substituting these values in the above equation (3.48) and simplifying them, the resulting Re_a (equation- 3.51) for this heat exchanger becomes a consolidated form of expression as:

$$Re_a = \frac{0.04649\dot{m}_a}{\mu_a} \tag{3.52}$$

The above expression is good for calculating air flow Reynolds number only for the heat exchanger used in the wind tunnel for the current study. For other heat exchanger with different dimensions, the above expression (equation-3.52) may not apply.

3.8 Air-side Heat Transfer Calculation

To characterize the heat exchanger, air-side heat transfer parameters need to be taken into account. The relevant parameters are summarized in this section.

3.8.1 Log Mean Temperature Difference (LMTD)

As per Newton's Law of cooling, for a two-fluid cross flow heat exchanger the following equation can be applied.

$$\dot{Q}_{avg} = UAF\Delta T_{lm} \tag{3.53}$$

Where, $\dot{Q}$ is the average heat transfer rate and ΔT_{lm} is the log mean temperature difference that can be expressed as:

$$\Delta T_{lm} = \frac{\Delta T_1 - \Delta T_2}{ln\left(\frac{\Delta T_1}{\Delta T_2}\right)} \tag{3.54}$$

$$\Delta T_1 = T_{coolant\ in} - T_{air\ out}$$

$$\Delta T_2 = T_{coolant\ out} - T_{air\ in}$$

In equation (3.53) A is the heat-transfer surface area, and *'F'* is the correction factor for a cross-flow heat exchanger. The heat-transfer surface area A can be the surface area of any of the fluids, either internal or the external. In the current study, the internal surface area is easily computable, so the heat-transfer surface area of the ATF $(A_{tot\text{-}mc})$ will be considered in this case while using the above equation. The correction factor in the equation (3.53) is basically the ratio of the true mean temperature difference to the log mean temperature difference, $F = \Delta T_m/\Delta T_{lm}$. The ΔT_m is the average of the inlet and the outlet temperature differences, $\Delta T_m = (\Delta T_1 + \Delta T_2)/2$. For different configuration and flow arrangement usually ΔT_{lm} remains the same whereas ΔT_m may be changed. If the difference between ΔT_1 and ΔT_2 is less than 40%, the error using ΔT_m is less (*1%*), but with the increase in the difference of the ΔTs, the effects of the errors increase. The ΔT_{lm} is basically the exponential decay of the local temperature difference. For a cross cross-flow exchanger, value of F is less than or equal to unity, $F \leq 1$. The limiting value of *'F = 1*, indicates a counter flow heat exchanger. The correction factor *'F'* is basically the measure of the deviation of ΔT_{lm} from the corresponding value of the case if the heat exchanger is a counter flow one. The factor *'F'* is available from the charts if the value of P and R are handy. 'P' is the effectiveness of temperature loadings and 'R' is the capacity rate ratio. If the liquid inlet and outlet temperatures are considered as t_1 and t_2 and the air inlet and outlet temperatures as T_1 and T_2 respectively, for a cross cross-flow exchanger, the 'P' and 'R' can be calculated as:

$$p = \frac{t_2 - t_1}{T_1 - t_1}, \ \ and \ \ R = \frac{T_1 - T_2}{t_2 - t_1} \tag{3.55}$$

Although the values of *F* are available in most of the heat transfer book by calculating the value of *P* and *R*, the values usually vary between 0.994 and 0.998 [55]. Bowman et al (1940) in their investigation, for a value of $R = 1$ and $P = 0.5$, tabulated values of different heat exchanger configurations and fluid flow arrangements. The authors showed the value of $F = 0.91$ for a single-pass cross flow heat exchanger [83]. Al-Obaidi, (2011), Khan, (2011), Dasgupta, (2011), and Siddiqui, (2011) carried out research for their study on the same heat exchangers and used the value of $F = 1$ in computing values of average heat transfer rate [8, 55, 67, 70]. Therefore, the same value $F = 1$ will be considered for the calculation in the current study due to same heat exchanger configuration and fluid flow arrangements.

3.8.2 Overall Thermal Resistance

Thermal resistance is almost similar to electrical resistance in series. The two-fluid thermal resistances are due to liquid inside the heat exchanger core, heat exchanger core fluid separating wall, and the flowing air. The overall thermal resistance of the working system in the current investigation can be computed from the following equation [71, 76]:

$$R_{total} = (R_L + R_w + R_a) = \frac{1}{UA} = \frac{F\Delta T_{lm}}{\dot{Q}} \tag{3.56}$$

Here, R_L is the resistance due to liquid, R_w resistance due to tube wall and the R_a resistance due to air flow. The above equation can be written in a specified form.

$$R_{total} = \frac{1}{UA} = \frac{1}{h_L A_{hx}} + R_w + \frac{1}{\eta_a h_a A_{Hxa}} \tag{3.57}$$

The heat-transfer resistance of the wall can be computed using the simple methods available in the heat transfer books for a circular geometry. In the current study, the slab of the heat exchanger contains 68 parallel channels drilled in the slab. The channel diameter is too small, only 1mm, and the slab thickness is also very small, 2mm only. The channels are spaced 0.5 mm apart. Additionally, the heat exchanger slab is made of high-quality aluminum, which has high conductivity. So, the channel outer geometry can be assumed circular. The assumption can be the best approximation which will lead to minimum error and greatly simplify the computation. The thermal resistance at the channel wall is very small compared to those of the liquid and the air. Therefore, the resistance can be considered negligible in finding overall thermal resistance. In such a case, the overall thermal resistance of the system can be expressed as follows:

$$R_{total} = \frac{1}{h_L A_L} + \frac{1}{\eta_a h_a A_a} \tag{3.58}$$

The core of the test specimen is quite new, and no fouling or scale resistance exists on either side of the heat exchanger, so the fouling or scaling resistance is not included in the above equation. The notation η_a represents the air side extended surface efficiency or temperature effectiveness due to the fins. This efficiency is related to the fin efficiency and can be expressed as follows [71]:

$$\eta_a = 1 - \frac{A_{fin}}{A_{Hxa}}\left(1 - \eta_f\right) \tag{3.59}$$

Here η_f is the fin efficiency, and it can be different for different fin geometry and arrangements. A_{fin} represents the fin area, and the A_{Hxa} represents total air side heat

transfer surface area which is equivalent to $A_{fin} + A_{slab.}$ The fins in the present study are wavy fins and following equation applies [72]:

$$\eta_f = \frac{tanh(ML)}{ML} \tag{3.60}$$

$$M = \sqrt{\frac{2h_a}{K_{fin}t_{fin}}} \tag{3.61}$$

$$L = The\ fin\ length\ from\ the\ root\ to\ the\ center\ of\ the\ fin = \frac{H}{2} \tag{3.62}$$

Here H is the height of the fin from the root to root or in other words this is the distance from the slab to slab.

3.8.3 Air-Side Heat Transfer Coefficient (h_a)

The air side heat transfer coefficient can be calculated using the formula given below:

$$h_a = \frac{\dot{Q}_a}{\eta_a A_{Hxa}(T_s - T_{ba})} \tag{3.63}$$

The computation of η_a of the heat exchanger is a critical task and several steps, and iterations are required to find it. Finding the air side heat transfer coefficient, another approach can also be adopted as:

$$h_a = \frac{1}{\eta_a A_{Hxa} R_a} \tag{3.64}$$

R_a is the thermal resistance in the air side flow. The method of calculating R_a will be discussed in the later section.

The air side heat transfer coefficient can be computed once the surface area and the geometry are known for the extended surface. From equation (3.57), the h_a can be obtained as follows:

$$h_a = \frac{1}{\eta_a A_{Hxa}\left(R_{total} - \frac{1}{h_L A_{hx}}\right)} \tag{3.65}$$

Iterative methods are needed to be used to find the values of h_a using equations (3.58-3.65). The stepwise methods are shown below:

1. First calculate the value of *UA* form equation (3.53) and get $R_{total} = 1/UA$.

2. Initially consider the value of $\eta_a = 1$and substitute in equation (3.65) to get h_a.

3. Replace the value of h_a in equation (3.61) to get *M*.

4. Calculate *L* and put the value of *M* and *L* in the equation (3.60) to compute η_f.

5. Put this value in equation (3.59) to get new η_a.

6. Repeat the process from step 2 to 5 until η_a converges to a constant value.

7. Finally use that value to compute h_a in equation (5.65).

After a little iteration, finally the air side heat transfer coefficient h_a can be obtained.

Another way of computing h_a is the surface temperature method which is shown equation (3.63). After getting the values of h_a from two different methods, the values can be compared for their correctness.

3.9 Heat Exchanger Performance

Heat exchanger performance can be evaluated by two distinct methods: Log Mean Temperature Difference (LMTD) method and the Effectiveness-NTU method. The LMTD method is considered as the best method followed by the effectiveness-NTU method. The LMTD method has been explained in detailed in section 3.8.1. The effectiveness-NTU method is summarized here.

3.9.1 Heat Exchanger Number of Transfer Unit (NTU)

The number of transfer units or in short *NTU* is defined as a ratio of the overall thermal conductance *UA* to the smaller heat capacity rate C_{min} as:

$$NTU = \frac{UA}{C_{min}} = \frac{1}{C_{min}} \int UdA \tag{3.66}$$

The *NTU* may also be defined as the relative magnitude of the heat transfer rate compared to the rate of enthalpy change of the smaller heat capacity rate fluid. It is a design parameter for the heat exchangers and indicates the non-dimensional thermal size not the geometrical or the physical size of the exchangers. Therefore, a larger value of *NTU* usually does not indicate that the heat exchanger is large enough in physical size rather, it indicates the thermal size. However, for a specific application when comparing heat exchangers, U/C_{min} almost remains constant. For such a case a higher magnitude of *NTU* indicates that the physical size of the heat exchanger is larger. So, the magnitude of *NTU* sometimes refers to a size factor of the heat exchanger. A higher value of *NTU* can be obtained by increasing either U or the heat transfer surface area (A) or both. Another

way of achieving higher value of *NTU* is by decreasing the value of C_{min}. By doing the change in C_{min} affects *NTU* directly.

3.9.2 Effectiveness (ε)

The effectiveness of a heat exchanger is the measure of its thermal performance or thermal efficiency. It is defined as a ratio of the actual heat transfer rate from the hot fluid to the cold fluid in a heat exchanger to the maximum possible heat transfer rate which is thermodynamically permitted. The term effectiveness should not be confused with efficiency; it is used to designate the efficiency of a heat exchanger. The heat exchanger may have any configuration in the flow arrangements such as; counter flow, cross flow, parallel and the like. The effectiveness of a heat exchanger can be formulated as [71, 76]:

$$\varepsilon = \frac{\dot{Q}_{actual}}{\dot{Q}_{max(possible)}} = \frac{C_h(T_{hi}-T_{ho})}{C_{min}(T_{hi}-T_{ci})} = \frac{C_c(T_{co}-T_{ci})}{C_{min}(T_{hi}-T_{ci})} \tag{3.67}$$

Here *Cs* are heat capacity rates, which are the product of mass flow rate and the heat capacity; C_p. Effectiveness can be expressed in another way as:

$$\varepsilon = \frac{UA}{C_{min}} \frac{\Delta T_m}{\Delta T_{max}} \tag{3.68}$$

From equation (3.65) a non-dimensionalized temperature can be obtained.

$$\frac{\Delta T_m}{\Delta T_{max}} = \varepsilon \frac{C_{min}}{UA} \tag{3.69}$$

The effectiveness (ε) ranges from 0-1 and increases rapidly when the value of $NTU \leq 1.50$. It increases monotonically for the value of $NTU > 1.50$ [76]. From the heat-transfer

point of view, a larger value of ε is always desirable but from the point of economic justification the larger ε is undesirable because it causes a larger value of *NTU*. Therefore, from the design point of view the ε should be considered based on the real field application factors. Basically ε is a function of *NTU* and C^* (Capacity Rate Ratio, $C^* = C/C_{min}$) and for a given value of *NTU* and C^*, counter current heat exchangers have the highest ε followed by the cross flow heat exchangers. In the current study, the heat exchanger configuration is a cross-flow heat exchanger. For a given *NTU* the ε is maximum when $C^* = 0$ and minimum when $C^* = 1$, also for a given capacity rate ratio (C^*) the ε approaches to a value of unity when the value of *NTU* is large.

CHAPTER IV

EXPERIMENTAL SETUP: INSTRUMENTATION AND MANAGEMENT

The current investigation has been carried out in a well-equipped laboratory which is known as "Integrated Thermal Management Research Laboratory" (ITMRL) in the department of Mechanical, Automotive and Materials Engineering (MAME). This experimental setup is capable of examining heat transfer and fluid flow characteristics of single-phase air to liquid cross-flow minichannel and microchannel heat exchangers under different operating conditions. The specialty of this lab is its automated instrumental system and the control of the system components. Another important feature of the laboratory is its versatility in using working fluids for heating or cooling while flowing through the narrow-channel heat exchangers which may be considered as the heart of the research work. The ITMRL is also useful for investigating only the air flow characteristics or heat pipes. The integrated wind tunnel system has the following three major components:

A. Fully controlled liquid handling system.

B. Controlled air handling and management system

C. Automated Data Acquisition system (DAQ)

A schematic diagram of the full instrumental network is shown in Figure 4.1. The full network will be discussed with full details in the subsequent sections.

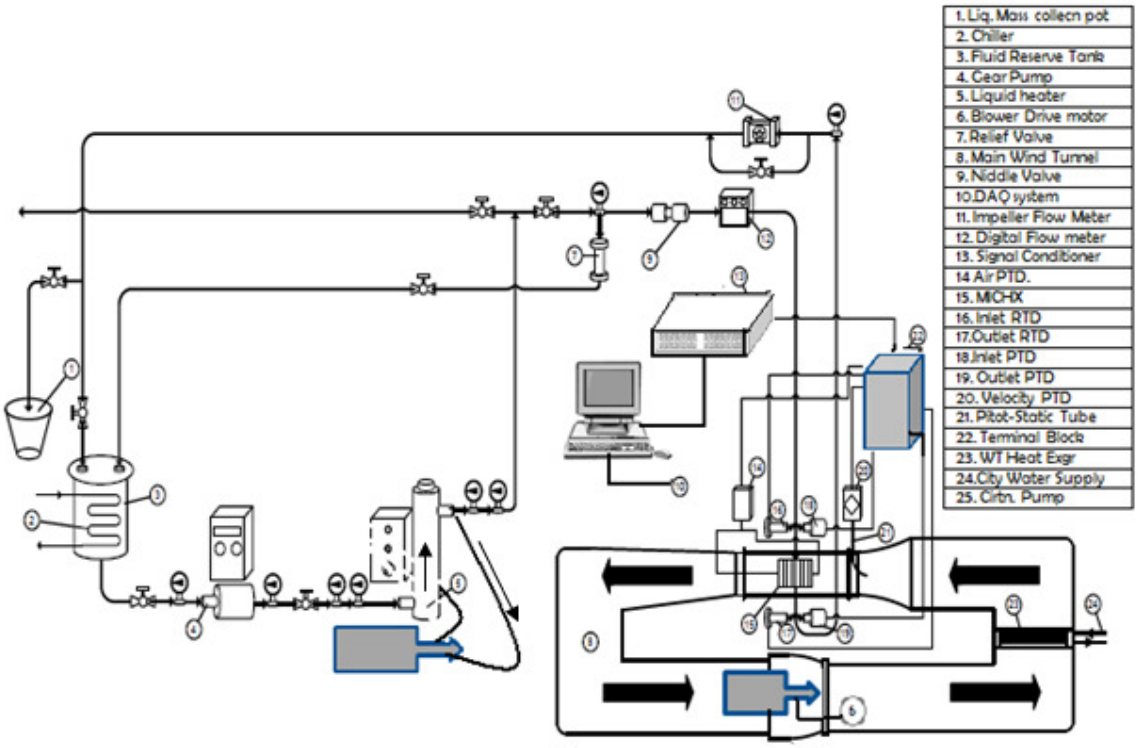

Figure-4. 1: Schematic Diagram of the Instrumental Network

4.1 Liquid Handling System

The liquid handling system comprises several self-controlled equipment. The components of the system are divided into mainly two groups; the feeding or operational components and the measuring and flow control devices. The major feeding components are;

1) Reservoir Tank

2) Gear Pumps

3) Recirculation Pump

4) Electric Heater, and

5) Chiller

The measuring and flow control devices in the liquid handling network are;

1) Needle Gauge for temperature and pressure monitoring

2) Pressure transducers (PTD)

3) Resistance Temperature Detector (RTD)

4) Micro-filter

5) Digital Flow Meter (DFM)

6) Impeller Flo Meter (IFM)

7) Flow Control and Directional valves

4) Tubing and Fittings

4.1.1 Reservoir Tank

In the system network in Figure 4.1, item number 3 shows the reservoir tank. Prior to starting the experiment, the tank is usually filled with the liquid. The liquid moves through the whole system and comes back to the tank after receiving or releasing heat at the heat exchanger. The tank has the dimension of height = 60cm, diameter = 43cm, wall thickness = 4cm, and overall volume of 87 liters. It can resist about 100^{o}C temperature. The returned liquid temperature usually does not exceed 70^{o}C, so it works well during the experiment.

4.1.2 Gear Pump with Frequency-Controlled Motor

The pump which has been used in this investigation is the external gear pump which has the capacity of 17.4 gpm with a maximum pressure of 150 psi at its outlet. This gear pump is the positive displacement pump, a pump in which a measured quantity of liquid is entrapped in a space; its pressure is raised, and then it is delivered. A Positive displacement pump imparts energy by applying mechanical force directly to the liquid. The pump in the current study is a frequency controlled pump shown in Figure 4.2. For this pump, only by changing the motor running frequency, the pump capacity can be varied. The 'Make' of the pump is OMEGA and the model is FPUGR205 – RCB. For controlling the pump outlet pressure at its nominal value, an inbuilt relief valve gets actuated on pressure rise and bypasses the fluid to keep the system safe. It has the working temperature range of -54 to 121^{o}C. It is capable of handling all types' non-corrosive fluids with a maximum viscosity of 100.000 SUS (Saybolt Universal Second) which is equivalent to a kinematic viscosity of 21,630 cSt. At a maximum pressure, the pump Water Horse Power is 3.6HP.

Figure-4. 2: Positive Displacement Gear Pump

The pump is coupled with a variable speed (variable frequency) motor drive. The maximum motor speed is 1725 rpm with a rated horse power of 7.5 hp or 5.6 kW. The main advantage of using such a gear pump is the positive displacement principle. At a higher pressure, it will not lose its head and efficiency like a centrifugal pump. Another advantage of the pump is the smooth supply of liquid. Other types of pumps like vane pump, rotary pump or screw pumps are also positive displacement pump, but the major hurdles of such pumps are the prices and the availability.

In the current study, the working fluid is ATF, which has higher viscosity at lower temperatures. Ideally, the pump volumetric efficiency increases with the increase in viscosity and decreases with lower viscosity. The pumps cannot be operated if the viscosity of the fluid exceeds 750 cP. At peak operating conditions, including peak temperatures, the fluid viscosity is often too low and results in decreased pump efficiency, inadequate flow rates, reduction in load carrying capacity, and system overheating [84]. A centrifugal pump shows the worst-case scenario at such conditions.

4.1.3 Recirculation Pump

While the transmission undergoes an operation, a huge amount of heat generates. The heat generation occurs mainly due to the friction between the mating parts and the fluid movement. This heat energy is usually carried away by the ATF to keep the transmission cooled. The temperature rise due to metal friction is always higher than the normal operating temperature of the ATF. Although the ATF is in contact with the high heated mating parts, normally it is not burnt or damaged because of its rapid motion inside the transmission and appropriate cooling.

In the current study, a liquid heater was used to raise the ATF temperature up to 75^{o}C. The skin temperature of the heater core is even higher than 120^{o}C, which can easily burn the ATF and shorten its life. To avoid this burning risk, an attempt has been made to create an environment inside the heater similar to that of the automatic transmission where the ATF takes the heat and quickly leaves the surface. Figure 4.3 shows the recirculation pump with heater core open. When the pump runs, it draws the liquid from the top and forces it through the bottom of the heater. The flow direction is also shown in the figure. The flow motion occurs in the same direction as the liquid motion created by the main gear pump. As the unit creates continuous agitation inside the heater cylinder, the system offers some advantages explained below:

a) Agitates ATF as it is agitated inside the transmission and the Torque converter.

b. It prevents the ATF from burning as a result of heater core high skin temperature.

b) Better mixing of the hot and cold fluid inside the heater

c) Better stabilization of ATF temperature due to better mixing

d) Since, the primary gear pump and the recirculation pump both create fluid motion in the same direction of fluid flow (from bottom to up); the recirculation pump helps the primary pump to work efficiently by creating additional motion in the same direction inside the heater.

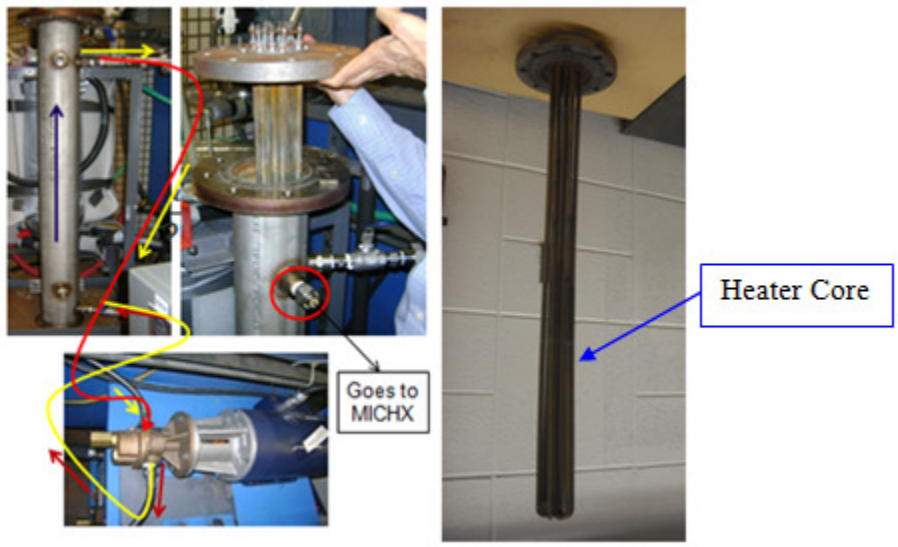

Figure-4. 3: **Recirculation Pump and Heater Element**

4.1.4 Electric Heater with PID Controller

In the instrumental network item number 5 and in Figure 4.3 the liquid heater is shown. The heater element in the system has a heat producing capacity of 6 kW. The heater cylinder has a diameter of 4" which allows the element to have watt density of 4.6 W/cm2. The heater is capable of handling water, glycol, ATF, Engine oil, etc. It can withstand a pressure of up to 6.8 MPa and temperature of 150°C. It is integrated with a PID controller which allows setting and controlling liquid temperature through an inbuilt

thermocouple inserted from the top of the heater and connected to the controller. The heater Model number is MFLI606X2818, from Wattco, and the controller Model number is SD6C-HJAAAARG. After setting the desired temperature, the heater first achieves that temperature and then goes to the on-off control switches for keeping steady-state temperatures. The heater is completely insulated using glass-wool which helps keeping the temperature constant and steady.

4.1.5 Chiller

In the current study, ATF temperature was raised, so no chiller was used. Although no chiller was used the system network has a provision of adding the chiller to lower the fluid temperature depending on experimental necessity.

4.1.6 Needle Gauges for Temperature and Pressure Monitor

Needle indicator temperature and pressure gauges are also the part of the system network. These gauges are not used for measuring or recording system temperature or pressure, rather they are used as monitoring devices for safety purposes. The location of the pressure gauges are; just after the pump outlet to monitor pump working pressure, after the heater to monitor heater pressure and before the micro-filter to observe the pressure rise. The locations of the pressure gauge are shown in Figure 4.1, the system network. Another pressure gauge was placed just before the impeller flow meter for outlet pressure monitor. The capacity of the gauges varies from 200 psi to 600 psi.

Temperature gauges are placed before and after the gear pump and liquid heater, before the micro-filter and the impeller flow meter for system temperature monitoring. The capacity of the temperature gauges ranges up to 120^{o}C.

4.1.7 Pressure Transducers (PTD)

A pressure transducer is a device which converts pressure into an analog electrical signal. The most common is the strain-gage base transducer. The conversion of pressure into an electrical signal is achieved by the deformation of strain gages which are embedded into the diaphragm of the pressure transducer and is wired into a Wheatstone bridge configuration. The transducer requires a nominal 24 VDC power source to operate the signal loop. When the pressure is applied on a diaphragm, and it gets deflected, the deflection causes the length changes in the strain gage, and that change in length causes changes in resistance. Most of the cases the strain gages are wired into a Wheatstone bridge circuit as shown in Figure 4.4. The circuit resistances cause voltage output that is measured for calibration. As the strain gage system works under the Wheatstone bridge, using voltage dividing rule, the bridge sensitivity can be estimated as [97]:

$$\frac{\delta V_o}{V_{ref}} = \left[\frac{(R_2\delta R_1 - R_1\delta R_2)}{(R_1+R_2)^2} - \frac{(R_4\delta R_3 - R_3\delta R_4)}{(R_3+R_4)^2}\right] \tag{4.1}$$

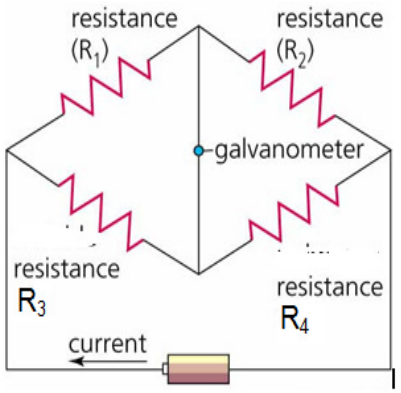

Figure-4. 4: Wheatstone Bridge Circuit

From the output voltage the corresponding pressures can be calculated.

In this study, the liquid pressures are recorded by two pressure transducers (PTD). At the inlet of the main header to the heat exchanger, a PTD is mounted to measure the inlet pressure. Another PTD is mounted just after the outlet header to record outlet pressure and thus to get the system pressure drops Figure 4.5-6. They have the capacity of reading 0-5 volts. The specifications and the calibration curves are produced in chapter 5.

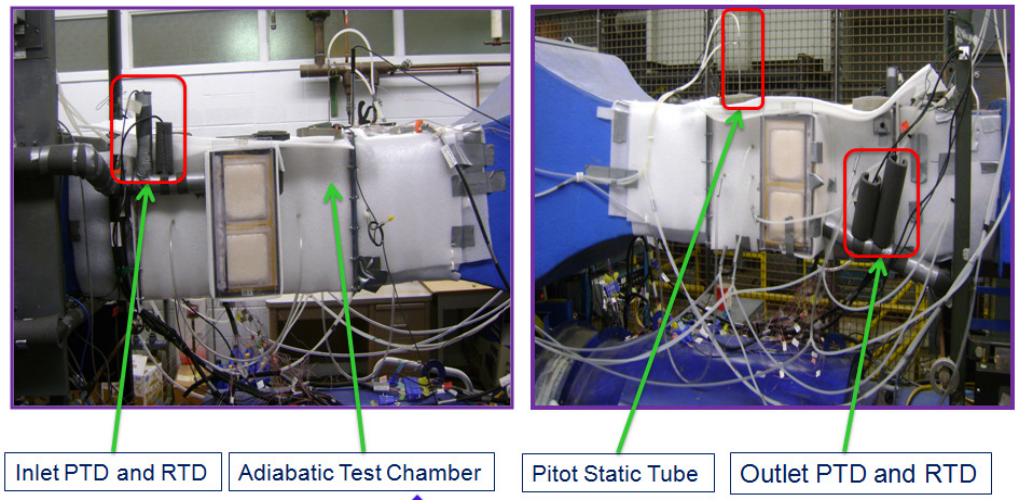

Figure-4. 5: Pressure Transducers (Inlet and Outlet) and the Test Chamber

Figure-4. 6: Pressure Transducer (PTD) & Resistance Temperature Detector (RTD)

4.1.8 Resistance Temperature Detector (RTD)

Resistance Temperature Detector (RTD) is basically a temperature-sensitive resistor (Figure 4.6). An RTD is a temperature recording sensor made of metal, which has known resistance and changes at different temperatures. RTDs have several advantages: a wide temperature range of -50 to 500°C for thin-film and -200 to 850°C for wire-wound type RTDs. It has better accuracy than thermocouples, better interchangeability, and long-term stability. The working principle of the RTDs is also based on the Wheatstone bridge circuit. Once the resistance of the RTD is known, the corresponding output voltage can be obtained. The voltage is generated due to resistance change. The resistance change occurs due to temperature effect. The following formula is applied in this case [97].

$$R_x = \frac{R_b R_c}{R_a} \tag{4.2}$$

$$\frac{V_b}{V_{in}} = \left[\frac{R_x}{R_x + R_c} - \frac{R_b}{R_b + R_a}\right] \tag{4.3}$$

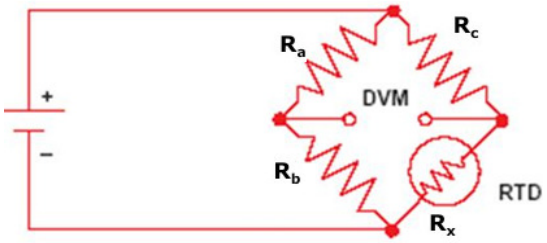

Figure-4. 7: Wheatstone Bridge Circuit for RTDs

The Callendar-Van Dusen equation is applied to approximate relationship between resistance and temperature as shown below [98]:

$$\frac{R_t}{R_0} = 1 + \alpha\left[t - \delta\left(\frac{t}{100} - 1\right)\left(\frac{t}{100}\right) - \beta\left(\frac{t}{100} - 1\right)\left(\frac{t}{100}\right)^3\right] \tag{4.4}$$

By fixing alpha, in above equation, from 0°C and 100°C resistances and modifying the Callendar-Van Dusen equation, it can be directly used for laboratory data. The equation can be modified as:

$$R_t = R_0[1 + At + Bt^2 + C(t - 100^oC)t^3] \quad (4.5)$$

Where, R_t = Resistance at temperature *t*

R_0 = Resistance at the ice point, *0* deg

$$A = \alpha\left(1 + \frac{\delta}{100}\right)$$

$$B = -10^{-4}\alpha\delta$$

$$C = -10^{-8}\alpha\beta$$

$$C = 0\ when\ t > 0^oC$$

In the current study, the liquid temperatures were recorded by two RTDs. One located at the inlet of the main header to the heat exchanger to measure the inlet temperature, and the other RTD is mounted just after the outlet header to record outlet temperature of the system temperature as in Figure 4.5-6. In the temperature measurement process Omega ultra precise immersion RTD sensors were used. They have the capacity of reading 0-5 volts. The specifications and the calibration curves are produced in Appendix A.

4.1.9 Micro-Filter

In the instrumental setup, the micro-filter is located just before the Digital flow meter to protect the system from any clogging and unwanted pressure development. For any kind of blockage in the micro-filter can cause a high pressure rise at the pump outlet and can result in pump failure. Therefore, any high pressure difference between the inlet PTD and the pump outlet indicates the micro-filter clogging problem. If the micro-filter is clogged, it can be easily cleaned by removing it from the tube lines. Two types of micro-filters are available; 230 and 420 micron. In the system, 230 micron filter is good for the water but for ATF and any other high viscous fluid, 420 micron filter is applicable to avoid any high system pressure on the gear pump.

4.1.10 Flow Meters

In the current study, two types of flow meters were employed; Digital Flow Meter (DFM) and the Impeller Flow Meter (IFM). The DFM is located in the inlet side of the MICHX to measure flow rate, pressure and the temperature of the working fluid. The 'Make' of DFM is Proteus and the model is FLUID-VISION 4000, which has the features of measuring flow rate, temperature and pressure of water, water/glycol mixtures, Galden®, Fluorinert®, ATF, and other liquids within the kinematic viscosity range of 120 cSt. It provides output in voltage within the range of 0–5 VDC, 0–10 VDC or 4–20 mA outputs. Figure 4.9 shows digital flow meters. It can measure the temperature by a semiconductor transducer which is embedded in stainless steel housing. It can sense the temperature of the liquid over the range of -40 to 140°C. The meter is a current actuated device so; first, it produces an output current. This produced current is proportional to the absolute

temperature with a unit of 1 μA/°K. Later the current is converted to an output voltage of 1 mV/°K. So the final output voltage gives the temperature measurement of the flowing liquid.

Figure-4. 8: Digital Flow Meter (DFM)

It is a temperature-compensated device and has an operating range of > 250 psi. In the current study initially the device was set to recognize a maximum pressure of 100 psi. So the device needed recalibration to withstand system pressure of 150 psi. The pressure range over which it can be calibrated is determined by the materials of the sensors. The pressure outputs are given as 0–5 VDC, 0–10 VDC or 4–20 mA. A 24 ± 10% VDC, 200 mA supply is necessary for its actuation. It has a safety feature of over voltage protection.

Proteus meters are viscosity dependent. Therefore, use of the same meter with different viscosity fluid, the output signals will be different. The existing flow meter can be re-calibrated to a different viscosity like the transmission fluid if it operates at high viscosity. Typically, Proteus meter can handle fluids with a viscosity up to 120 cSt.

The Impeller Flow Meter (IFM) is located at the exit line of the test specimen. It helps verifying flow rate of the DFM if there is any leakage or loss of fluid on the way back to the reserve tank. The IFM works over the range of 160° F (70° C) temperature and 150

PSI (10 bar) pressure. It is made by OMEGA, and the model is FPR-301 with a capacity of 0.3 ~ 19 LPM.

Figure-4. 9: Impeller Flow Meter

In addition to the above devices, the instrumental network comprises few flow control and directional valves in order to make the system operation easier. The tubing network has a tube size of 0.50 inch diameter and made of stainless steel. The whole system is capable of withstand very high pressure.

4.2 Air Handling System

The air-handling system consists of the following major components;

1. The Thermal Wind Tunnel

2. The Test Chamber

3. Air Temperature Measurement System

4. Surface Temperature Measuring Thermocouples

5. Air Pressure Measuring System

4.2.1 Integrated Closed Loop Thermal Wind Tunnel

The air-handling system comprises several equipment and devices. The main and the largest component is the thermal wind tunnel itself Figure 4.10. The closed loop thermal wind tunnel has a dimension of 544 cm length, 75 cm width, and 164 cm height. The material of the wind tunnel body is fiber glass with high insulating quality. The wall thickness is 1cm but capable of withstanding low scale twisting or bending loads. It has honeycomb porous aluminum plates just before the contraction section to stabilize flow stream lines. It has a contraction section near the test section to allow air flow measurement and controlled air inlet to the test specimen. The contraction ratio of the wind tunnel is 6.25.

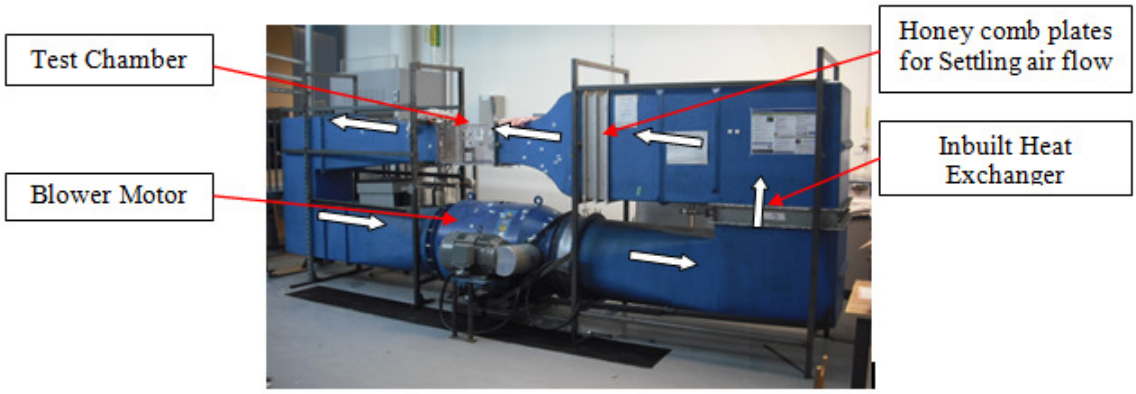

Figure-4. 10: Winds Tunnel with Blower Motor

In the closed-loop wind tunnel, the air flow is generated by a blower which is driven by a frequency controlled variable-speed motor. The induction motor has a capacity of 20 HP at full load with a rated speed of 1750 rpm. The motor controller has a nominal operating frequency of 60 Hz at which the blower produces a free stream air velocity of 30 m/s at the test section with no heat exchanger.

An inbuilt heat exchanger maintains the inlet air temperature using city water supply. The heat exchanger has a capacity of 6 KW to add or remove heat from the air. The heat exchanger is a tube fin heat exchanger. A hot and cold water mixing network properly mixes the hot, and the cold supply water before it enters into the heat exchanger.

4.2.2 Test Chamber

The test chamber is the key point of the experimental setup where the test specimen stays on. In Figure 4.11 the test chamber without and with the heat exchanger is shown. It has an overall dimension of 304.8 mm width, 304.8 mm height, and 609.6 mm length along the flow direction. It has a slot at the middle to barely fit the heat exchanger. The test chamber is made of 6.5 mm thick Plexiglas with the thermal conductivity of 0.19 W/m-°C. It has a flange at the end to easy fit with the wind tunnel by nut and bolt with proper insulation.

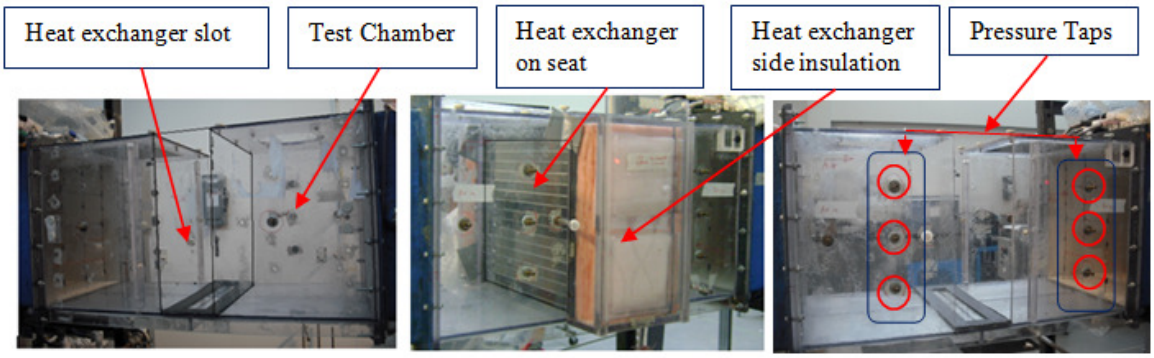

Figure-4. 11: Test Chamber and the Heat Exchanger

The side and the top of the test chamber have removable lids to allow the easy insertion of the heat exchanger and also to install a pitot static tube, a hot wire anemometer, and humidity sensor. To make the test chamber thermally insulated, additional insulating

materials are wrapped around it Figure-4.5. The thick walled test chamber with additional insulation forms a sealed cubicle which prevents the system from participating in any heat-transfer activity with the outside environment.

Holes are drilled at the top, middle, and bottom of the test chamber side wall, and fittings are placed to facilitate measuring air pressures by connecting the differential pressure transducers. To measure the inlet air velocity, the static and total pressure, and the air dynamic pressure at the test section; a 12-inch Pitot static probe, model P012A-CF, is placed at a location referred by ASHRAE as shown in Figure 4.5.

4.2.3 Air Temperature Measurement

To measure the upstream and downstream air temperatures, thermocouple placement grids are installed both at the upstream and downstream to the test specimen. The thermocouple probes are equally and appropriately distributed in the grid so that they can best record temperatures, Figure 4.12. The upstream grip consists of 3x3 = 9 T-type thermocouple (channel number- T100 to T108) whereas the downstream 5x5 = 25 similar thermocouples (channel number- T109 to T131 and T200 to T201).

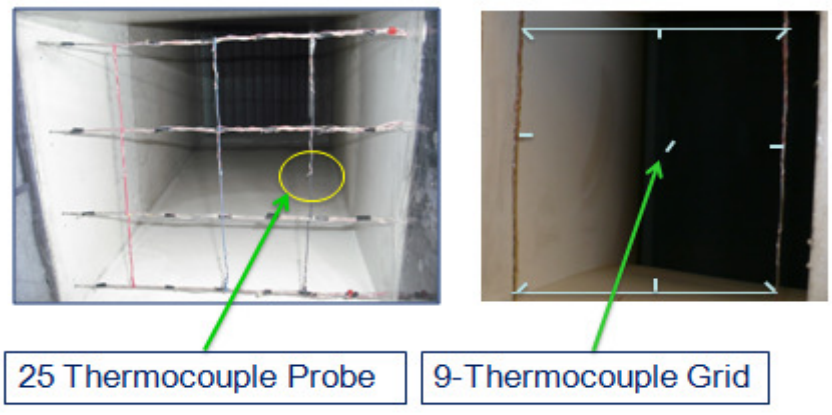

Figure-4. 12: Outlet and Inlet Thermocouple Grids

All the thermocouples are well calibrated and connected to the signal conditioner of the data acquisition system. For data reduction and analysis, the average temperatures are taken as shown below:

$$T_{ai} = \left[\frac{(T100+\cdots+T108)}{n}\right] \tag{4.6}$$

The above equation is applied for the inlet air temperature where *n = 1 to 9.*

For the downstream temperature averaging:

$$T_{ao} = \left[\frac{(T109+\cdots+T131+T20+T201)}{n_1+n_2}\right] \tag{4.7}$$

For the downstream the *n* indicates the number of thermocouples where n_1 *= 1 to 23* and n_2 *= 2.*

4.2.4 Surface Temperature Measurement

The surface temperature measurement is one of the major issues for a dense finned serpentine structure. To measure the surface temperatures, the TC probes are strategically and very precisely placed just at the base of the serpentine where it starts forming curvature and on the other side at 180^o where the curvature ends as shown in Figure 4.13. Along the air flow direction, the serpentine/slab width is 100 mm where the fins form eight waves. The TC probes are placed at the 2^{nd} and the 6^{th} valley of the waves so that they can measure uniform temperature at the airflow direction. The arrangement measures all the temperatures at the beginning of channels as well as the ending of the channels. The mean of the temperatures gives the average outside surface temperatures. For three different loops with twelve serpentines, forty eight thermocouples are equally

set for measuring total average surface temperatures. The TC temperature measuring channels are T202 to T231 and T300 to T317. The average surface temperatures are computed as follows:

$$T_{s,avg} = \left[\frac{(T202+\cdots+T231+T300+\cdots+T317)}{n_1+n_2}\right] \tag{4.8}$$

Here n indicates the number of thermocouples where $n_1 = 1$ *to* 30 and $n_2 = 1$ *to*18. Inappropriate connection, calibration or any probe damage may cause erroneous reading in thermocouple temperatures. Therefore, connections should be checked carefully during such faulty readings.

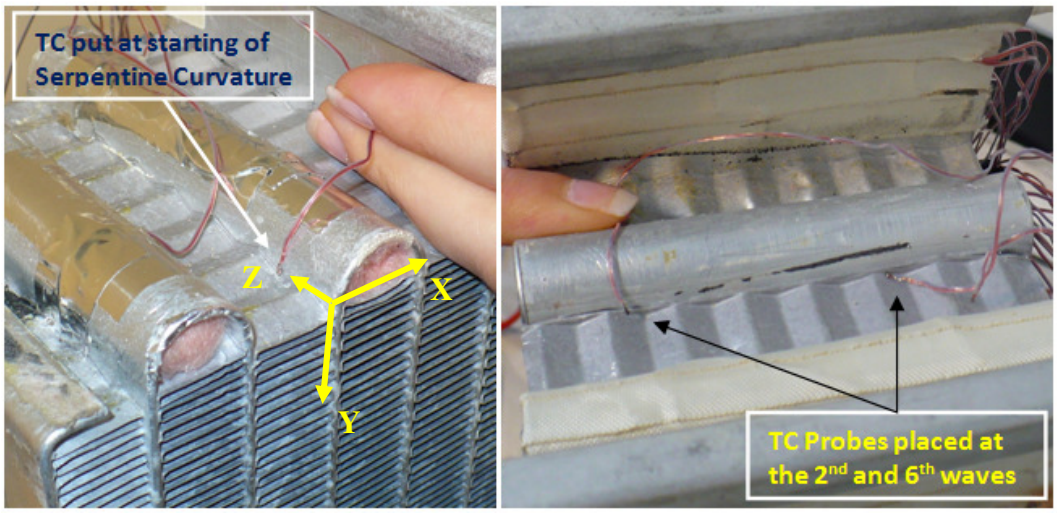

Figure-4. 13: Placement of TC Probe for Surface Temperature Measurement

4.2.5 Air Pressure Measurement

In the test chamber, taps are drilled at the upstream and downstream to trap pressure differences, Figure 4.11. Each upstream and downstream has three pressure traps. From the taps narrow plastic tubes are connected to the Differential Pressure Transducers

(DPTD) as well as to the flow kinetic device which will be explained separately. Two types of DPTDs are used for the experimental setup, model PX653 and PX277, Figure 4.14.

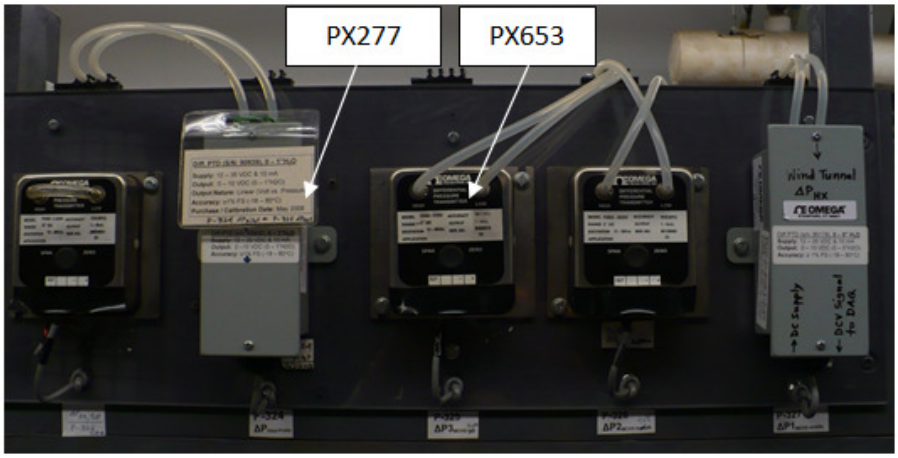

Figure-4. 14: Differential Pressure Transducers (DPTD)

One of the two PX277 DPTDs which is connected to the DAQ system, channel P-327, records the middle differential pressure, while the other PX277 is connected to the pitot static tube (DAQ channel P-325). Among the two PX653 series DPTDs, one is connected to record the top portion pressure drops, and the second one records the lower portion pressure drops in the test section.

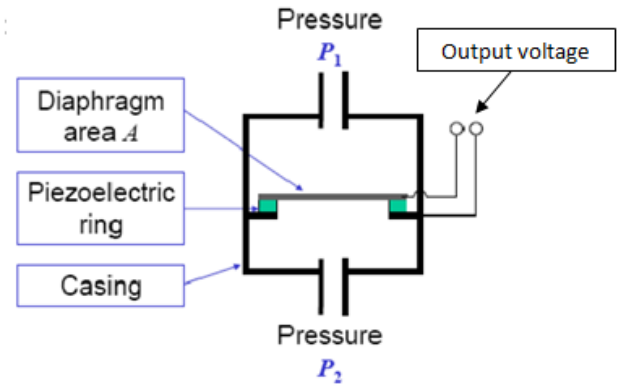

Figure-4. 15: Differential Pressure Transducer Working Diagram

A DPTD usually works as the following working principle.

A Piezoelectric sensor converts force to voltage. The force applied to the sensor diaphragm is given by:

$$F = A(P_1 - P_2) \tag{4.9}$$

Here, *P1* = Absolute upstream pressure, *P2* = Absolute downstream pressure. The applied force due to pressure is converted to voltage. From the output voltage, the respective pressures can be calculated as per calibration.

4.3 Automated Data Acquisition (DAQ) System

In the instrumental setup, Data Acquisition (DAQ) system is the main part where all the results are accumulated for further data reduction. DAQ system allows automated collection of huge data sets with higher accuracy and an integrated manner. The whole DAQ system comprises so many components among which the following are the most important components.

1. Main power supply

2. Back-up battery (UPS)

3. Flow-Kinetics device, FKT

4. PC computer and monitor

5. VDC power supply

6. Terminal Block

7. Signal Conditioner

8. Ratemeter

9. Pressure Transducers

10. RTDs

The connectivity of the devices and the equipments to the DAQ system, and power supply diagram are schematically portrayed below;

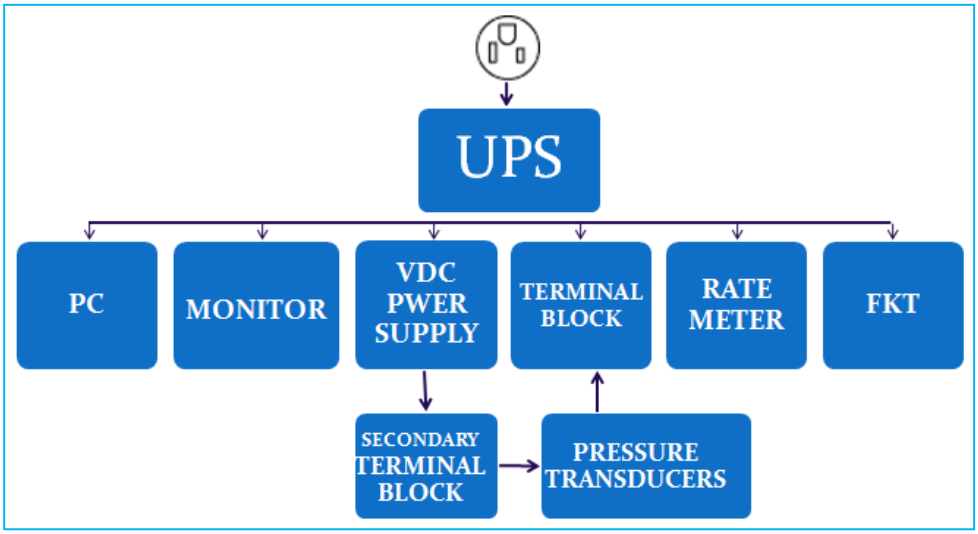

Figure-4. 16: Power Supply Connectivity

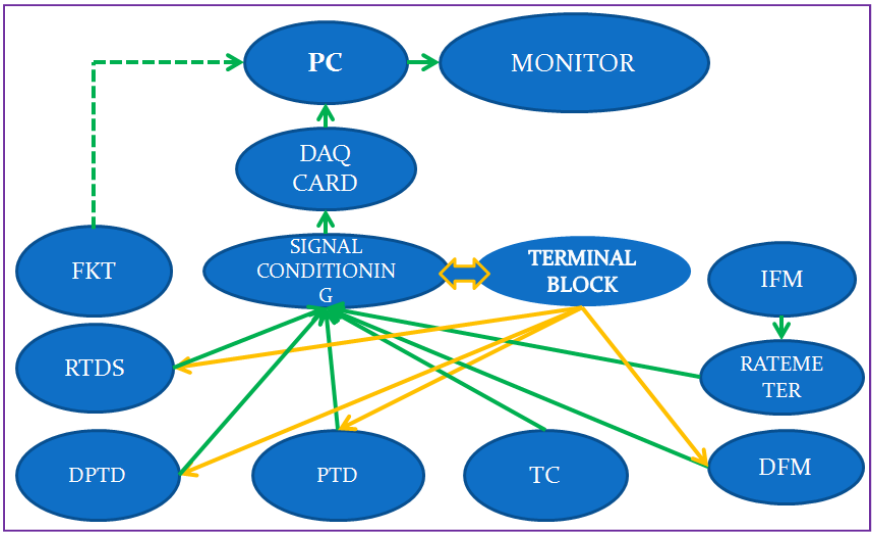

Figure-4. 17: Flow Diagram for the DAQ System Device Connectivity

The above Figure 4.17 shows the connectivity of the data acquisition system. The PTDs, DPTDs, RTDs, and the DFM are connected to the terminal block to have to be voltage actuated or current actuated as necessary. The IFM is connected first to the rate-meter. The rate-meter, DFM, all the thermocouples, PTDs, DPTDs, RTDs, and if necessary the FKT are connected to the signal conditioner. The signal conditioner gives input to the data acquisition card which is connected to the computer PC and finally, everything can be monitored by the computer monitor.

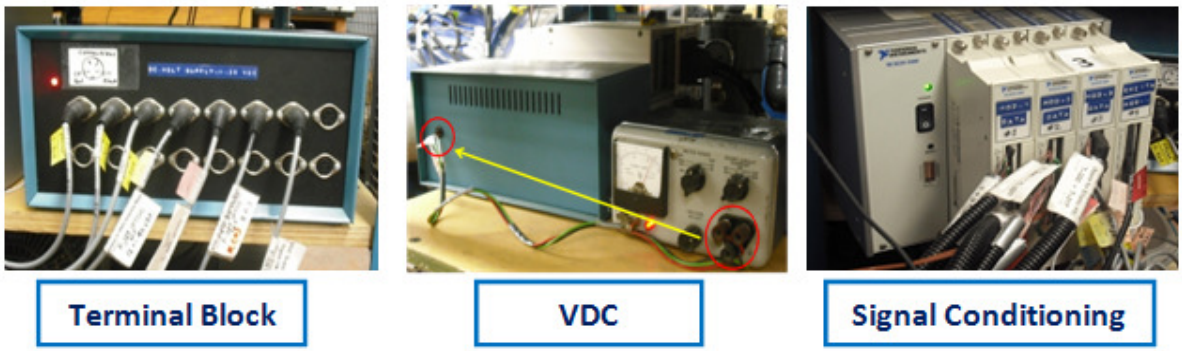

Figure-4. 18: Terminal Block, VDC and the Signal Conditioner

The DAQ system consists of so many vital components, which are integrated to each other in order to complete the full data collection and record. The components are explained below:

4.3.1 DC Voltage Supply Unit and Secondary Terminal Block

The whole DAQ system runs with a Direct Current Voltage supply range of 20-30 VDC where the actual working voltage is 24 VDC. Mainly, the UPS supplies the power but for the secondary terminal block, a separate VDC is connected (Figure 4.18). The VDC is powered by the UPS which receives AC supply and converts it to DC supply. This device basically works as a voltage converter for the primary terminal block due to no inbuilt converter in it. The VDC is connected to the terminal block.

The secondary terminal block is the main junction point for all the pressure transducers and RTDs to have power for actuation. The cable which comes from the PTDs and RTDs are just plug and play system (Figure-4.18). The basic function of the terminal block is to supply power to necessary components such as PTDs and DFM.

4.3.2 SCXI Signal Conditioning

In the DAQ system, the component which receives signals from the PTDs, RTDs, TCs, and the flow-meters is the SCXI signal conditioning unit which processes the data and conditions them as required by the lab view software, Figure 4.18. It has four main components:

1. SCXI -1300/1303 Terminal Block that makes provisions to connect the thermocouples and other probe wires. `It has four terminals out of which one is SCXI-1300. RTDs are

current exited, so this SCXI-1300 block supplies current to the RTDs. The other ends of the RTDs are directly connected to one of the rest of the three SCXI-1303 blocks to get connected to the Module. Each block contains a provision for 32 channels.

2. The SCXI- 1102 Module which conditions signals as readable by the 16-bit high resolution data acquisition card. The data acquisition card is NI 6052E (National Instrument) which interfaces to an SCXI system so that over 3,000 analog signals from thermocouples, resistance temperature detectors (RTDs), strain gauges, voltage sources, or current sources can be acquired.

3. The SCXI-1000 is the Chassis which holds other components and supply power to other modules.

4. Data acquisition cable that connects to the PC to record data.

As the signal conditioning system consists of four blocks, and each block provides 32 channels, the system allows a total number of 128 channels for acquiring data.

The 128-channel DAQ system has multiplex mode reception. The theory of the multiplex system is that; all input channels of the SCXI module are multiplexed into a single analog input channel of the E Series DAQ device. Multiplexed mode operation is ideal for high channel count systems where the power of SCXI multiplexed mode scanning is its ability to route many input channels to a single channel. The multiplexing operation of the analog input signals is performed solely by the multiplexers in the SCXI modules. It does not happen inside the E Series DAQ device or SCXI chassis. The scheme can do sample data at a rate of 100 kHz. In the current study, the configuration of the DAQ system is

capable of monitoring, reading, and recording data for 96 individual experimental parameters through 96 channels.

The DAQ system which is used in this experimental setup is from National Instruments. The National Instruments software can convert a thermistor voltage to the thermistor temperature. The system takes the output voltage of the temperature sensor, the reference voltage, and the precision resistance and finally returns the thermistor temperature.

4.3.3 Flow-Kinetic (FKT)

The Flow-Kinetics, Model FKT-3DP1A-0.4-5-1and Make FlowKineticsTM-LLC, is a multifunction device which allows simultaneous measurement of three (P1, P2, and P3) differential and one absolute pressures (P_{abs})of the wind tunnel air in conjunction with a pitot static tube (Figure 4.19) placed at the upstream of the heat exchanger. It also records air humidity, flow velocity, air instant density and the relative humidity.

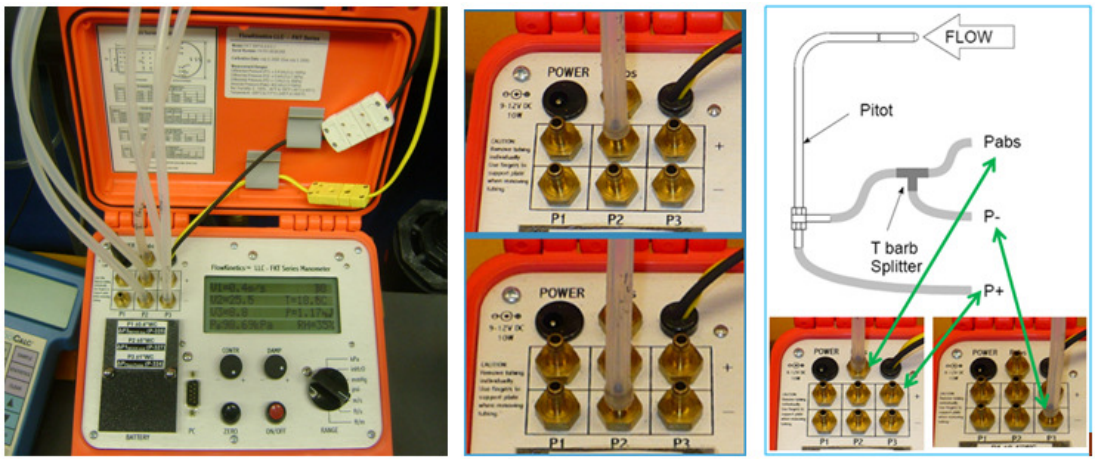

Figure-4. 19: Flow Kinetics and Pitot Static Tube Configuration

The FKT is connected with the Pitot Static Tube in such a way that it offers three pressure drops measurements simultaneously as shown in Figure 4.19. Among these three

pressure drops, P3 records the dynamic pressure which is used in computing air velocities as per equation (3.50).

4.3.4 LabView Data Acquisition System

The data logging system used in the current study is the LabVIEW (Laboratory Virtual Instrumentation Engineering Workbench) version-8 from National Instruments. It ensures automated data acquisition at a sampling rate of 100 kHz. . It is integrated with the National Instrument data acquisition card, NI-PCI-6052E multi-function I/O Board, which is installed in the PC.

4.4 Minichannel Heat Exchanger

The Minichannel Heat Exchanger (MICHX) is the key point of this study. The MICHX under the study is a slab structured serpentine shape heat exchanger (Figure 4.20-21) with cross flow configuration. The heat exchanger core is made of high-quality aluminum alloy. It comprises three loops where each loop has five slabs and four serpentines. Although the physical shape looks very simple to construct but making parallel channels in a 2 mm thick plate is really a challenging task because of high level smoothness inside the channel. The slab thickness is 2mm and width is100 mm. There are 68 parallel channels of 1mm diameter, spacing 0.5mm from each other. The channels are constructed by the laser beam method in order to make the channel flow surface smoother and thus keeping the roughness coefficient as minimum as possible. The MICHX making process can be considered very simple, as if a long piece of aluminum plate (1838 mm long) with required dimensions was drilled to get the channel holes. The plate is then alternately bent four times with equal length of 304 mm, and serpentine curvature of 22 mm to make

the basic structure. The two ends of the newly formed structure are then welded to the headers/distributors (Horizontal). The wavy fins are precisely welded as per specifications. All three loops are then connected to the common inlet and outlet manifolds (vertical pipes) which are connected with copper inlet and outlet tubes of 4.76 mm diameter. The purpose of the inlet and outlet common manifold is to serve as accumulators for the liquid flowing through the manifolds. The headers equally distribute the liquid to 68 channels.

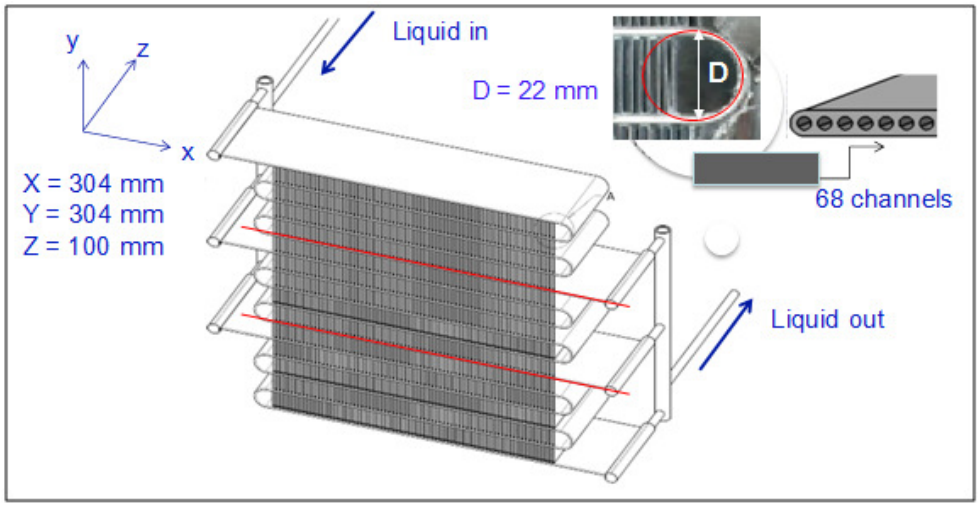

Figure-4. 20: Heat Exchanger Dimensions

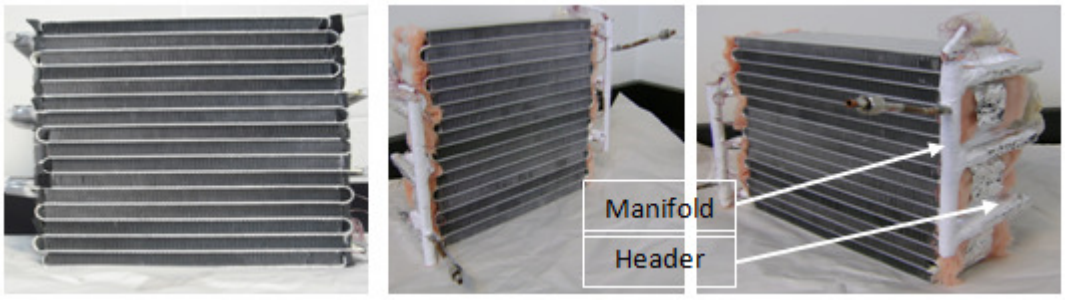

Figure-4. 21: Heat Exchanger Slab and the Manifold

The MICHX has a frontal area of 0.08669 m2. The fin height is 18mm with the fin density of 12 fins per 25.4 mm.

4.5 Operating Conditions

In the current study, the liquid under investigation is ATF whose properties are very susceptible to the temperature variation. ATF has large functionalities inside the Auto-transmission. As such, considering all possible situations to match real-world application and accordingly setting the operating conditions for the experiment is a vital task. Four major variables which are essential to be altered during the experiment for characterization of fluid heat transfer and flow behaviours are the liquid mass flow rate and inlet temperature, and the air inlet velocity and temperature. ATF achieves the highest operation life when the temperature is maintained below 80^{o}C. Throughout the whole experiment, the ATF inlet temperature has been maintained constant at 75^{o}C.

Usually, the high-way vehicle maximum speed is 100 km/h. Due to the obstructions in front of the radiator; it has been considered that maximum 60% air flows to the radiator. It means that the radiator face velocity of air is maximum 60 km/h which is equivalent to 18 m/s face velocity of inlet air to the heat exchanger inside the wind tunnel test chamber. On the other hand, the urban normal running average speed is 35-40 km/h which is equivalent to the face velocity of 6 m/s when the heat exchanger is set inside the test chamber. Considering all these applicable situations the minimum and maximum air velocities, the face velocities of the heat exchanger in the wind tunnel test chamber, have been estimated as 6 m/s and 18 m/s respectively. Other intermediate speeds, including the

peak torque speed are considered as 10 m/s and 16 m/s. The whole experiment has been designed to run by varying the air velocities of 6 m/s, 10 m/s, 16 m/s, and 18 m/s.

The inlet air temperatures are controlled by the city water supply flowing through the in-built wind tunnel heat exchanger. During the experiment, the achievable minimum temperature of air is 15°C, and the maximum temperature is 43°C. Within this range of temperature three other temperatures, 22°C, 29°C, and 36°C, have been considered.

ATF is highly viscous at lower temperatures. Therefore, the flow through a one mm diameter channel can cause high pressure at higher mass flow rates. To maintain a system pressure within the limit of the equipment and devices, the ATF mass flow rates have been kept limited. For a particular inlet air temperature, four different mass flow rates have been selected. For each fixed mass flow rate of ATF, all four air velocities were applied. A pictorial representation of the set conditions is given in Figure 4.22.

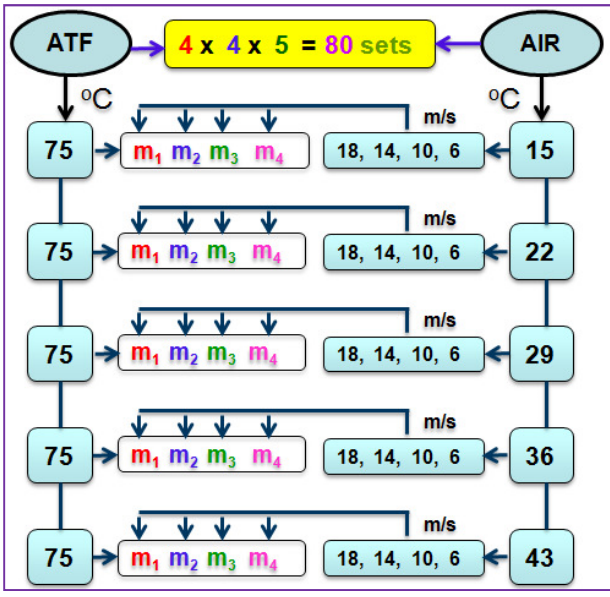

Experimental Operating Conditions				
ATF inlet Temp °C	Air inlet Temp °C	Air Velocity, m/s	ATF Mass Flow Rate kg/min	Remarks
75	15	6, 10, 14, 18	1.180 - 0.530	ATF: 4 mass flow rates
75	22	6, 10, 14, 18	2.472 - 0.484	ATF: 4 mass flow rates
75	29	6, 10, 14, 18	3.260 - 0.835	ATF: 4 mass flow rates
75	36	6, 10, 14, 18	3.660 - 1.057	ATF: 4 mass flow rates
75	43	6, 10, 14, 18	3.87 - 1.288	ATF: 4 mass flow rates

Figure-4. 22: Operating Conditions and Experimental Set Points

4.6 Experimental Methods

The main purpose of this study is to experimentally investigate heat transfer and fluid flow characteristics of ATF when it flows through an air-cooled Minichannel Heat Exchanger (MIHX) in a cross-flow orientation. In this investigation, the hot fluid (ATF) flows through the MICHX core whereas the air flows through the fins. Therefore, the fluid flow directions are perpendicular to each other. As ATF is the hot fluid, and air is cold, naturally the exit ATF will lower its temperature whereas air will gain the temperature. For a steady-state condition, ATF exit temperature can never be lower than the air exit temperature. Any piece of deviation from such temperature bindings will certainly lead to an erroneous data output. In that case, the experiments must be repeated.

Before running the experiment, the piping system and the MICHX was properly dried by blowing high pressure air. Once the system was dried, the reservoir liquid tank was filled up with a right amount of ATF. The level of ATF in the tank was maintained such that the tank would never be dried or emptied during operation. The data acquisition system was then started first to check all channels that represent different sensor locations and functions. The whole system was carefully checked and the main switches for the heater, gear pump, and the blower motor were turned on. City water supply was also opened. First, the recirculation pump was started. The gear pump switch was turned on, and the pump speed was slightly raised by changing the control frequency. The heater was turned on for heat up the ATF, and the temperature setting point was raised by the heater controller. The blower motor started running. The heater temperature was increased to maintain a steady-state temperature of $75 \pm 0.5^{o}C$ and it was kept unchanged throughout

the whole experiment. The blower speed was increased to achieve the maximum air velocity of 18m/s. The city water supply was controlled to achieve inlet air temperature of 15^{o}C. The fluid gear pump was maintained at a speed to achieve maximum flow rate of ATF within the pressure limit of the system. With the current settings, the experiment was run for few hours to investigate system response, stability, and accuracy of the instrumental readings. Upon receiving the steady-state response, the data was recorded for the first time. Although the DAQ system automatically records the ATF mass flow rates in terms of voltage readings, a physical measurement system of bucket and kitchen scale was applied to verify the readings of the DFM. Stop watch was used to record the collection time for the returned ATF. After collecting exit ATF for few minutes into the bucket, it was weighed in a précised kitchen scale and verified with the results from the DFM and IFM. Very negligible deviation which may happen due to human error was noticed in this process. The data was verified, and it looked satisfactory. As a part of the preparation for second set of data, the air velocity was changed to 14 m/s while keeping other parameters unchanged. Upon receiving a steady condition by running the system at list 25 minutes, second set of data was recorded. Next the air velocities were varied at 10 m/s and 6 m/s for other two readings.

To record the next set of experimental data, the mass flow rate was changed and a similar way four sets of data were collected by varying inlet air velocities from 18 me/s to 14m/s, 10 m/s, and then 6 m/s while other parameters keeping the constant. The processes were repeated for four different mass flow rates, where four different air velocities were applied. Therefore, at 15^{o}C air temperature, four mass flow-rates and for each mass flow rate, four air velocities were applied that offered a total set of 4x4 = 16 data points.

Hot and cold water was mixed to achieve 22°C inlet air temperature. For this temperature, another mass flow rate was set such that the flow rate developed similar system pressure as it was reached during the experiment with the air temperature of 15°C. For the 22°C air inlet temperature, all the steps were followed as those of the steps followed at air temperature of 15°C. Another sixteen sets of data points were recorded for this temperature.

The whole processes were repeated for air temperatures of 29°C, 36°C and 43°C. At the end of the experiment, sixteen times five equal eighty sets of data points were available for subsequent analysis. The number of data sets in-hand was considered enough for the analysis of ATF fluid flow and heat transfer characterization. The experimental data offered a Reynolds number range of $3 \leq Re \leq 30$ and the Prandtl number of $180 \leq Pr \leq 285$ within the prevailing temperature range. The maximum and minimum mass flow rates for individual air temperatures are shown in Figure-22. The ATF mass flow rates ranged within a minimum of 0.484 kg/min to the maximum of 3.870 kg/min. The ATF mass flow rates were controlled by setting the gear pump control frequency.

CHAPTER V

RESULTS AND DISCUSSIONS

The main focus of this study was the experimental investigation on heat transfer and fluid flow characteristics of a highly viscous fluid and established relationships among the key parameters. In order to successfully attain the goal, efforts were concentrated on the working fluid flow behaviours and convective heat transfer phenomena. Important parameters of the fluids in connection with heat transfer and fluid flow, such as heat transfer rate, Reynolds number, Nusselt number, Prandtl number, and heat transfer coefficients were carefully examined. These characteristics of the MICHX were investigated: the effectiveness and NTU, pressure drop, friction factor, curvature effect of the serpentine structure on the flow field and heat transfer enhancement, and some other non-dimensional parameters.

The ATF temperature was maintained at 75 ± 0.5^{o}C, whereas the air inlet temperatures were varied in five different steps as: 15, 22, 29, 36, and 43^{o}C. The details of the liquid mass flow rate and temperatures, and the air velocities and temperatures are displayed in Figure 4.22, section 4.5. Based on the prevailing liquid mass flow rates and velocities, the liquid Reynolds numbers varied from $3 \leq Re_L \leq 30$, and the Prandtl number varied from $180 \leq Pr \leq 285$ at bulk temperature. In order to determine the developing conditions of the liquid flow, the velocity boundary layer entrance length as well as the hydraulic boundary layer entrance length was estimated using equations 3.32 and 3.34. The hydrodynamic entrance length within the range of 0.12-1.462 mm (0.04-0.481% of one slab length), and the thermal entrance length of 33-277 mm (11-91% of same slab length)

were estimated. To define the entrance length ranges, the maximum and minimum values of *Re* and *Pr* were considered. The calculated entrance lengths indicated that the flow was hydrodynamically fully developed along most of the parts of the channels, while at the entry region, it was developing. On the other hand, the flow was thermally developing for the major portion of the total length. This phenomenon of developing thermal entrance length happened due to higher *Pr* values. Therefore, in this study the total effect of the flow regime will be termed as 'developing laminar flow' for heat transfer parameters and assumed to be 'fully developed laminar flow' for pressure drop calculations.

5.1 ATF Properties

As the ATF behaves very peculiar at different conditions of temperature, its properties need to be discussed. A brief summary of the fluid thermo-physical properties has been given in the following sections. Although the conductivity and the specific heat capacity were used for this study, those were not tested in the laboratory. Hence, those two properties have been placed in Appendix A.

5.1.1 Viscosity

ATF was tested in the laboratory in order to get some ideas on its thermo-physical behaviours. The test was conducted in the laboratory, owned by Can-Am Instrument Ltd., Oakville ON. The viscosity and density of ATF were tested in that Laboratory. The viscosity data has been plotted against the temperature as shown in Figure 5.1. Different plotting schemes such as exponential, logarithmic, power-law, and the poly-fit have been

applied to predict the best fit. Among the schemes, only poly-fit offered the best fit as illustrated below.

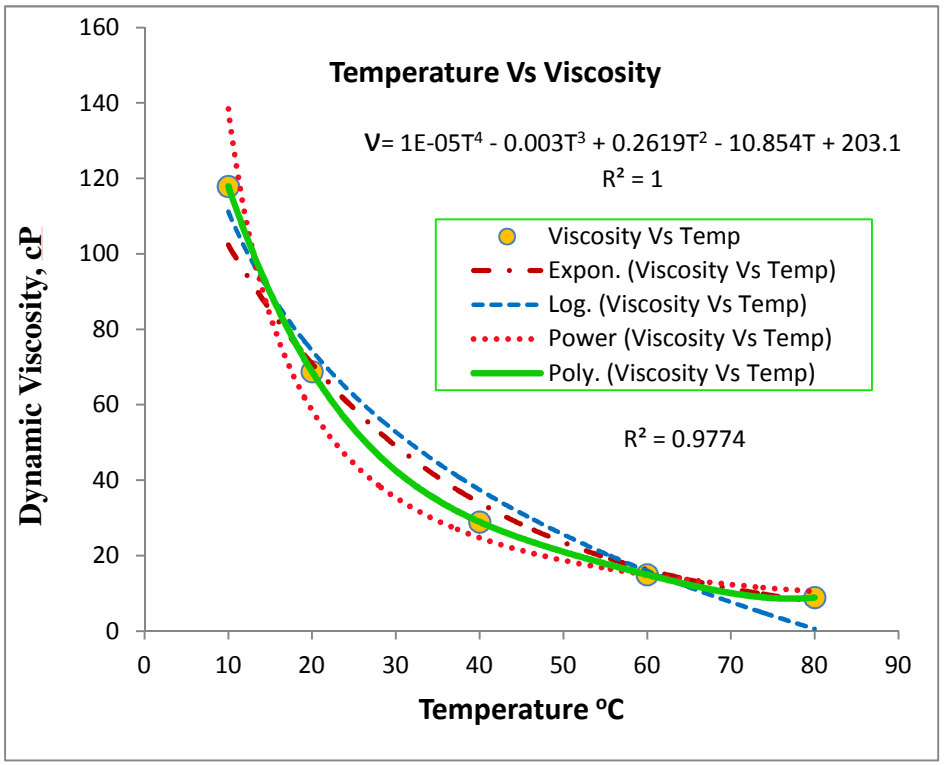

Figure-5. 1: Viscosity Variation with Temperature Change

The most important physical property of ATF is the viscosity. From the figure, it is evident that the viscosity makes sharp changes at temperatures below 20-22^{o}C, whereas above 60^{o}C the trend of viscosity change gets slower. It is highly viscous at lower temperatures, but at higher temperatures the viscosity remarkably decreases. The viscosity-change with temperature gives a 4th order polynomial equation as:

$$\upsilon = 1E^{-0.05}T^4 - 0.003T^3 + 0.2619T^2 - 10.854T + 203.10 \qquad (5.1)$$

The information from the viscosity plot can give an insight in analyzing subsequent data. Some of the non-dimensional parameters such as Re_L, Pr_L, N_{Br}, are the function of

viscosity. The viscosity governs the magnitude of such numbers and parameters. The uncertainty of the viscosity measurement in Can-Am lab has been shown in Table 5.1.

Table-5. 1: Uncertainty in Viscosity Measurement

Temp T	Torque %	Torque	1% of Torque	cP	Error	% Error
0	88.7	0.887	0.0089	221.7	1.9665	0.0197
10	78.6	0.786	0.0079	117.87	0.9265	0.0093
20	68.8	0.688	0.0069	68.79	0.4733	0.0047
40	77.2	0.772	0.0077	28.94	0.2234	0.0022
60	69.8	0.698	0.0070	14.95	0.1044	0.0010
80	59.5	0.595	0.0060	8.92	0.0531	0.0005

Within the temperature range of 0 to 80^{o}C, the error is very low; hence, the data can be considered reliable.

Kemp, S. P. et al (1990) made an investigation on physical and chemical properties of the similar grade ATF. The authors plotted viscosity and temperature data in log scale that resulted in a straight line [31]. The plot enabled to interpolate or extrapolate additional data. The viscosity plot from the authors' data and the Can-Am lab experimental data displayed a good match in the trend line.

5.1.2 Density

The density of ATF was also tested in Can-Am laboratory. Figure 5.2 illustrates density of ATF which linearly decreases with the increase in temperature. The change in density with temperature is very monotonous. From the plot, it is clearly evident that with a huge change in temperature 0-150^{o}C, density changes only about 100kg/m^{3}.

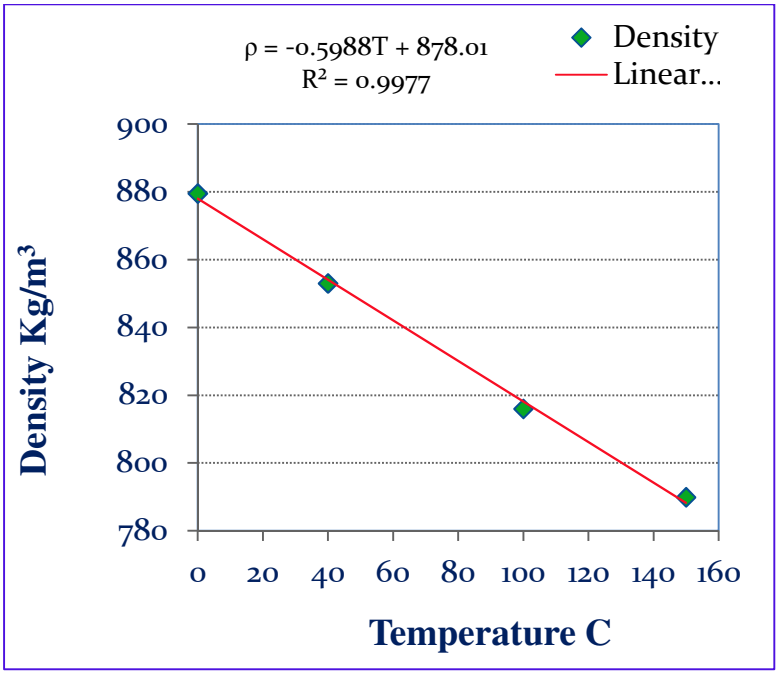

Figure-5. 2: Density Variation with Temperature Change

5.1.3 ATF Mass Flow Rate

Figure 5.3 shows the effect of the viscosity on ATF mass flow rates at constant system pressure that can be withstood by the instrumental setup used for this experiment. The result indicates that the system flow-rate is a smooth function of viscosity (Equation-3.46). As the viscosity increased, the mass flow rate decreased within the limit of the pressure measuring instrument and the pump maximum pressure handling capacity. For a

fluid that contains Viscosity Index Improver (VII), the viscosity and VII of the liquid may not be the indicative to its performance because the fluid viscosity may be substantially decreased as a result of the permanent or temporary shearing of the VII. This loss in viscosity may result in low pump flow-rate and excessive increase in fluid temperature [85]. The gear pumps are positive displacement pumps, which are known as "constant flow machines." However, due to some leakage at a higher pressure, the flow rate decreases with the decrease in viscosity, and this is the common principle for an ideal case. The relationship between the parameters may be described as [85]:

$$\tilde{V}_{actual} = \tilde{V}_{nominal} - C\left(P_{discharge} - P_{inlet}\right)/\mu \tag{5.2}$$

Usually, the inlet pressure is always less than atmosphere due to negative suction head. So, P_{inlet} in equation 5.2, can be eliminated. In that case, the volume flow rate of the pump can be expressed as [85]:

$$\tilde{V}_{actual} = \tilde{V}_{nominal} - C\left(P_{discharge}\right)/\mu \tag{5.3}$$

Here, C is the geometrical factor which is the pump characteristic. From the above equation, the pump volumetric efficiency can be shown as:

$$V_{eff} = \frac{Q_{actual}}{Q_{nominal}} * 100 \tag{5.4}$$

From the above expressions, it is evident that volumetric efficiency increases with the increase in dynamic viscosity. In the present investigation, an opposite phenomenon has been observed due to the persisting conditions. The MICHX under the study has a channel diameter of 1mm; in contrast a highly viscous fluid has been passed through it.

Due to the high viscosity, a high rate of shear stress developed which caused high pressure drops.

The discharge capacity of a pump is a direct function of the pump speed, especially for a positive displacement pump. Therefore, in general, pump discharge increases with the increase in pump speed in case of a gear pump; but it yields pressure rise in the system. To keep the pressure rise within the limit of the network system, the pump speed needs to be controlled. Under such a condition, the fluid pump needs to be driven with a limiting speed to maintain limited system pressure that results in a reasonably decreased flow-rate. A correlation has been developed between the mass flow rates and the dynamic viscosity of ATF at a certain constant system pressure. A third order polynomial equation has been obtained as:

$$\dot{m} = -49028\mu^3 + 1867\mu^2 - 24.30\mu + 0.173 \tag{5.5}$$

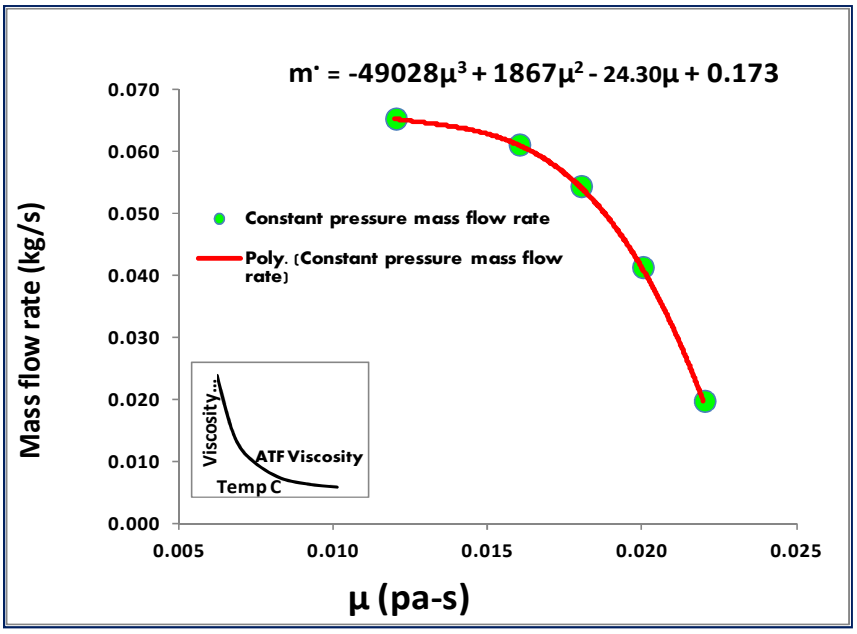

Figure-5. 3: Effect of Viscosity on Mass Flow Rate

The correlation indicates that any increase in dynamic viscosity will lower the pump discharge at a condition of constant system pressure.

The above phenomena implies that during the cold start of a vehicle, a bypass strategy is required to be followed for warming up ATF to reach a certain temperature. This task is important for avoiding a high pressure rise in the Automatic Transmission system during cold start, when ATF viscosity is very high. Semel, (2000) conducted similar investigation on improved automotive transmission warm-up that resulted in better automatic transmission performance [37].

5.2 Heat transfer characteristics

Some basic parameters which govern the heat-transfer phenomena are explained below. These are the key points which set the heat-transfer characteristics.

5.2.1 Inlet-Outlet Temperature Difference and Re_L

The relation between the ATF Reynolds number and its inlet-outlet temperature differences *(*ΔT) have been plotted for all *Re* of air in Figure 5.4. The plot shows that, the higher the inlet air temperature, the lower the ΔTs are which represent higher ATF outlet temperature. Since the Re_L increases, the ΔT deceases. Basically, Re_L increases due to the combined effect of higher mass flow rate and velocity and lower dynamic viscosity at higher ATF temperature. The plot also indicates that the air Re_a does not play a big role in heat transfer phenomenon. At a particular temperature of the inlet air, the ΔT does not decrease as much as the Re_L increases. Therefore, it can be concluded that the change in ATF ΔT mainly occurs due to the effect of inlet-air temperatures.

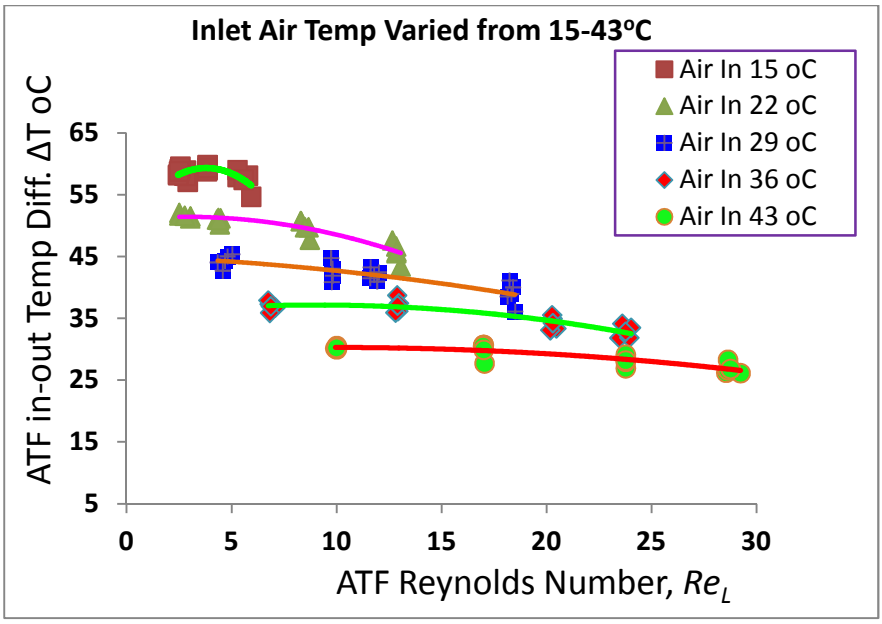

Figure-5. 4: ATF Inlet-Outlet Temperature Difference, $\Delta T^{o}C$

5.2.2 Heat Balance

The test chamber is the most important part of the closed-loop wind tunnel. For better performance, it was perfectly insulated. So, it was considered as an adiabatic test chamber. This assumption may be valid for an ideal case, but in practice it usually does not happen. Therefore, it is necessary to verify the heat balances within what percentages they exist. Heat Balances (HB) have been calculated using equations 3.19. To get a clear idea of the heat-transfer deviation, heat balance has also been calculated based on average heat transfer rate using equation 3.21. According to ASME PTC 30-1991 [90], the recommended Heat Balance (HB) limit is ± 15%. Figure 5.5 shows detailed HB, plotted against liquid Re_L. In the current study, the HB remains within the range of ± 5%, which is quite below the ASME limit of ± 15%. Therefore, collected data at the test chamber can be considered fairly good for subsequent calculations.

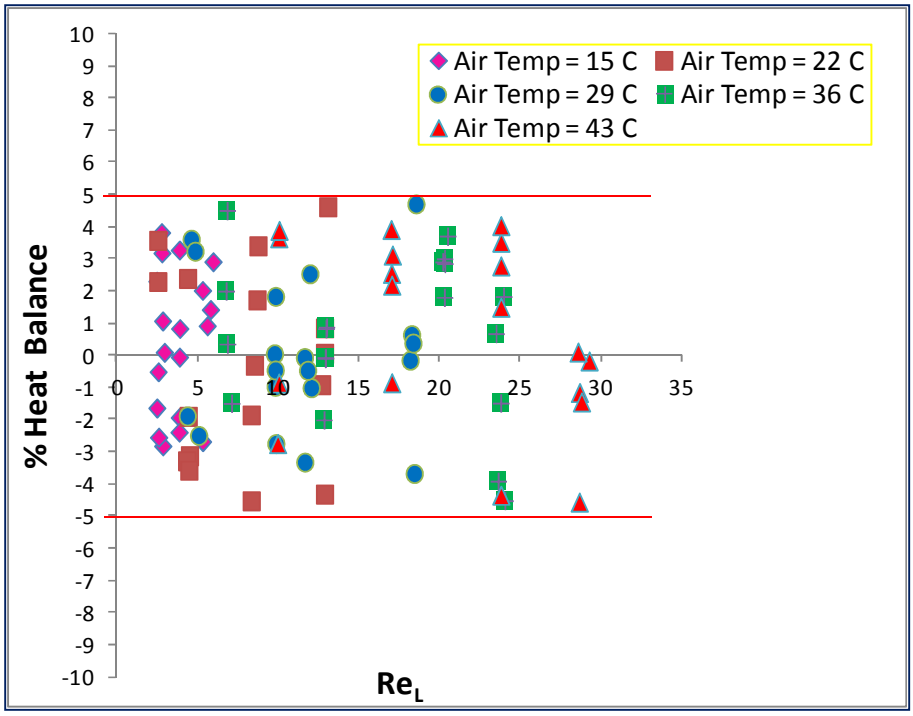

Figure-5. 5: Heat Balance Vs Liquid Reynolds Number

5.2.3 Heat Transfer Rate

ATF heat transfer rates $\dot{Q}$ and the corresponding Reynolds number Re_L have been plotted in Figure 5.6. For five different inlet air temperatures, five different curves have been fitted with power-law relation. From the plot, it is evident that the heat transfer rate increases with the increase in Re_L. For a certain value of Re_L, the heat transfer rates are comparatively lower at higher inlet air temperatures than the lower air-temperatures. Furthermore, it is evident that at lower inlet-air temperatures, the curve slope is steeper whereas at higher temperatures it is comparatively flatter indicating lower heat transfer performance. This occurred due to higher ΔT of ATF.

From the heat transfer observation, it has been found that the maximum heat transfer rate $4607 \geq \dot{Q} \geq 854\ W$ ($4727\text{-}876\ W/m^2$) occurred at 29°C inlet-air temperature.

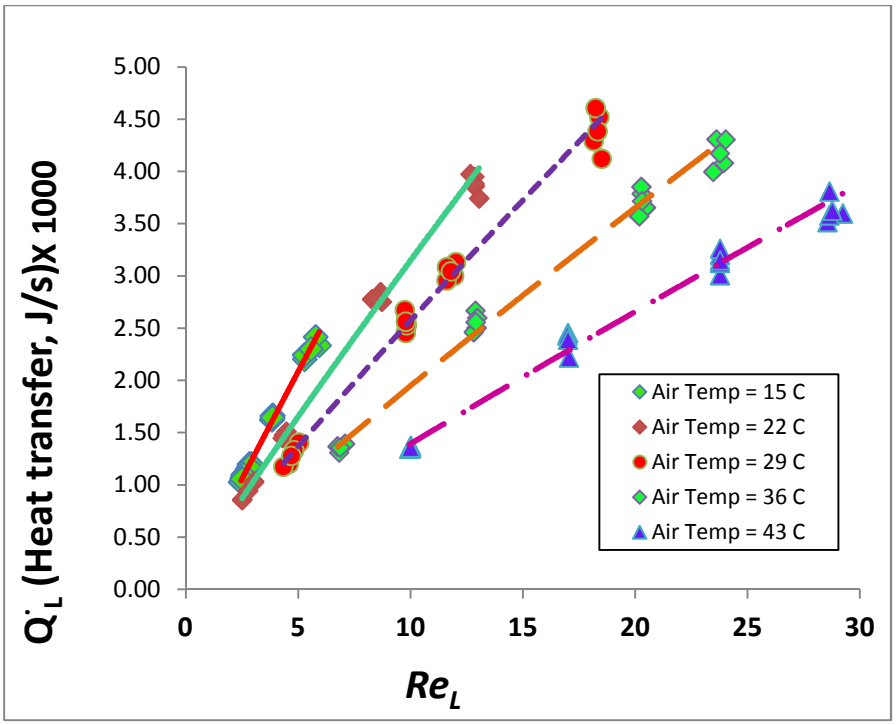

Figure-5. 6: ATF Heat Transfer Rate with Respect to ATF Reynolds Number

5.2.4 Normalized Heat Transfer and Liquid Reynolds Number

To analyze heat transfer characteristics, the non-dimensional heat transfer rate is an important parameter. It can be calculated as:

$$Q^* = \frac{Q}{\Delta T A_f}, \quad or \quad Q^* = \frac{\dot{Q}_L}{(\Delta T A_f)} \tag{5.6}$$

Q^* is the normalized heat transfer rate, $\dot{Q}_L$ is the liquid heat transfer rate in BTU/min, ΔT is the temperature difference between the ATF inlet-temperature and air inlet-temperatures, and A_f is the frontal area of the heat exchanger in square feet. The normalized heat transfer rate has been plotted against the liquid Re_L to justify the effect of the Re_L on the non-dimensional heat transfer rate in Figure 5.7. The plot shows that with the increase in

Re_L, the non-dimensional heat transfer rate increases in a power-law relation. A correlation has been developed with the following expression:

$$Q^* = 0.486Re_L^{0.80} \tag{5.7}$$

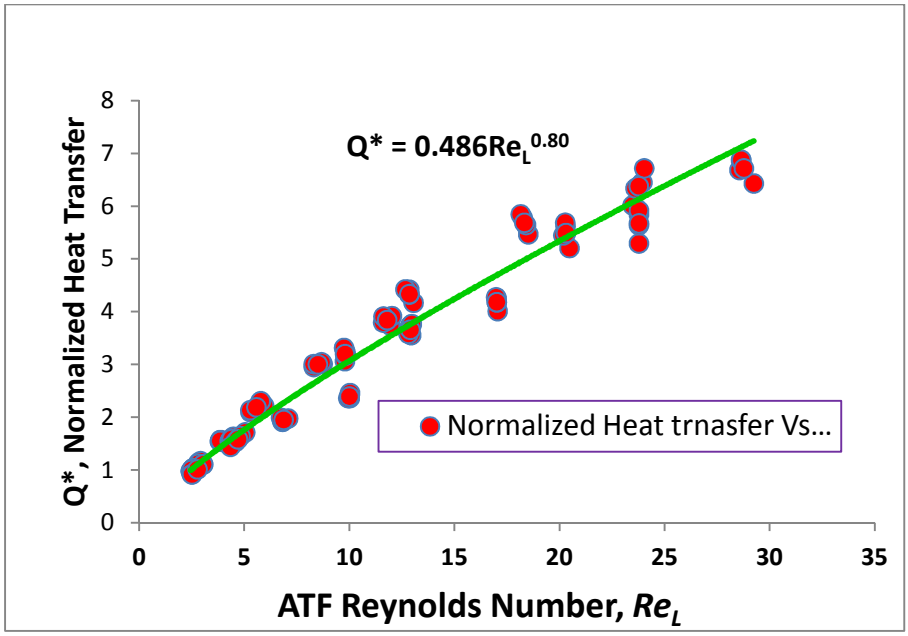

Figure-5. 7: Effect of Liquid Re_L on Normalized Heat Transfer

Therefore, from the investigation it is evident that the heat transfer rate is always dependent on Re_L, whether non-dimensional or direct.

5.2.5 Effect of Re_L on Non-Dimensional Temperature

The non-dimensional temperature is the ratio of the inlet-outlet temperature differences to the inlet temperature as shown below:

$$T_{non-dimensional} = \frac{T_i - T_o}{T_i} = \frac{\Delta T}{T_i} \tag{5.8}$$

The non-dimensional temperatures have been plotted against the liquid Reynolds number (Re_L) shown in Figure 5.8. The dimensionless temperature decreases with increasing

liquid Reynolds number in a polynomial relation. For a particular Reynolds number, the non-dimensional temperature is higher at the lower temperatures due to the same reasons explained in section 5.2.1 with Figure 5.4.

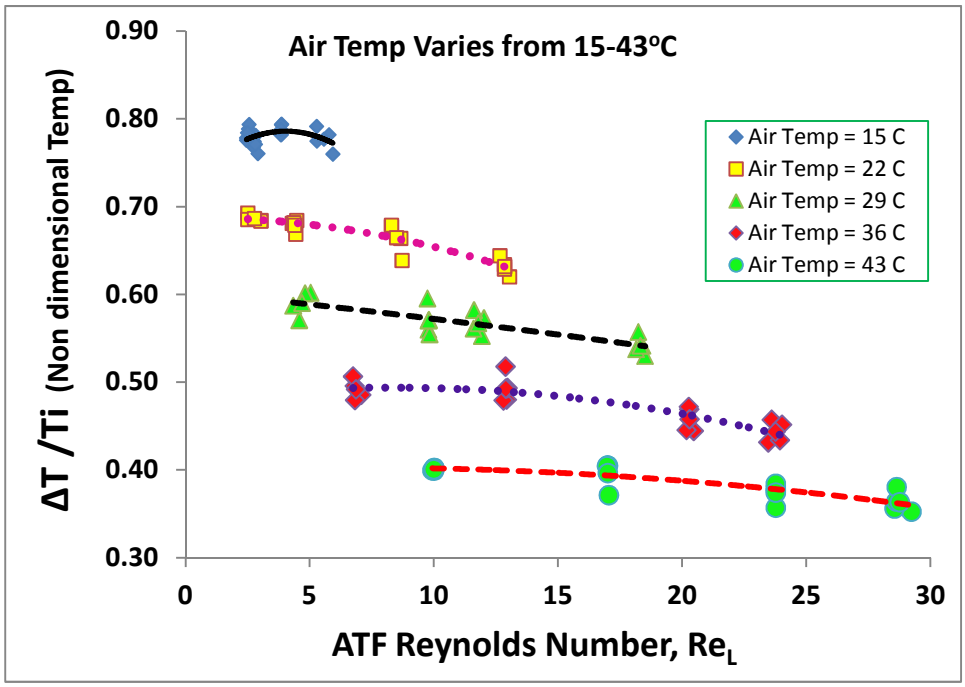

Figure-5. 8: Effect of ATF Reynolds Number on Dimensionless Temperature

Another dimensionless temperature is the Log Mean Temperature Difference (LMTD). It is one of the most important performance evaluation methods of a heat exchanger. If the desired inlet and outlet temperatures of the participating fluids in a heat exchanger are known, the heat-transfer area and the size of the heat exchanger can be determined through the LMTD method. In Figure 5.9(a) the LMTD values at different inlet air temperatures have been plotted against Re_L. The plot implies that for a particular Re_L, the lower inlet air temperature offers higher LMTD, whereas higher temperature gives lower LMTD.

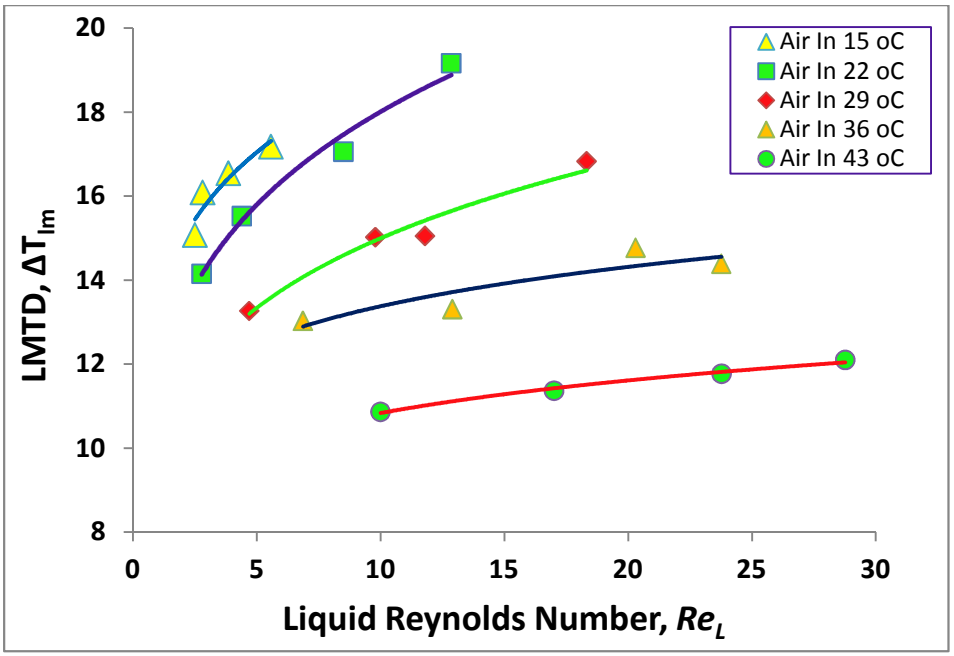

Figure-5. 9 (a): Effect of Liquid Reynolds Number on LMTD

Another important fact to notice is that the LMTD increases with the increase in Re_L. Also, the slope at lower air temperature gets steeper, while at a higher temperature it is flattened. It may seem to be quite fictitious; how the LMTD be higher at higher Re_L for a particular inlet air temperature. The fact is that in equation 3.54 (ΔT_{lm} = (ΔT_1-ΔT_2)/($ln(\Delta T_1/\Delta T_2)$) for calculating LMTD, the denominator is the subtraction of values in two natural logs that does not change much as the numerator changes due to fluid temperature change. The result is the higher LMTD at higher Re_L. In equation 3.53, the heat transfer rate increases with an increase in LMTD. Therefore, it is obvious that the LMTD should be increased with the increase in Re_L to offer more heat transfer rates.

Khan, et al (2010) conducted an investigation on ethylene glycol-water to predict the LMTD trend and found the similar trends for a multi-port serpentine meso-channel heat exchanger with a single slab [25].

The nature of the non-dimensional temperature differences and the non-dimensional LMTD are worth to analyze.

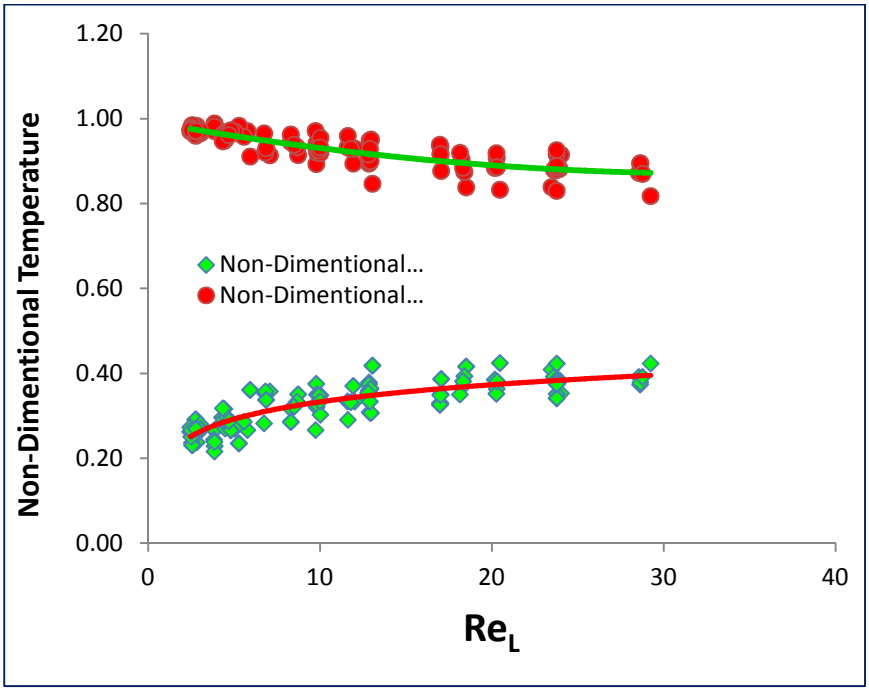

Figure-5. 10 (b): Effect of Liquid Reynolds Number on Non-Dimensional Temperatures (ΔT & LMTD)

Figure 5.9(b) shows non-dimensional temperatures both for ΔT and LMTD which are calculated based on $\Delta T_{n\text{-}di}=(T_{Li}-T_{Lo})/(T_{Li}-T_{ai})$ and $LMTD_{n\text{-}di}=(LMTD)/(T_{Li}-T_{ai})$ respectively. The plot illustrates that with the increase in Re_L the non-dimensional ΔT decreases whereas the non-dimensional LMTD increases as expected. The reasons after such an opposite trends of the plot have been explained earlier in the current section. The plot includes all the air temperatures and the velocities. The figure also explains that the curves at higher Re_L are getting flattened with the indication of heat transfer increments at a slower rate.

5.2.6 Convective Heat Transfer Coefficient

Convective heat transfer coefficient implies how faster the heat transfer occurs due to convection. Figure 5.10 shows a correlation between the liquid-side Reynolds number and the heat transfer coefficient. With the increase in liquid Re_L, heat transfer coefficient increases in a power-law relation. The correlation obtained is shown in equation 5.9.

$$h_L = 17.70 Re_L^{1.044} \tag{5.9}$$

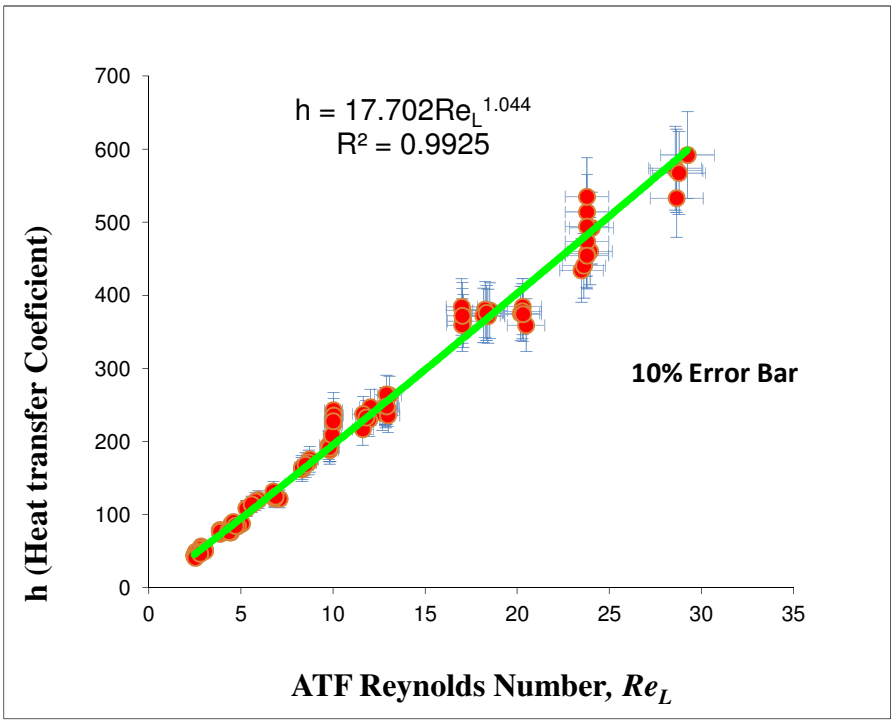

Figure-5. 11: Effect of ATF *Re* on Heat Transfer Coefficient

Karamavruc, et al (2011) found a similar trend in heat transfer phenomenon inside a transmission, while investigating empirical heat transfer coefficient for predicting interface temperature of continuously slipping clutches for ATF [62].

In the current study, the correlation shows that the heat transfer coefficient changes almost linearly with an exponent of 1.044. This relation is valid for the attained Re_L and Pr. For a higher Re_L range, the obtained correlation may not be applied.

5.2.7 Effect of Re_L on Nusselt Number

The Nusselt number indicates how faster the heat transfer occurs due to convection compared to the fluid conduction. The Nu_L has been calculated based on equation 3.11. As ATF thermo-physical properties are highly dependent on temperature, the Nu_L was corrected with viscosity ratio for temperature as equation 3.12. In order to justify the effects of liquid Re_L, the Nu_L has been plotted against the ATF Re. The plot in Figure 5.11 shows that Nu_L increases with the increase in Re_L. To investigate the actual nature of Nu_L with Re_L and to obtain the best correlation between them, different curve fittings have been tried. The data is best fitted in a power-law relation. This relationship entails all the data points within ±10% data variations. Warnakulasuriya, et al (2008) used poly-fit as a power function for developing correlation between Nu and Re for a plate type heat exchanger while using viscous fluid and found similar trends [38].

Two different curves have been shown in Figure 5.11. The dotted line represents the temperature corrected values with viscous effect as a variable property ratio. Both curves showed good agreement with the open literature in the case of the MICHX. As the Nu_L was corrected at its wall temperature with the property ratio, the actual corrected values have been found slightly lower than the original values. That happened because of the higher viscosities at the lower temperatures near the wall which indicates a lower heat transfer rate.

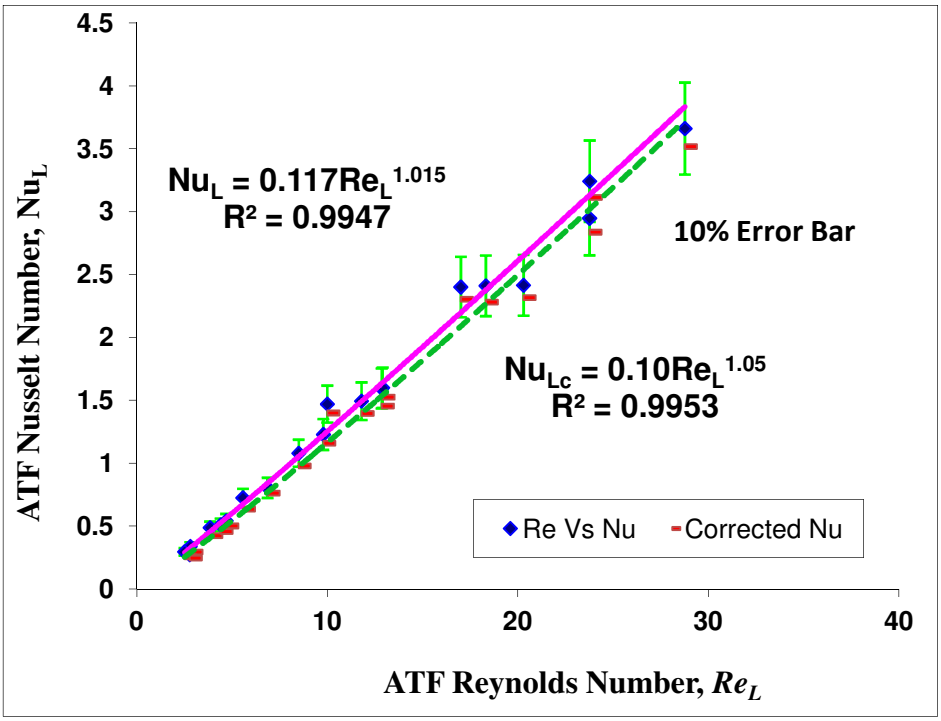

Figure-5. 12: Effect of Liquid *Re* on Liquid *Nu*

Kumar, et al (2007) found similar results for water and die-ethylene glycol [40]. In their investigation under cooling conditions, the value for *Nu*, when viscosity was corrected with temperature, was lower than the constant-property values for both fluids. That happened because of the change in the thermo-physical properties, mainly viscosity, at the inner portion of the tube.

As *Nu* has been corrected with the viscosity at wall temperatures, the value of the exponent 'n' in equation 3.12 has been considered 0.14 [71, 75]. For the case of a circular tube, the flow with laminar regime, Yang used the value n = 0.11 at the thermal entry region. However, Deissler suggests n = 0.14 for fully developed flow conditions [75]. Kumar, V. et al surveyed the value as n = 0.14 [40]. Shah, et al (2003) stated that the value of the exponent is not available in the literature however, the exponent n = 0.14 may be the best choice to represent the best primary corrections [71]. Basically, there is

no definite way of accepting the value of the exponent 'n' because of lack of adequate research findings on this matter. To define the suitability of choosing the value of 'n' for calculation, particular case of experiment is scarce in open literatures. For a design purpose, both values can be considered [40, 71, 75]. In this study, the value of 'n' has been chosen 0.14 based on most of the authors' selections in open literatures.

For a constant property case, the correlation followed by the Nu_L in Figure 5.11 is given below:

$$Nu_L = 0.117(Re_L)^{1.015} \tag{5.10}$$

After the Nu_L was corrected with variable property ratio, the values were found lower than the original, and a slightly different correlation resulted as shown in equation 5.11:

$$Nu_{Lc} = 0.100(Re_L)^{1.05} \tag{5.11}$$

Comparing the correlations, it is evident that the slopes and the exponents in the correlation differed from each other. The phenomenon emphasized the necessity of viscosity correction due to temperature variations. For both cases, the viscous dissipation effect is not considered.

The relationship between the non-dimensional parameters, such as liquid Re_L, Pr_L, and Nu_L, has been investigated. Figure 5.12 shows the correlation between the effects of Re_L and Pr_L on Nu_L. The investigation shows that the Nu_L increases with the increase in Re_L and the Pr_L. The dependency of Nu_L on Re_L and Pr_L followed a power-law relation. As Prandtl number (Pr_L) is a fluid property, which indicates relative effectiveness of momentum as well as energy transport by diffusion, the values decreased with the

increase in temperature, mainly due to viscosity. It is important to notice that Pr_L is a function of fluid viscosity and conductivity. At a certain temperature it remains constant because no other fluid-properties get changed at that particular temperature. The correlation between the Re_L, Pr_L, and Nu_L at bulk temperature found as:

$$Nu_L = 0.016 Re_L^{1.10} Pr_L^{0.33} \tag{5.12}$$

Based on the correlation developed, the behaviours of the curves have been compared with the study conducted by other investigators on a similar type of MICHX.

Khan, et al (2010) conducted a study on Ethylene Glycol-Water for characterizing heat transfer and fluid-flow through a similar two slab single serpentine minichannel heat exchanger. For a developing flow, their observation resulted in a correlation of $Nu_g = 0.152 Re_g^{0.4912} Pr_g^{0.33}$ [25]. The correlation obtained in the present study showed a good match with this correlation. There are slight variations in the numerical values which may appear due to the differences in the thermo-physical properties of two different fluids, Glycol-water & ATF. Moreover, their investigation was conducted within the liquid Reynolds number ranging from 400-1900 only for two slabs; whereas in the current study, the Re_L value ranges from 3-30 and total number of slabs are 15 in three loops.

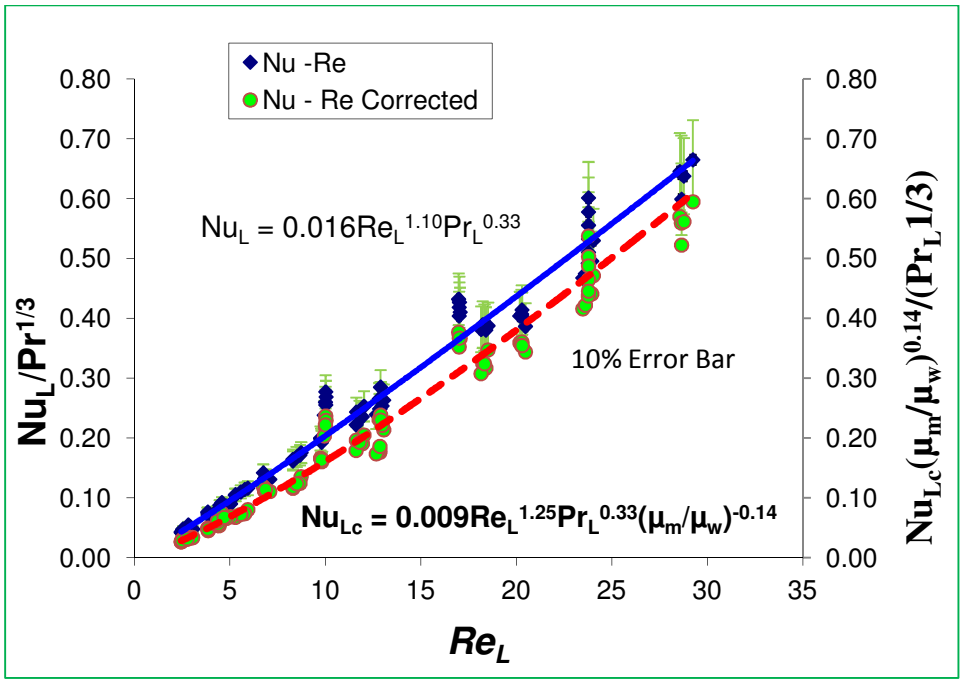

Figure-5. 13: Effect of Re_L and Pr_L on Nusselt number (Nu_L)

As explained in section 3.3.7, again the Nusselt number was corrected with the viscosity ratio while making correlation with Re_L and Pr_L. Upon correcting the values of Nu_L and taking the value of Pr_L at wall temperature, the new correlation has been found as:

$$Nu_{Lc} = 0.009{Re_L}^{1.25}{Pr_L}^{0.33}\left(\frac{\mu_m}{\mu_w}\right)^{-0.14} \tag{5.13}$$

In this case, the value of the exponent (n = 0.14) for the variable property ratio method has been considered. Comparing the above correlations, it is evident that upon correcting the values of Nu_L with variable property ratio and taking Pr_L at wall temperature, the Nusselt number decreases from the constant property values for cooling the transmission fluid. This decline in Nu_L is due to temperature variation between the wall and bulk temperatures or mean temperature.

Observation: For a fully developed laminar flow in a circular geometry, the Nu_L should be 3.66 upon maintaining a constant surface temperature (T_s) boundary condition. In this study, the Nu_L varied $3.687 \geq Nu_{Lc} \geq 0.235$ at variable property-corrected condition, and $3.819 \geq Nu_L \geq 0.263$ at constant property conditions. Ideally, the Nu_L should not be less than 1, although some values are less than unity in this study. Three possible reasons have been identified after the fact: (a) a constant surface temperature boundary condition could not be maintained perfectly due to the flow arrangements of the fluids and the geometry of the MICHX that keeps a temperature gradient between the inlet and outlet, (b) a viscous dissipation occurred due to a highly viscous fluid, but the effect could not be perfectly quantified due to the lack of appropriate boundary condition of constant heat flux, and (c) axial heat conductions in solid-wall and the liquid occurred, but those could not be taken into account.

5.3 Non-Dimensional Numbers

Some non-dimensional numbers are very important in characterizing fluid-flow and heat transfer, especially in the case of a curved geometry with highly viscous fluid-flow. The effects of curvature in a channel on heat transfer and flow-field have been explained in this section.

5.3.1Dean Number (De)

Dean Number (*De)* is the ratio of the viscous force acting on a fluid flowing in a curved pipe to the centrifugal force. It is very important to address the contribution of a viscous fluid like ATF when it flows through serpentine heat exchanger. The purpose of taking the *De* into account is to know the effects of this parameter on fluid-flow and heat-

transfer characteristics due to serpentines. One of the approaches in evaluating the effects of these serpentines on flow field is by finding the friction factor at the curvature and thus predicting the flow characteristics. A friction factor at the curvature, if different from that of the straight part of the channel, may be considered as an indicative to the presence of different flow field at that curved location. *De* was calculated using equation 3.10. As *De* was investigated and explained in sections 3.5.13, 5.5.1, and 5.5.4, the *De* did not have any effect on fluid-flow characteristics because of very low *De* values which ranged from $0.523 \leq De \leq 6.235$. For a value of *De* less than 11.6, the friction factors at the straight part of the channel and at the serpentine becomes the same ($f_s = f_c$) [82, 86]. In this case the *De* data were plugged in equation 3.40 in which case the calculation became redundant. The *De* values were also fitted in equation 3.41; again the ratio f_c/f_s became unity which proved both friction factors are the same in magnitude. Hence, the analysis from two different approaches through equations 3.40 and 3.41offered a similar result. In this study, one of the reasons for lower *De* is the liquid Reynolds number and $D/2R = 0.04545$ which is very small. Therefore, in this investigation, it is clear that due to a lower *De* the serpentine showed no effect on flow keeping the flow field undistorted.

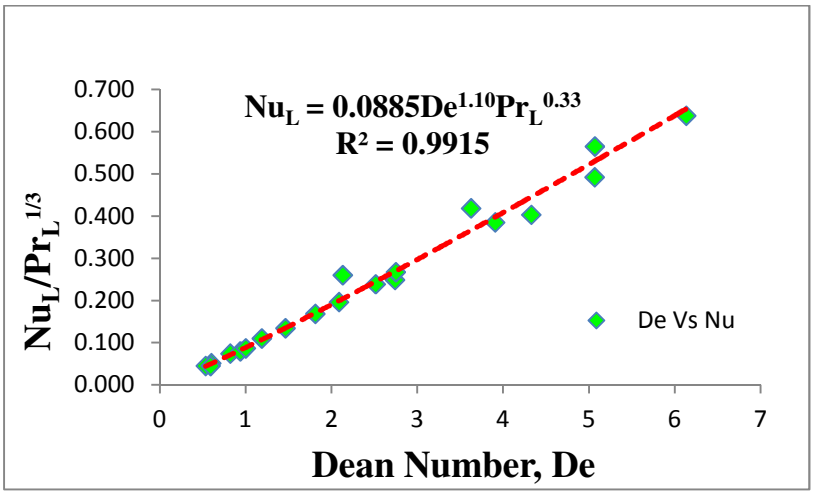

Figure-5. 14: Effect of *De* on Nusselt number, *Nu*

Under the current investigation, although serpentine does not have any influence on flow-field due to low Re_L, it is necessary to predict its effects on heat transfer enhancement. One method of evaluating heat transfer enhancement due to curvature is finding the local *Nu* at the straight part as well as the serpentine and then comparing them as: $q_{Nu} = (Nu_{serpentine}/Nu_{straight})$. Finding local *Nu* was beyond the capacity of this study due to the lack of appropriate instrumentation at the serpentine part. Another important matter for the current MICHX is its configuration. The serpentines are properly insulated, so they are considered adiabatic. Thus, under the scope of this study, finding *Nu* at an adiabatic condition may lead to an impossible task. Therefore, it has been recommended that future researchers may concentrate their views to look at these matters.

Although *De* is only valid for explaining curvature effect on flow-field and heat transfer enhancement, it can also be applied for visualizing heat transfer characteristics even at the straight part due to the presence of Re_L in the expression $De = Re_L(D/2R)^{0.5}$. Figure 5.13 shows that Nu_L increases with the increase in *De* in a power-law correlation. As *De* is a function of Re_L, it demonstrates that the pattern of Nu_L increment with the increase in *De* is similar to that of the explanation in section 5.2.7. As Nu_L increases with the increase in *De* as a power-law function, it offers a correlation as:

$$Nu_L = 0.0885De^{1.10}{Pr_L}^{0.33} \tag{5.14}$$

This correlation is exactly similar to that of the equation 5.12 except the slope. This slope in equation 5.14 is different from that in equation 5.12 because of the curvature ratio in *De* expression.

5.3.2 Eckert Number

A highly viscous fluid, ATF, has been investigated while it was flowing through the minichannel. To characterize the viscous dissipation due to such viscous fluid-flow and the change in kinetic energy inside the channel due to inertia or velocity, Eckert number *(Ec)* was calculated based on equation 3.9. The calculated *Ec* has been plotted against the mass flux (G) in Figure 5.14 and Nu_L against *Ec* in Figure 5.15 to investigate heat transfer characteristics. The *Ec* increases with the increase in mass flux (*G*). In the present investigation *Ec* varied between the values of $8.087E^{-08} \leq Ec \leq 1.818E^{-05}$, which is very small in magnitude. Although the numbers are very small, they should be taken into account due to their importance in contributing viscous heating. Since *Ec* is the ratio of the kinetic energy of the flow to the boundary layer enthalpy difference, the kinetic energy is much smaller compared to the enthalpy difference. Once the kinetic energy due to inertia or velocity increases, the *Ec* increases. The increase in *Ec* indicates that the viscous dissipation occurred at higher velocities of the flow. Therefore, how smaller the *Ec* or the viscous dissipation is, it cannot be neglected for a viscous fluid. It is also evident that at a higher temperature of the inlet-air, the fluid becomes hotter, and gives higher kinetic energy due to lower viscosity allowing easy movement of fluid. This may happen because $Ec = (V^2/(C_p (T_b-T_w)))$, the term T_b-T_w decreases due to the addition of viscous heating, and the higher T_w at higher inlet-air temperatures. Due to lower viscosity at higher wall temperature, in this case, V^2 increases resulting in larger *Ec*. An appropriate boundary condition of constant heat flux would result even in higher *Ec*.

Figure 5.15 shows the effect of *Ec* on the heat transfer phenomenon. As the *Ec* increases, the Nu_L increases in a power-law mode. The figure indicates that, while making a

correlation with *Ec* and Nu_L, the inlet air temperature does not play a big role on Nu_L. Basically, this increase in Nu_L does not mean heat transfer is enhanced; this indicates that the temperature increases with the increase in *Ec* which is the result of the viscous dissipation due to high viscosity of ATF.

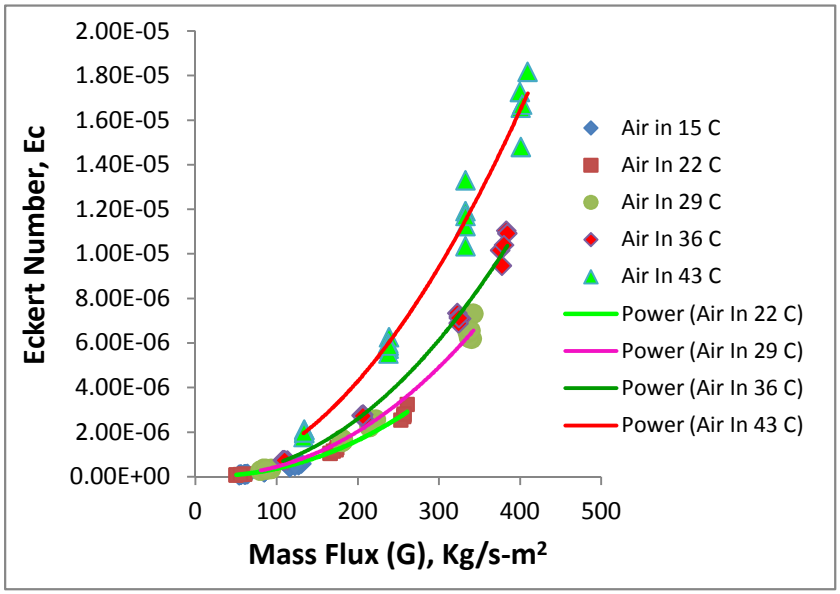

Figure-5. 15: Effect of Mass Flux, *G* on *Ec*

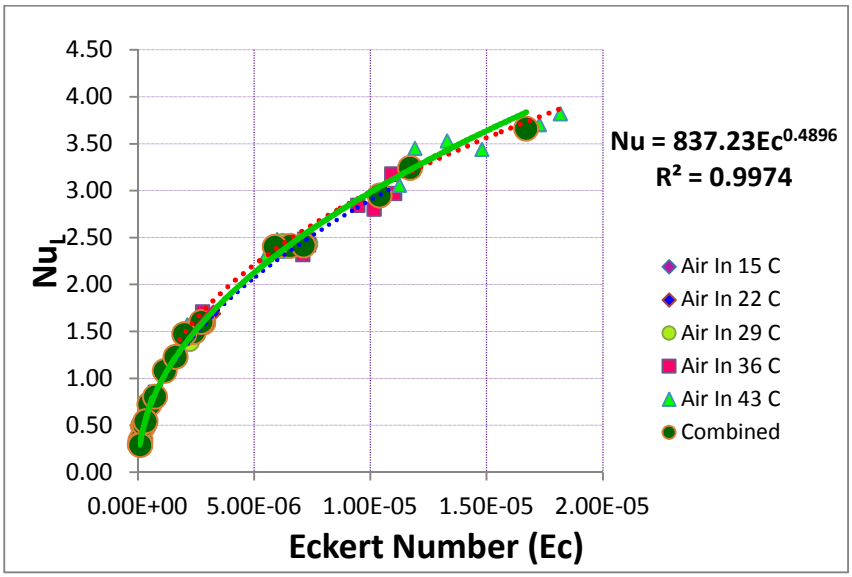

Figure-5. 16: Effect of *Ec* on Nusselt Number, Nu_L

Herwig, et al (2003) investigated unusual behaviour of dissipation effects in the narrow pipes. Tso, et al (2000) made an experimental investigation in micro-flow devices to find the micro-effects. Eckert numbers, *Ec*, in their study were found in the order of $Ec = 10E^{-09}$, which is very small. The authors mentioned that the dissipation effects can be neglected in the limit $Ec \rightarrow 0$. They claimed that, the variations of the Eckert number may be responsible for an unexpected heat transfer behaviour in their study. They called these effects as ''secondary Brinkman effects'' in view of the Brinkman number expression as $N_{Br} = EcPr$ to relate the non-dimensional numbers. So the temperature rise in an adiabatic micro-channel has an important contribution to heat transfer characteristics. In the current investigation, an empirical correlation has been developed:

$$Nu_L = 837Ec^{0.50} \tag{5.15}$$

This correlation is developed at a boundary condition of constant surface temperature (T_s) at a cooling mode. At a boundary condition of constant heat flux with heating mode offers the actual value of *Ec* which will be larger than the obtained values. As those conditions were not possible to maintain in this study, the calculated *Ec* is far below the real values. These values basically illustrate the presence of the viscous heating, not the actual heating amount. Therefore, the above correlation is valid only for the existing conditions.

5.3.3 Brinkman Nunber

There is no basic difference between the Eckert number and the Brinkman number, because both numbers contain the flow velocity and the temperature difference. Furthermore, they are related as $N_{Br} = EcPr$. Therefore, both numbers fundamentally

measure the viscous dissipation. The N_{Br} has been calculated based on equation 3.9. Since N_{Br} contains the dynamic viscosity term which is highly dependent on temperature variation, it usually gets higher with high viscosity-fluid yielding high rate of viscous dissipation. In this case, similar explanation can be applied, which is explained in section 5.3.2 regarding *Ec*.

Due to the effect of viscous dissipation, under some conditions, it can lead to a significant change in flow and temperature field. It can cause instability in flow, hydrodynamic thermal explosion, and oscillatory motion. Figure 5.16 shows the effect of mass velocity over N_{Br}. As G increases, N_{Br} increases with power-law fit. It is known that N_{Br} is a function of *Ec* and *Pr,* and *Pr* being a fluid property that remains constant at a certain temperature; it is important to notice that for a particular inlet-air temperature, the N_{Br} changes only due to the change in *Ec*. This increase in N_{Br} occurs due to the higher heat release as a result of viscosity. This viscous heating is higher than that of the thermal conduction at higher mass flux or velocities resulting in higher N_{Br} as per equation 3.14.

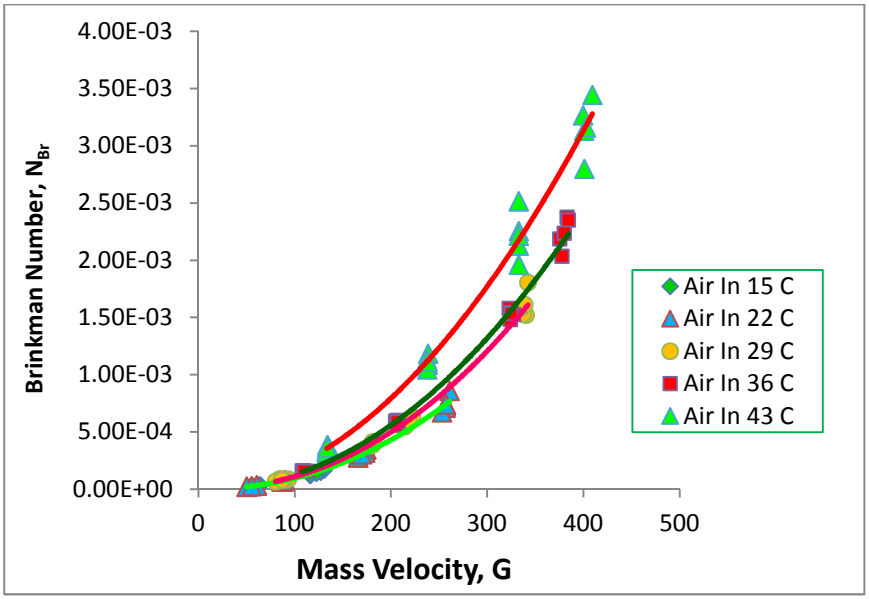

Figure-5. 17: Effect of Mass Flux, G on N_{Br}

Tso, et al (2000) carried out experimental investigation on water flowing through microchannel specimen and found $N_{Br} \approx 10^{-8}–10^{-5}$. This value has been considered non-realistic [60, 89]. A larger value of N_{Br} as of the order of unity or larger, it can influence the film temperature (T_f) directly.

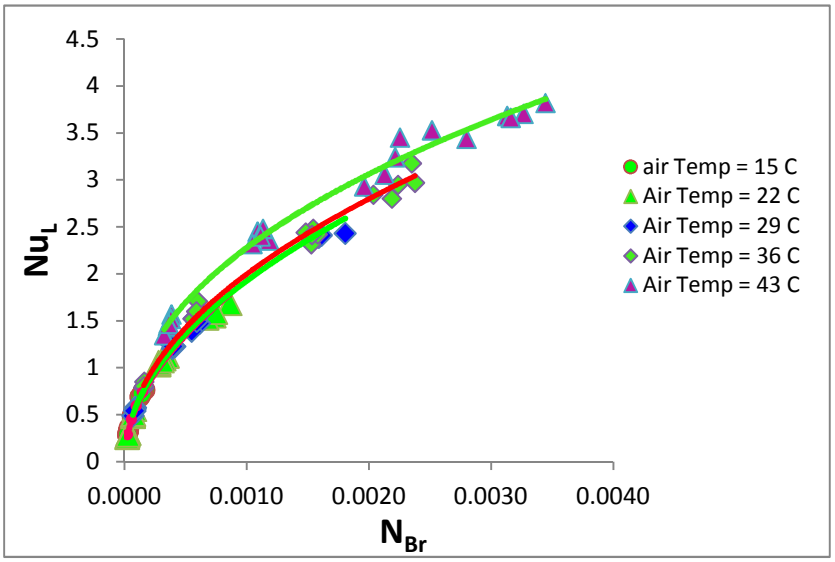

Figure-5. 18: Effect of N_{Br} on Nusselt Number, Nu_L

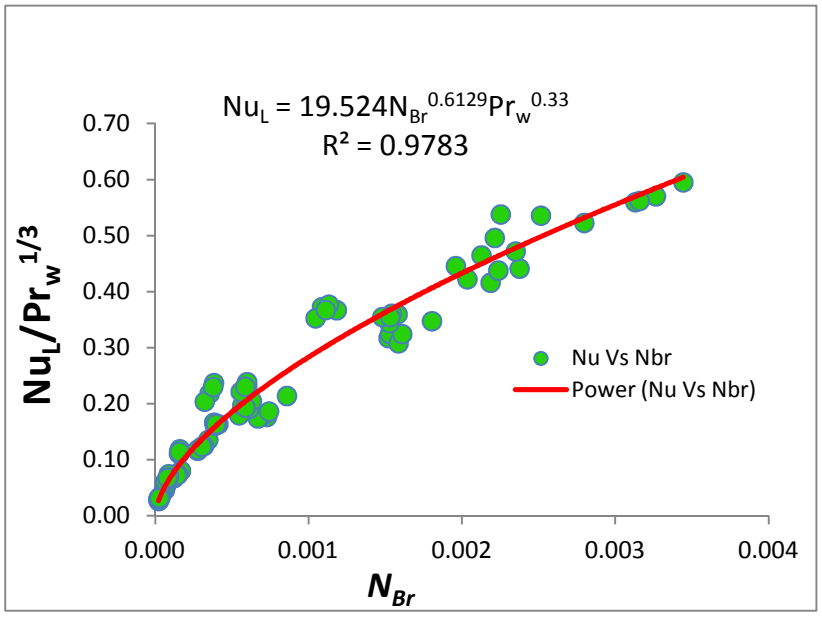

Figure-5. 19: Effect of N_{Br} on Nusselt Number, Nu_L

In the current investigation, the N_{Br} varies from $2.13E^{-05} < N_{Br} < 3.44E^{-03}$ within the Re_L range of 3-30, whereas C.P. Tso and S.P. Mahulikar made their investigation with the *Re* of *80-107* to obtain $N_{Br} \approx 10^{-8}–10^{-5}$. It is anticipated that in this study, a possible higher Re_L range may offer significantly increased N_{Br}. The value of N_{Br} is already higher compared to those of 'Tso' even at lower Re_L. Even though the values of N_{Br} are very small, it cannot be considered negligible because of the facts that the N_{Br} should be measured at boundary conditions of constant heat flux at heating mode. In the present investigation, the experiments have been carried out in such a way that ATF loses heat all the way to its travel through the channel core where heat flux also decreases. The decrasing heat flux implies that the calculated N_{Br} does not reflect the actual value due to the absence of required boundary conditions. Therefore, it can be concluded that ATF, as a highly viscous fluid, causes viscous dissipation in minichannel heat exchangers even at lower Reynolds numbers.

Figure 5.18 shows the relation of N_{Br}, Pr_w, and liquid Nu_L. An empirical correlation at a possible constant temperature boundary condition has been developed as:

$$Nu_L = 19.52 N_{Br}^{0.61} {Pr_L}^{0.33} \tag{5.16}$$

5.4 Air-Side Heat Transfer

Although liquid-side heat transfer parameters have been given the priority in this study, air-side heat transfer parameters need to be addressed. A brief summary of the heat transfer is presented in this section.

5.4.1 Air-Side Heat Transfer Coefficient

Air side heat transfer coefficient (h_a) has been calculated by an iteration method as described in sections 3.8.3. The h_a has been plotted against the air Reynolds number while considering a particular liquid Reynolds number which is constant for that condition. Figure 5.19 shows the effects of air-side Reynolds number (Re_a) on h_a. The air-side h_a increases in a polynomial relation with the increase in Re_a. It is important to know that h_a increased with the increase in liquid Re_L also. The maximum h_a value has been achieved at the maximum Re_L value of 28.77, and the minimum h_a value at the minimum Re_L value of 5.6. So, air-side heat transfer coefficient has direct relation with air-side as well as the liquid side Reynolds number. The plot also illustrates that air-side Re_a has less effect on h_a than the liquid Re_L. When the Re_a changes from 1700 to 5000, for an example (at Re_L = 5.6), the change in h_a occurs from 33 to 37 only. On the other hand, h_a changes from 33 to 98 with the change in liquid Re_L of 5.6 to 28.77.

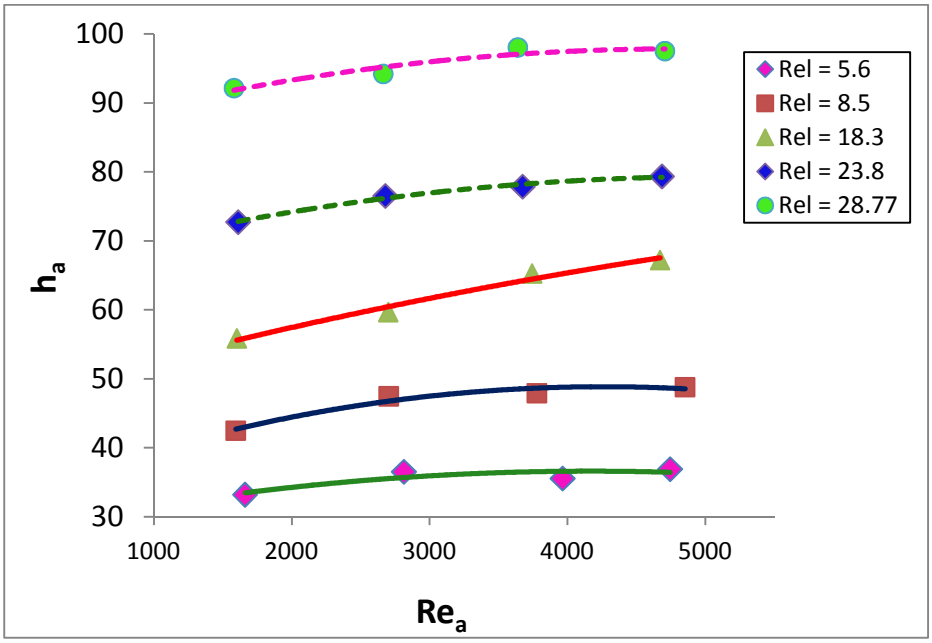

Figure-5. 20: Effect of Air-Side Re_a on Air Heat Transfer Coefficient, h_a

Therefore, the liquid Re_L plays dominating effect on Re_a in a convective heat transfer phenomena to characterize ATF heat-transfer mechanism for the case of a serpentine cross flow MICHX. From the above discussion it is also evident that the air velocity has negligible effect on heat transfer parameters for a multiport minichannel heat exchanger.

5.4.2 Air-Side Nusselt Number

Air-side Nusselt number (Nu_a) has been computed for all air inlet temperatures and plotted against the air Reynolds number while considering a particular liquid Reynolds number which is constant for those conditions.

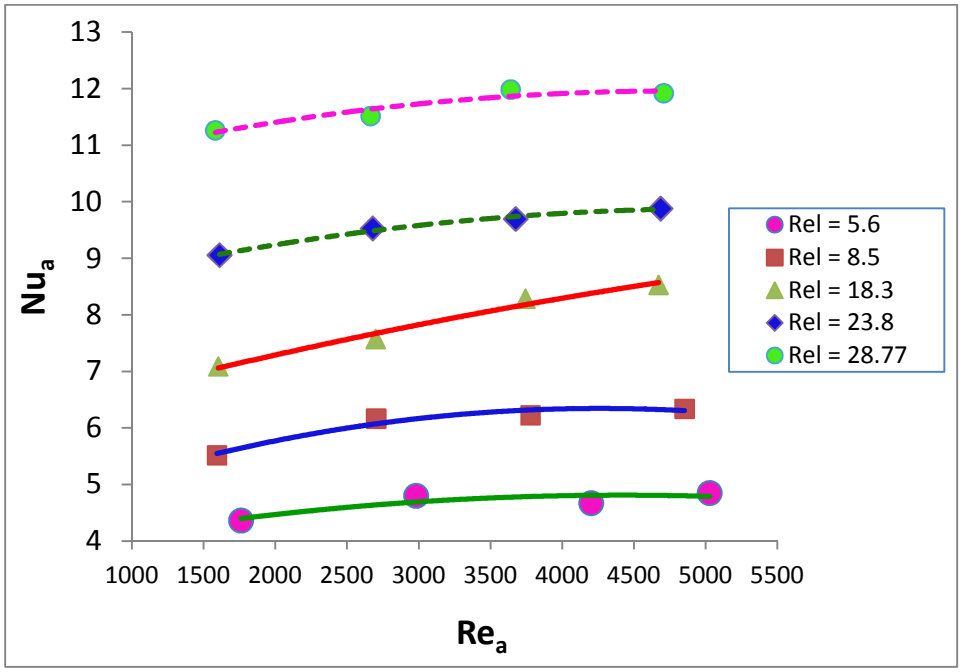

Figure-5. 21: Effect of Air-Side Re_a on Air Nusselt Number Nu_a

Figure 5.20 shows the effects of air-side Reynolds number (Re_a) on air Nusselt number (Nu_a). The Nusselt number of air increases in a polynomial relation with the increase in Re_a. The nature of change in the curves is similar to that of the patterns of the air convective heat transfer coefficients. It is noticed that the Nu_a increases with the increase

in liquid Re_L. The air Re_a has less effect on the Nu_a than the liquid Re_L. For an example (at Re_L = 5.6), Nu_a changes only 4.3 to 4.8 with the Re_a change of 1700 to 5000, whereas Nu_a changes from 4.3 to 11.6 with the change in liquid Re_L from 5.7 to 28.77. So, the effect of the liquid Re_L is prominent in a convective heat transfer phenomenon in case of ATF cooling through serpentine slab structure MICHX and air velocity has less effect on the air Nusselt number. This is because of the high mass flow rate of air even at lower Re_a (1700-5000) compared to a very little mass flow rate of ATF resulting in very low Re_L.

5.5 Pressure Drops

A highly viscous fluid like ATF creates a high pressure drop, especially in case of a narrow-channel. In this study, the channel hydraulic diameter is 1mm which is a minichannel. Therefore, pressure drops and friction factors are the prime factors in evaluating serpentine shape MICHX performances. Although based on thermally developing boundary condition, the flow has been considered developing flow. However, the flow is hydrodynamically fully developed. Additionally, the serpentines played no roles in flow-fields. Therefore, logically the pressure drops can be calculated considering a fully developed flow. The pressure drop parameters are summarized in this section.

5.5.1 Pressure Drop Analysis in MICHX

Due to the narrow-channel geometry and a highly viscous fluid, high pressure drops occurred when it flows through the heat exchanger. From the investigation, the ATF Reynolds number (Re_L) was achieved within the range of 3.00 to 30.00, which is very low. Although the Re_L was very low due to high wall shear stress, an increased friction

factor has been found that resulted in high pressure drops. The flow entrance length has been calculated as 0.12-1.462 mm, which is so small compared to the channel length of 1658 mm or the *L/D = 1658/1=1658*. Therefore, as explained in sections 3.6, 3.6.1-2**,** approach-friction factor or pressure drop due to entrance effect can be neglected. Based on this assumption, the total pressure drop for the channel length of 1658 mm has been calculated based on equation 3.39 where the serpentine length and effect have also been considered. Pressure drops have been computed using equations 3.37-42 for calculating different parameters required to estimate total channel pressure. For computing pressure drop at the straight part of the channels, equation 3.37 has been applied. For the serpentine part equations 3.38 and 3.39 were used. As the Darcy's friction factor f_d or Fanning friction factor (f_f) is required to calculate f_c in equations 3.40 and 3.41, equation 3.26 has been applied to compute f_d which is the friction factor at the straight part of the channels. To find the friction factors at the serpentine, equation 3.40 or 3.41 is necessary to be verified. To get full in-sight of the serpentine friction factor, both equations have been verified. For the cases of using empirical formula 3.40 of White or the equation 3.41 of Topakoglu, Dean Number is required. The biggest Dean Number has been found as 6.24. As White, (1929) investigated that for a Dean number *De* less than *11.6*, the ratio f_c/f_s comes to unity. This explains that the friction factor at the curvature is equal to the friction factor at the straight part of the tube in magnitude. In the present investigation, the calculated Dean number is maximum 6.24. While substituting this value in equation 3.40 for calculating f_c/f_s, the calculations become redundant. On the other hand, equation 3.41 outlined by Topakoglu, (1967) offered a calculated value of f_c/f_s=1, which supported the observation of White [86]. Hence, the friction factor at straight part and the serpentine

are the same. Therefore, the total length of the channel for calculating the friction factor and the pressure drop is the sum of the straight part and the serpentine part which equals 1658 mm. In the current investigation, although the serpentine does not have any effect on the friction factor due to curvature (f_c) as stated above, the radial component contributes a bit to the total pressure. So the total pressure drops along the channels are the contribution from equations 3.37 or 3.39 and 3.38. Any of the two equations 3.37 or 3.39 gives the same ΔP values because the origin of both equations is same. The difference between them is just the method of expression.

The calculated values of the friction factors have been corrected with viscosity effect due to temperature change as explained in section 3.5.1. In this case, equation 3.29 has been applied for the correction. Based on the corrected values of the friction factors, the actual pressure drops along the core have been calculated using equation 3.39.

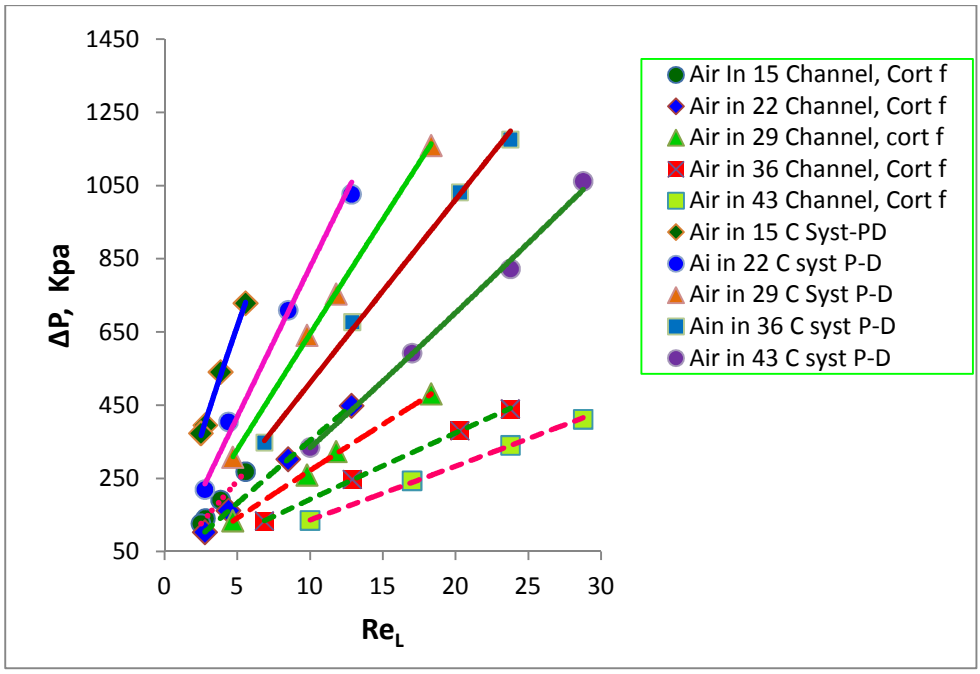

Figure-5. 22: Effect of Re_L on System Pressure and the Pressure along the Channel

Figure 5.21 shows relation between the calculated channel core pressure drops and Re_L, while Figure 5.22 shows pressure drops and mass velocity G. In addition to the channel pressure drops, Figure 5.21 also contains the total system pressure which is much higher than the core pressure drops (the solid lines). The dotted lines indicate pressure drops only at the channel core when they are corrected with variable property ratio. The plots showed the effect of Re_L on the pressure drops for five different inlet-air temperatures, while liquid inlet-temperatures remained constant. For all the data points in the range of obtained $3 \leq Re_L \leq 30$, the measured total system pressure drops as well as the calculated channel pressure drops varied non-linearly with Re_L in a power-law relation. For a particular Re_L, the plot shows that the pressure drops are higher at lower inlet air temperatures. This happens due to higher viscosity and shear stress.

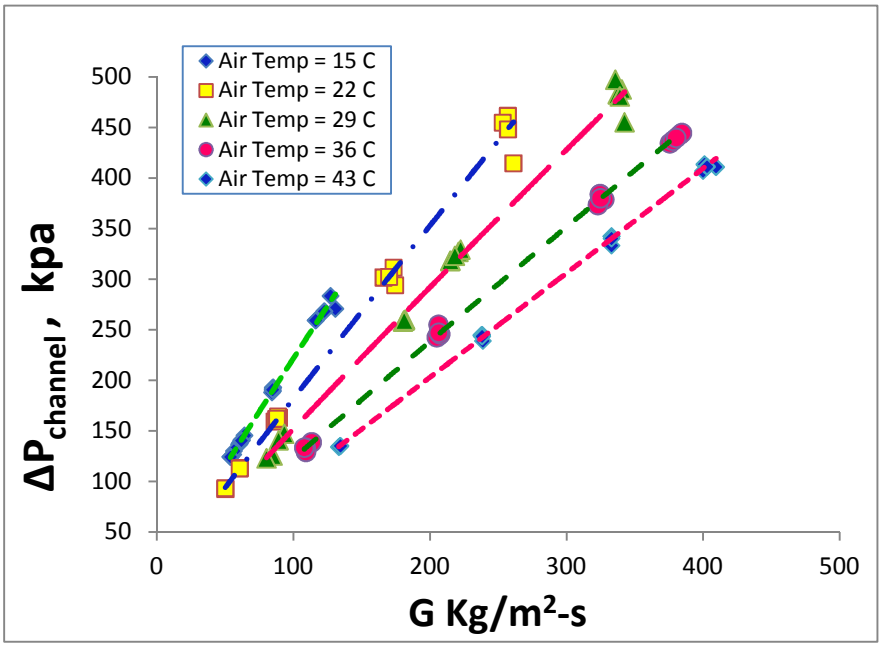

Figure-5. 23: Effect of ATF Mass Velocity (*G*) on Pressure along the Channel

Qu, et al (2002) conducted an experimental and numerical study on pressure drop and heat transfer in a single-phase micro-channel heat sink [57]. The authors in their

investigation found a similar trend of the curves when examining the effect of *Re* on measured pressure drops at different heat transfer rates. The result showed increasing pressure drops with increasing Re_L.

Khan, (2011) conducted an investigation on the single slab MICHX to estimate channel core pressure drop for hot glycol-water mixture flowing through it. The author made an investigation for a *Re* range of $346 \leq Re \leq 1637$ to find the pressure drop of hot glycol-water mixture per unit length of the core channel [54]. The pressure drops were calculated by eliminating all other pressure drops from the measured total system pressure drops and finally, the remaining pressure drop was the pressure drop at channel core. The investigation showed a range of 17 to 138 kpa/m pressure drops along the channel core. In the current investigation, the pressure drops calculated varied as 56-300 kpa/m for the channel core. In this case, serpentine effects have been considered although they are very small in magnitude (0.00027- 0.0182kpa). In this investigation, even for low Re_L, the rise in the pressure drop which is greater than Khan et al is due to the higher viscosity of ATF.

Figure 5.22 illustrates the effect of mass flux (*G)* on pressure drop. The figure indicates that the pressure drop increases with the increase in mass velocity linearly, and for a particular *G* value the higher inlet air temperature offers lower pressure drops due to lower viscosity offering lower shear stress.

5.5.2 Effect of Re_L Over Pressure-Drop Mass-Flux (*G*) Ratio

To investigate the effect of Re_L over the pressure-drop mass-flux ratio ($\Delta P/G$), the data has been plotted against Re_L. By substituting the value of *L/D* for the MICHX under

investigation and rearranging all the parameters, the *ΔP/G* becomes a direct function of velocity and friction factor as shown in equation 5.17 where f is the Fanning friction factor and V is the liquid velocity.

$$\frac{\Delta P}{G} = 2\frac{L}{D}fV = 3316fV \tag{5.17}$$

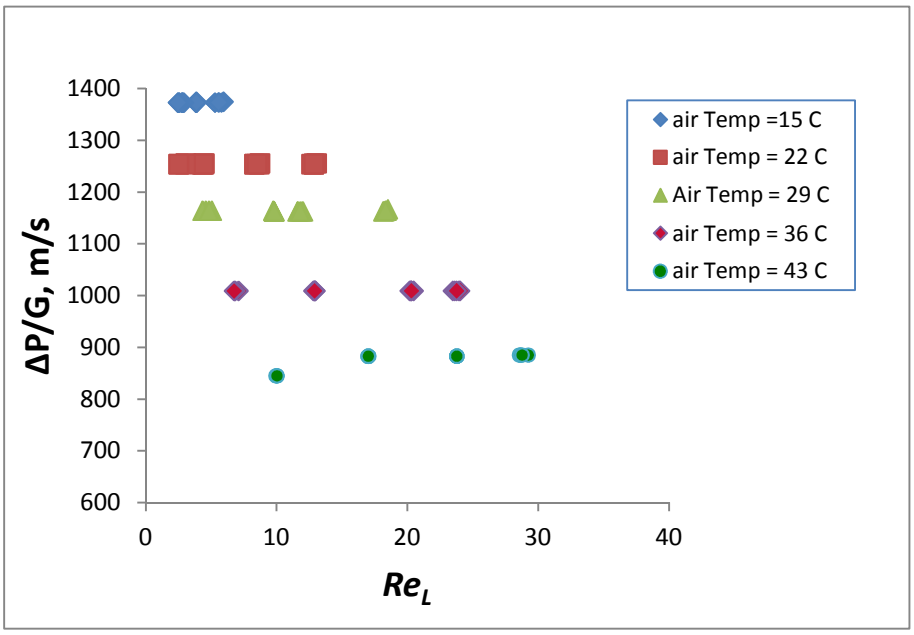

Figure-5. 24: Effect of Re_L on Pressure Drop-Mass Velocity Ratio

In Figure 5.23, the plot indicates that for a particular temperature, the Re_L has almost no effect on the *ΔP/G* ratio. At lower air temperature, the pressure-drop mass-flux ratio is higher. Again, the fact implies that with the increase in mass flux, the pressure drops increases with the same multiplication factor for a particular temperature to keep the ratio a constant. The *ΔP/G* ratio is higher at a lower temperature, whereas lower at the higher temperatures.

5.5.3 Effect of Temperature on Pressure Drop (ΔP)

The system pressure drops have been determined from the measurement of the pressure transducer located at the inlet and the outlet of the heat exchanger. For a certain temperature, it is obvious that the pressure drop increases with the increase in mass flow rates. So, the pressure drops can be normalized based on mass flux. Figure 24 shows the normalized pressure drops against the liquid bulk mean temperature. When the bulk temperature increases, the pressure drop decreases in a power-law function as:

$$\Delta P = 683681 T_B^{-3.049} G \tag{5.18}$$

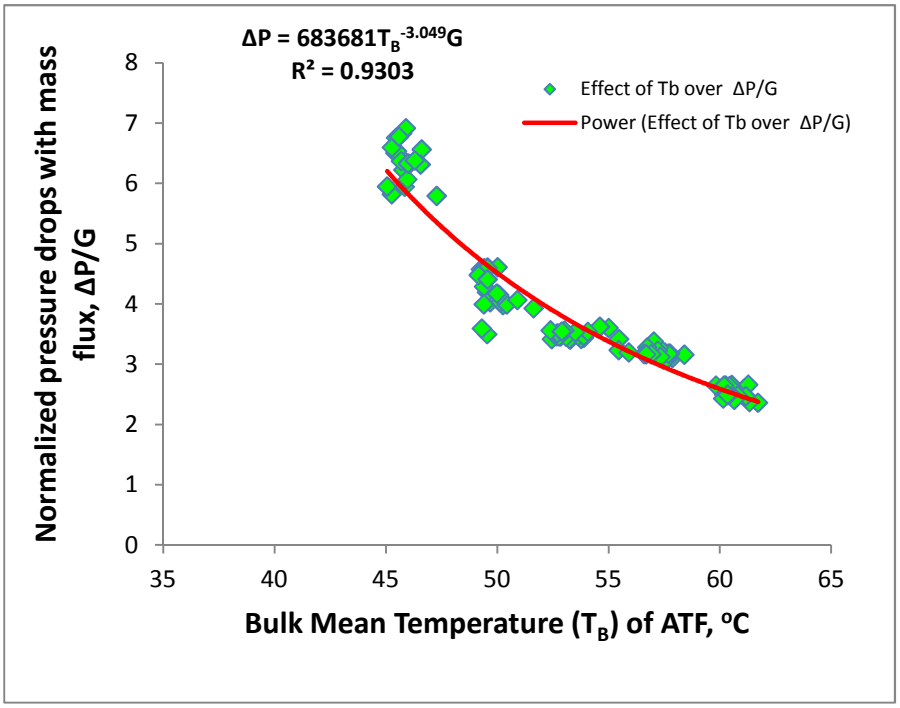

Figure-5. 25: Effect of Temperature on Normalized Pressure Drops w. r. t. (ΔP/G)

5.5.4 Friction Factor

The pressure drops and the friction factors are correlated to each other as per equations 3.28 (Darcy's friction factor) or 3.39 (Fanning's friction factor). In this study, two types of friction factors have been calculated. One is based on the traditional Poiseuille flow (equation 3.26) which is not corrected with viscosity effect, and the other is based on making the correction with viscosity change as mentioned in section 3.5.1 as per equation 3.29. A correlation has been established through a best fit of the curves as portrayed in Figure 5.25. In this case, the Darcy's friction factor makes the correlation with the Re_L as a power-law function, when considering constant properties. The relation is given as:

$$f_d = 64.044 Re_L^{-1} \tag{5.19}$$

For a fully developed laminar flow in a circular tube, the flow reaches to the Poiseuille (Po) flow, and the relation comes to f_d *=64/Re.* The current investigation shows $f_d Re_L$*=64.044* which is almost 64. As the friction factors have been corrected with the viscosity ratio for temperatures (equation 3.29), the curve shows a slight deviation from the Poiseuille equation and makes a different correlation from equation 5.19. The new correlation based on variable property ratio is shown in equation 5.20 within the prevailing Re_L.

$$f_{cort} = 118 {Re_L}^{-1.15} (\mu_m/\mu_w)^{0.50} \tag{5.20}$$

The plot explains that at lower Re_L, the deviation of the corrected friction factor (f_{cort}) from the Poiseuille flow is higher and gradually collapsed to overlap each other at higher Re_L and finally follows Poiseuille law. The influencing factor is the viscosity.

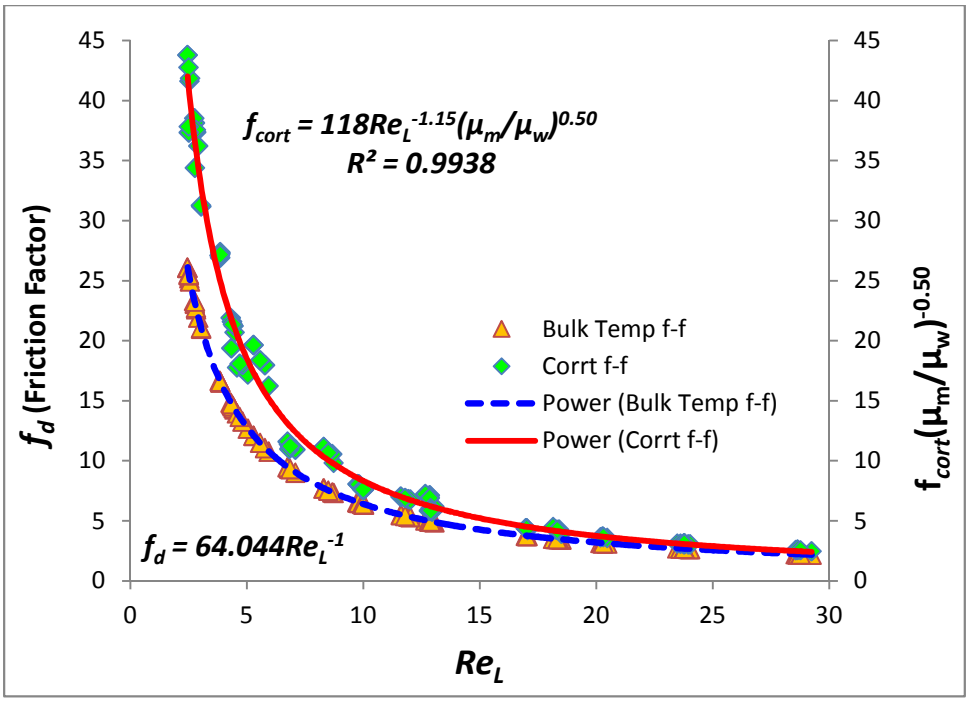

Figure-5. 26: Relation Between Darcy's Friction Factor f_d and the Re_L

The Reynolds number is an inverse function of dynamic viscosity, which decreases with an increase in temperature resulting in higher Re_L. Hence, at higher temperatures the viscosity effects are not so prominent in separating the curves from each other. So, the dominating viscosity effects cause higher friction factors with the result of higher pressure drops.

The data for the corrected friction factors has also been plotted in log-log scale. As expected, Figure 5.26, the f_{cort} values linearly decreased with the increase in Re_L, the effect which shows strong dependency on Re_L. As the curve shows a straight line, and no directional changes occur, it implies there is no Blasius zone or turbulence in the flow.

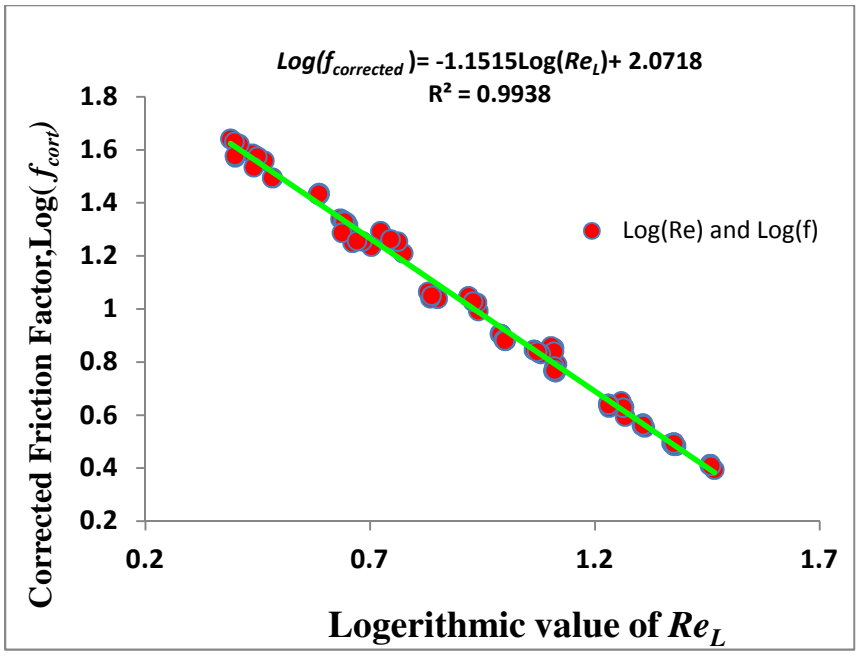

Figure-5. 27: Relation Between Darcy's Friction Factor f_d and the Re_L in a log-log Plot

Khan, (2011) made an investigation on water while using a similar type of single serpentine two-slab heat exchanger and found the similar trend of the curves within the laminar flow regime. The author established the correlation of $fRe = 67$, which is 5% over the theoretical value of Poiseuille equation [55].

Many authors have so many differences in their opinions on channel diameter and the *fRe* (*Po*) numbers. Statistics among the researchers who worked on the microchannel shows that 24% researchers argued in favor of increased value of *Po*, 11% opined that *Po* should be lower, while 31% opined that the *Po* should always be constant with a value of 64 even in the case of a microchannel [64]. In the current study, the channel diameter is considered a minichannel and for this minichannel serpentine heat exchanger core flow, the *Po* is 64.044 with no correction for viscosity. However, on correcting with viscosity ratio, the flow does not follow the conventional Poiseuille form *fRe = 64,* rather it

produces $fRe_L^{1.152} = 118$ or an average value of $fRe_L \approx 85.48$. At higher Re_L the corrected variable property curve collapsed to the constant property Poiseuille curve although they are separated at lower Re_L. Therefore, it can be concluded that, ATF as a viscous fluid flowing through minichannel, the flow in the laminar regime behaves in two different ways: it follows the conventional Poiseuille flow theory at higher Re_L to yield $fRe = 64$, whereas at lower Re_L, it results in higher fRe values that disregards Poiseuille law. The governing factor is the fluid viscosity. This effect may not be prominent in case of low viscous fluid but very important for a highly viscous fluid.

5.6 Heat Exchanger Performance

Heat transfer performance is characterized by the Effectiveness-NTU analysis which are summarized here.

5.6.1 Effectiveness

The effectiveness (ε) for the test specimen under investigation has been calculated using equation 3.67. Figure 5.27 shows that the effectiveness increases with the increase in the air-side Reynolds number; this implies the air velocity dependency of the effectiveness. Five different curves against five different inlet air temperatures have been plotted in the figure. The plot shows that within the air Re_a of 1400-5200 and a temperature range of 15– 43^{o}C, the effectiveness varied from 82-95%, which indicates that the heat exchanger is almost at its maximum effectiveness. The plot also illustrates that for all temperatures of the inlet air except a very low temperature (15^{o}C), no big change in effectiveness occurs. With the increse in air Re_a the effectiveness increases monotonically. So, it is

evident that air velocity and temperature both play less important roles in heat exchanger performance.

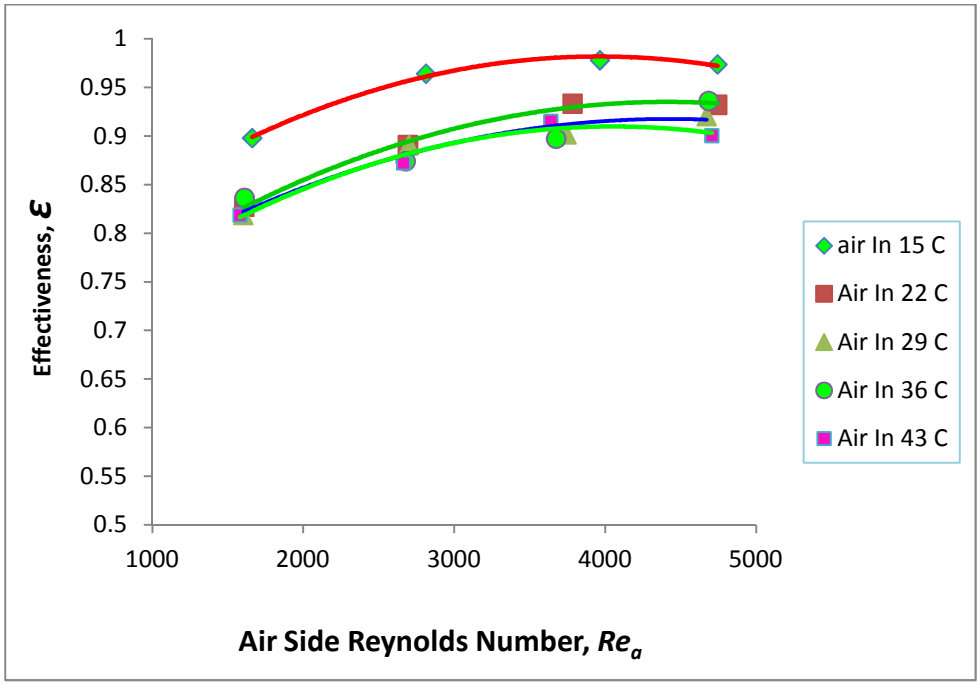

Figure-5. 28: Effect of Re_a on Effectiveness

In Figure 5.28 the effectiveness and the ATF Reynolds number have been plotted to illustrate the effect of the ATF Re_L on ε within the Re_L value of 3- 30. For a given operating condition, especially the flow regime such as a laminar flow, the plot can provide with values of ε for a heat exchanger design and optimized operating point for a defined heat duty. As the ATF Re_L increases, the effectiveness decreases in a power-law fit as shown in Figure 5.28 and equation 5.21. In this case the ε is higher at lower Re_L because at lower Re_L the velocity of ATF is low resulting in higher dwaling time which allows higher heat tranfer ratio, $\varepsilon = \dot{Q}/\dot{Q}_{max}$ (of course the $\dot{Q}$ value is less than the value at higher Re_L). In this case the correlation obtained as:

$$\varepsilon = 1.03Re_L^{-0.05} \tag{5.21}$$

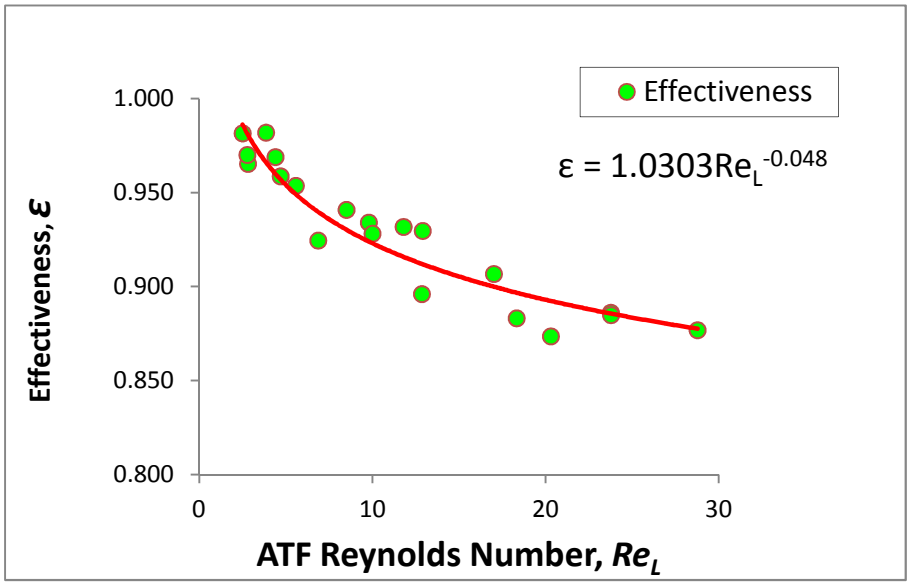

Figure-5. 29: Effect of Re_L on Effectiveness, ε

Khan, (2011) worked on a similar heat exchanger with a shorter length and found the similar trend of decreasing $\boldsymbol{\varepsilon}$ with increasing Re_L while using ethylene glycol-water as working fluid [55]. The effect of liquid Re_L has more influence on effectiveness than the air-side Re_a. Therfore, for a design purpose the liquid Re_L should be considered as higher influencing factor.

5.6.2 Number of Transfer Unit (NTU)

The *NTU* is another aspect of a heat exchanger design. It gives the economic size of the heat exchanger. The observed *NTU* has been plotted against the air Re_a for four different Re_L in Figure 5.29. The figure illustrates that for a particular Re_L, the *NTU* increases with the increase in an air-side Reynolds number. The figure also explains that the liquid Re_L values dominate the *NTU* numbers. At lower Re_L, the *NTU* is higher than that of the *NTU* at higher Re_L.

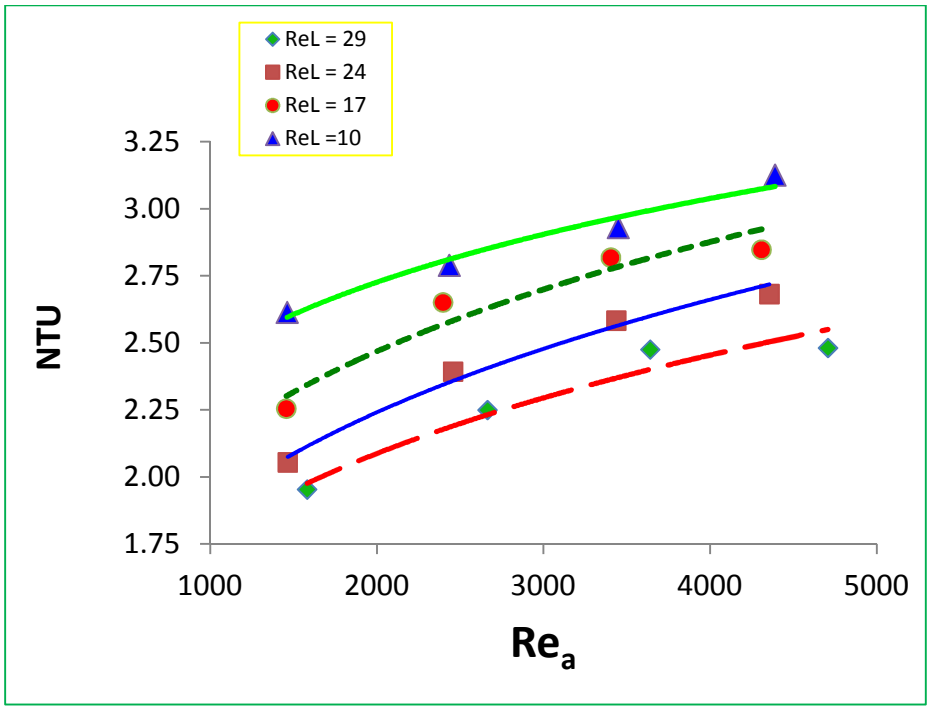

Figure-5. 30: Effect of Re_a on NTU

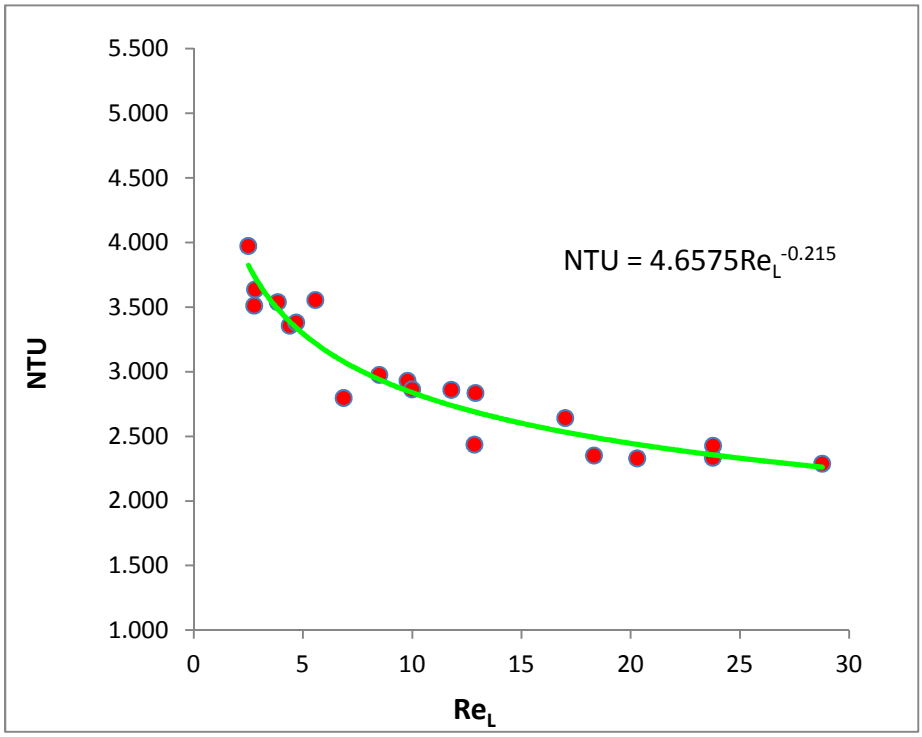

Figure-5. 31: Effect of Re_L on NTU

Figure 5.30 shows the *NTU* against the Re_L in a precise way which shows decreasing values with increasing Re_L in a power-law correlation as:

$$NTU = 4.66Re_L^{-0.22} \tag{5.22}$$

As illustrated in Figure 5.31, the ε- *NTU* results are plotted against the Capacity Rate Ratio (C^*). For design purpose, the *NTU* and the ε are tightly related to each other. In a general rule, the effectiveness increases rapidly for an *NTU* value up to *1.5* and then the ε increment rate happens monotonously. In the current study, the *NTU* values range from 2.25 to 4.00. So the range of rapid change in ε is not applicable, rather it is in the monotonous range.

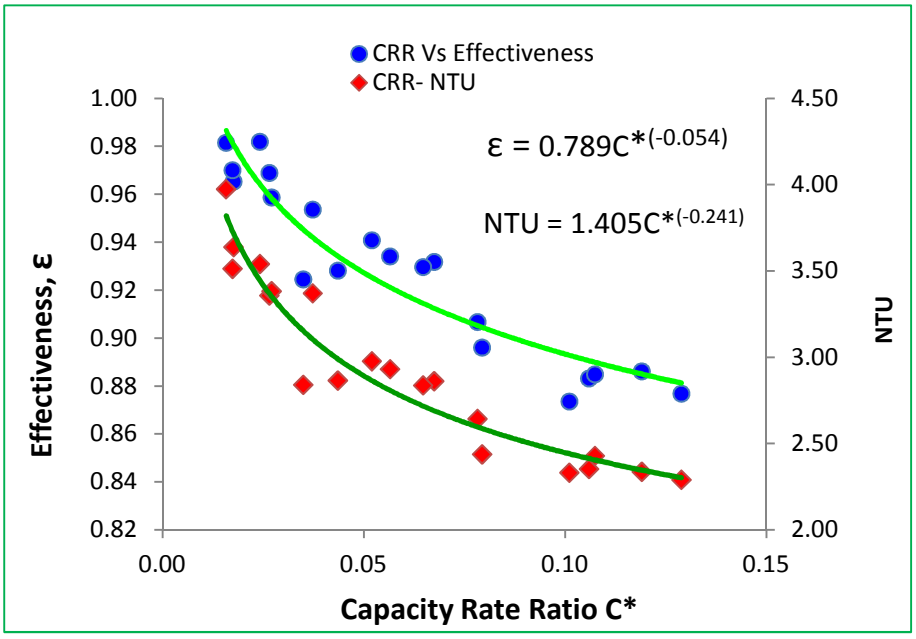

Figure-5. 32: Effect of ε-*NTU* and Heat Capacity Rate Ratio (CRR), C^*

The plot gives two power-law equations for ε and *NTU* as shown below:

$$\varepsilon = 0.79C^{*(-0.05)} \tag{5.23}$$

$$NTU = 1.405C^{*(-0.24)} \tag{5.24}$$

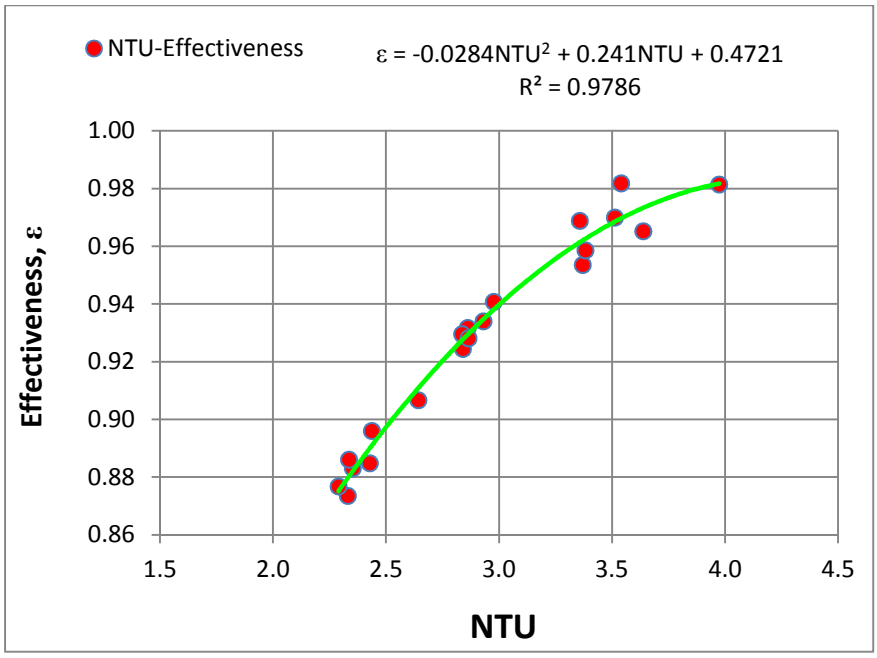

Figure-5. 33: *ε-NTU* Relations

A larger value of *NTU* (usually > 3) is not economically justifiable [76]. The investigation on the test specimen shows that most of the data remains within *2.2* ≥ *NTU* ≥ *3.5* (Figure 5.32), which implies that the heat exchanger under the current operating condition just crosses the margin of the economic limit at few points. The Figure 5.31 also shows that, with the increase in C^*, the *ε-NTU* decreases. Ideally, C^* ranges $0 \geq C^* \geq 1$, for a particular value of *NTU*, *ε* gets maximum when $C^* = 0$ and minimum when 1. In this investigation, C^* varies from 0.016 – 0.129 which is far below the maximum value of 1. So, the heat exchanger for the cooling of ATF at the prevailing operating conditions worked at the best-performing limits. As the *ε-NTU* are at the maximum level, no enlargement in physical channel length of the heat exchanger can be recommended.

5.6.3 Heat Exchanger Conductance (UA)

To investigate the effect of liquid-side Reynolds number (Re_L) on heat exchanger conductance (*UA),* the results have been plotted as shown in Figure 5.33. The *UA* is the overall conductance of the heat exchanger, which is basically the inverse of total resistance (R_{total}). Conductance is the measure of how well heat can be transferred through the heat exchanger. This is directly related to *NTU*. By determining *UA* value for a particular heat exchanger, other parameters are easy to calculate. Basically, *NTU* has been calculated from equation 3.66. The conductance increases with the increase in Re_L and hence the heat transfer coefficient h_L increases. The increment of the conductance follows a power function with the polynomial curve fit as:

$$UA_{Th} = -0.1918Re_L^2 + 14.874Re_L + 37.36 \tag{5.25}$$

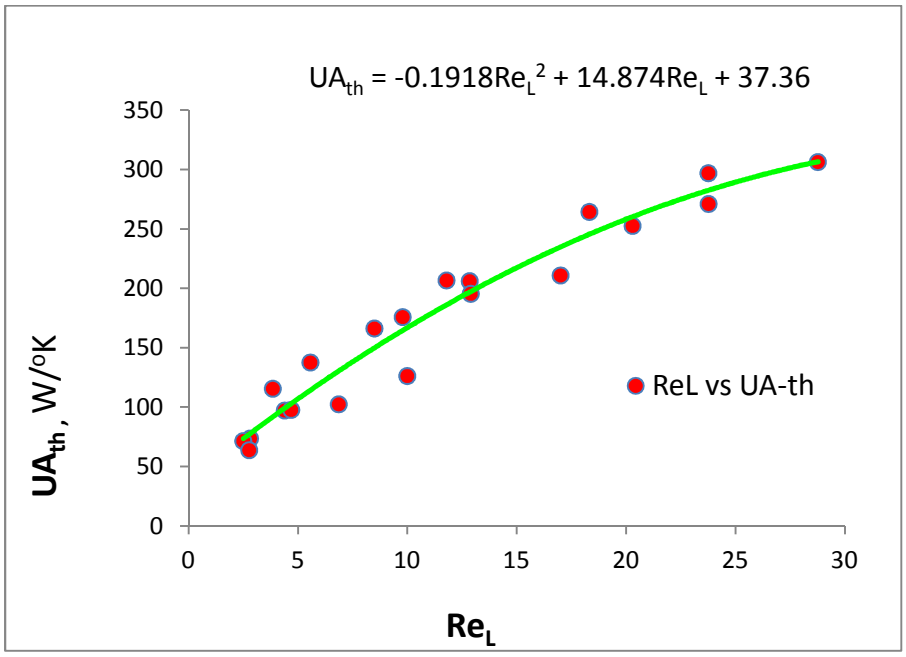

Figure-5. 34: Effect of ATF Re_L on Overall Thermal Conductance

Siddiqui, (2011) conducted an investigation on 50% ethylene glycol using the same heat exchanger for his M. A. Sc program, and he found a similar trend in increasing values of *UA* with the increase in an air-side Reynolds number [70]. In the current investigation, the thermal conductance varies as $64 \geq UA \geq 307$. As the value is high, the thermal resistance gets lower and the heat transfer occurs faster.

Khan, (2011) investigated overall thermal resistance (*1/UA*) and found the maximum value of 0.0175. In this case the author conducted experiments on 50 ethylene glycol using a similar type of heat exchanger within the *Re* maximum value of 400-1800 [55]. In the current investigation, the overall thermal resistance obtained is maximum 0.026, which is higher than what Khan found. This is due to the facts of operating conditions, fluid flow length, and the fluid itself.

CHAPTER VI

CONCLUSIONS AND RECOMMENDATIONS

6.1 Conclusions

An experimental investigation has been conducted in order to characterize ATF heat transfer and fluid flow behaviours flowing through an air-cooled MICHX in a cross-flow orientation. The main focus of this study is to investigate the appropriateness of cooling ATF using a MICHX. The key parameters, such as heat transfer rates, *NTU*, Effectiveness, friction factor and pressure drop behaviours, and overall thermal resistance have been studied. This study entails experimental investigation on the effects of dimensionless parameters such as: Reynolds number (*Re*), and Nusselt number (*Nu*) for both fluids upon heat and mass flow behaviour. Attention has been paid to other non-dimensional parameters such as: Prandtl number (*Pr*), Brinkman number (N_{Br}) Eckert number (*Ec*), and Dean Number (*De*). Empirical relationships have been established between the heat transfer and key fluid-flow non-dimensional parameters.

Eighty different operating conditions were maintained in order to obtain the key heat transfer and fluid flow characteristics. ATF temperature has been kept constant at 75^{o}C throughout the experiment while air temperatures were kept at 15, 22, 29, 36 and 43^{o}C. ATF mass flow rates were varied and for each mass flow rate, four air velocities: 18, 14, 10, and 6 m/s were applied.

Based on in-depth investigation on the matters related to ATF heat transfer and mass-flow characteristics while using a MICHX, the following observations have been made:

1. Inlet air temperature governs major parts of the liquid-side (ATF) heat transfer characteristics such as: heat transfer rate, heat transfer coefficient, and Nusselt number. It has dominating effect on flow behaviours such as: Reynolds number, mass flow rate, pressure drops, and friction factor. The lower inlet air temperatures offered higher heat transfer enhancements.
2. In light of how the ATF behaves with temperature, the Nusselt number has been corrected with the viscosity ratio at mean and wall temperatures. The correlations found are:

   Nusselt number before correction with viscosity:

$$Nu_L = 0.016 {Re_L}^{1.10} {Pr_L}^{0.33} \tag{6.1}$$

   Nusselt number after correction with variable property ratio:

$$Nu_{Lc} = 0.009 {Re_L}^{1.25} {Pr_L}^{0.33} \left(\frac{\mu_m}{\mu_w}\right)^{-0.14} \tag{6.2}$$

3. Liquid heat transfer parameters: heat transfer rate, LMTD, convective heat transfer coefficient, Nusselt number, and normalized heat transfer rate are strong functions of liquid Reynolds number. The parameters increase with the increase in liquid Reynolds number and fit power-law correlations.
4. Pressure drops and friction factor increase with the increase in Re_L. The friction factor followed the 'Poiseuille law' when calculated based on constant properties, but upon correction with the variable property ratio, it did not follow the Poiseuille law at lower Re_L. However, it collapsed to the Poiseuille law at higher

Re_L. The Poiseuille number (Po) was found very high in the corrected plot. The correlation established is different from the Poiseuille constant, $f = 64Re$.

The new correlation can be presented as:

$$f_{cort} = 118Re_L^{-1.15}(\mu_m/\mu_w)^{0.50} \quad (6.3)$$

5. The serpentine played no role in developing a new velocity profile and hence no secondary flow developed.
6. From the investigation, some important non-dimensional parameters which are intricately related to viscosity were quantified as: Eckert number $8.087E^{-08} \leq Ec \leq 1.818E^{-04}$ and Brinkman number $2.13E^{-05} \leq N_{Br} \leq 3.33E^{-03}$. Although these quantities are small in magnitude, they implied that ATF contributed to viscous dissipation even for a low Re_L. For quantifying Ec at constant temperature boundary condition with a cooling mode, an empirical correlation has been developed as:

$$Nu = 837Ec^{0.50} \quad (6.4)$$

The correlation for the Brinkman number (N_{Br}) found as:

$$Nu = 19.52N_{Br}^{0.61}Pr^{0.33} \quad (6.5)$$

7. Heat exchanger performances, as evaluated by effectiveness-NTU, decreases with the increase in liquid Reynolds number (Re_L) and capacity rate ratio (Q^*); in contrast, the parameters increase with the increase in air-side Reynolds number (Re_a) in a slower rate. Both factors make a power-law relation with Re_L and C^* as:

$$\varepsilon = 1.03Re_L^{-0.05} \quad (6.6)$$

$$NTU = 4.66Re_L^{-0.22} \quad (6.7)$$

$$\varepsilon = 0.79C^{*(-0.05)} \tag{6.8}$$

$$NTU = 1.405C^{*(-0.24)} \tag{6.9}$$

8. The *NTU* values ranged from 2.25 to 4.00, the effectiveness ranged from 82-98%, and the Capacity rate ratio ranged from 0.016 - 0.129. So the heat exchanger performed at the uppermost margin of economic design. At this condition, the heat exchanger was working almost at its maximum thermal size.
9. For the air side, Reynolds number variation of $1450 \leq Re_a \leq 5250$, the coefficient in air side heat transfer(h_a) and Nusselt number (Nu_a) increased. The higher the liquid side Re_L, the higher these two parameters are.
10. Due to highly viscous fluid and flow limitations in minichannels, the serpentine structure MICHX under investigation can be recommended for the light weight hybrid car transmission cooling because of a high cooling performance.

A significant number of correlations has been established based upon the experimental investigation for heat transfer, fluid flow and MICHX characteristics. These correlations and the information summary might be a useful source for power-train thermal management and system designers. Due to the lack of previous information in the open literature regarding the heat transfer and fluid behaviours of ATF through any kind of heat exchangers, the findings of this study could not be compared to any other research. Based upon the significance of the present research and the information summary, it can be considered as a future reference to the researchers. Additionally, the research outcome might be a valuable source for other research works, and can supplement as an aid to the performance evaluation of heavy equipment and devices used in industries such

as chemical plants, food processing, petro-chemical, and refineries dealing with viscous fluids. It can also be used as a shunt device while testing the performance of heavy equipment in those industries.

6.2 Recommendations

Although every attempt has been made to highlight the most important information observed from the experimental investigation, there is still considerable information in existance that could not be presented. The heat exchanger could not be maintained at its appropriate boundary conditions, yet the observations made from the present study may substantiate the necessity of undertaking future projects and further research in the field of heat transfer and thermo-fluid characterization. Based on the difficulties, constraints, and limitations, the following recommendations can be made for short and long-term future activities:

1. Although a promising heat transfer enhancement has been observed in MICHX for ATF cooling, further research can be extended to investigate the effect of channel diameter to find the optimum channel size that will permit higher mass flow rate for such a highly viscous fluid.
2. The necessity of a thorough investigation in characterizing heat transfer and fluid-flow behaviours of viscous fluids due to the effect of a serpentine has been realized.
3. The temperature distribution and heat transfer phenomena at the upper and lower slabs formed as a result of the curved geometry that creates a counter-flow in liquid can be carefully investigated.

4. In-depth investigation is recommended to quantify the viscous heating inside the channel by maintaining appropriate thermal boundary conditions.
5. Comparatively lower values always appeared in quantifying non-dimensional parameters, especially the Nusselt number (*Nu*), Prandtl number, and the friction factor while using the slab structure parallel-channel geometry. Research on these matters in a broader scale can be conducted to identify the insight of the problems. Axial heat conduction through the liquid and the solid, can be investigated to address such phenomena.
6. An accurate fluid pressure measurement inside the channel is absolutely a difficult task for a serpentine slab structure MICHX. Appropriate instrumentation, such as a high-performance strain gauge, can be implanted at the inlet and outlet of the heat exchanger slab as well as on the serpentine part in order for estimating channel pressure drops.
7. Future projects can be taken to obtain an exact picture of the thermal distribution and temperature profile inside and outside the channel core through a thermal imaging system for better measurement of the local fluid temperatures as well as the surface temperature.
8. The channel outside diameters are always assumed to be circular, although physically they are not. In-depth investigation is required to characterize the geometry of the heat exchanger in terms of heat transfer and temperature distribution.

APPENDICES

APPENDIX A

INSTRUMENT CALIBRATION AND SPECIFICATION

A.1 General Overview

The Integrated Thermal Management and Research Laboratory (ITMRL) in the Department of Mechanical Engineering comprise a plentiful number of instrument and devices. The output of most of the instrument is in the form of voltage. Therefore, it is very important to have the instrument be calibrated or should have enough calibration information of the instrument and devices. The calibration information including other specification of the major instrument and devices are summarized here.

A.1.1 Digital Flow Meter (DFM)

The information of the digital flow meter is given in the following table.

Table A. 1: Digital Flow Meter (DFM)

Features	Specifications
Make	Proteus Instrument
Model:	FLUID-VISION 4000
Power Requirements	24 ± 10% VDC, 200 mA
Flow Rate	0.02 to 60.0 GPM / 0.1 to 227 LPM
Pressure	75, 100, or 250 psi
Temperature	from -40º C to 140º C
Output Voltage	0–5 VDC, 0–10 VDC or 4–20 mA outputs
Accuracy	± 1% Full Scale
Linearity	± 1.5% Full Scale
Repeatability	± 0.50% Full Scale

Although the instrument calibration is viscosity dependent, the viscosity effect on the calibration for different fluids is dominant at higher mass flow rates. In the current study the maximum mass flow rate is under 4 kg/min. So the viscosity will not affect the output voltage and flow rates. A typical calibration curve is shown for the volume flow rates of ATF.

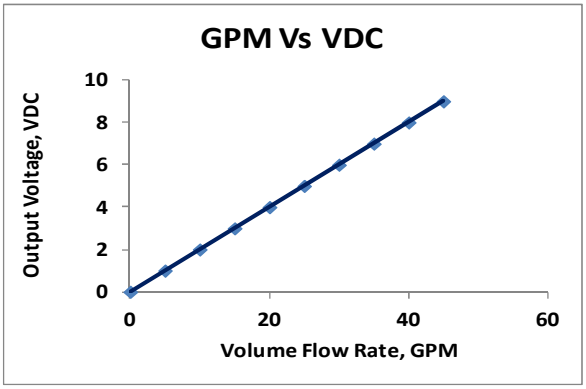

Figure A. 1: DFM Calibration Curve

A.1.2 Impeller Flow Meter (IFM)

The impeller flow meter (IFM) is basically the back up of the DFM and it is installed at the outlet of the liquid flow system through the heat exchanger. The information and the calibration curve are given below.

Table A. 2: Impeller Flow Meter Specification

Features	Specifications
Make	OMEGA
Model:	FPR300
Power Requirements	5-24 Vdc, 2 mA min
Pressure	150 PSI (10 bar)
Temperature	160° F (70° C)
Output Voltage	Current sinking pulse, 6-24 Vdc
Accuracy	+1% of full scale
Response	Linear

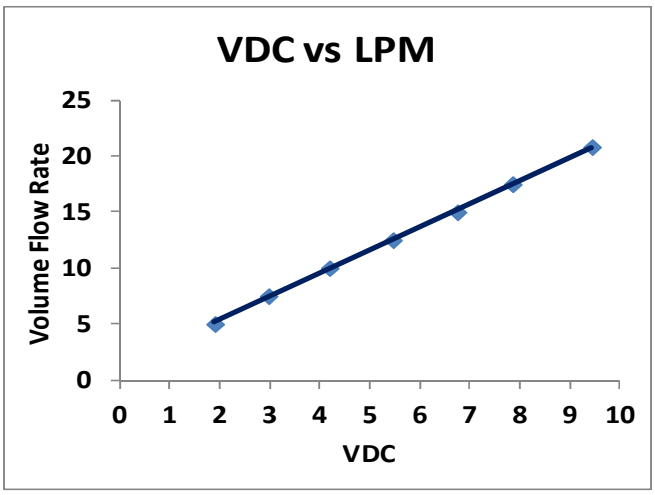

Figure A. 2: IFM Calibration Curve

A.2.1 Pressure Transducer (PTD)

To measure the inlet and outlet pressures of the liquid, pressure transducers are placed just near the inlet to the test specimen and just at the outlet manifold. The outputs of the PTDs are in terms of voltage. So it needs to be calibrated to get the exact pressure. The output pressures of the PTDs have a fair linear relation with output voltage. The system was run and some data were collected to check the calibration. After plotting the data the curve showed good agreement with the company supplied calibration curve. The specification and the calibration information are shown below.

A.2.2 Liquid inlet Pressure Transducer

The calibration curve and the instrumental information are given below;

Table A. 3: Liquid inlet Pressure Transducer Specification

Features	Specifications
Make	OMEGA
Model:	PX 309

Power Requirements	24 ± 5 VDC
Output Voltage	0 to 5 Vdc or 0 to 10 Vdc
Pressure	0-500 pis
Temperature	-40 to 85°C (-40 to 185°F)
Accuracy	±0.25% FS BSL at 25ºC; includes linearity, hysteresis and repeatability
Response Time	<1 ms
Compensated Temperature	0 to 50°C (32 to 122°F) for 5 psi range
Proof Pressure	300% or 20psi, for <50 psig range
Burst Pressure	500% of capacity or 25 psi

Pressure Transducer	Application	Measuring Limit	Range, R1	Output votage	Voltage range, R2	Equipment Sensitivity (Multiplication factor), R1/R2
PX309	Liquid	0- 500 psig	500	0-5	5	100

VDC out	PSI	kpa
0.152	15.234	105.037
0.275	27.468	189.394
0.431	43.081	297.046
0.659	65.924	454.547
0.949	94.878	654.186
1.061	106.143	731.856

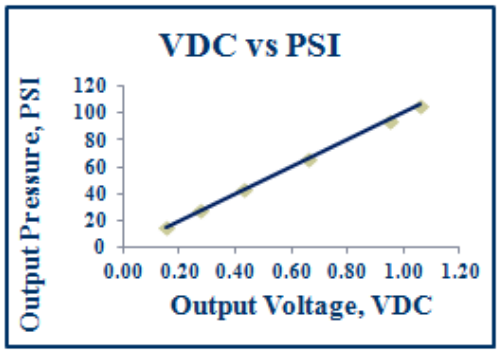

Figure A. 3: PTD inlet Calibration data and Curve

A.2.3 Liquid outlet Pressure Transducer

The calibration curve and the instrumental information are given below:

Table A. 4: Liquid outlet Pressure Transducer specification

Features	Specifications
Make	OMEGA
Model:	PX 309
Power Requirements	24 ± 5 VDC
Output Voltage	0 to 5 Vdc
Pressure	0-50 psi
Temperature	-40 to 85°C (-40 to 185°F)
Accuracy	±0.25% FS BSL at 25ºC; includes linearity, hysteresis and repeatability
Response Time	<1 ms

Pressure Transducer	Application	Measuring Limit	Range, R1	Output votage	Voltage range, R2	Equipment Sensitivity (Multiplication factor), R1/R2
PX309	Liquid	0-50 psig	50	0-5	5	10

VDC out	PSI	kpa
0.152	1.523	10.504
0.275	2.747	18.939
0.431	4.308	29.705
0.659	6.592	45.455
0.949	9.488	65.419
1.061	10.614	731.856

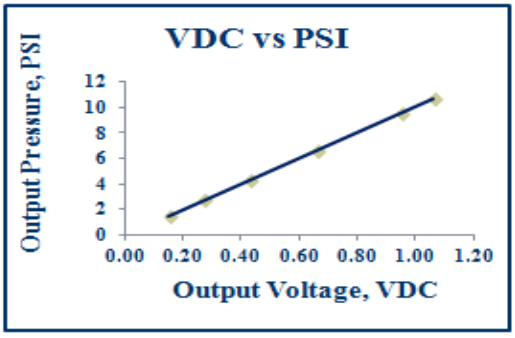

Figure A. 4: PTD Outlet Calibration data and Curve

A.2.4 Gas Differential Pressure Transducer (DPTD)

The differential pressure transducers read the pressure difference between the upstream and downstream pressure of the heat exchanger in the test chamber. The detailed of the

locations and the functionalities were explained in section 4.2.B.5. The calibration information of the DPTDs is explained here.

A.2.5 Test Chamber Middle Location DPTD

The DPTD which is connected to the DAQ, channel P-327, records the middle differential pressure while the other one is connected to the pitot static tube, DAQ channel P-325. Both are same in specification which is given below.

Table A. 5: Test Chamber Middle Location DPTD Specification

Features	Specifications
Make	OMEGA
Model:	PX277
Power Requirements	12 to 35 Vdc
Output Voltage	0 to 5 or 0 to 10 Vdc selectable
Proof Pressure	10 psi
Temperature	-18 to 80°C (0 to 175°F)
Compensated Temp	-4 to 65°C (25 to 150°F)
Media Compatibility	Clean dry air or inert gas
Accuracy	± 1% Full Scale

Pressure Transducer	Application	Measuring Limit	Range, R1	Output votage	Voltage range, R2	Equipment Sensitivity (Multiplication factor), R1/R2	Remarks
PX277	Gas	0-5 " H2O	5	0-10	10	0.5	Middle

Voltage, VDC (in)	H2O Height	Pressure, psig	Pressure, Kpa
0.560	0.280	0.010	0.070
1.205	0.602	0.022	0.150
2.086	1.043	0.038	0.260
3.052	1.526	0.055	0.380
4.304	2.152	0.078	0.536

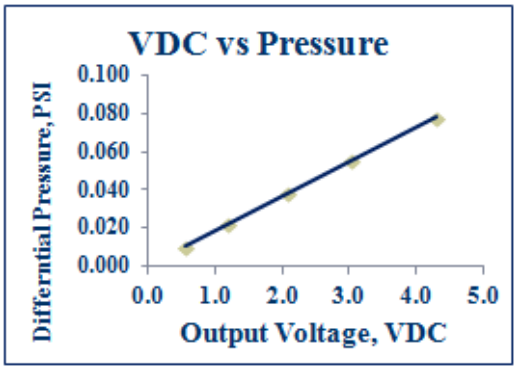

Figure A. 5: DPTD Middle Location Calibration data and Curve

Pressure Transducer	Application	Measuring Limit	Range, R1	Output votage	Voltage range, R2	Equipment Sensitivity (Multiplication factor), R1/R2	Remarks
PX277	Gas	0-1 " H2O	1	0-5	5	0.2	Pitot-Static Tube

Data analysis, PX277 Pitot			
Voltage, VDC (in)	H2O Height	Pressure, psig	Pressure, Kpa
0.163	0.033	0.001	0.008
0.542	0.108	0.004	0.027
1.123	0.225	0.008	0.056
1.825	0.365	0.013	0.091
2.803	0.561	0.020	0.140

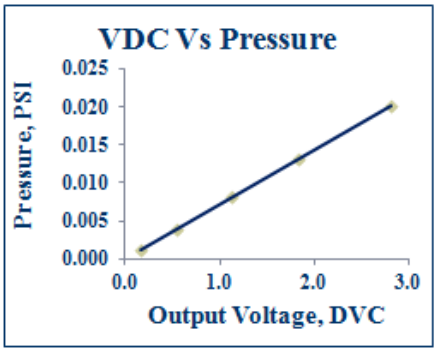

Figure A. 6: DPTD Pitot Static Calibration data and Curve

A.2.6 Test Chamber Top Location DPTD

Among the two PX653 series DPTDs, one is connected to record the top portion pressure drops and the other one record the lower portion pressure drops in the test section. The

transducer shows linear relation with the output voltage and fair relation with the supplied calibration information. The detail specification is given below.

Table A. 6: Test Chamber Top Location DPTD Specification

Features	Specifications
Make	OMEGA
Model:	PX 653
Power Requirements	12 to 36 Vdc
Output Voltage	1 to 5 Vdc (3 wire)
Proof Pressure	15 psi
Burst Pressure	20 psi
Operating Temperature	-29 to 72°C (-20 to 160°F)
	Linearity: 0.3%, Hysteresis: 0.02%, Repeatability: 0.05%
Response Time	250 ms

Pressure Transducer	Application	Measuring Limit	Range, R1	Output votage	Voltage range, R2	Equipment Sensitivity (Multiplication factor), R1/R2	Remarks
PX653	Gas	0-2 "H2O	2	1-5)	4	0.5	Bottom

Data analysis, PX653 Bottom			
Voltage, VDC (in)	H2O Height	Pressure, psig	Pressure, Kpa
1.341	0.671	0.024	0.167
1.778	0.889	0.032	0.221
2.359	1.179	0.043	0.294
2.997	1.498	0.054	0.373
3.825	1.912	0.069	0.476

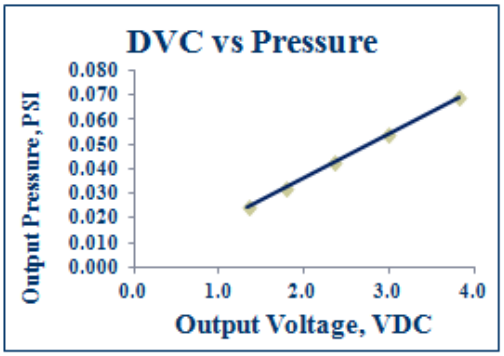

Figure A. 7: DPTD at Bottom Location Calibration Data and Curve

A.3.1Thermal Conductivity

The thermal conductivity linearly changes downwards similar to that of density. Thermal conductivity of ATF was not tested in the laboratory; rather necessary data have been extracted from the SAE technical paper to fulfill the requirement [31]. The thermal conductivity of ATF decreases very slowly with increasing temperature. In Figure 6.3 the plot shows that, with the change in temperature from 0-150^{o}C, the conductivity changes only 0.022 w/m-k. For the current investigation, conductivity does not play a significant role in heat transfer characterization. The temperature difference (ΔT) of ATF occurred within $26 \geq \Delta T \geq 60^{o}$C. For this change in ΔT, the conductivity did not have significant effects on heat transfer contribution due to the small values.

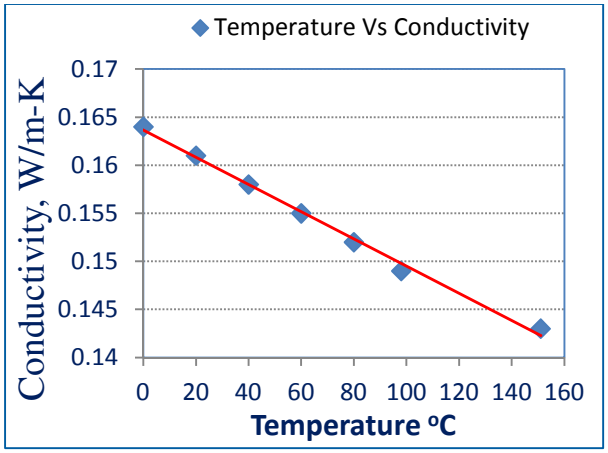

Figure A. 8: Thermal Conductivity Variation with Temperature Change

A.3.2 Specific Heat Capacity (C_p)

Although some of the ATF thermo-physical properties decrease with increasing temperature, specific heat capacity increases with the increase in temperature. This is only the property which increases with temperature increase. The increment with

temperature is linear. This property was not tested in the laboratory. The data have been extracted from the same SAE technical paper [31]. For a 150°C temperature difference (ΔT) in ATF, the Specific heat capacity (C_p) changes only 0.55 KJ/kg-K.

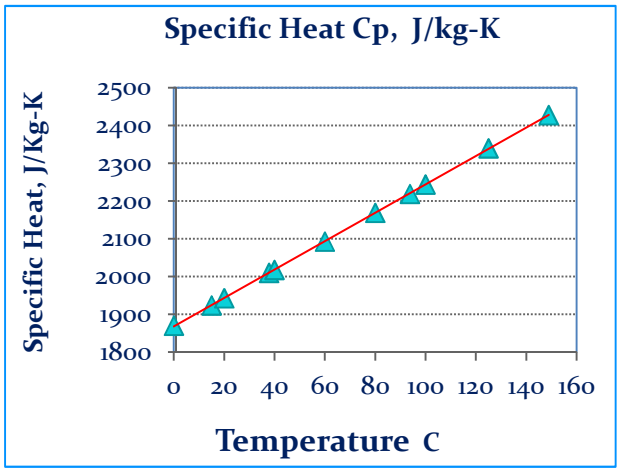

Figure A. 9: Specific Heat capacity (C_p) Variation with Temperature Change

APPENDIX B

UNCERTAINTY ANALYSIS

In the current study a considerable number of data were collected for both fluids. Numbers of instruments and devices were used for the experiments. Also a significant number of formulae were applied to compute and analyze data sets for achieving research objectives. During the use of such instruments, there were chances of the instrumental errors that might lead to some deviation from the actual values. Similarly progressive error could happen due to the use of measured data in the analysis while applying for some particular formula. Therefore, the intensity of the error should be taken into account for better understanding of the closeness to the accuracy in findings.

The scope of calculating uncertainties include the instrumental uncertainties, such as errors in the form of bias, accuracy, linearity, hysteresis and repeatability, precision etc., which are given by the manufacturers. The instruments which are involved in such errors are explained in chapter-4. The formula used for data reduction and analysis may be considered another source of errors. These formulae are outlined in chapter-3. The uncertainty of such sources is summarized in this section.

Mainly two types, dependent and independent variables are account for such errors. In the current study, both variables are identified. The variables or the parameters which are directly measured or recorded during the data acquisition are the independent variables. The dependent variables are the function of the independent parameters based on which the subsequent calculations are done. The Reynolds number, Prandtl number, Nusselt number, liquid velocity, heat transfer rate, these are the dependent parameters.

The following expression can be attributed to show the relationship between the dependent and the independent variables.

$$Y = f(X_1, X_2, X_3, \dots, X_n) \tag{B.1}$$

Xs are the independent variables. The basic principle of computing such errors is the Root Sum Squire (RSS) method. The methods of calculating uncertainties are explained below:

B.1 Bias

The Bias error can be computed using the Root Sum Square (RSS) method as:

$$U_B = \pm\sqrt{{B_1}^2 + {B_2}^2 + \cdots + {B_n}^2} \tag{B.2}$$

B.2 Precision

Precision error can be calculated as:

$$U_P = \pm\sqrt{{P_1}^2 + {P_2}^2 + \cdots + {P_n}^2} \tag{B.3}$$

B.3 Repeatability

The errors from a device or instrument can be estimated as:

$$U_R = \pm\sqrt{{R_1}^2 + {R_2}^2 + \cdots + {R_n}^2} \tag{B.4}$$

The combined error due to bias, precision, and repeatability using the RSS method can be shown as:

$$U_X = \pm\sqrt{B^2 + P^2 + R^2} \tag{B.5}$$

B.4 Uncertainty in Independent Variables

The uncertainty in an independent variable can be expressed in terms of absolute and relative uncertainties. For an example uncertainty due to bias and precision may be calculated in these two forms of expressions. If a single point is measured by an instrument and X an arbitrary measurement, for bias and precision the following expressions can be used.

Absolute uncertainty: $$U_{XBP} = \sqrt{B^2 + P^2} \tag{B.6}$$

Relative uncertainty: $$\frac{U_{XBP}}{X} = \sqrt{\frac{B^2+P^2}{X^2}} \tag{B.7}$$

B.5 Uncertainty in Dependent Variables

The uncertainty of the dependent parameters can be computed as a combination of the individual error as:

$$U_Y = \sqrt{\left(\frac{\partial Y}{\partial X_1}U_{X_1}\right)^2 + \left(\frac{\partial Y}{\partial X_2}U_{X_2}\right)^2 + \left(\frac{\partial Y}{\partial X_3}U_{X_3}\right)^2 + \left(\frac{\partial Y}{\partial X_n}U_{X_n}\right)^2} \tag{B.8}$$

If an arbitrary variable 'W' is considered, the relative uncertainty can be expressed as;

$$\frac{U_y}{W_x} = \sqrt{\frac{\left(\frac{\partial Y}{\partial X_1}U_{X_1}\right)^2+\left(\frac{\partial Y}{\partial X_2}U_{X_2}\right)^2+\left(\frac{\partial Y}{\partial X_3}U_{X_3}\right)^2+\left(\frac{\partial Y}{\partial X_n}U_{X_n}\right)^2}{\{W=f(W_1,W_2,W_3,\ldots\ldots,W_n)\}^2}} \tag{B.9}$$

The uncertainty of a parameter can be represented in the form of an absolute value as $Y \pm U_Y$.

$$Y \pm U_Y = Y \pm \sqrt{\left(\frac{\partial Y}{\partial X_1}U_{X_1}\right)^2 + \left(\frac{\partial Y}{\partial X_2}U_{X_2}\right)^2 + \left(\frac{\partial Y}{\partial X_3}U_{X_3}\right)^2 + \left(\frac{\partial Y}{\partial X_n}U_{X_n}\right)^2} \tag{B.10}$$

B.6 Uncertainty in Thermo-physical properties

The thermo-physical properties of the fluid such as viscosity, specific heat, density, and conductivity were taken at the liquid bulk temperature from property table or curves. In such cases, the uncertainties are considered as bias. Or calculating error, the maximum and minimum values are usually considered. The uncertainty of the maximum and minimum values at bulk temperatures can be calculated as:

$$U_{prop,fluid} = \frac{1}{2}\{[Fluid_{prop,}\, T_{b,max}] - [Fluid_{prop,}\, T_{b,min}]\} \tag{B.11}$$

B.6.1 Uncertainty in the Liquid Side Temperatures

To measure the inlet and the outlet temperatures of ATF, RTDs were used. From the available data obtained from the sources supplied by the equipment manufacturers and on-site measurements during experiments, the following formula can be used:

$$U_T = \pm\sqrt{\left[\frac{6.033\times10^{-6}}{3.908\times10^{-5}-1.16038\times10^{-8}|T|}\right]^2 + \left[\frac{1}{10}(0.3+0.005|T|)\right]^2 + \left[1.96\frac{S_{RTD,T}}{\sqrt{N}}\right]^2} \tag{B.12}$$

B.6.2 Bulk Temperature

The bulk temperature of the ATF can be calculated as:

$$T_b = \frac{T_i+T_o}{2} \tag{B.13}$$

And its uncertainty is found as:

$$U_{T_b} = \pm\sqrt{\left(\frac{\partial T_b}{\partial T_i}U_{T_i}\right)^2 + \left(\frac{\partial T_b}{\partial T_o}U_{T_o}\right)^2} \tag{B.14}$$

$$\frac{\partial T_b}{\partial T_i} = \frac{1}{2} \tag{B.15}$$

$$\frac{\partial T_b}{\partial T_o} = \frac{1}{2} \tag{B.16}$$

B.6.3 Uncertainty in the Liquid Side Density

The uncertainty of the ATF density can be found as:

$$U_\rho = \frac{1}{2}\left|\left[\rho@T_{b,max}\right] - \left[\rho@T_{b,min}\right]\right| \tag{B.17}$$

B.6.4 Uncertainty in the Liquid Side Specific Heat

The uncertainty of the ATF specific heat can be found as follows:

$$U_{c_p} = \frac{1}{2}\left|\left[c_p@T_{b,max}\right] - \left[c_p@T_{b,min}\right]\right| \tag{B.18}$$

B.6.5 Uncertainty Related to the Liquid Mass Flow Rate

The mass flow rate of ATF can be calculated as:

$$\dot{m}_L = \dot{\forall}_L \rho_L \tag{B.19}$$

$$\frac{\partial \dot{m}_L}{\partial \rho_L} = \dot{\forall}_L \tag{B.20}$$

$$\frac{\partial \dot{m}_L}{\partial \dot{\forall}_L} = \rho_L \tag{B.21}$$

The overall uncertainty of the liquid mass flow rate is:

$$U_{\dot{m}_L} = \pm\sqrt{\left[\frac{\partial \dot{m}_L}{\partial \rho_L} U_{\rho_L}\right]^2 + \left[\frac{\partial \dot{m}_L}{\partial \dot{\forall}_L} U_{\dot{\forall}_L}\right]^2} \tag{B.22}$$

B.6.6 Uncertainty in the Liquid Reynolds Number

The Reynolds number of ATF depends on it mass flow rate, viscosity, density, and channel geometry. It can be expressed as:

$$Re_L = \frac{\dot{m}_L}{51\pi\mu_L D} \tag{B.23}$$

$$\frac{\partial Re_L}{\partial \dot{m}_L} = \frac{1}{51\pi\mu_L D} \tag{B.24}$$

$$\frac{\partial Re_L}{\partial \mu_L} = -\frac{\dot{m}_L}{51\pi\mu_L D} \tag{B.25}$$

$$\frac{\partial Re_L}{\partial D} = -\frac{\dot{m}_L}{51\pi\mu_L D^2} \tag{B.26}$$

The resultant uncertainty associated with ATF Reynolds number can be shown as:

$$U_{Re_L} = \pm\sqrt{\left[\frac{\partial Re_L}{\partial \dot{m}_L}U_{\dot{m}_L}\right]^2 + \left[\frac{\partial Re_L}{\partial \mu_L}U_{\mu_L}\right]^2 + \left[\frac{\partial Re_L}{\partial D}U_D\right]^2} \tag{B.27}$$

B.6.7 Uncertainty in the liquid Heat Transfer Rate

The glycol heat transfer rate depends on the liquid mass flow rate, temperature difference between the inlet and the outlet, and the specific heat.

$$\dot{Q}_g = \dot{m}_L c_p\left(T_{g,i} - T_{g,o}\right) \tag{B.28}$$

$$\frac{\partial \dot{Q}_L}{\partial \dot{m}_L} = c_p \Delta T_g \tag{B.29}$$

$$\frac{\partial \dot{Q}_L}{\partial c_p} = \dot{m}_L \Delta T_L \tag{B.30}$$

$$\frac{\partial \dot{Q}_L}{\partial \Delta T_L} = c_p \dot{m}_L \tag{B.31}$$

$$U_{\dot{Q}_L} = \pm\sqrt{\left[\frac{\partial \dot{Q}_L}{\partial \dot{m}_L}U_{\dot{m}_L}\right]^2 + \left[\frac{\partial \dot{Q}_L}{\partial c_p}U_{c_p}\right]^2 + \left[\frac{\partial \dot{Q}_L}{\partial \Delta T_L}U_{\Delta T_L}\right]^2} \tag{B.32}$$

B.7.1 Uncertainty in the Airside Temperatures

For air temperature measurement, 2 grids were used; one at the inlet and the other at the outlet. The thermocouples are well calibrated, so no significance effect on the uncertainty calculation. Yet some errors need to be considered.

The bias error from the thermocouples is assumed to be 0.1℃.

$$B_1 = 0.1℃ \tag{B.33}$$

There is no precision error due to the instrumentation since they only deal with the design stage uncertainty. The precision error from the number of samples, N=180000~240000 and can be accounted as:

$$P_2 = \frac{S_T}{\sqrt{M}} B_1 = 0.1℃ \tag{B.34}$$

Where,

$$S_T = \sqrt{\frac{\sum_{m=1}^{M} (\bar{T}_m - \langle \bar{T} \rangle)^2}{M-1}} \tag{B.35}$$

$$\bar{T}_m = \frac{1}{N} \sum_{n=1}^{N} T_{mn} \tag{B.36}$$

$$\langle \bar{T} \rangle = \frac{1}{M} \sum_{m=1}^{M} \bar{T}_m \tag{B.37}$$

$$v_2 = M - 1 \tag{B.38}$$

S_T: The standard deviation of each thermocouple at the inlet and outlet

$\bar{T}_m$: Mean of the samples number for a specific thermocouple

v_2: Degree of freedom

$\langle \bar{T} \rangle$: The mean of each thermocouples reading at the inlet and outlet

The precision error from the temporal variation is:

$$P_3 = \frac{(S_p)}{\sqrt{MN}} \tag{B.39}$$

Where,

$$S_p = \sqrt{\frac{\sum_{m=1}^{9}\sum_{n=1}^{N}(\bar{T}_{mn}-\langle\bar{T}\rangle)^2}{M(N-1)}} \tag{B.40}$$

$$v_3 = M(N-1) \tag{B.41}$$

S_p: The pooled standard deviation of all the thermocouple and samples

v_3: Degree of freedom

The degree of freedom used with the precision error is found using Welch-Satterthwaite (W-S) method as:

$$v = \frac{\left(\sum_{i=1}^{3} P_i^2\right)^2}{\sum_{i=1}^{3}\left(\frac{P_i^4}{v_i}\right)} = \frac{\left(P_2^2+P_3^2\right)^2}{\frac{P_2^4}{v_2}+\frac{P_3^4}{v_3}} \tag{B.42}$$

$$t_{v,95} = 1.96\ (N > 1000) \tag{B.43}$$

The total uncertainty associated with the thermocouples reading includes the bias and the precision error, and it is found using the RSS method as:

$$U_{thermocouples} = \pm\sqrt{B^2 + \left(t_{v,95}P\right)^2} \tag{B.44}$$

To convert the voltage reading of the thermocouples to a ℃ reading, and include it with the uncertainty calculation, the sensitivity is found as:

$$\frac{\partial V}{\partial T}_{thermocouple} = 43 \times 10^{-6}\,\frac{V}{℃} \tag{B.45}$$

$$U_{DAQ} = \pm\frac{6.033\times10^{-6}V}{\frac{\partial V}{\partial T}_{thermocouple}} = \frac{6.033\times10^{-6}\text{V}}{43\times10^{-6}\text{V/℃}} = 0.14℃ \tag{B.46}$$

The total uncertainty is:

$$U_{T_a} = \pm\sqrt{U_{DAQ}^2 + U_{thermocouple}^2} \tag{B.47}$$

The mean temperature of the air inlet-outlet temperatures can be given as:

$$T_{a,b} = \frac{T_{a,i}+T_{a,o}}{2} \tag{B.48}$$

$$U_{T_{a,b}} = \pm\sqrt{\left(\frac{\partial T_{a,b}}{\partial T_{a,i}} U_{T_{a,i}}\right)^2 + \left(\frac{\partial T_{a,b}}{\partial T_{a,o}} U_{T_{a,o}}\right)^2} \tag{B.49}$$

Where,

$$\frac{\partial T_{a,b}}{\partial T_{a,i}} = \frac{1}{2} \tag{B.50}$$

$$\frac{\partial T_{a,b}}{\partial T_{a,o}} = \frac{1}{2} \tag{B.51}$$

B.7.2 Uncertainty in the Air Reynolds Number

The expression of the Reynolds number for air can be expressed as:

$$Re_a = \frac{G_a D_{h,a}}{\mu_a} \tag{B.52}$$

Where G_a is the air-mass velocity and can be calculated as:

$$G_a = \frac{\dot{m}_a}{A_{a,min}} \tag{B.53}$$

$$\frac{\partial G_a}{\partial \dot{m}_a} = \frac{1}{A_{a,min}} \tag{B.54}$$

$$\frac{\partial G_a}{\partial A_{a,min}} = -\frac{\dot{m}_a}{(A_{a,min})^2} \tag{B.55}$$

The uncertainty of the mass velocity can be found as follows:

$$U_{G_a} = \pm\sqrt{\left[\frac{\partial G_a}{\partial \dot{m}_a} U_{\dot{m}_a}\right]^2 + \left[\frac{\partial G_a}{\partial A_{min,a}} U_{A_{min,a}}\right]^2} \tag{B.56}$$

Therefore, the uncertainty of air can be calculated as:

$$\frac{\partial Re_a}{\partial G_a} = \frac{D_{h,a}}{\mu_a} \tag{B.57}$$

$$\frac{\partial Re_a}{\partial D_{h,a}} = \frac{G_a}{\mu_a} \tag{B.58}$$

$$\frac{\partial Re_a}{\partial \mu_a} = -\frac{G_a D_{h,a}}{{\mu_a}^2} \tag{B.59}$$

$$U_{Re_a} = \pm\sqrt{\left[\frac{\partial Re_a}{\partial G_a} U_{G_a}\right]^2 + \left[\frac{\partial Re_a}{\partial D_{h,a}} U_{D_{h,a}}\right]^2 + \left[\frac{\partial Re_a}{\partial \mu_a} U_{\mu_a}\right]^2} \tag{B.60}$$

B.7.3 Uncertainty in the Air Heat Transfer Rate

$$\dot{Q}_a = \dot{m}_a c_p \left(T_{a,o} - T_{a,i}\right) \tag{B.61}$$

$$\frac{\partial \dot{Q}_a}{\partial \dot{m}_a} = c_p \Delta T_a \tag{B.62}$$

$$\frac{\partial \dot{Q}_a}{\partial c_p} = \dot{m}_a \Delta T_a \tag{B.63}$$

$$\frac{\partial \dot{Q}_a}{\partial \Delta T_a} = c_p \dot{m}_a \tag{B.64}$$

$$U_{\dot{Q}_a} = \pm\sqrt{\left[\frac{\partial \dot{Q}_a}{\partial \dot{m}_a} U_{\dot{m}_a}\right]^2 + \left[\frac{\partial \dot{Q}_a}{\partial c_p} U_{c_p}\right]^2 + \left[\frac{\partial \dot{Q}_a}{\partial \Delta T_a} U_{\Delta T_a}\right]^2} \tag{B.65}$$

B.8 Uncertainty in the Average Heat Transfer Rate

The heat transfer rate can be found from the following relationship:

$$\dot{Q} = \frac{\dot{Q}_L + \dot{Q}_a}{2} \tag{B.66}$$

$$\frac{\partial \dot{Q}}{\partial \dot{Q}_L} = \frac{1}{2} \tag{B.67}$$

$$\frac{\partial \dot{Q}}{\partial \dot{Q}_a} = \frac{1}{2} \tag{B.68}$$

$$U_{\dot{Q}} = \pm\sqrt{\left[\frac{\partial \dot{Q}}{\partial \dot{Q}_L} U_{\dot{Q}_L}\right]^2 + \left[\frac{\partial \dot{Q}}{\partial \dot{Q}_a} U_{\dot{Q}_a}\right]^2} \tag{B.69}$$

B.9 Uncertainty in Effectiveness

The effectiveness of a heat exchanger depends on the average heat transfer rate, liquid mass flow rate, and the inlet temperatures difference of the two fluids. Effectiveness can be expressed as:

$$\varepsilon = \frac{\dot{Q}}{\dot{Q}_{max}} \tag{B.70}$$

$$\varepsilon = \frac{\dot{Q}}{(\dot{m}c_p)_{min}(T_{g,i}-T_{a,i})} \tag{B.71}$$

$$\frac{\partial \varepsilon}{\partial \dot{Q}} = \frac{1}{\dot{m}_L c_p (T_{g,i}-T_{a,i})} \tag{B.72}$$

$$\frac{\partial \varepsilon}{\partial \dot{m}_L} = -\frac{\dot{Q}}{\dot{m}_L{}^2 c_p (T_{g,i}-T_{a,i})} \tag{B.73}$$

$$\frac{\partial \varepsilon}{\partial c_p} = -\frac{\dot{Q}}{\dot{m}_L c_p{}^2 (T_{g,i}-T_{a,i})} \tag{B.74}$$

$$\frac{\partial \varepsilon}{\partial T_{L,i}} = -\frac{\dot{Q}}{\dot{m}_L c_p (T_{L,i}-T_{a,i})^2} \tag{B.75}$$

$$\frac{\partial \varepsilon}{\partial T_{a,i}} = \frac{\dot{Q}}{\dot{m}_L c_p (T_{L,i}-T_{a,i})^2} \tag{B.76}$$

Therefore, the total uncertainty in effectiveness is:

$$U_\varepsilon = \pm \sqrt{\begin{matrix}\left[\frac{\partial \varepsilon}{\partial \dot{Q}} U_{\dot{Q}}\right]^2 + \left[\frac{\partial \varepsilon}{\partial \dot{m}_L} U_{\dot{m}_L}\right]^2 + \left[\frac{\partial \varepsilon}{\partial c_p} U_{c_p}\right]^2 \\ + \left[\frac{\partial \varepsilon}{\partial T_{L,i}} U_{T_{L,i}}\right]^2 + \left[\frac{\partial \varepsilon}{\partial T_{a,i}} U_{T_{a,i}}\right]^2\end{matrix}} \tag{B.77}$$

B.10 Uncertainty in the Heat Capacity Rate Ratio

The capacity rate ratio can be expressed as:

$$C^* = \frac{\dot{m}_L c_{p_g}}{\dot{m}_L c_{p_a}} \tag{B.78}$$

$$\frac{\partial C^*}{\partial \dot{m}_L} = \frac{c_{p_g}}{\dot{m}_a c_{p_a}} \tag{B.79}$$

$$\frac{\partial C^*}{\partial c_{p_L}} = \frac{\dot{m}_L}{\dot{m}_a c_{p_a}} \tag{B.80}$$

$$\frac{\partial C^*}{\partial \dot{m}_a} = -\frac{\dot{m}_L c_{p_g}}{(\dot{m}_a)^2 c_{p_a}} \tag{B.81}$$

$$\frac{\partial C^*}{\partial c_{p_a}} = -\frac{\dot{m}_L c_{p_g}}{\dot{m}_a \left(c_{p_a}\right)^2} \tag{B.82}$$

The total uncertainty is:

$$U_{C^*} = \sqrt{\left[\frac{\partial C^*}{\partial \dot{m}_L} \times U_{\dot{m}_L}\right]^2 + \left[\frac{\partial C^*}{\partial c_{p_L}} \times U_{c_{p_L}}\right]^2 + \left[\frac{\partial C^*}{\partial \dot{m}_a} \times U_{\dot{m}_a}\right]^2 + \left[\frac{\partial C^*}{\partial c_{p_a}} \times U_{c_{p_a}}\right]^2} \tag{B.83}$$

y (C_p) Variation with Temperature Change

B.11Example of Calculating Uncertainty

Some examples of the important parameters are shown below:

B.11.1 Uncertainty in ATF Reynolds Number

$$Re_L = \frac{\dot{m}_L}{51\pi\mu_L D} \tag{B.23}$$

From the experimental data:

$$\frac{\partial Re_L}{\partial \dot{m}_L} = \frac{1}{51\pi\mu_L D} = 1/(51*\pi*0.02*0.001) = 312 \tag{B.24}$$

$$\frac{\partial Re_L}{\partial \mu_L} = -\frac{\dot{m}_L}{51\pi\mu_L D} = 0.0351/(51*\pi*0.02\text{^}2*0.001) = 547 \tag{B.25}$$

$$\frac{\partial Re_L}{\partial D} = -\frac{\dot{m}_L}{51\pi\mu_L D^2} = 0.0351/(51*\pi*0.02*(0.001)\text{^}2) = 10953 \tag{B.26}$$

The resultant uncertainty associated with ATF Reynolds number can be calculated as:

$$U_{Re_L} = \pm\sqrt{\left[\frac{\partial Re_L}{\partial \dot{m}_L} U_{\dot{m}_L}\right]^2 + \left[\frac{\partial Re_L}{\partial \mu_L} U_{\mu_L}\right]^2 + \left[\frac{\partial Re_L}{\partial D} U_D\right]^2} \tag{B.27}$$

$$U_{Re_L} = \pm\sqrt{[312 * 0.03015]^2 + [547 * 0.00096]^2 + [10953 * 0.0000348]^2}$$

$= \pm 0.727$

The relative Uncertainty can be calculated as:

$$\frac{U_{Re_L}}{Re_L} * 100 = \pm \frac{0.727}{7.132} * 100 = 10.19\%$$

B.11.2 Uncertainty in ATF Prandtl Number

$$Pr_L = \frac{\mu C_p}{k}$$

$$U_{Pr_L} = \sqrt{\left(\frac{\partial Pr}{\partial \mu} U_\mu\right)^2 + \left(\frac{\partial Pr}{\partial C_p} U_{C_p}\right)^2 + \left(\frac{\partial Pr}{\partial k} U_k\right)^2}$$

$$\frac{\partial Pr}{\partial \mu} = \frac{C_p}{k} = 13182$$

$$\frac{\partial Pr}{\partial C_p} = \frac{\mu}{k} = 0.128$$

$$\frac{\partial Pr}{\partial k} = -\frac{\mu C_p}{k^2} = -695$$

$$U_\mu = -0.00096$$

$$U_{C_p} = 3.49$$

$$U_k = -0.00014$$

$$U_{Pr_L} = \sqrt{(13182 * -0.00096)^2 + (0.128 * 3.49)^2 + (-695 * -0.00014)^2}$$

$$U_{Pr_L} = \pm 12.6$$

The relative uncertainty of the Prandtl is:

$$\frac{U_{Pr_L}}{Pr_L} * 100 = \frac{12.6}{518} * 100 = 2.43\%$$

B.11.3 Uncertainty in ATF Nusselt Number

The Nusselt number can be calculated as:

$$Nu_L = \frac{h_L D_h}{k}$$

The uncertainty can be calculated as:

$$U_{Nu_L} = \pm\sqrt{\left(\frac{\partial Nu_L}{\partial h_L} * U_{h_L}\right)^2 + \left(\frac{\partial Nu_L}{\partial D_h} * U_{D_h}\right)^2 + \left(\frac{\partial Nu_L}{\partial k} * U_k\right)^2}$$

$$\frac{\partial Nu_L}{\partial h_L} = \frac{D_h}{k} = 0.00641$$

$$\frac{\partial Nu_L}{\partial D_h} = \frac{h_L}{k} = 867$$

$$\frac{\partial Nu_L}{\partial k} = -\frac{h_L D_h}{k^2} = 5.56$$

$$U_{Nu_L} = \pm\sqrt{(0.00641 * 12.76)^2 + (867 * 0.0000348)^2 + (5.56 * -0.00014)^2}$$

$$U_{Nu_L} = 0.088$$

The relative uncertainty is:

$$\frac{U_{Nu_L}}{Nu_L} * 100 = \frac{0.088}{0.868} * 100 = 10.11\%$$

B.12 Uncertainty of the instrument and devices used

All the laboratory instruments and devices used in the present experiment were previously used by some researchers. All of them estimated uncertainties for those equipments in details.

Khan, M. G., (2011) used this laboratory for long time for his PhD research and calculated uncertainties of all the equipment he used. He presented these uncertainties in his thesis and published literatures [55]. Al-Obaidi S (2011), Dasgupta, E. S, (2011), and Siddiqui, F. A., (2011) used this laboratory for their M A Sc research works. They

estimated uncertainties for all the equipment and devices including data acquisition system [8, 67, 70].

In the current investigation, same laboratory instrument and devices were used. So, the uncertainties were taken from those works for data analysis to avoid repetition of similar works. The uncertainties are given below:

Table B. 1: Uncertainties of Key Parameters Related to the MICHX

Dimensional Parameters	**Brief description of the parameters**	**Numerical value**	**Uncertainty %**
L_{slab}	Length of a single slab participating in heat transfer	0.304 m	± 0.15
W_{slab}	Width of a single slab participating in heat transfer	0.100 m	± 0.20
T_{slab}	Thickness of a single slab participating in heat transfer and containing the channels	0.002 m	± 0.50
N_{fin}	No. of fins per slab	144	± 0.30
N_{slab}	Total No. of slab	15	
H_{hx}	Height of the Heat Exchanger	0.287 m	± 0.25
A_{fin}	Total Heat transfer Area of the fins	7.771 m^2	± 0.45
$A_{front,\ fin\ \&\ slab}$	Area of fin & slab that blocks the air flow	1.587×10^{-2}	± 6.79
A_{front}	Frontal Area of the Heat Exchanger $A_{front} = L_{slab}$ X H_{hx}	8.748×10^{-2} m^2	± 0.29
A_{slab}	Combined total area of only the slabs participating in heat transfer for the whole heat exchanger due to air flow.	0.834 m^2	± 1.55

Table B. 2: DAQ System and Measured Parameters

Dimensional Parameters	**Numerical value**	**Uncertainty %**
Data acquisition Card	$3.025\times10^{(-6)}$	$\pm3.025\times10^{(-4)}$
Signal Conditioning	$5.22\times10^{(-6)}$	$\pm5.22\times10^{(-4)}$
Data acquisition System	$6.033\times10^{(-6)}$	$\pm6.033\times10^{(-4)}$
Digital Flow meter	±0.020615 FS	±2.0615 FS
RTD	0.0042	±0.42
ATF Mass Flow rate	0.03015	±3.015
ATF Dynamic Viscosity	0.00096	±0.096
Channel Hydraulic Diameter	0.0000348	±0.00384
Air Side Hydraulic Diameter	0.0087	± 0.87
Air Side Temperature	0.0273	± 2.73
Air Mass flow rate	0.074	± 2.74
Air Reynolds Number	0.0312	±3.12
ATF Specific Heat Capacity	3.49	±34.9
ATF Conductivity	0.00014	±0.014
ATF Reynolds Number	0.1019	±10.19
ATF Prandtl Number	0.0243	±2.43
ATF Nusselt Number	0.1011	±10.11
Heat exchanger effectiveness	0.055	±5.5
Heat exchanger NTU	0.0776	±7.76

APPENDIX C

EXPERIMENTAL DATA

The following table contains the processed data as a source of information.

ATF inlet Temp	Air inlet Temp	ATF Mass Flow Rate	ATF Mass Flow Rate	Air Inlet Average Temp	Air Outlet Average Temp	Air Side Surface Average Temp, T_{so}
°C	°C	kg/min	kg/sec	°C	°C	°C
75	15	1.256	0.021	14.59	18.10	26.78
75	15	1.223	0.020	14.47	16.64	23.55
75	15	1.119	0.019	14.74	16.21	23.95
75	15	1.118	0.019	14.56	15.75	23.19
75	15	0.816	0.014	14.68	17.12	23.87
75	15	0.811	0.014	15.24	16.72	23.78
75	15	0.819	0.014	14.65	15.70	22.27
75	15	0.816	0.014	14.93	15.73	22.18
75	15	0.586	0.010	14.54	16.20	23.23
75	15	0.580	0.010	15.23	16.22	23.17
75	15	0.598	0.010	15.50	16.30	23.48
75	15	0.617	0.010	16.56	17.16	23.27
75	15	0.537	0.009	14.84	16.43	22.47
75	15	0.543	0.009	14.58	15.58	21.41
75	15	0.519	0.009	15.08	15.76	21.36
75	15	0.519	0.009	15.04	15.54	21.65
75	22	2.510	0.042	22.08	27.72	36.03
75	22	2.471	0.041	21.52	25.13	32.01
75	22	2.470	0.041	22.51	25.28	32.12
75	22	2.435	0.041	22.63	24.78	31.52
75	22	1.678	0.028	22.56	26.73	34.11
75	22	1.667	0.028	21.61	24.20	32.16
75	22	1.596	0.027	21.23	23.11	30.72
75	22	1.596	0.027	22.07	23.57	30.61
75	22	0.861	0.014	21.98	24.35	30.70
75	22	0.828	0.014	21.67	23.07	29.51
75	22	0.840	0.014	22.02	22.99	29.34
75	22	0.854	0.014	22.16	22.96	29.18
75	22	0.585	0.010	21.96	23.49	29.02
75	22	0.584	0.010	22.21	23.13	28.52
75	22	0.483	0.008	21.75	22.31	28.74
75	22	0.482	0.008	22.33	22.76	28.10
75	29	3.292	0.055	30.46	36.69	43.08
75	29	3.273	0.055	28.15	32.56	39.46
75	29	3.244	0.054	28.36	31.47	39.18

75	29	3.228	0.054	29.80	32.14	39.02
75	29	2.123	0.035	28.32	32.89	39.31
75	29	2.138	0.036	28.41	31.40	38.60
75	29	2.064	0.034	29.49	31.50	38.14
75	29	2.067	0.034	29.21	30.89	37.95
75	29	1.741	0.029	29.68	33.64	40.85
75	29	1.748	0.029	30.01	32.48	39.96
75	29	1.744	0.029	29.73	31.47	38.92
75	29	1.733	0.029	29.09	30.51	37.70
75	29	0.815	0.014	30.17	31.97	39.60
75	29	0.897	0.015	28.60	29.99	35.55
75	29	0.772	0.013	28.52	29.37	36.64
75	29	0.857	0.014	28.62	29.30	35.96
75	36	3.611	0.060	35.85	42.12	46.97
75	36	3.683	0.061	37.32	41.12	46.99
75	36	3.632	0.061	35.90	39.00	45.77
75	36	3.696	0.062	37.59	40.03	46.62
75	36	3.149	0.052	35.01	40.41	46.82
75	36	3.104	0.052	36.87	40.20	46.82
75	36	3.120	0.052	36.02	38.55	45.70
75	36	3.118	0.052	36.63	38.66	45.75
75	36	1.990	0.033	35.17	39.09	45.91
75	36	1.971	0.033	35.75	38.16	45.75
75	36	1.983	0.033	34.00	35.82	44.11
75	36	1.995	0.033	36.55	37.92	44.99
75	36	1.090	0.018	35.49	37.76	44.97
75	36	1.048	0.017	34.81	36.06	44.96
75	36	1.050	0.018	35.86	36.75	45.52
75	36	1.038	0.017	35.60	36.31	44.86
75	43	3.936	0.066	42.20	48.00	53.50
75	43	3.844	0.064	43.60	46.95	52.94
75	43	3.854	0.064	43.38	45.99	51.87
75	43	3.855	0.064	42.79	44.87	51.45
75	43	3.200	0.053	43.01	47.75	54.96
75	43	3.200	0.053	43.24	46.51	53.83
75	43	3.200	0.053	43.79	45.90	52.55
75	43	3.200	0.053	44.38	46.11	52.86
75	43	2.295	0.038	43.05	46.60	53.83
75	43	2.290	0.038	42.36	44.84	52.95
75	43	2.288	0.038	42.95	44.64	52.66
75	43	2.285	0.038	42.95	44.26	52.94
75	43	1.290	0.022	42.69	44.87	53.96
75	43	1.290	0.022	42.91	44.25	53.92
75	43	1.281	0.021	42.91	43.87	53.18
75	43	1.292	0.022	43.62	44.34	53.86

Inlet Air Temp	Liquid Inlet Temp (RTDi)	Liquid outlet Temp (RTDo)	Liquid inlet Press	Liquid inlet Press	Liquid outlet Press	Liquid outlet Press
°C	°C	°C	Psi	Kpa	Psi(o)	Kpa
15	74.64	19.93	137.59	948.66	27.79	191.62
15	74.33	16.20	134.16	925.00	26.78	184.65
15	74.74	16.83	131.70	908.06	26.61	183.47
15	74.57	15.54	128.05	882.88	27.69	190.91
15	75.48	16.46	93.27	643.07	18.56	127.95
15	75.25	16.41	96.04	662.20	18.05	124.42
15	75.33	15.52	98.45	678.79	18.09	124.73
15	75.42	15.59	98.45	678.80	17.98	123.96
15	75.12	16.96	67.16	463.06	11.23	77.46
15	75.68	17.53	68.81	474.43	11.37	78.37
15	75.48	16.51	68.33	471.11	11.20	77.20
15	75.13	17.99	69.99	482.55	11.20	77.20
15	75.04	15.87	64.65	445.73	9.89	68.21
15	75.06	15.48	64.02	441.43	9.98	68.84
15	74.87	16.59	64.50	444.72	11.00	75.81
15	75.00	16.81	65.12	448.99	10.99	75.76
22	73.35	29.92	178.29	1229.27	29.50	203.41
22	72.48	26.90	178.12	1228.11	27.92	192.53
22	73.60	26.93	176.78	1218.89	28.37	195.63
22	73.96	26.33	176.94	1219.94	28.85	198.92
22	74.80	27.02	123.32	850.29	20.38	140.49
22	74.99	25.19	124.77	860.25	20.41	140.71
22	74.93	24.17	121.38	836.88	20.40	140.67
22	74.81	24.02	123.46	851.21	20.20	139.25
22	74.89	23.64	69.75	480.90	10.31	71.10
22	74.93	23.91	68.38	471.48	10.97	75.63
22	75.21	23.94	68.87	474.85	10.47	72.21
22	75.14	24.90	70.21	484.07	10.82	74.59
22	75.32	23.78	35.57	245.23	4.67	32.22
22	74.92	23.71	36.42	251.08	4.78	32.97
22	75.23	23.10	37.26	256.90	4.59	31.67
22	75.42	23.72	37.32	257.32	5.25	36.17
29	73.54	37.42	198.87	1371.13	29.15	200.97
29	73.92	33.87	198.65	1369.65	28.71	197.92
29	73.87	32.70	196.30	1353.46	29.45	203.03
29	71.74	33.16	196.33	1353.62	29.89	206.06
29	74.13	33.15	129.01	889.50	17.80	122.75
29	74.09	31.62	129.68	894.08	17.97	123.91
29	74.01	32.47	123.32	850.26	16.81	115.90

29	74.30	31.03	126.33	871.02	18.30	126.19
29	75.45	34.57	108.54	748.36	13.95	96.19
29	75.58	33.65	109.45	754.61	13.87	95.65
29	75.42	32.35	105.14	724.92	13.85	95.49
29	75.17	30.41	104.41	719.90	13.94	96.12
29	74.87	32.13	49.36	340.32	5.93	40.86
29	75.41	30.00	54.43	375.29	6.81	46.97
29	75.07	30.98	48.06	331.37	6.57	45.32
29	74.93	29.87	52.85	364.36	6.78	46.76
36	73.81	41.95	195.66	1349.03	26.50	182.73
36	73.47	41.58	198.91	1371.47	26.51	182.75
36	74.73	40.56	195.83	1350.22	26.86	185.20
36	74.21	40.69	197.92	1364.63	26.12	180.06
36	75.11	41.71	172.00	1185.88	21.92	151.16
36	74.32	41.20	170.65	1176.62	21.87	150.81
36	74.54	39.57	171.17	1180.17	21.87	150.77
36	75.32	39.76	172.10	1186.57	21.86	150.75
36	75.36	39.17	113.10	779.79	14.61	100.73
36	75.02	39.06	114.99	792.81	14.54	100.25
36	74.84	36.08	111.30	767.40	14.53	100.17
36	75.95	38.48	111.76	770.59	14.63	100.89
36	75.72	38.95	57.00	392.98	5.66	39.01
36	75.26	37.95	55.80	384.74	5.64	38.90
36	74.88	38.97	55.80	384.74	5.63	38.83
36	74.88	36.94	55.58	383.19	5.53	38.10
43	74.18	48.02	177.65	1224.86	23.59	162.65
43	73.65	47.42	177.64	1224.79	23.59	162.65
43	73.15	46.51	177.65	1224.88	23.68	163.30
43	74.42	46.10	177.65	1224.88	23.70	163.37
43	75.47	48.52	132.53	913.79	18.50	127.56
43	75.68	46.98	132.62	914.40	18.01	124.15
43	74.36	46.35	139.88	964.41	19.81	136.61
43	75.85	46.70	148.00	1020.40	19.51	134.48
43	74.66	46.93	97.65	673.24	11.69	80.58
43	75.90	45.17	97.65	673.25	11.76	81.07
43	75.85	45.11	97.65	673.25	11.75	81.00
43	75.47	44.95	97.65	673.24	11.75	81.00
43	75.92	45.38	52.27	360.37	5.35	36.92
43	75.16	45.15	52.47	361.80	5.15	35.48
43	75.49	45.32	53.64	369.85	5.43	37.44
43	75.34	45.05	56.96	392.74	5.41	37.31

Inlet Air Temp.	Air Dyn Pressure ΔP (FKT-P3)	ATF Pressure drop, ΔP	ATF Bulk Temperature	Air Mean Temp	ATF Inside wall Temp, T_w (Tsi)	ATF in & out Temp Diff. ΔT
°C	kpa	Kpa	°C	°C	°C	°C
15	0.02	757.04	47.28	16.35	27.65	54.71
15	0.06	740.35	45.26	15.56	24.45	58.13
15	0.12	724.59	45.79	15.47	24.79	57.90
15	0.18	691.97	45.06	15.15	24.02	59.04
15	0.02	515.12	45.97	15.90	24.49	59.02
15	0.06	537.78	45.83	15.98	24.39	58.85
15	0.12	554.05	45.42	15.18	22.89	59.81
15	0.20	554.84	45.50	15.33	22.79	59.83
15	0.02	385.60	46.04	15.37	23.66	58.17
15	0.06	396.07	46.61	15.73	23.59	58.15
15	0.12	393.91	45.99	15.90	23.94	58.97
15	0.19	405.35	46.56	16.86	23.72	57.14
15	0.02	377.52	45.45	15.63	22.88	59.17
15	0.06	372.59	45.27	15.08	21.83	59.59
15	0.12	368.91	45.73	15.42	21.75	58.29
15	0.20	373.23	45.90	15.29	22.03	58.19
22	0.02	1025.86	51.64	24.90	37.40	43.43
22	0.06	1035.58	49.69	23.33	33.46	45.58
22	0.11	1023.26	50.26	23.90	33.63	46.67
22	0.18	1021.02	50.15	23.70	33.02	47.64
22	0.02	709.80	50.91	24.64	35.12	47.78
22	0.06	719.55	50.09	22.90	33.22	49.80
22	0.11	696.21	49.55	22.17	31.77	50.76
22	0.19	711.96	49.41	22.82	31.68	50.79
22	0.02	409.81	49.27	23.16	31.27	51.25
22	0.06	395.85	49.42	22.37	30.06	51.02
22	0.11	402.64	49.57	22.50	29.89	51.27
22	0.19	409.49	50.02	22.56	29.75	50.24
22	0.02	213.01	49.55	22.73	29.40	51.54
22	0.06	218.11	49.31	22.67	28.89	51.21
22	0.11	225.23	49.17	22.03	29.06	52.13
22	0.19	221.15	49.57	22.55	28.42	51.69
29	0.02	1170.15	55.48	33.58	44.59	36.12
29	0.06	1171.73	53.90	30.36	41.19	40.04
29	0.11	1150.43	53.28	29.92	40.90	41.17
29	0.17	1147.57	52.45	30.97	40.63	38.58
29	0.02	766.75	53.64	30.61	40.42	40.97
29	0.06	770.17	52.85	29.91	39.78	42.47
29	0.11	734.36	53.24	30.50	39.25	41.53
29	0.19	744.83	52.67	30.05	39.13	43.27
29	0.02	652.17	55.01	31.66	41.78	40.88
29	0.06	658.96	54.61	31.25	40.93	41.93
29	0.11	629.43	53.88	30.60	39.88	43.08

29	0.18	623.79	52.79	29.80	38.70	44.77
29	0.02	299.46	53.50	31.07	40.04	42.73
29	0.05	328.31	52.71	29.29	36.09	45.41
29	0.10	286.05	53.02	28.94	37.08	44.08
29	0.19	317.60	52.40	28.96	36.45	45.06
36	0.02	1166.30	57.88	38.98	48.47	31.85
36	0.06	1188.71	57.52	39.22	48.51	31.89
36	0.11	1165.02	57.64	37.45	47.41	34.17
36	0.18	1184.57	57.45	38.81	48.27	33.52
36	0.02	1034.72	58.41	37.71	48.16	33.39
36	0.06	1025.81	57.76	38.53	48.14	33.12
36	0.11	1029.40	57.06	37.28	47.10	34.97
36	0.18	1035.82	57.54	37.65	47.18	35.56
36	0.02	679.06	57.27	37.13	46.85	36.19
36	0.06	692.56	57.04	36.96	46.69	35.96
36	0.11	667.23	55.46	34.91	45.11	38.75
36	0.18	669.70	57.22	37.24	45.96	37.48
36	0.02	353.97	57.34	36.63	45.50	36.77
36	0.06	345.85	56.60	35.44	45.45	37.31
36	0.11	345.91	56.92	36.30	46.01	35.92
36	0.18	345.09	55.91	35.95	45.37	37.94
43	0.02	1062.21	61.10	45.10	54.86	26.15
43	0.06	1062.15	60.54	45.28	54.26	26.23
43	0.11	1061.58	59.83	44.69	53.24	26.64
43	0.18	1061.51	60.26	43.83	52.89	28.32
43	0.02	786.23	62.00	45.38	56.08	26.95
43	0.06	790.25	61.33	44.88	55.05	28.70
43	0.11	827.80	60.35	44.84	53.71	28.00
43	0.17	885.92	61.28	45.24	54.06	29.15
43	0.02	592.66	60.80	44.82	54.65	27.73
43	0.05	592.17	60.53	43.60	53.87	30.73
43	0.11	592.25	60.48	43.80	53.57	30.73
43	0.17	592.24	60.21	43.61	53.84	30.52
43	0.02	323.46	60.65	43.78	54.46	30.55
43	0.05	326.32	60.15	43.58	54.43	30.02
43	0.11	332.41	60.41	43.39	53.70	30.17
43	0.18	355.44	60.19	43.98	54.36	30.29

Inlet Air Temp	ATF Specific Heat Cp, at Bulk Temp	ATF Specific Heat Cp, at Wall Temp	ATF Density ρ, at bulk Temp	ATF Conductivity k, at Bulk Temp	ATF Conductivity k, at Wall Temp	ATF Dynamic Viscosity at Bulk Temp, μ_m
°C	J/Kg-K	J/Kg-K	kg/m^3	W/m-K	W/m-K	Kg/m-s
15	2040	1970	849	0.157	0.160	0.022
15	2040	1960	850	0.157	0.160	0.022
15	2040	1960	850	0.157	0.160	0.022
15	2040	1960	850	0.157	0.160	0.022
15	2040	1960	849	0.157	0.160	0.022
15	2040	1960	850	0.157	0.160	0.022
15	2040	1960	850	0.157	0.160	0.022
15	2040	1960	850	0.157	0.160	0.022
15	2040	1960	850	0.157	0.160	0.022
15	2040	1960	850	0.157	0.160	0.022
15	2040	1960	850	0.157	0.160	0.022
15	2040	1960	850	0.157	0.160	0.022
15	2040	1955	850	0.157	0.160	0.022
15	2040	1950	850	0.157	0.160	0.022
15	2040	1950	850	0.157	0.160	0.022
15	2040	1950	850	0.157	0.160	0.022
22	2060	2010	845	0.156	0.158	0.020
22	2056	1992	846	0.156	0.159	0.020
22	2056	1992	846	0.156	0.159	0.020
22	2056	1990	846	0.156	0.159	0.020
22	2060	2000	845	0.156	0.159	0.020
22	2056	1992	846	0.156	0.159	0.020
22	2056	1990	846	0.156	0.159	0.020
22	2056	1990	846	0.156	0.159	0.020
22	2056	1985	845	0.156	0.159	0.020
22	2056	1980	846	0.156	0.159	0.020
22	2056	1980	846	0.156	0.159	0.020
22	2056	1980	846	0.156	0.159	0.020
22	2056	1980	845	0.156	0.159	0.020
22	2056	1980	846	0.156	0.159	0.020
22	2056	1980	846	0.156	0.159	0.020
22	2056	1973	846	0.156	0.159	0.020
29	2080	2032	841	0.156	0.158	0.019
29	2070	2020	843	0.156	0.158	0.019
29	2070	2020	844	0.156	0.158	0.019
29	2068	2020	844	0.156	0.158	0.019
29	2070	1990	844	0.156	0.158	0.019
29	2070	1990	844	0.156	0.158	0.019
29	2070	2013	844	0.156	0.158	0.019
29	2070	2013	844	0.156	0.158	0.019
29	2070	2020	844	0.156	0.158	0.019
29	2070	2020	844	0.156	0.158	0.019
29	2070	2020	844	0.156	0.158	0.019
29	2068	2013	843	0.156	0.158	0.019

29	2070	2020	843	0.156	0.158	0.019
29	2070	2002	843	0.156	0.158	0.019
29	2070	2008	843	0.156	0.158	0.019
29	2070	2002	843	0.156	0.158	0.019
36	2085	2050	841	0.155	0.157	0.016
36	2085	2050	841	0.155	0.157	0.016
36	2083	2050	841	0.155	0.157	0.016
36	2085	2050	841	0.155	0.157	0.016
36	2085	2050	841	0.155	0.157	0.016
36	2085	2050	841	0.155	0.157	0.016
36	2083	2045	841	0.155	0.157	0.016
36	2085	2045	841	0.155	0.157	0.016
36	2085	2045	841	0.155	0.157	0.016
36	2085	2050	841	0.155	0.157	0.016
36	2083	2040	841	0.155	0.157	0.016
36	2085	2040	841	0.155	0.157	0.016
36	2085	2040	841	0.155	0.157	0.016
36	2085	2040	841	0.155	0.157	0.016
36	2083	2040	841	0.155	0.157	0.016
36	2085	2040	841	0.155	0.157	0.016
43	2098	2075	839	0.155	0.156	0.014
43	2093	2070	839	0.155	0.156	0.014
43	2093	2070	839	0.155	0.156	0.014
43	2093	2070	839	0.155	0.156	0.014
43	2093	2080	841	0.155	0.156	0.014
43	2093	2075	841	0.155	0.156	0.014
43	2093	2070	841	0.155	0.156	0.014
43	2098	2070	841	0.155	0.156	0.014
43	2093	2075	841	0.155	0.156	0.014
43	2093	2070	841	0.155	0.156	0.014
43	2093	2070	841	0.155	0.156	0.014
43	2093	2070	841	0.155	0.156	0.014
43	2093	2070	841	0.155	0.156	0.013
43	2093	2070	841	0.155	0.156	0.013
43	2093	2070	841	0.155	0.156	0.013
43	2093	2072	841	0.155	0.156	0.013

Inlet Air Temp	ATF Dynamic Viscosity at Wall Temp, μ_w	Viscosity Ratio, μ_m/μ_w	Viscosity Ratio, $(\mu_m/\mu_w)^{0.14}$	Viscosity Ratio, $(\mu_m/\mu_w)^{-0.50}$	ATF Reynolds Number, (Re_L), at Bulk Temp	ATF Velocity, (V)
°C	Kg/m-s					m/s
15	0.050	0.440	0.891	1.508	5.94	0.154
15	0.058	0.379	0.873	1.624	5.78	0.150
15	0.058	0.379	0.873	1.624	5.29	0.137
15	0.058	0.379	0.873	1.624	5.29	0.137
15	0.058	0.379	0.873	1.624	3.86	0.100
15	0.058	0.379	0.873	1.624	3.83	0.099
15	0.060	0.367	0.869	1.651	3.87	0.100
15	0.060	0.367	0.869	1.651	3.86	0.100
15	0.060	0.367	0.869	1.651	2.77	0.072
15	0.060	0.367	0.869	1.651	2.74	0.071
15	0.060	0.367	0.869	1.651	2.83	0.073
15	0.060	0.367	0.869	1.651	2.92	0.076
15	0.060	0.367	0.869	1.651	2.54	0.066
15	0.062	0.355	0.865	1.679	2.57	0.066
15	0.062	0.355	0.865	1.679	2.45	0.064
15	0.062	0.355	0.865	1.679	2.45	0.063
22	0.032	0.625	0.936	1.265	13.05	0.309
22	0.041	0.488	0.904	1.432	12.85	0.304
22	0.041	0.488	0.904	1.432	12.85	0.304
22	0.041	0.488	0.904	1.432	12.66	0.299
22	0.036	0.556	0.921	1.342	8.73	0.207
22	0.041	0.488	0.904	1.432	8.67	0.205
22	0.042	0.476	0.901	1.449	8.30	0.196
22	0.042	0.476	0.901	1.449	8.30	0.196
22	0.042	0.476	0.901	1.449	4.48	0.106
22	0.044	0.460	0.897	1.475	4.31	0.102
22	0.044	0.460	0.897	1.475	4.37	0.103
22	0.044	0.460	0.897	1.475	4.44	0.105
22	0.044	0.455	0.895	1.483	3.04	0.072
22	0.044	0.455	0.895	1.483	3.03	0.072
22	0.043	0.465	0.898	1.466	2.51	0.059
22	0.044	0.455	0.895	1.483	2.51	0.059
29	0.024	0.771	0.964	1.139	18.51	0.407
29	0.028	0.661	0.944	1.230	18.40	0.404
29	0.028	0.661	0.944	1.230	18.24	0.400
29	0.030	0.617	0.935	1.273	18.15	0.398
29	0.030	0.617	0.935	1.273	11.94	0.262
29	0.030	0.617	0.935	1.273	12.02	0.264
29	0.030	0.617	0.935	1.273	11.61	0.254
29	0.030	0.617	0.935	1.273	11.62	0.255
29	0.028	0.661	0.944	1.230	9.79	0.215
29	0.028	0.661	0.944	1.230	9.83	0.215
29	0.028	0.661	0.944	1.230	9.81	0.215
29	0.028	0.661	0.944	1.230	9.74	0.214

29	0.030	0.617	0.935	1.273	4.58	0.101
29	0.034	0.544	0.918	1.356	5.04	0.111
29	0.032	0.578	0.926	1.315	4.34	0.095
29	0.034	0.544	0.918	1.356	4.82	0.106
36	0.021	0.762	0.963	1.146	23.48	0.447
36	0.021	0.762	0.963	1.146	23.94	0.456
36	0.021	0.762	0.963	1.146	23.61	0.449
36	0.021	0.762	0.963	1.146	24.03	0.457
36	0.021	0.762	0.963	1.146	20.47	0.389
36	0.021	0.762	0.963	1.146	20.18	0.384
36	0.022	0.727	0.956	1.173	20.29	0.386
36	0.022	0.727	0.956	1.173	20.27	0.386
36	0.022	0.727	0.956	1.173	12.94	0.246
36	0.022	0.727	0.956	1.173	12.81	0.244
36	0.024	0.667	0.945	1.225	12.89	0.245
36	0.022	0.727	0.956	1.173	12.97	0.247
36	0.024	0.681	0.948	1.212	7.09	0.135
36	0.024	0.681	0.948	1.212	6.81	0.130
36	0.022	0.727	0.956	1.173	6.83	0.130
36	0.024	0.667	0.945	1.225	6.75	0.128
43	0.018	0.778	0.965	1.134	29.24	0.488
43	0.019	0.757	0.962	1.150	28.56	0.477
43	0.019	0.737	0.958	1.165	28.64	0.478
43	0.019	0.737	0.958	1.165	28.65	0.478
43	0.019	0.737	0.958	1.165	23.78	0.396
43	0.018	0.778	0.965	1.134	23.78	0.396
43	0.019	0.737	0.958	1.165	23.78	0.396
43	0.019	0.737	0.958	1.165	23.78	0.396
43	0.018	0.778	0.965	1.134	17.05	0.284
43	0.019	0.737	0.958	1.165	17.02	0.283
43	0.019	0.737	0.958	1.165	17.00	0.283
43	0.019	0.737	0.958	1.165	16.98	0.283
43	0.019	0.705	0.952	1.191	10.01	0.160
43	0.019	0.705	0.952	1.191	10.01	0.160
43	0.019	0.705	0.952	1.191	9.94	0.158
43	0.019	0.705	0.952	1.191	10.03	0.160

Inlet Air Temp	ATF Heat Transfer rate Q,	ATF Heat Transfer rate Q	Heat Flux, (q)	Liq Heat Transfer rate Q	Hydrodynamic Entry length, $L_h=0.05ReD_h$,	Hydrodynamic Entry length, % of Total Length
°C	W	KW	W/m^2	BTU/min	Mm	%
15	2336.31	2.34	2397.05	132.81	0.297	0.098
15	2416.33	2.42	2479.15	137.36	0.289	0.095
15	2203.04	2.20	2260.32	125.24	0.265	0.087
15	2244.05	2.24	2302.40	127.57	0.264	0.087
15	1637.57	1.64	1680.15	93.09	0.193	0.063
15	1622.63	1.62	1664.82	92.24	0.192	0.063
15	1664.65	1.66	1707.93	94.63	0.194	0.064
15	1659.93	1.66	1703.09	94.36	0.193	0.063
15	1158.88	1.16	1189.01	65.88	0.139	0.046
15	1146.72	1.15	1176.53	65.19	0.137	0.045
15	1198.89	1.20	1230.06	68.15	0.141	0.047
15	1198.66	1.20	1229.83	68.14	0.146	0.048
15	1080.13	1.08	1108.21	61.40	0.127	0.042
15	1099.46	1.10	1128.05	62.50	0.128	0.042
15	1028.50	1.03	1055.25	58.47	0.123	0.040
15	1026.08	1.03	1052.76	58.33	0.123	0.040
22	3742.42	3.74	3839.73	212.74	0.653	0.215
22	3859.18	3.86	3959.53	219.38	0.643	0.211
22	3950.03	3.95	4052.73	224.55	0.642	0.211
22	3975.03	3.98	4078.38	225.97	0.633	0.208
22	2752.39	2.75	2823.96	156.46	0.436	0.144
22	2844.45	2.84	2918.41	161.70	0.434	0.143
22	2775.94	2.78	2848.12	157.80	0.415	0.137
22	2777.72	2.78	2849.94	157.90	0.415	0.137
22	1511.92	1.51	1551.23	85.95	0.224	0.074
22	1447.60	1.45	1485.24	82.29	0.215	0.071
22	1475.75	1.48	1514.12	83.89	0.218	0.072
22	1470.20	1.47	1508.42	83.58	0.222	0.073
22	1033.73	1.03	1060.61	58.76	0.152	0.050
22	1023.95	1.02	1050.57	58.21	0.152	0.050
22	862.97	0.86	885.41	49.06	0.126	0.041
22	854.34	0.85	876.55	48.57	0.125	0.041
29	4122.33	4.12	4229.51	234.34	0.926	0.304
29	4521.64	4.52	4639.20	257.04	0.920	0.303
29	4607.41	4.61	4727.20	261.92	0.912	0.300
29	4292.06	4.29	4403.66	243.99	0.908	0.299
29	3001.13	3.00	3079.16	170.60	0.597	0.196
29	3132.68	3.13	3214.14	178.08	0.601	0.198

29	2957.54	2.96	3034.44	168.13	0.580	0.191
29	3085.45	3.09	3165.68	175.40	0.581	0.191
29	2455.06	2.46	2518.90	139.56	0.489	0.161
29	2528.91	2.53	2594.66	143.76	0.492	0.162
29	2591.97	2.59	2659.36	147.34	0.490	0.161
29	2673.96	2.67	2743.49	152.01	0.487	0.160
29	1201.53	1.20	1232.77	68.30	0.229	0.075
29	1405.26	1.41	1441.80	79.88	0.252	0.083
29	1174.12	1.17	1204.64	66.74	0.217	0.071
29	1332.32	1.33	1366.96	75.74	0.241	0.079
36	3996.94	4.00	4100.87	227.21	1.174	0.386
36	4081.31	4.08	4187.43	232.01	1.197	0.394
36	4308.28	4.31	4420.30	244.91	1.181	0.388
36	4305.64	4.31	4417.59	244.76	1.201	0.395
36	3654.24	3.65	3749.25	207.73	1.024	0.337
36	3571.93	3.57	3664.81	203.05	1.009	0.332
36	3788.01	3.79	3886.50	215.34	1.014	0.334
36	3852.68	3.85	3952.85	219.01	1.014	0.333
36	2502.62	2.50	2567.69	142.27	0.647	0.213
36	2462.42	2.46	2526.44	139.98	0.641	0.211
36	2667.65	2.67	2737.01	151.65	0.645	0.212
36	2598.16	2.60	2665.72	147.70	0.649	0.213
36	1392.75	1.39	1428.96	79.17	0.354	0.117
36	1358.80	1.36	1394.13	77.24	0.341	0.112
36	1309.25	1.31	1343.29	74.43	0.341	0.112
36	1368.51	1.37	1404.10	77.80	0.337	0.111
43	3599.15	3.60	3692.73	204.60	1.462	0.481
43	3517.14	3.52	3608.59	199.94	1.428	0.470
43	3581.00	3.58	3674.11	203.57	1.432	0.471
43	3808.65	3.81	3907.68	216.51	1.432	0.471
43	3008.49	3.01	3086.71	171.02	1.189	0.391
43	3203.17	3.20	3286.46	182.09	1.189	0.391
43	3125.66	3.13	3206.93	177.68	1.189	0.391
43	3261.55	3.26	3346.35	185.41	1.189	0.391
43	2219.81	2.22	2277.53	126.19	0.853	0.280
43	2454.54	2.45	2518.36	139.53	0.851	0.280
43	2453.02	2.45	2516.80	139.45	0.850	0.280
43	2432.86	2.43	2496.12	138.30	0.849	0.279
43	1374.62	1.37	1410.36	78.14	0.501	0.165
43	1350.66	1.35	1385.78	76.78	0.501	0.165
43	1348.04	1.35	1383.09	76.63	0.497	0.164
43	1365.35	1.37	1400.85	77.62	0.501	0.165

Inlet Air Temp	Thermal entry Length, $L_{Th}=0.05RePrD_h$	Thermal entry Length, % of total length	ATF Heat transfer Coefficient, h_L	Prandtl Number at Bulk Temp, Pr_b	Prandtl Number at wall Temp, Pr_w	Nusselt Number at Bulk Temp, Nu	Corrected Nusselt Number, Nu_{cort}
°C	mm	%	W/m^2-K				
15	84.67	27.85	120.32	285.13	615.63	0.764	0.681
15	82.41	27.11	118.25	285.13	710.50	0.751	0.656
15	75.43	24.81	109.11	285.13	710.50	0.693	0.605
15	75.36	24.79	108.39	285.13	710.50	0.689	0.601
15	55.01	18.09	78.97	285.13	710.50	0.502	0.438
15	54.67	17.98	78.59	285.13	710.50	0.499	0.436
15	55.18	18.15	75.48	285.13	735.00	0.480	0.417
15	55.01	18.09	73.78	285.13	735.00	0.469	0.407
15	39.50	12.99	52.28	285.13	735.00	0.332	0.289
15	39.10	12.86	50.15	285.13	735.00	0.319	0.277
15	40.31	13.26	56.57	285.13	735.00	0.359	0.312
15	41.59	13.68	53.82	285.13	735.00	0.342	0.297
15	36.19	11.91	49.22	285.13	733.13	0.313	0.272
15	36.58	12.03	48.74	285.13	755.63	0.310	0.268
15	34.99	11.51	44.37	285.13	755.63	0.282	0.244
15	34.96	11.50	43.59	285.13	755.63	0.277	0.240
22	172.39	56.71	263.45	264.10	407.09	1.689	1.581
22	169.38	55.72	242.92	263.59	513.66	1.557	1.408
22	169.31	55.70	249.05	263.59	513.66	1.596	1.444
22	166.92	54.91	239.30	263.59	513.14	1.534	1.387
22	115.25	37.91	175.89	264.10	454.26	1.127	1.038
22	114.27	37.59	171.50	263.59	513.66	1.099	0.994
22	109.40	35.99	161.73	263.59	525.66	1.037	0.934
22	109.40	35.99	164.36	263.59	525.66	1.054	0.950
22	59.02	19.41	87.57	263.59	524.34	0.561	0.506
22	56.76	18.67	78.01	263.59	541.70	0.500	0.449
22	57.58	18.94	76.01	263.59	541.70	0.487	0.437
22	58.54	19.26	75.74	263.59	541.70	0.486	0.435
22	40.12	13.20	51.47	263.59	547.92	0.330	0.295
22	40.00	13.16	50.23	263.59	547.92	0.322	0.288
22	33.12	10.89	43.25	263.59	535.47	0.277	0.249
22	33.06	10.88	40.97	263.59	545.99	0.263	0.235
29	228.30	75.10	379.31	246.67	309.64	2.431	2.344
29	225.89	74.30	371.77	245.48	359.11	2.383	2.249
29	223.89	73.65	380.64	245.48	359.11	2.440	2.302
29	222.57	73.21	372.73	245.24	384.76	2.389	2.233
29	146.52	48.20	230.05	245.48	379.05	1.475	1.378
29	147.55	48.54	247.16	245.48	379.05	1.584	1.481
29	142.45	46.86	216.93	245.48	383.43	1.391	1.300
29	142.65	46.93	237.76	245.48	383.43	1.524	1.424
29	120.13	39.52	191.39	245.48	359.11	1.227	1.158
29	120.67	39.69	192.17	245.48	359.11	1.232	1.162
29	120.36	39.59	188.18	245.48	359.11	1.206	1.138

29	119.49	39.31	194.74	245.24	357.87	1.248	1.178
29	56.25	18.50	89.96	245.48	384.76	0.577	0.539
29	61.91	20.36	87.84	245.48	432.18	0.563	0.517
29	53.28	17.53	76.28	245.48	407.97	0.489	0.453
29	59.15	19.46	84.34	245.48	432.18	0.541	0.496
36	252.64	83.10	434.27	215.23	274.20	2.802	2.697
36	257.68	84.76	460.45	215.23	274.20	2.971	2.860
36	253.86	83.51	440.61	215.02	274.20	2.843	2.736
36	258.59	85.06	492.39	215.23	274.20	3.177	3.058
36	220.32	72.47	359.13	215.23	274.20	2.317	2.230
36	217.17	71.44	375.28	215.23	274.20	2.421	2.331
36	218.10	71.74	384.57	215.02	286.56	2.481	2.373
36	218.15	71.76	378.21	215.23	286.56	2.440	2.334
36	139.24	45.80	245.47	215.23	286.56	1.584	1.515
36	137.87	45.35	246.56	215.23	287.26	1.591	1.521
36	138.60	45.59	264.65	215.02	311.85	1.707	1.613
36	139.58	45.91	235.81	215.23	285.86	1.521	1.455
36	76.26	25.09	121.61	215.23	305.35	0.785	0.743
36	73.32	24.12	122.26	215.23	305.35	0.789	0.747
36	73.39	24.14	122.85	215.02	285.86	0.793	0.758
36	72.62	23.89	131.85	215.23	311.85	0.851	0.804
43	277.07	91.14	592.03	189.50	239.42	3.820	3.688
43	269.97	88.80	574.21	189.05	245.48	3.705	3.563
43	270.67	89.04	570.72	189.05	252.12	3.682	3.528
43	270.77	89.07	533.04	189.05	252.12	3.439	3.295
43	224.74	73.93	514.09	189.05	253.33	3.317	3.178
43	224.74	73.93	535.00	189.05	239.42	3.452	3.332
43	224.74	73.93	473.90	189.05	252.12	3.057	2.929
43	225.28	74.11	454.47	189.50	252.12	2.932	2.809
43	161.18	53.02	365.00	189.05	239.42	2.355	2.273
43	160.83	52.91	379.83	189.05	252.12	2.451	2.348
43	160.69	52.86	359.45	189.05	252.12	2.319	2.222
43	160.48	52.79	384.37	189.05	252.12	2.480	2.376
43	90.60	29.80	223.88	180.94	252.12	1.444	1.375
43	90.60	29.80	243.05	180.94	252.12	1.568	1.493
43	89.97	29.59	208.90	180.94	252.12	1.348	1.283
43	90.74	29.85	235.67	180.94	252.36	1.520	1.448

nlet Air Temp	Mass Flux (G)	Total System Pressure drop (ΔP)	Total System Pressure drop ΔP	System Pressure drop per mass flux	ATF Capacity rate, C_L	Pressure Ratio, P_{in}/P_o
°C	Kg/m^2-s	kpa	pa	ΔP/G		
15	130.65	757.04	757042.09	5.79	42.70	4.95
15	127.17	740.35	740350.38	5.82	41.57	5.01
15	116.40	724.59	724589.79	6.22	38.05	4.95
15	116.30	691.97	691973.38	5.95	38.01	4.62
15	84.88	515.12	515123.72	6.07	27.74	5.03
15	84.36	537.78	537779.08	6.37	27.57	5.32
15	85.15	554.05	554053.79	6.51	27.83	5.44
15	84.88	554.84	554843.63	6.54	27.74	5.48
15	60.96	385.60	385600.61	6.33	19.92	5.98
15	60.33	396.07	396066.06	6.56	19.72	6.05
15	62.21	393.91	393912.27	6.33	20.33	6.10
15	64.18	405.35	405349.22	6.32	20.98	6.25
15	55.85	377.52	377515.37	6.76	18.25	6.53
15	56.45	372.59	372589.07	6.60	18.45	6.41
15	53.99	368.91	368907.37	6.83	17.65	5.87
15	53.95	373.23	373228.46	6.92	17.63	5.93
22	261.10	1025.86	1025855.03	3.93	86.18	6.04
22	257.04	1035.58	1035581.41	4.03	84.67	6.38
22	256.94	1023.26	1023259.19	3.98	84.64	6.23
22	253.30	1021.02	1021016.77	4.03	83.44	6.13
22	174.55	709.80	709804.32	4.07	57.61	6.05
22	173.41	719.55	719548.00	4.15	57.12	6.11
22	166.02	696.21	696212.85	4.19	54.69	5.95
22	166.02	711.96	711957.92	4.29	54.69	6.11
22	89.56	409.81	409805.60	4.58	29.50	6.76
22	86.13	395.85	395845.75	4.60	28.37	6.23
22	87.38	402.64	402642.73	4.61	28.78	6.58
22	88.84	409.49	409487.21	4.61	29.26	6.49
22	60.88	213.01	213007.91	3.50	20.06	7.61
22	60.70	218.11	218112.50	3.59	19.99	7.62
22	50.25	225.23	225225.30	4.48	16.55	8.11
22	50.17	221.15	221146.94	4.41	16.53	7.11
29	342.44	1170.15	1170153.93	3.42	114.12	6.82
29	340.47	1171.73	1171731.35	3.44	112.92	6.92
29	337.45	1150.43	1150427.72	3.41	111.92	6.67
29	335.78	1147.57	1147567.09	3.42	111.26	6.57
29	220.84	766.75	766746.75	3.47	73.24	7.25
29	222.40	770.17	770167.96	3.46	73.76	7.22
29	214.70	734.36	734363.60	3.42	71.21	7.34
29	215.01	744.83	744828.10	3.46	71.31	6.90

29	181.06	652.17	652171.57	3.60	60.05	7.78
29	181.87	658.96	658960.93	3.62	60.32	7.89
29	181.42	629.43	629428.02	3.47	60.17	7.59
29	180.27	623.79	623786.49	3.46	59.73	7.49
29	84.78	299.46	299459.36	3.53	28.12	8.33
29	93.31	328.31	328313.82	3.52	30.95	7.99
29	80.31	286.05	286048.75	3.56	26.63	7.31
29	89.15	317.60	317600.13	3.56	29.57	7.79
36	375.63	1166.30	1166300.72	3.10	125.48	7.38
36	383.12	1188.71	1188714.65	3.10	127.98	7.50
36	377.81	1165.02	1165022.54	3.08	126.09	7.29
36	384.47	1184.57	1184569.12	3.08	128.44	7.58
36	327.57	1034.72	1034721.05	3.16	109.43	7.85
36	322.89	1025.81	1025808.05	3.18	107.86	7.80
36	324.58	1029.40	1029402.94	3.17	108.33	7.83
36	324.34	1035.82	1035822.28	3.19	108.35	7.87
36	207.03	679.06	679062.26	3.28	69.16	7.74
36	204.99	692.56	692561.90	3.38	68.48	7.91
36	206.27	667.23	667231.06	3.23	68.84	7.66
36	207.53	669.70	669698.46	3.23	69.33	7.64
36	113.38	353.97	353971.78	3.12	37.88	10.07
36	109.02	345.85	345848.44	3.17	36.42	9.89
36	109.22	345.91	345913.07	3.17	36.45	9.91
36	107.98	345.09	345087.38	3.20	36.07	10.06
43	409.40	1062.21	1062211.48	2.59	137.62	7.53
43	399.85	1062.15	1062145.27	2.66	134.09	7.53
43	400.90	1061.58	1061583.21	2.65	134.44	7.50
43	401.05	1061.51	1061510.31	2.65	134.49	7.50
43	332.87	786.23	786229.76	2.36	111.63	7.16
43	332.87	790.25	790253.89	2.37	111.63	7.37
43	332.87	827.80	827804.25	2.49	111.63	7.06
43	332.87	885.92	885915.94	2.66	111.89	7.59
43	238.73	592.66	592657.63	2.48	80.06	8.35
43	238.21	592.17	592171.45	2.49	79.88	8.30
43	238.00	592.25	592250.88	2.49	79.81	8.31
43	237.69	592.24	592243.49	2.49	79.71	8.31
43	134.19	323.46	323456.46	2.41	45.00	9.76
43	134.19	326.32	326317.93	2.43	45.00	10.20
43	133.25	332.41	332406.51	2.49	44.69	9.88
43	134.40	355.44	355436.21	2.64	45.07	10.53

Inlet Air Temp	Air Temp Diff ΔT	Air TH Conductivity (K air)	Air Density ρ	Air velocity , (V)	Air Mass Flow Rate	Air Specific Heat Cp
°C	°C	W/m-C	Kg/m^3	m/Sec	Kg/sec	KJ/Kg-K
15	3.51	0.025	1.200	5.80	0.64	1.01
15	2.18	0.025	1.200	9.82	1.09	1.01
15	1.47	0.025	1.200	13.84	1.54	1.01
15	1.19	0.025	1.110	17.91	1.84	1.01
15	2.44	0.025	1.200	6.15	0.68	1.01
15	1.48	0.025	1.200	10.04	1.11	1.01
15	1.06	0.025	1.200	14.02	1.56	1.01
15	0.80	0.025	1.200	18.04	2.00	1.01
15	1.66	0.025	1.200	6.08	0.67	1.01
15	0.99	0.025	1.200	10.00	1.11	1.01
15	0.79	0.025	1.200	13.98	1.55	1.01
15	0.60	0.025	1.200	18.00	2.00	1.01
15	1.59	0.025	1.200	6.14	0.68	1.01
15	1.00	0.025	1.200	10.08	1.12	1.01
15	0.67	0.025	1.200	13.98	1.55	1.01
15	0.49	0.025	1.200	18.20	2.02	1.01
22	5.64	0.026	1.140	5.98	0.63	1.01
22	3.61	0.026	1.140	10.01	1.05	1.01
22	2.77	0.026	1.140	14.06	1.48	1.01
22	2.15	0.026	1.140	17.62	1.86	1.01
22	4.17	0.026	1.150	5.97	0.63	1.01
22	2.59	0.026	1.150	10.10	1.07	1.01
22	1.88	0.026	1.150	14.08	1.50	1.01
22	1.50	0.026	1.150	18.08	1.92	1.01
22	2.37	0.026	1.140	6.21	0.65	1.01
22	1.40	0.026	1.140	10.09	1.06	1.01
22	0.97	0.026	1.140	13.97	1.47	1.01
22	0.80	0.026	1.140	18.05	1.90	1.01
22	1.53	0.026	1.140	6.10	0.64	1.01
22	0.91	0.026	1.140	10.07	1.06	1.01
22	0.56	0.026	1.140	14.13	1.49	1.01
22	0.44	0.026	1.140	18.09	1.91	1.01
29	6.23	0.026	1.130	6.01	0.63	1.01
29	4.41	0.026	1.130	10.12	1.06	1.01
29	3.11	0.026	1.130	14.04	1.47	1.01
29	2.34	0.026	1.130	17.51	1.83	1.01
29	4.56	0.026	1.130	6.11	0.64	1.01
29	2.99	0.026	1.130	10.08	1.05	1.01
29	2.01	0.026	1.130	14.00	1.46	1.01
29	1.68	0.026	1.130	18.10	1.89	1.01

29	3.96	0.026	1.130	5.96	0.62	1.01
29	2.47	0.026	1.130	10.02	1.05	1.01
29	1.74	0.026	1.130	13.95	1.46	1.01
29	1.42	0.026	1.130	17.97	1.88	1.01
29	1.81	0.026	1.130	6.11	0.64	1.01
29	1.40	0.026	1.130	9.82	1.03	1.01
29	0.85	0.026	1.130	13.40	1.40	1.01
29	0.68	0.026	1.130	18.10	1.89	1.01
36	6.26	0.027	1.120	6.09	0.63	1.01
36	3.80	0.027	1.120	10.13	1.05	1.01
36	3.10	0.027	1.110	14.03	1.44	1.01
36	2.44	0.027	1.110	17.88	1.83	1.01
36	5.40	0.027	1.130	6.21	0.65	1.01
36	3.33	0.027	1.120	10.02	1.04	1.01
36	2.53	0.027	1.120	13.96	1.44	1.01
36	2.04	0.027	1.120	17.87	1.85	1.01
36	3.93	0.027	1.130	6.02	0.63	1.01
36	2.41	0.027	1.120	10.01	1.04	1.01
36	1.82	0.027	1.130	13.98	1.46	1.01
36	1.37	0.027	1.130	17.93	1.87	1.01
36	2.27	0.027	1.120	5.98	0.62	1.01
36	1.24	0.027	1.130	9.94	1.04	1.01
36	0.89	0.027	1.130	14.02	1.46	1.01
36	0.71	0.027	1.120	18.06	1.87	1.01
43	5.80	0.027	1.100	6.09	0.62	1.01
43	3.35	0.027	1.100	10.26	1.04	1.01
43	2.61	0.027	1.100	14.02	1.43	1.01
43	2.08	0.027	1.120	17.80	1.84	1.01
43	4.74	0.027	1.100	6.05	0.61	1.01
43	3.27	0.027	1.100	10.01	1.02	1.01
43	2.11	0.027	1.100	14.00	1.42	1.01
43	1.73	0.027	1.090	17.90	1.80	1.01
43	3.55	0.027	1.070	6.10	0.60	1.01
43	2.48	0.027	1.080	9.94	0.99	1.01
43	1.69	0.027	1.080	14.12	1.41	1.01
43	1.30	0.027	1.080	17.87	1.78	1.01
43	2.18	0.027	1.100	5.95	0.61	1.01
43	1.34	0.027	1.090	10.01	1.01	1.01
43	0.97	0.027	1.100	14.05	1.43	1.01
43	0.72	0.027	1.100	17.88	1.82	1.01

Inlet Air Temp	Air Specific Heat Cp,	Air Heat Transfer Rate, $\dot{Q}$	Air Heat Transfer Rate, $\dot{Q}$	Air Heat Transfer Rate $\dot{Q}$	Heat Balance	Air Dyn. Viscosity μ_a
°C	J/Kg-K	KW	W	Btu/min	HB	Kg/m-s
15	1005.00	2.27	2268.92	128.98	2.88	0.000018
15	1005.00	2.38	2382.50	135.44	1.40	0.000018
15	1005.00	2.26	2262.65	128.62	-2.71	0.000018
15	1005.00	2.20	2199.32	125.02	1.99	0.000018
15	1005.00	1.67	1669.60	94.91	-1.96	0.000018
15	1005.00	1.66	1661.80	94.47	-2.41	0.000018
15	1005.00	1.65	1651.17	93.86	0.81	0.000018
15	1005.00	1.61	1606.03	91.30	3.25	0.000018
15	1005.00	1.12	1122.29	63.80	3.16	0.000018
15	1005.00	1.10	1103.24	62.72	3.79	0.000018
15	1005.00	1.23	1232.94	70.09	-2.84	0.000018
15	1005.00	1.20	1197.82	68.09	0.07	0.000018
15	1005.00	1.09	1085.91	61.73	-0.54	0.000018
15	1005.00	1.13	1127.74	64.11	-2.57	0.000018
15	1005.00	1.05	1045.60	59.44	-1.66	0.000018
15	1005.00	1.00	1002.68	57.00	2.28	0.000018
22	1005.00	3.57	3570.48	202.97	4.59	0.000018
22	1005.00	3.83	3827.22	217.56	0.83	0.000018
22	1005.00	4.12	4121.37	234.29	-4.34	0.000018
22	1005.00	4.01	4012.22	228.08	-0.94	0.000018
22	1005.00	2.66	2659.35	151.17	3.38	0.000019
22	1005.00	2.80	2796.13	158.95	1.70	0.000018
22	1005.00	2.83	2828.04	160.76	-1.88	0.000018
22	1005.00	2.90	2904.07	165.09	-4.55	0.000018
22	1005.00	1.56	1559.49	88.65	-3.15	0.000018
22	1005.00	1.50	1495.42	85.01	-3.30	0.000018
22	1005.00	1.44	1440.85	81.91	2.37	0.000018
22	1005.00	1.52	1523.09	86.58	-3.60	0.000018
22	1005.00	0.99	988.02	56.17	4.42	0.000018
22	1005.00	0.98	975.26	55.44	4.76	0.000018
22	1005.00	0.83	832.33	47.32	3.55	0.000018
22	1005.00	0.83	834.94	47.46	2.27	0.000018
29	1005.00	3.93	3929.28	223.37	4.68	0.000018
29	1005.00	4.69	4688.79	266.54	-3.70	0.000018
29	1005.00	4.58	4578.89	260.29	0.62	0.000018
29	1005.00	4.30	4299.56	244.42	-0.17	0.000018
29	1005.00	2.93	2925.78	166.32	2.51	0.000019
29	1005.00	3.17	3165.02	179.92	-1.03	0.000019
29	1005.00	2.96	2960.24	168.28	-0.09	0.000019
29	1005.00	3.19	3188.61	181.26	-3.34	0.000019
29	1005.00	2.48	2479.33	140.94	-0.99	0.000019
29	1005.00	2.60	2598.89	147.74	-2.77	0.000019
29	1005.00	2.55	2545.08	144.68	1.81	0.000019
29	1005.00	2.67	2673.34	151.97	0.02	0.000019
29	1005.00	1.16	1158.43	65.85	3.59	0.000019
29	1005.00	1.44	1440.60	81.89	-2.52	0.000019
29	1005.00	1.20	1196.50	68.02	-1.91	0.000019
29	1005.00	1.29	1289.52	73.30	3.21	0.000019

36	1005.00	3.97	3970.84	225.73	0.65	0.000018
36	1005.00	4.01	4007.69	227.82	1.80	0.000018
36	1005.00	4.48	4477.98	254.56	-3.94	0.000018
36	1005.00	4.50	4501.18	255.88	-4.54	0.000018
36	1005.00	3.52	3519.70	200.08	3.68	0.000019
36	1005.00	3.47	3469.01	197.20	2.88	0.000019
36	1005.00	3.68	3675.08	208.92	2.98	0.000019
36	1005.00	3.78	3784.16	215.12	1.78	0.000019
36	1005.00	2.48	2482.52	141.12	0.80	0.000019
36	1005.00	2.51	2512.47	142.83	-2.03	0.000019
36	1005.00	2.67	2670.28	151.80	-0.10	0.000019
36	1005.00	2.58	2576.03	146.44	0.85	0.000019
36	1005.00	1.41	1413.86	80.37	-1.52	0.000019
36	1005.00	1.30	1297.93	73.78	4.48	0.000019
36	1005.00	1.30	1304.99	74.18	0.33	0.000019
36	1005.00	1.34	1341.49	76.26	1.97	0.000019
43	1005.00	3.61	3606.27	205.00	-0.20	0.000018
43	1005.00	3.51	3514.33	199.78	0.08	0.000018
43	1005.00	3.75	3745.32	212.91	-4.59	0.000018
43	1005.00	3.85	3853.67	219.07	-1.18	0.000018
43	1005.00	2.93	2925.58	166.31	2.76	0.000020
43	1005.00	3.34	3343.33	190.06	-4.38	0.000019
43	1005.00	3.02	3016.51	171.48	3.49	0.000019
43	1005.00	3.13	3130.78	177.97	4.01	0.000019
43	1005.00	2.15	2151.18	122.29	3.09	0.000019
43	1005.00	2.48	2476.10	140.76	-0.88	0.000019
43	1005.00	2.39	2391.09	135.93	2.52	0.000019
43	1005.00	2.34	2338.30	132.92	3.89	0.000019
43	1005.00	1.32	1324.73	75.31	3.63	0.000019
43	1005.00	1.36	1362.61	77.46	-0.88	0.000019
43	1005.00	1.39	1385.33	78.75	-2.77	0.000019
43	1005.00	1.31	1312.66	74.62	3.86	0.000019

Inlet Air Temp	Air Reynolds Number, Re_a	Log Mean Temperature Difference	Air Side Capacity Rate, C_a	Average heat transfer Q_{avg}	Capacity rate ratio, C*
°C	Re (air)	ΔTlm		W	
15	1761.00	21.69	646.69	2302.61	0.066
15	2981.43	15.96	1094.86	2399.41	0.038
15	4201.78	16.94	1543.01	2232.84	0.025
15	5027.66	14.13	1846.29	2221.69	0.021
15	1866.80	16.20	685.54	1653.58	0.040
15	3047.63	14.66	1119.17	1642.21	0.025
15	4256.24	13.90	1563.00	1657.91	0.018
15	5475.65	13.08	2010.81	1632.98	0.014
15	1846.13	17.70	677.95	1140.58	0.029
15	3035.01	17.58	1114.54	1124.98	0.018
15	4243.59	14.28	1558.36	1215.91	0.013
15	5464.43	15.28	2006.68	1198.24	0.010
15	1862.68	14.24	684.03	1083.02	0.027
15	3060.20	13.98	1123.79	1113.60	0.016
15	4243.59	15.69	1558.36	1037.05	0.011
15	5524.50	16.40	2028.74	1014.38	0.009
22	1705.94	21.45	633.43	3656.45	0.136
22	2854.08	19.29	1059.74	3843.20	0.080
22	4009.68	18.34	1488.82	4035.70	0.057
22	5024.98	17.58	1865.81	3993.63	0.045
22	1688.83	18.34	637.76	2705.87	0.090
22	2864.63	17.81	1078.27	2820.29	0.053
22	4004.19	17.02	1503.94	2801.99	0.036
22	5142.10	15.08	1931.33	2840.90	0.028
22	1752.32	14.32	657.80	1535.70	0.045
22	2860.76	15.79	1068.06	1471.51	0.027
22	3961.14	15.23	1478.88	1458.30	0.019
22	5120.25	16.77	1911.63	1496.64	0.015
22	1729.56	14.94	645.73	1010.88	0.031
22	2855.83	14.19	1066.21	999.61	0.019
22	4007.18	14.06	1496.07	847.65	0.011
22	5131.26	14.12	1915.74	844.64	0.009
29	1698.44	17.93	630.64	4025.81	0.181
29	2861.37	18.02	1062.45	4605.21	0.106
29	3967.18	16.70	1473.04	4593.15	0.076
29	4950.33	14.69	1838.09	4295.81	0.061
29	1690.18	16.98	641.37	2963.46	0.114
29	2802.79	15.25	1057.85	3148.85	0.070
29	3894.07	14.88	1469.73	2958.89	0.048
29	5034.48	13.11	1900.15	3137.03	0.038
29	1649.65	17.20	625.99	2467.20	0.096

29	2785.64	15.97	1051.38	2563.90	0.057
29	3878.22	14.65	1463.75	2568.52	0.041
29	4997.65	12.30	1886.25	2673.65	0.032
29	1699.32	13.28	641.37	1179.98	0.044
29	2731.07	12.67	1030.78	1422.93	0.030
29	3727.07	14.80	1406.70	1185.31	0.019
29	5031.76	12.33	1899.12	1310.92	0.016
36	1707.40	15.53	633.97	3983.89	0.198
36	2838.82	13.85	1054.07	4044.50	0.121
36	3894.65	15.25	1446.11	4393.13	0.087
36	4965.42	12.94	1843.69	4403.41	0.070
36	1670.39	17.02	651.92	3586.97	0.168
36	2670.11	14.44	1042.09	3520.47	0.104
36	3720.26	14.01	1451.94	3731.54	0.075
36	4763.94	13.63	1859.27	3818.42	0.058
36	1619.82	14.64	632.19	2492.57	0.109
36	2667.73	13.91	1041.16	2487.44	0.066
36	3760.73	12.60	1467.74	2668.96	0.047
36	4822.46	12.10	1882.11	2587.10	0.037
36	1592.85	14.40	621.66	1403.31	0.061
36	2672.44	14.27	1043.00	1328.36	0.035
36	3769.23	13.97	1471.06	1307.12	0.025
36	4812.95	11.10	1878.40	1355.00	0.019
43	1675.74	13.54	622.21	3602.71	0.221
43	2823.13	11.77	1048.25	3515.74	0.128
43	3857.49	11.12	1432.31	3663.16	0.094
43	4987.74	11.99	1851.98	3831.16	0.073
43	1552.48	13.75	617.62	2967.03	0.181
43	2603.80	12.38	1022.59	3273.25	0.109
43	3642.01	10.76	1430.32	3071.09	0.078
43	4615.25	10.76	1812.54	3196.16	0.062
43	1543.31	12.23	606.10	2185.49	0.132
43	2539.91	11.76	997.50	2465.32	0.080
43	3607.08	10.88	1416.60	2422.05	0.056
43	4565.02	10.62	1792.81	2385.58	0.044
43	1548.99	11.59	608.33	1349.68	0.074
43	2580.15	10.92	1013.30	1356.64	0.044
43	3653.82	11.36	1434.96	1366.68	0.031
43	4650.95	9.60	1826.56	1339.00	0.025

Inlet Air Temp	UA= $q_{avg}/F\Delta T_{lm}$	Number of Transfer Unit	Effectiveness	Overall resistance R_{tot}	Air side heat transfer Coefficient, h_a	Air Nusselt Number, Nu_a
°C	W/°K	NTU	ε	°K/W	W/m²-K	
15	107.23	2.51	0.8980	0.0093	33.21	4.36
15	151.90	3.65	0.9643	0.0066	36.53	4.80
15	133.12	3.88	0.9782	0.0070	35.55	4.67
15	158.78	4.18	0.9738	0.0067	36.91	4.85
15	103.10	3.72	0.9803	0.0097	26.95	3.54
15	113.14	4.10	0.9923	0.0089	28.41	3.73
15	120.49	4.33	0.9817	0.0083	30.83	4.05
15	126.10	4.55	0.9731	0.0090	30.62	4.02
15	65.10	3.27	0.9449	0.0150	19.14	2.52
15	64.65	3.28	0.9437	0.0155	19.44	2.55
15	86.03	4.23	0.9972	0.0164	22.52	2.96
15	79.19	3.77	0.9752	0.0176	20.39	2.68
15	76.80	4.21	0.9855	0.0230	21.28	2.80
15	80.49	4.36	0.9978	0.0224	28.27	3.71
15	66.77	3.78	0.9830	0.0250	22.68	2.98
15	62.47	3.54	0.9595	0.0260	19.98	2.63
22	172.15	2.00	0.8276	0.0055	50.92	6.61
22	201.20	2.38	0.8907	0.0047	58.75	7.63
22	222.21	2.63	0.9334	0.0047	59.19	7.69
22	229.48	2.75	0.9323	0.0046	64.04	8.32
22	149.00	2.59	0.8991	0.0066	42.48	5.52
22	159.96	2.80	0.9249	0.0067	47.48	6.17
22	166.25	3.04	0.9542	0.0060	47.92	6.22
22	190.35	3.48	0.9850	0.0068	48.79	6.34
22	108.31	3.67	0.9838	0.0148	29.02	3.77
22	94.12	3.32	0.9738	0.0150	27.54	3.58
22	96.74	3.36	0.9525	0.0147	27.37	3.55
22	90.13	3.08	0.9654	0.0155	29.02	3.77
22	68.37	3.41	0.9445	0.0236	15.97	2.07
22	71.14	3.56	0.9485	0.0237	16.60	2.16
22	60.90	3.68	0.9574	0.0265	17.28	2.24
22	60.42	3.66	0.9627	0.0297	16.60	2.16
29	226.81	1.99	0.8189	0.0045	55.86	7.09
29	258.19	2.29	0.8911	0.0040	59.68	7.57
29	277.86	2.48	0.9018	0.0036	65.30	8.29
29	295.35	2.65	0.9207	0.0034	67.23	8.53
29	176.31	2.41	0.8833	0.0057	47.74	6.06
29	208.58	2.83	0.9346	0.0048	55.19	7.00
29	200.85	2.82	0.9334	0.0050	61.76	7.84
29	241.66	3.39	0.9757	0.0049	60.42	7.67
29	144.92	2.41	0.8977	0.0068	40.51	5.14

29	162.20	2.69	0.9328	0.0060	47.31	6.00
29	177.16	2.94	0.9343	0.0057	52.49	6.66
29	219.63	3.68	0.9714	0.0055	55.39	7.03
29	89.77	3.19	0.9389	0.0111	24.45	3.10
29	113.44	3.67	0.9821	0.0129	30.69	3.89
29	80.88	3.04	0.9561	0.0126	34.77	4.41
29	107.41	3.63	0.9574	0.0190	31.85	4.04
36	259.07	2.06	0.8365	0.0038	72.72	9.06
36	294.90	2.30	0.8742	0.0033	76.52	9.53
36	290.98	2.41	0.8974	0.0036	77.86	9.70
36	343.71	2.57	0.9363	0.0029	79.34	9.88
36	212.84	1.95	0.8176	0.0046	52.30	6.51
36	246.32	2.28	0.8715	0.0040	59.14	7.36
36	269.05	2.48	0.8942	0.0036	66.76	8.31
36	282.90	2.61	0.9108	0.0035	66.02	8.22
36	171.94	2.49	0.8967	0.0059	46.32	5.77
36	180.59	2.64	0.9251	0.0059	48.71	6.07
36	213.96	3.11	0.9495	0.0057	57.14	7.12
36	215.91	3.11	0.9471	0.0055	59.62	7.42
36	98.42	2.60	0.9209	0.0105	31.85	3.97
36	94.02	2.58	0.9019	0.0129	32.05	3.99
36	94.51	2.59	0.9189	0.0126	36.40	4.53
36	123.31	3.42	0.9561	0.0190	36.97	4.60
43	268.81	1.95	0.8188	0.0037	92.15	11.26
43	301.65	2.25	0.8724	0.0033	94.21	11.52
43	332.75	2.48	0.9154	0.0030	98.05	11.99
43	322.88	2.48	0.9007	0.0029	97.52	11.92
43	217.99	1.95	0.8188	0.0050	48.76	5.96
43	267.10	2.39	0.9041	0.0042	52.69	6.44
43	288.34	2.58	0.9001	0.0034	69.98	8.55
43	300.13	2.68	0.9076	0.0030	73.50	8.98
43	180.52	2.25	0.8635	0.0054	100.06	12.23
43	211.76	2.65	0.9202	0.0052	92.05	11.25
43	224.91	2.82	0.9225	0.0044	96.86	11.84
43	226.98	2.85	0.9205	0.0043	108.28	13.24
43	117.63	2.61	0.9025	0.0092	33.32	4.07
43	125.51	2.79	0.9348	0.0087	39.92	4.88
43	121.52	2.93	0.9386	0.0080	45.01	5.50
43	140.88	3.13	0.9367	0.0069	55.19	6.75

REFERENCES

[1] Gomes, C. "Global Auto Report", *Global Economic Research,* November 29, 2011, Scotia Economics, Web. 11 Dec 2011.

http://www.scotiacapital.com/English/bns_econ/bns_auto.pdf.

[2] "2010 Production Statistics." OICA. International Organization of Motor Vehicle Manufa, 2011. Web. 11 Dec 2011. <http://oica.net/category/production-statistics/>.

[3] Raschke. K., "Heat Transfer between the Plant and the Environment" Annual Review of Plant Physiology 11: 111-126, June 1960) DOI: 10.1146/annurev.pp.11.060160.000551.

[4] Mehendale, S.S., Jacobi, A. M., and Shah, R.K., "Fluid Flow and Heat Transfer at Micro- and Meso-scales with Application to Heat Exchanger Design," ASME Appl. Mech. Rev., 53(7):175-193, 2000, doi:10.1115/1.3097347.

[5] Kandlikar, S. G., and Grande, W. J., "Evolution of Microchannel Flow Passages-Thermohydraulic Performance and Fabrication Technology," J. of Heat Transfer Engineering, 24(1):3-17, 2003.

[6] Dasgupta, E. S., Siddiqui, F. A., Quaiyum, M. A., Al-Obaidi, S., and Fartaj, A., "Experimental Study on Air Side Heat Transfer and Flow Characteristics of Mesochannel Crossflow Heat Exchanger," Proc. 9th *International Conference on Nanochannels, Microchannels and Minichannels*, M.E. Alberta, Canada, ICNMM2011-58257, June 19-22, 2011.

[7] Taylor, J. B., Carrano, A. L., and Kandlikar, S. G., "Characterization of the Effect of Surface Roughness and Texture on Fluid Flow – Past, Present, And Future", *Proc. of 3rd International Conference on Microchannels and Minichannels,* Toronto, Ontario, Canada, ICMM2005 June 13-15, 2005

[8] Al-Obaidi S., "Second Law Analysis of a Multiport Serpentine Microchannel Heat Exchanger," M.A.Sc. Thesis, Mechanical Engineering Department, University of Windsor, Canada, 2011.

[9] Zimparov V. Energy Conservation through Heat Transfer Enhancement Techniques. *Int. J. Energy Research* 2002; 26:675-696.

[10] Kang, S. W., Chang, Y. T., and Chang, G. S., "The Manufacture and Test of (110) Orientation Silicon Based Micro Heat Exchanger", *Tamkang Journal of Science and Engineering,* 5(3):129–136, 2002.

[11] Fan, Y., and Luo, L., "Recent Applications of Advances in Microchannel Heat Exchangers and Multi-Scale Design Optimization" *Heat Transfer Engineering*, 29(5):461–474, 2008, DOI: 10.1080/01457630701850968.

[12] Lee, P-S., Garmilla, S. V., and Liu, D., "Investigation of Heat Transfer in Rectangular Microchannels", International Journal of Heat and Mass Transfer 48(9): 1688–1704, 2005.

[13] Shah R. K., Webb R. L. *Compact and Enhanced Heat Exchangers;* ISSN: 961-91393-0-5: 425-468

[14] Taborek J, Hewitt GF, Afgan N. *Heat Exchangers: Theory and Practice*; (Eds.) McGraw-Hill: ISBN:9780070628069 New York, USA,1983.

[15] Luo L, Fan Y, Tondeur D. "Heat exchanger: from micro- to multi-scale design optimization". *International Journal of Energy Research,* 30:1266-1274, 2007.

[16] Owhaib, W., and Palm, Bjorn., "Experimental investigation of single-phase convective heat transfer in circular microchannels", Experimental Thermal and Fluid Science, 28: 105–110, 2004, doi.org/10.1016/S0894-1777(03)00028-1.

[17] Tuckerman, D. B., and Pease, R. F. W., "High-Performance Heat Sinking for VLSI," IEEE Electron Device Letters (EDL) 2:126-129, 1981.

[18]Tuckerman, D. B., Pease, R. F. W, Guo, Z., Hu, J. E., Yildirim, O., Deane, G., and Wood, L., "Microchannel Heat Transfer: Early History, Commercial Application and Emerging Opportunities", Proc. 9th *International Conference on Nanochannels, Microchannels and Minichannels*, M.E. Alberta, Canada, ICNMM2011-58308, June 19-22, 2011

[19] Steinke, M. E., and Kandlikar, S. G., "Single-Phase Liquid Heat Transfer in Plain and Enhanced Microchannels", ICNMM2006-96227, *Fourth International Conference on Nanochannels, Microchannels and Minichannels* June 19-21, 2006, Limerick, Ireland

[20] Carrier, "Microchannel Technology - More Efficient, Compact, and Corrosion Resistant Technology for Air-Cooled Chiller Applications", *Carrier Corporation,* New York, USA, 2006.

[21] Westphalen, D., Roth, K. W., and Brodrick, J., "Emerging Technologies: Microchannel Heat Exchangers", ASHRAE Journal, 45(12):107-109, December 2003.

[22] Kim, J-H., Groll, E. A., "Microchannel Heat Exchanger Defrost Performance and Reliability (ASHRAE 1195-RP)", Final report, Ray W. Herrick Labs, Purdue University, April 2003.

[23] Dehghandokht, M., Khan, M. G., Fartaj, F., and Sanaye, S., "Numerical Study of Fluid Flow and Heat Transfer in a Multi-Port Serpentine Meso-Channel Heat Exchanger," J. of Applied Thermal Engineering 31(10):1588-1599, 2011, doi: 10.1016/j.applthermaleng.2011.01.035.

[24] Dehghandokht, M., Khan, M. G., Fartaj, F., and Sanaye, S., "Flow and Heat Transfer Characteristics of Water and Ethylene Glycol-water in a Multi-Port Serpentine Meso-Channel Heat Exchanger," Int. J. of Thermal Sciences 50(8): 1615-1627, 2011, doi: 10.1016/j.ijthermalsci.2011.03.004.

[25] Khan, M. G., and Fartaj, A., "Heat Transfer Experiments of Ethylene Glycol-Water Mixture in Multi-Port Serpentine Meso-Channel Heat Exchanger Slab," FEDSM-ICNMM2010-31131, Proc. *3rd Joint US-European Fluids Engineering Summer Meeting (FEDSM) and 8th International Conference on Nanochannels, Microchannels, and Minichannels (ICNMM),* Montreal, Quebec, CANADA, August 1-5, 2010.

[26] United States environmental Protection Agency, EPA-420-F-10-014, April 2010.

[27] National Association of State Foresters, "Automatic Transmission Fluid Overheating: New Jersey Forest Fire Service's Solution to High Temperature Problems in Ford F-350 and F-450", REC Newsnote #15, December 2005.

[28] Neil, C., "Cooling Automatic Transmission Fluids More Efficiently", Tribology & Lubrication Technology, 19 Oct, 2011.

http://findarticles.com/p/articles/mi_qa5322/is_200503/ai_n21367574/?tag=mantle_skin;content

[29] GM, Ford, Chrysler Automatic Transmission Fluids http://ls1tech.com/forums/833909-post39.html

[30] Salah, M. H., Mitchell, T.H., Wagner, J. R., Dawson, D. M., "Multiple Cooling Loops in Advanced Vehicle Thermal Management Systems", *IEEE/ASME Transactions on Mechatronics,* June 2007.

[31] Kemp, S. P., and Linden, J. L., "Physical and Chemical properties of a Typical Automatic Transmission Fluid," SAE International, 902148, 1990.

[32] Henderson, H. E., and Swinney, B., "High Quality Base Oil for Next Generation Automatic Transmission Fluids," SAE Technical Paper 982666, 1998.

[33] Sarkar, R., Devlin, M. K., Li, S., Glasgow, M. B., and Jao, T-C., "Low and High Temperature Non-Newtonian Behaviour of Automatic Transmission Fluids," SAE Technical Paper 2002-01-1695.

[34] Totten, G. E., "Hand Book of Lubrication and Tribology, Application and Maintenance," Second Edition, ISBN 978-0849320958, 1:2.1-2.14, 2006.

[35] Rudnick, L. R., and Shubkin, R. L., "Synthetic Lubricant and High-Performance Functional Fluids," CRC Press, Technology & Engineering, ISBN 978-0824701949, 77:461-476, 1999.

[36] Yamamori, k., Saitou, K., kobiki, Y., and Ogawa, A., "Development of New Automatic Transmission Fluid for Fuel Economy", SAE Technical Paper 2003-01-3258.

[37] Semel, R. R., "Fuel Economy Improvements through Improved Automatic Transmission Warmup – Stand Alone Oil to Air (OTA) Transmission Cooling Strategy with Thermostatic Cold Flow Bypass valve," SAE Technical Paper 2001-01-1760.

[38] Warnakulasuriya, F. S. K., and Worek, W. M., "Heat Transfer and Pressure Drop Properties of High Viscous Solutions in Plate Heat Exchangers," Int. J. of Heat and Mass Transfer, 51(1-2):52–67, 2008, doi:10.1016/j.ijheatmasstransfer.2007.04.054.

[39] Rennie, T. J., and Raghavan, G. S. V., "Thermally Dependent Viscosity and Non-Newtonian Flow in a Double-Pipe Helical Heat Exchanger," Applied Thermal Engineering, 27:862-868, 2007.

[40] Kumar, V., Gupta, P., and Nigam, K. D. P., "Fluid Flow and Heat Transfer in Curved Tubes with Temperature-Dependent Properties," Ind. Eng. Chem. Res. 46(10): 3226-3236, 2007, DOI: 10.1021/ie0608399.

[41] Wang, C-C., Jeng, Y-R., Chien, J-J., and Chang, Y-J., "Frictional Performance of Highly Viscous Fluid in Minichannels," Applied Thermal Engineering, 24(14-15):2243–2250, 2004.

[42] Koo, J., and Kleinstreuer, C., "Viscous Dissipation Effects in Microtubes and Microchannels," Int. J. of Heat and Mass Transfer, 47(14-16):3159–3169, 2004.

[43] Sahin, A. Z., "Effect of Viscosity on Effectiveness of Parallel Flow Heat Exchanger," Energy Convers. Mgmt 12 (39):1233-1238, 1998.

[44] Genic´, S. B., Jac´imovic´, B. M., and Janjic, B., "Experimental Research of Highly Viscous Fluid Cooling in Cross-Flow to a Tube Bundle," Int. J. of Heat and Mass Transfer, 50(7-8):1288–1294, 2007.

[45] Nonino, C., Giudice, S. D., and Savino, S., "Temperature Dependent Viscosity Effects on Laminar Forced Convection in The Entrance Region of Straight Ducts," Int. J. of Heat and Mass Transfer, 49(23-24):4469–4481, 2006.

[46] Murakami, Y., and Miki´C, B. B., "Parametric Investigation of Viscous Dissipation Effects on Optimized Air Cooling Microchanneled Heat Sinks," Int. J. of Heat Transfer Engineering, 24(1):53–62, 2003.

[47] Page, R. W., and Kozierowski, H. J., "Thermal Management for the 21st Century – Improved Thermal Control & Fuel Economy in an Army Medium Tactical Vehicle", SAE Technical Paper, 2005-01-2068.

[48] Soares, A. A., Ferreira, J. M., Caramelo, L., Anacleto, J., and Chhabra, R. P., "Effect of Temperature-Dependent Viscosity on Forced Convection Heat Transfer From a Cylinder in Crossflow of Power-Law Fluids," Int. J. of Heat and Mass Transfer 53(21-22):4728–4740, 2010.

[49] Morini, G. L., "Viscous Heating in Liquid Flows in Micro-Channels," Int. J. of Heat and Mass Transfer 48(17):3637–3647, 2005.

[50] Cheng, C-Y., "The Effect of Temperature-Dependent Viscosity on the Natural Convection Heat Transfer from a Horizontal Isothermal Cylinder of Elliptic Cross Section," Int. Communications in Heat and Mass Transfer 33(8):1021–1028, 2003.

[51] Kleinstreuer, J. K., "Viscous Dissipation Effects in Microtubes and Microchannels," Int. J. of Heat and Mass Transfer 47(14-16):3159–3169, 2004.

[52] Celata, G. P., Morini, G. L., Marconi, V., Marconi, S. J., and Zummo, G., "Using Viscous Heating to Determine the Friction Factor in Microchannels an Experimental Validation," Experimental Thermal and Fluid Science 30(8):725–731, 2006.

[53] Vashisth, S., Kumar, V., and Nigam, K. D. P., "A Review on the Potential Applications of Curved Geometries in Process Industry", Industrial & Engineering Chemistry Research, 47 (10): 3291-3337, 2008, DOI: 10.1021/ie701760h.

[54] Yang, Y., Lam, R. C., Chen, Y. F., and Yabe, H., "Modeling of Heat Transfer and Fluid Hydrodynamics for a Multidisc Wet Clutch," SAE Technical Paper 10.4271/950898, 1995.

[55] Khan, M. G., "Experimental Investigation of Heat Transfer and Pressure Drop Characteristics of Water and Glycol-Water Mixture in Multi-Port Serpentine Microchannel Slab Heat Exchangers," Ph.D. Thesis, Mechanical Engineering Department, University of Windsor, Ontario, Canada, 2011.

[56] Hosseini, R., Hosseini-Ghaffar, A., and Soltani, M., "Experimental Determination of Shell Side Heat Transfer Coefficient and Pressure Drop for an Oil Cooler Shell-and-Tube Heat Exchanger with Three Different Tube Bundles," Applied Thermal Engineering 27(5-6):1001–1008, 2007.

[57] Qu, W., and Mudawar, I., "Experimental and Numerical Study of Pressure Drop and Heat Transfer in a Single-Phase Micro-Channel Heat Sink," Int. J. of Heat and Mass Transfer 45:2549–2565, 2002.

[58] Obot, N. T., Das, L., Vakili, D. E., and Green, R. A., "Effect Of Prandtl Number on Smooth-Tube Heat Transfer and Pressure Drop", *International Communications in Heat and Mass Transfer,* 24(6):889-896, October 1997.

[59] Akehurst, S., "An Investigation in to the Loss Mechanisms Associated With a Pushing Metal V-Belt Continuously Variable Transmission", PhD Thesis, Department of Mechanical Engineering, University of Bath, United Kingdom, 2001.

[60] Hetsroni , G., Mosyak , A., Pogrebnyak, E., and Yarin, L.P "Fluid flow in micro-channels", Int. J. of Heat and Mass Transfer, 48(10):1982–1998, 2005

[61] Hetsroni, G., Mosyak, A., Pogrebnyak, E., and Yarin, L.P., "Heat Transfer in Micro-Channels: Comparison of Experiments with Theory and Numerical Results", Int. J. of Heat and Mass Transfer 48:5580–5601, 2005.

[62] Karamavruc, A., Shi, z., and Gunther, D., "Determination of Empirical Heat Transfer Coefficient via CFD to Predict the Interface Temperature of Continuously Sleeping Clutches," SAE Technical Paper 2011-01-0313.

[63] Sobhan, C. B., and Garimella, S. V., "A Comparative Analysis of Studies on Heat Transfer and Fluid Flow in Microchannels," CTRC Research Publications, Microscale Thermophysical Engineering, 5:293–311, 2001.

[64] Khan, M. G., and Fartaj, A., "A Review on Microchannel Heat Exchangers and Potential Applications," Int. J. of Energy Research 35(7): 553-582, 2010, doi: 10.1002/er.1720.

[65] Khan, M. G., and Fartaj, A., "Experiment of Ethylene Glycol-Water in Multiport Circular Straight Microchannel Slab," SAE Technical Paper 2010-01-0326, 2010, doi: 10.4271/2010-01-0326.

[66] Celata, G.P., Cumo, M., Guglielmi, M., and Zummo, G, "Experimental Investigation of Hydraulic and Singlephase Heat Transfer in 0.130-Mm Capillary Tube", Microscale Thermophysical Engineering, 6:85–97, 2002, DOI: 10.1080/1089395029005323 1.

[67] Dasgupta, E. S., "Experimental Study on Heat Transfer and Flow Characteristics of Air Cooling through Cross-flow Microchannel Heat Exchanger," M.A.Sc. Thesis, Mechanical Engineering Department, University of Windsor, Canada, 2011.

[68] Murakami, Y., and MikiC, B. B., "Parametric Investigation of Viscous Dissipation Effects on Optimized Air Cooling Microchanneled Heat Sinks," Int. J. of Heat Transfer Engineering, 24(1): 53-62, 2003, DOI: 10.1080/01457630304047.

[69] Soares, A. A., Ferreira, J. M., Caramelo, L., Anacleto, J., and Chhabra, R. P., "Effect of Temperature-Dependent Viscosity on Forced Convection Heat Transfer from a

Cylinder in Crossflow of Power-Law Fluids," Int. J. of Heat and Mass Transfer 53:4728-4740, 2010, doi: 10.1016/j.ijheatmasstransfer.2010.06.019.

[70] Siddiqui, F. A., "A Study of Cross-Flow Air Heating via a Multiport Serpentine Microchannel Heat Exchanger," M.A.Sc. Thesis, Mechanical Engineering department, University of Windsor, Canada, 2011.

[71] Shah, R. K, and Sekulic, D. P., "Fundamentals of Heat Exchanger Design," John Wiley & Sons, Inc., USA, ISBN 0-471-32171-0, 2003.

[72] Kakac, S. and Hongtan, L., "Heat Exchangers: Selection, Rating and Thermal Design," CRC: New York, ISBN 9780849309021, 2002.

[73] Yovanovich, M. M., and Muzychka, Y. S., "Solutions of Poisson Equation within Singly and Doubly Connected Prismatic Domains," National Heat Transfer Conference, Baltimore, MD, 97-3880, Aug 10-12, 1997.

[74]Muzychka, Y. S., and Yovanovich, M. M., "Pressure Drop in Laminar Developing Flow in Noncircular Ducts: A Scaling and Modeling Approach", Journal of Fluids Engineering, Vol. 131 / 111105-1, NOVEMBER 2009

[75] Kays, W. M., and London, A. L., "Compact Heat Exchangers: Third Edition," Krieger Publishing Company, Florida, ISBN 1-57524-060-2:102-107, 1998.

[76] Cengel, Y. A., "Heat Transfer -A Practical Approach," McGraw-Hill, New York, ISBN 0-07-245893-3, 2007.

[77] Muzychka, Y. S., "Generalized Models for Laminar Developing Flows in Heat Sinks and Heat Exchangers", Proc. 9th *International Conference on Nanochannels, Microchannels and Minichannels*, M.E. Alberta, Canada, ICNMM2011-58294, June 19-22, 2011.

[78] Giudice, S. D., Nonino, C., and Savino, S., "Effects of viscous dissipation and temperature dependent viscosity in thermally and simultaneously developing laminar flows in microchannels", Int. J. of Heat and Fluid Flow, 28: 15–27, 2007.

[79] Bahrami, M., Yovanovich, M. M., and Culham, J. R., "A Novel Solution for Pressure Drop in Singly Connected Microchannels of Arbitrary Cross-Section", Int. J. of Heat and Mass Transfer 50:2492–2502, 2007.

[80] Zimparov, V., "Energy Conservation through Heat Transfer Enhancement Techniques", Int. J. Energy Research, 26:675-696, 2002, DOI: 10.1002/er.810.

[81] Fox, R. W., McDonald, A. T. Pritchard, P. J. "Introduction to Fluid Mechanics, 8th Edition" John Wiley & Sons Inc., ISBN-13 9780470547557:328-402, 2010.

[82] Topakoglu, H. C. "Steady state laminar flow in incompressible viscous fluid in curved pipes", Math Mech. 16, 1321, 1967.

[83] Bowman, R. A., Mueller, A. C., and Nagle, W. M., "Mean Temperature Difference in Design." Transactions of the ASME 62(1): 283-294, 1940.

[84] Placek, D., Herzog, S. N., Neveu, C. D., "Reducing Energy Consumption with Multigrade Hydraulic Fluids", *Proc. of the 9th Annual Fuels & Lubes Asia Conference and Exhibition,* F&L Asia, Inc., Singapore, 21-24 January, 2003.

[85] Herzog, S.N., Hyndman, C.W., Simko, R.P., and Neveu, C.D., "Effect of Operation Time on Oil Viscosity and Pump Efficiency", NCFP I05-9.3.

[86] White, C. M., "Fluid friction and its Relation to Heat Transfer", *Trans. Inst. Chem. Eng.* (London) 10, 66, 1929.

[87] Kumar, V, and Nigam, K.D.P., "Laminar convective heat transfer in chaotic configuration", Int. J. of Heat and Mass Transfer, 50, 2469–2479, 2007.

[88] Herwig, H. and Hausner, O., "Critical View on ''New Results in Micro-Fluid Mechanics: an Example", Int. J. of Heat and Mass Transfer, 46: 935–937, 2003, doi: 10.1016/S0017-9310(02)00306-X.

[89] Tso, C. P. and Mahulikar, S. P., "Experimental Verification of the Role of Brinkman Number in Microchannels Using Local Parameters", Int. J. of Heat and Mass Transfer, 43: 1837-1849, 2000.

[90] ASME. Air cooled heat exchangers. An American National Standard, Performance Test Code (PTC) 30-1991. American Society of Mechanical Engineers (ASME): NY, USA, 1991.

[91] Mott, R. L., "Applied Fluid Mechanics," Pearson Prentice Hall, Upper Saddle River, New Jersey, ISBN 0-13-114680-7: 2006.

[92] Dean, W. R., 1928 "The streamline motion of fluid in a curved pipe", Phil. Mag. S7 5: 673-695, 1928.

[93] Johnson, M., and Kamm, R. D., "Numerical Studies of Steady Flow Dispersion at Low Dean Number in a Gently Curving Tube", J. of Fluid Mech. vol. 172: 329-345, 1986.

[94] Nield, D.A., Kuznetsov, A.V., and Xiong, M., "Thermally Developing Forced Convection in a Porous Medium: Parallel Plate Channel with Walls at Uniform Temperature, with Axial Conduction and Viscous Dissipation Effects", Int. J. of Heat and Mass Transfer 46: 643–651, 2003.

[95] White, F. M., "Fluid Mechanics", McGraw-Hill Companies, Burr Ridge, IL, ISBN 13: 9780072402179, 2003.

[96] Lienhard, J. H, "A Heat Transfer Textbook", Phlogiston Press, Cambridge, MA, ISBN 13: 9780133850895.

[97] DeSilva, C. W., "Sensors and Actuators: Control System Instrumentation", CRC Press, Taylors and Francis Group, New York, ISBN: 9 781420 044836, 2007.

[98] "FE-EIT PM - Mechanical Engineering (REA) - The Best Test Prep for the EIT Exam", Research and Education association, New Jersey, ISBN: 0-87891-262-2, 1999.

VITA AUCTORIS

NAME: Md. Abdul Quaiyum

PLACE OF BIRTH: Chapai Nowabgonj, Bangladesh

YEAR OF BIRTH: October, 1964

EDUCATION:

[1] In 1973 completed elementary school from Shonaichandi Primary School, Chapai Nowabgonj, Bangladesh with residential scholarship and promoted to Grade VI.

[2] In 1976 attended district scholarship examination in grade VIII and secured 2nd position in the district competition from Alinagar Multilateral High School, Chapai Nowabgonj, Bangladesh.

[3] In 1979 completed Secondary School Certificate (SSC) examination from Alinagar Multilateral High School, Chapai Nowabgonj, Bangladesh securing 1st division with distinction.

[4] In 1981 completed Higher Secondary School Certificate (HSC) examination from Rajshahi Government College, Rajshahi, Bangladesh securing 1st division.

[5] In 1988 received the Degree of Bachelor of Science (honours) in Agricultural Engineering, Major Farm Power and Machinery from Bangladesh Agricultural University, Mymensingh, Bangladesh.

[6] In 2005 received the Degree of Bachelor of Applied Science (B. A. Sc) in Mechanical Engineering from the University of Windsor, ON, Canada.

[7] In 2010 received the Degree of Master of Engineering (M Eng) in Mechanical Engineering from the University of Windsor, ON, Canada.

[8] In 2011-12 pursuing the Degree of Master of Applied Science (M. A. Sc) in Mechanical Engineering in the University of Windsor, ON, Canada. Expecting to graduate in February, 2012.

EMPLOYMENT EXPERINCE:

[1] ***Engineer and Senior Engineer*** from 1989-2000 in Barind Multipurpose Development Authority, Bangladesh: The principal responsibilities include; on-field diesel engine and machinery performance test, managing projects on agricultural mechanization, irrigation and water management, and command area development. The duty includes imparting training to the practicum engineers, mechanics, operators, and machinery drivers on engine and machinery operation, maintenance, overhaul, and troubleshooting.

Additional responsibilities were diesel engine performance test in test cells located in Bangladesh Diesel Plant, Dhaka, Bangladesh.

[2] ***Test Engineer*** 2006 in Nemak of Canada, Windsor, ON: Was responsible for non-destructive test of engine head and block.

[3] ***Diesel Engine Performance Development Engineer*** from 2006-2008 in Caterpillar Inc. Illinois, USA: The main responsibilities include diesel engine performance development and emission calibration compliant to EPA, CARB, and EU regulations based on ISO 8178 duty cycles.

[4] ***Research and Development Engineer*** from 2008-2009 in Dusan Infracore America Corporation, Georgia, USA: The main responsibilities include compressed natural gas (CNG) engine performance development and emission calibration compliance with EPA, and CARB regulations based on 40 CFR duty cycles.

[5] ***Calibration Engineer*** from 2012-present in ISUZU Motors, Michigan, USA: The main responsibilities include diesel engine calibration and emission control compliance with EPA, and CARB regulations based on 40 CFR and ISO 8178 duty cycles.